Transient Slurry Flow Phenomena after Bends in the Vertical Plane

An experimental study and analysis into the origin and development of density waves within pipeline systems using a sedimentation and erosion unbalance model

T. van der Voort

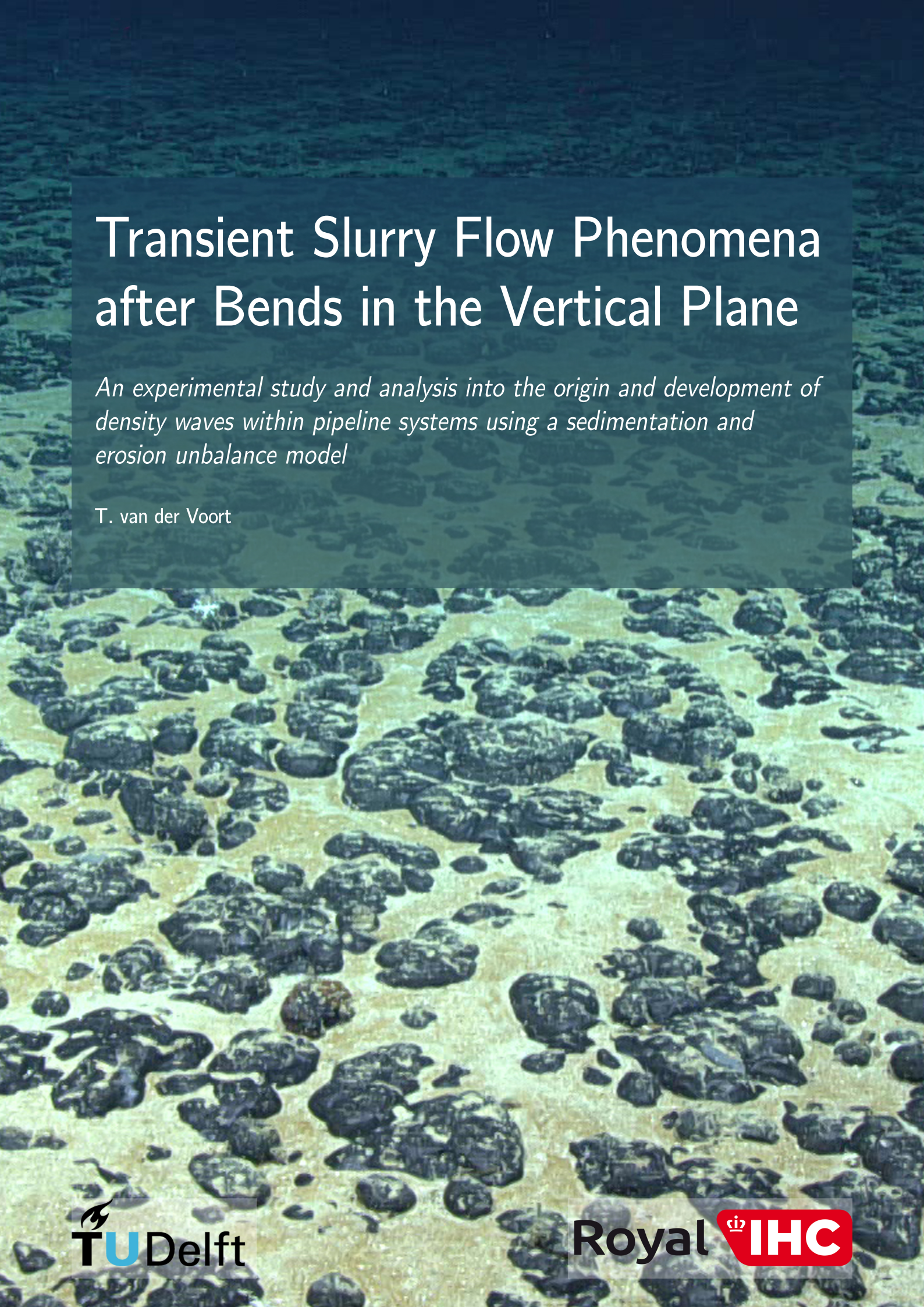

TU Delft

Royal IHC

Transient Slurry Flow Phenomena after Bends in the Vertical Plane

An experimental study and analysis into the origin and development of density waves within pipeline systems using a sedimentation and erosion unbalance model

by

T. van der Voort
4288017

in partial fulfilment of the requirements for the degree of,
Master of Science

in Civil Engineering

at the Delft University of Technology
to be defended publicly on Monday **July 5**, *2021 at 14:30*

Date:	June 22, 2021	
Project duration:	16th of March 2020 - 5th of July 2021	
Thesis committee:	Prof. dr. ir. C. van Rhee,	TU Delft - *Chair*
	Dr. ir. A. M. Talmon,	TU Delft
	Ir. E. de Hoog,	TU Delft | Royal IHC

Faculty of Civil Engineering and Geosciences,
Delft University of Technology

Royal IHC,
Department Technology

Figure on frontpage is retrieved and adapted from NOAA Office of Ocean Exploration and Research (2019)

Delft University of Technology

Prof. Dr. ir. C. van Rhee
Professor of Dredging Engineering, Faculty CEG, Department HE / Faculty 3ME, Department MTT
c.vanrhee@tudelft.nl

Dr. ir. A.M. Talmon
Assistant professor Dredging Engineering, Faculty 3ME, Department MTT
a.m.talmon@tudelft.nl

Royal IHC | Technology

ir. E. de Hoog
PhD candidate transient slurry flows in pipelines, Faculty 3ME, Department MTT
Research Engineer - Dredging Technology, IHC | Technology
e.dehoog@royalihc.com

Preface

This thesis present my research regarding amplifying density waves due to the unbalance of erosion and sedimentation at high concentrations. Moreover, it is the end of my time as a student at the TU Delft, on which I can look back with great pleasure. Coming to this subject was not straight forward. During most of my high school period I wanted to become an architect. Only after visiting taster days I actually came to the conclusion that I preferred something with more technical substance. The next study in line was Civil Engineering. During my bachelor I became more and more interested in anything that involved water and less in the structural part of the curriculum. Hence, the choice for my master Hydraulic Engineering was obvious for me. During my master courses I found myself mostly interested in the courses that involved anything with offshore and dredging applications. So, eventually I decided that the dredging section within Hydraulic Engineering was the best choice for me to finish my Master's degree with. So, after contacting Cees van Rhee for any Thesis subjects, he introduced me to Edwin de Hoog who is working on his PhD in transient slurry flow phenomena. Edwin was still looking for a student to help him explain the density waves he saw during earlier experiments in 2018. Which I was happy to help him with.

Therefore, I would like to thank Edwin de Hoog for the necessary guidance throughout the whole process, the feedback he gave during the process and his enthusiasm whenever anything slurry flow related was discussed or shown. Moreover I want to thank Cees van Rhee and Arno Talmon for providing feedback on my report and help during the design and set up process of the dedicated flow loop.
The flow loop was build with the help of Andre van den Bosch, who I would like to thank for the drawings of the flow loop as well. Moreover, I want to thank Ed Stok for the installation of the measuring equipment and helping with the calibration thereof. Last, but certainly not least I would to thank Royal IHC foremost for the opportunity to graduate at a company during the COVID-19 pandemic, but also for the measurement equipment and the high speed camera I was able to use during the experiments.

Then I want to thank Syra, Felix, Hits, Daniel, Boaz, Rian, Tim, Mau, Seb and Kalk for the emotional support and the helpful distractions during my research. I would like to expressly thank my parents, sister and brother for the support they have given me throughout my student days. I would also like to thank Billy, Misha, Winkel, Vrinds and my friends from high school for all the good times, may there be many more. Some special thanks go out to Winkel for his help with the numerical model.

Ultimately, this thesis represent the end of my student life, in which I was able to travel to Chile to do a Multidisciplinary Project meet a lot of people and made a lot of friends. For now the time has come to end this all and start a new chapter in my life, in which I hopefully may work on hydraulic transport for the rest of my working days. Please enjoy reading this thesis!

Tjalie van der Voort
Delft, June 22, 2021

Table of Contents

Nomenclature

α	Calibration parameter in the van Rijn (2019) equation	[−]
β	Angle of the bed layer top in the 2LM in the pipeline cross-section	[rad]
β_s	Slope angle	[°]
ΔP	Pressure drop over a pipeline section	[Pa]
Δt	Difference between two time steps	[s]
Δy	height and width of a grid cell of the ERT	[m]
Δy_{bed}	Difference in bed height between two time steps	[m]
Δ	Friction parameter	[−]
Δ	Relative sediment density	[−]
$\frac{\partial \tilde{p}}{\partial x}$	Adjusted pressure loss	[Pa/m]
$\hat{w}$	Average vertical velocity due to the turbulent bursts	[m/s]
κ	Von Karman constant = 0.4	[−]
λ_b	Area of bursts per unit area of the bed	[−]
λ_f	Darcy-Weisbach friction coefficient	[−]
λ_s	Area of sweeps per unit area of the bed	[−]
C_D	Drag coefficient	[−]
μ_s	Coefficient of mechanical friction of solids against pipewall	[−]
ν	Kinematic viscosity	[m^2/s]
Φ_p	Non-dimensional pick-up rate	[−]
ϕ'_p	Adjusted non-dimensional pick-up rate of van Rhee (2010)	[−]
ψ	Grain shape factor ≈ 0.7 for real sand particles	[−]
ρ_f	Density of the carrier fluid	[kg/m^3]
ρ_i	In-situ density	[kg/m^3]
ρ_m	Density of the mixture	[kg/m^3]
ρ_s	Density of the solids	[kg/m^3]
ρ_w	Density of water	[kg/m^3]
σ_a	The extra stress necessary to accelerate sheared mass to flow velocity above the bed	[Pa]
τ_c	Critical bed shear stress	[N/m^2]
τ_1	Friction coefficient between fluid and pipe wall in the upper layer in the 2LM	[−]
$\tau_{2,f}$	Friction coefficient between fluid and pipe wall in the lower layer in the 2LM	[−]
$\tau_{2,s}$	Friction coefficient between solids and pipe wall in the lower layer in the 2LM	[−]
τ_2	Friction coefficient at the interface of the upper and lower layer in the 2LM	[−]
τ_{bed}	Bed shear stress	[Pa]
θ'	Bed related Shields parameter as defined by van Rijn, Bisschop, and van Rhee (2019)	[−]

θ_b	Shields parameter	[−]
θ_{cr}	Critical Shields parameter	[−]
θ'_{cr}	Altered critical Shields parameter as defined by van Rhee (2010)	[−]
φ	Angle of internal friction of the sediment	[°]
ξ	Slip ratio	[−]
ζ	Calibration parameter for the CCM in the exponential equation	[−]
ζ_2	Calibration parameter for the CCM in the Archie et al. (1942) equation	[−]
A	Coefficient = $1/(1-n_0) \approx 1.7$ for continuum	[−]
A	Cross-sectional area of the pipeline	[m^2]
A_1	Cross-sectional area of the upper layer in the 2LM in the pipeline	[m^2]
A_2	Cross-sectional area of the lower layer in the 2LM in the pipeline	[m^2]
A_b	Bed related cross-sectional area	[m^2]
B	Width of the cross-section	[m]
C'	Bed related Chézy coefficient	[$\sqrt{m}/s$]
c_f	Friction coefficient for the bed	[−]
C_v	Volumetric concentration of the slurry	[−]
c_{1992}	Depth-averaged concentration above the bed	[−]
C_1	Mean concentration of the upper layer in the 2LM in the pipeline cross-section	[−]
C_2	Mean concentration of the lower layer in the 2LM in the pipeline cross-section	[−]
c_{crit}	Critical value in the concentration profile to determine the bed height	[−]
c_{nb}	Near bed concentration	[−]
C_{vd}	Delivered volumetric concentration	[−]
C_{vi}	Spatial volumetric concentration	[−]
c_v	Volumetric concentration of the mixture	[−]
d	Grain size	[m]
D_*	Dimensionless grain size parameter	[−]
D_h	Bed related hydraulic diameter	[m]
D_h	Hydraulic diameter above the bed	[m]
D_{10}	Grain size at which 10% of the grains is smaller	[m]
D_{15}	Grain size at which 15% of the grains is smaller	[m]
D_{50}	Average grain size diameter	[m]
D_{60}	Grain size at which 60% of the grains is smaller	[m]
D_{90}	Grain size at which 90% of the grains is smaller	[m]
D_{inner}	The inner diameter of a pipeline	[m]
D_{pipe}	The diameter of the pipe	[m]
E	Erosion flux	[$kg/m^2 \cdot s$]
f	Friction coefficient for the adjusted pressure loss estimation	[−]

f_0	Friction coefficient of the bed	[−]
f_b	Darcy-Weisbach bed friction coefficient	[−]
f_D	Damping parameter in the van Rijn et al. (2019) pick-up function	[−]
g	Gravitational acceleration	[m/s^2]
h_f	Flow depth in the pipeline cross-section	[m]
h_s	Thickness of the sheared layer	[m]
i	Hydraulic gradient	[−]
i	Hydraulic gradient due to inward flow into the sand bed	[−]
k	Permeability	[m/s]
k_f	Conductivity of the carrier fluid	[μS/cm]
k_l	Permeability of sediment bed at minimum compaction	[m^2]
k_m	Conductivity of the mixture	[μS/cm]
k_s	bed roughness	[m]
k_{max}	Permeability at maximum porosity	[m/s]
L	Length of the pipeline section	[m]
M	Eroded mass in van Rijn (1984a) experiments	[kg]
m	Empirical exponent for the hindered settling according to Richardson and Zaki (1954)	[−]
m_s	Mass of the sediment	[g]
N_γ	Bearing capacity factor	[−]
n_i	In-situ porosity of the bed	[−]
n_l	Bed porosity, estimated as maximum porosity n_{max}	[−]
n_0	Bed porosity prior to erosion	[−]
n_{max}	Maximum porosity	[−]
n_{min}	Minimum porosity	[−]
O_1	Circumference of the lower layer in the 2LM in the pipeline cross-section	[m]
O_2	Circumference of the upper layer in the 2LM in the pipeline cross-section	[m]
O_{12}	Length of the interface between the upper and lower layer in the 2LM in the pipeline cross-section	[m]
p'	Turbulent wall stress	[Pa]
Q_m	Flow rate of mixture	[m^3/s]
Q_s	Flow rate of solids in mixture	[m^3/s]
R_p	Particle Reynolds number calculated as: $\frac{d\sqrt{\Delta g d}}{\nu}$	[−]
Re	Reynolds number	[−]
Re_p	Particle Reynolds number	[−]
S	Sedimentation flux	[kg/m$^2 \cdot$ s]
S_f	Specific density of the fluid	[−]
S_s	Specific density of the solids	[−]

T	Dimensionless transport parameter	[−]
T_B	Time scale of turbulent bursts	[s]
u	Flow velocity	[m/s]
u_*	Bed-shear velocity	[m/s]
u_2	Mean flow velocity above the bed layer	[m/s]
U_f	Volume of the carrier fluid	[m^3]
U_m	Volume of the mixture	[m^3]
U_s	Volume of the solids	[m^3]
$u_{*,c}$	Critical bed shear velocity according to Shields (1936)	[m/s]
v_e	Erosion velocity	[m/s]
V_f	The flow velocity of the carrier fluid	[m/s]
V_m	Mixture velocity	[m/s]
V_1	Mean flow velocity of the upper layer in the 2LM in the pipeline cross-section	[m/s]
V_2	Mean flow velocity of the lower layer in the 2LM in the pipeline cross-section	[m/s]
V_{crit}	Critical velocity	[m/s]
V_{dl}	Deposit limit velocity	[m/s]
V_{min}	Minimum velocity	[m/s]
v_{sed}	Sedimentation velocity	[m/s]
v_{sl}	Slip velocity	[m/s]
V_{sm}	Maximum velocity at the limit of stationary deposition	[m/s]
w_0	Terminal settling velocity	[m/s]
w_s	Hindered settling velocity	[m/s]
y_{bed}	Height of the sand bed in the pipeline	[m]
z	height at velocity u(z)	[m]
z_0	level at which the velocity is equal to zero	[m]
s	Specific grain density	[−]

Abstract

Royal IHC, as an equipment manufacturer, is one of the companies interested in exploring the possibilities of deep sea mining. However, before they can venture towards the deep sea, a lot of research required. This to ensure the safe transport of the nodules towards the surface. Due to the long distance, density variations within the slurry can be expected as these are introduced at the input side of the pipeline system. These variations can amplify and when they grow too large they can cause system blockages or pump drive failure (de Hoog, Talmon, & van Rhee, 2021). The causes of amplifying density have to be explored further to make deep sea mining as an operation economically attractive.

Density wave amplification was researched in the 1990's and 2000's, with the focus on long distance horizontal pipeline transport. Initially the cause of the amplifying density waves was attributed to a relation between slip and density. However, later research drew up the conclusion that the cause was to be found in the unbalance between erosion and sedimentation at high concentrations. Although, more recent research in inclined and vertical pipeline systems shows a different density wave amplification mechanism.

In this thesis it is investigated whether an unbalance between erosion and sedimentation at high concentration, causes density wave amplification. Furthermore, it is determined whether the erosion process in a pipeline can be modelled numerically as a 2LM based on the sedimentation-erosion balance using different pick-up functions for the erosion flux. An experimental study is done to research the unbalance between erosion and sedimentation at high concentrations. To assess the influence of of the mean grain size and the mixture concentration on the sedimentation and erosion unbalance, several sand types (Dorsilit nr.5G, Dorsilit nr.7, Dorsilit nr.8, Zilverzand and GEBA) and volumetric concentrations (5, 10, 20 and 30%), respectively, are used during the experiments.

For the experimental study a dedicated flow loop is build. The flow loop consists out of a main loop, in which the measurement section is located, and a bypass loop. These loops are connected with two gate valves.
Using a Electrical Resistance Tomography (ERT) system both the bed height evolution and the near bed concentration are determined. Moreover, a flow meter measures the mean flow velocity in the loop during the experiments and Conductance Concentration Meters (CCM) are placed in front and behind the measurement section to evaluate the transformation of the density wave. Within the bypass loop a mixture can be prepared to the desired volumetric concentration. At the same time a stationary bed is deposited in the measurement section. By opening the gate valves the prepared mixture is send over the stationary bed, leading to a process where sedimentation and erosion occur simultaneously.

The coarser sand types (Dorsilit) were transported as sheet flow and the ERT measurements showed sudden increases of the bed height. After complementary inspection of the high speed camera footage these could be attributed to the caterpillar-like behaviour of a shocking and sliding bed, as similarly described by Matoušek and Krupička (2013). This caterpillar-like movement of the stationary bed is associated to the sedimentation and erosion unbalance by de Hoog et al. (2021). From the experiments it can be concluded that the influence of the mean grain size diameter on the transport capacity of the flow is shown in the ability to form amplifying density waves in the horizontal measurement section. These density waves were present for the coarser sand types. Furthermore, the results show an initial growth of the bed at high mixture concentrations even though the flow velocity signal showed a steep drop. Shortly after the initial sedimentation, the erosion took over and caused a sharp decrease in the bed height. This confirms the erosion and sedimentation unbalance at high concentrations. It was found that the higher concentrations lead to erosion, while at low concentrations the particles within the mixture have a tendency to settle. The sudden increases of the bed height are found to a greater extent with increasing mixture concentration. Dorsilit nr.7 seems to be most susceptible to these shocking and sliding movements of the bed as the most amount of peaks in bed height are found for this sand type.

A numerical model based on the outcomes of the measurements and the sedimentation and erosion unbalance in a control volume around the bed interface is build to simulate the experiments. Subsequently, several erosion functions are implemented to investigate the applicability of these functions to experiments.
The pick-up function of Bisschop (2018) is found to be the best fit for Dorsilit nr.5G, Dorsilit nr.8 and for Dorslit nr.7 for the higher mixture concentrations. Furthermore, the pick-up function of Bisschop (2018) was

found to generally resemble the trend of most sand types with sufficient accuracy. However, some other erosion functions were found to fit the results of specific experiments even better. The pick-up function of van Rhee (2010) shows good results for the experiments with Dorsilit nr.7 and concentrations up to 10% and Dorsilit nr.8. The finer sand type Zilverzand showed good resemblance with the pick-up functions of Bisschop (2018); van Rhee (2010) and van Rhee and Talmon (2010). Lastly, based on the measurements of GEBA, it appeared that the van Rijn (1984a) equation was able to adequately simulate the bed height evolution. However, for higher concentrations (20 and 30%) the pick-up functions of van Rhee (2010) or Bisschop (2018) were much more in correspondence with the measurements.

Concluding, it is found that at higher concentrations the caterpillar-like movement of the bed is observed more frequently. Since these movements are attributed by de Hoog et al. (2021) to the erosion and sedimentation unbalance at high concentrations it is deemed proven that density wave amplification at high concentration is caused by an unbalance in erosion and sedimentation. Furthermore, if the right pick-up function is chosen the conditions measured during the experiments can be simulated with sufficient accuracy with the developed numerical model based on a 2LM that applies the sedimentation and erosion unbalance.

1

Introduction

Hydraulic transport has been part of dredging operations for a very long time. In deep sea mining this method of transport has been an idea for quite some time as well, as it is an efficient way to convey material towards the surface. The principle is that via a crawler the ore is mined and subsequently the material is pumped through a pipeline system up to the surface. At the surface a production support vessel processes the ore and it is transferred to a carrier vessel bringing the post-processed materials to shore. The principle of the subsea part of deep sea mining is shown in figure 1.1.

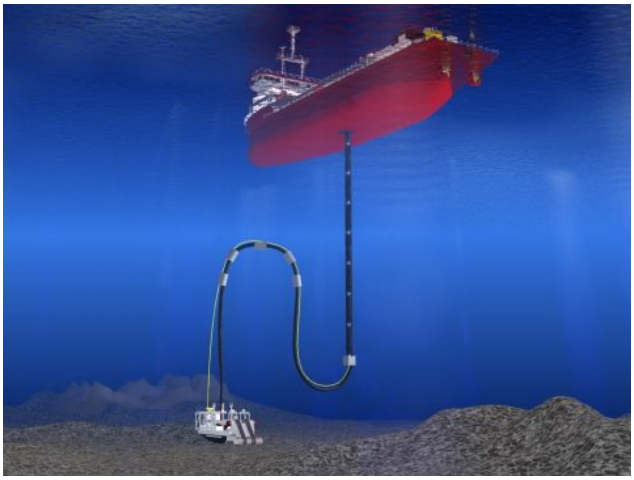

Figure 1.1: Principle of deepsea mining with hydraulic transport consisting of a crawler, riser pipeline system and centrifugal pumps, retrieved from Buitendijk (2020)

1.1 Background Information

Deep sea mining has been a subject for exploitation for many years, with an initial spike from 1972 to 1982 (Glasby, 2000). Recently the interest in venturing towards the depths of the sea has been growing again. Mostly due to the high demand for metallic compounds expected in the future, meaning that this journey might be an interesting business opportunity for mining companies. For now the exact environmental impacts are not known and policies for this industry are only in the developing stage (Halfar & Fujita, 2007; Hoagland et al., 2010; Wedding et al., 2015). Meaning that at this moment it is only allowed to enter an exploration contract of 15 years to mine these compounds (International Seabed Authority, 2013).

In manganese nodules minor components of non-ferrous material such as nickel, copper, cobalt, molybdenum and possibly manganese can be found (Blöthe et al., 2015; Hein, Koschinsky, & Kuhn, 2020; Monhemius, 1980). These materials are becoming an even more necessary resource in the future industrial production (Steele, Thorpe, & Turekian, 2009). The nodules are found on the seabed and are often surrounded by a thick layer of marine snow (Bischoff & Piper, 1979). This marine snow is easily picked up during the mining process and

consists of very fine material. This together with the nodules makes it a very interesting mixture for hydraulic transport when collected. Foremost, because of the small grain size of the marine snow and the much larger size of the nodules. The nodules have a potato-like form and fall within the size range of 4 to 10 cm (K. A. Miller, Thompson, Johnston, & Santillo, 2018). This transport therefore has some analogies with fine sediments mixed with coarse grains in a pipeline. These kinds of transports often lead to a fully stratified flow regime within the pipeline as the coarse grains are more sensitive to gravity and can thus form a sliding bed or sheet flow layer (Matoušek & Krupička, 2011; Vlasák, Chára, Krupička, & Konfršt, 2014; Wilson, Addie, Sellgren, & Clift, 2006).

Royal IHC is one of the companies interested in exploring the possibilities of deep sea mining. However, before they can venture towards the deep sea, a lot of research is needed first. This to ensure the safe transport of the nodules towards the surface. Due to the long distance, density variations within the slurry can be expected as these are introduced at the input side of the pipeline system. If these variations grow too large, they can cause system blockages as well as pump drive failure (de Hoog et al., 2021). These unknowns have to be explored first to make the exploitation of manganese nodules economically attractive. For Royal IHC, as a manufacturer, this means that a lot of research is required to develop adequate equipment to be able to sell this to operating companies.

1.2 Problem Definition

The phenomena of density waves in specifically horizontal slurry pipelines have been observed as early as in 1981. During the construction of the Prins Clausplein, a highway intersection in the Netherlands, several density fluctuations in the pipeline conveying sand were observed. The material was pumped from the mining site towards the building site 10 km away, showed a density wave within the system (Matoušek, 1995). These density waves appeared to be self-amplifying, therefore Matoušek (1995, 1996b) first hypothesised that material aggregation in density waves was caused by the variable particle slip due to the variation of the cross-sectional velocity distribution with the passage of density waves. However, Talmon (1999) did a linear stability analysis and came to the conclusion that a sedimentation and erosion unbalance at high mixture concentrations was most likely the cause of the amplification of the density waves. For this to be true the slurry concentration has to be high. In the cases of Talmon (1999) and Matoušek (1995, 1996b) it was found that the density waves were only present when the mixture velocity was approximately at the deposit limit velocity. Because around these velocities a stationary bed can be formed temporary, which increases the density of the flow once the deposits are entrained within the flow again.

Though with later research, conducted by de Hoog, in 't Veld, van Wijk, and Talmon (2017); de Hoog et al. (2021), it was shown that for coarse slurry flow in inclined and vertical transport a self-amplifying density wave is present for cases where the mixture velocity was far above the deposit limit velocity. Meaning that the limits of the transport capacity of a vertical pipeline system, such as for deep-sea mining, further decreases. Therefore de Hoog et al. (2021) hypothesised that different processes must be responsible for the occurrence thereof. de Hoog et al. (2021) reasoned that while a centrifugal pump may introduce a density wave within a system, due to acceleration of the mixture at increasing density, resultant of a higher pump pressure Wilson et al. (2006). However, this most likely is not the underlaying mechanism for the amplification of the density wave, but a transient material accumulation effect in horizontal components of a vertical transport transportation system is. This hypothesis forms the basis of the research subject for this thesis.

1.2.1 *Main Research Objective*

The above results in the following main objective:

"Investigate whether an unbalance between erosion and sedimentation at high concentration, causes density wave amplification and determine whether the erosion process in a pipeline can be modelled numerically as a 2LM based on the sedimentation-erosion balance using different pick-up functions for the erosion flux."

The objective regarding the unbalance between erosion and sedimentation at high concentration as an amplifying factor for density waves is assessed with a combination of an experimental study and numerical study. The latter consist of a sedimentation and erosion balance in a numerical model, in which the erosion flux is varied by using

different pick-up functions available in literature. The outcomes of the numerical simulation are then compared to measurements to verify the applicability of the pick-up functions.

1.2.2 *Scope of this thesis*

The scope of this thesis is defined as that this thesis is an experimental study into transient slurry flow phenomena. Physical processes regarding slurry transport are written in a program to model these processes. This regards the sediment transport capacity of highly concentrated slurry flows, such as in density waves. This is modelled using various pick-up functions and the hindered settling equation of Richardson and Zaki (1954).

As this study concerns transient slurry flow, actual steady state slurry flow phenomena are out of the scope. It is expected that a steady state will never be reached within the time scale of transient slurry flow effects. This due to the fact that a mixture is suddenly introduced, leading to a deceleration of the mean flow velocity in the system. The mixture is not able to fill the complete loop, mostly due to the open loop design.
In closed loops so-called closed loop phenomena may occur, i.e. growing density waves due to the influence of the pump, therefore it is opted for an open loop design to negate these effects.

A small-scale loop is build, hence scaling dimensionless numbers have to be accounted for in order to relate the tests to real life scenarios for deep sea mining operations or pipeline slurry transport in dredging operations.

This study is mostly interested in the general physical processes regarding the erosion capacity of highly concentrated slurry flows on a stationary bed. Therefore, very coarse gravels, able to resemble poly-metallic nodules, are excluded in the experiments.

To resemble the hypothesised mismatch in transport capacity it is opted for a horizontal measurement part behind a vertical section in the loop design. This is able to resemble the transition between the vertical transport system and the horizontal processing part in the deep-sea mining operations.

1.2.3 *Research questions*

To support the previous mentioned objective additional questions are drawn up. These sub-questions contribute to the assessment of the main research objective.

Theory

- What are the current described hypothesis in the literature for density wave amplification?
- What are the main differences between the various chosen pick-up functions?

Experimental Study

- What is the influence of the mean grain size diameter on the transport capacity of the slurry in the pipeline system?
- What is the influence of the mixture concentration on the transport capacity of the slurry?
- What are the limitations of the experimental study?

Physical Modelling

- How can the erosion due to a density wave be modelled using an erosion and sedimentation balance in a two layer model structure?
- Which pick-up function agrees best with the experimental results?

1.3 Reading Guide

This thesis is split up in four main parts, where Part 1, Literature review, contains an analysis of the available literature. Within this part, the basics of slurry flow and the intro to a two-layer model are elaborated in chapter 3. Thereafter, a historical review of the available research regarding the origins and development of amplifying density waves is conducted in chapter 4. Subsequently, the sedimentation and erosion unbalance is elaborated in chapter 5. These topics form the theoretical basis on which this thesis is build.

In Part II, Experimental Study, the experimental setup, with all the measurement equipment and how this equipment is used is explained in chapter 6. Based on these measurements, the post-processing of the data is explained in chapter 7. Moreover, the conclusions regarding the influences of the mean grain size diameter and concentration based on the measurements and post-processed data are drawn as well in this chapter.
Part III, Physical modelling, the sedimentation and erosion unbalance model using a two-layer model is explained in detail. In chapter 8 the schematisation and computational setup of the model are explained at first. Consequently, the mathematical implementation of the pick-up fluxes as described in chapter 5 in the two layered sedimentation and erosion unbalance model is elaborated in detail in this chapter as well. Part IV, Conclusions, presents the conclusion, and the recommendations of this thesis. The appendices form Part V and contain all the available data used for this thesis as well as the results of all of the simulations conducted with the different pick-up flux models.

2

Methodology

In this chapter the basis for the methodology is explained, which is used to achieve the progress and knowledge to find sufficient information to answer the questions posed in the research question section. This methodology follows a framework where, based on the current knowledge found in e.g. literature and books, a foundation is build to be able to dive deeper into the unknown processes regarding the origin of a self-amplifying density wave in a pipeline system.

2.1 Slurry Flow and Pick-up flux Theory

Using the theory available for hydraulic slurry transport the principles thereof are explained with a focus on the stratified slurry flow regimes. This demarcation is made because the mixture of manganese nodules with marine snow resembles a mixture of sand and gravel, which can be considered as a coarse slurry flow. A coarse slurry flow is characterised by a highly stratified character, either with a stationary or sliding bed and a homogeneous mixture flow above the bed. After summarising the basic principles of slurry flow the improved Two-layer model (2LM) of Wilson (1992) is explained and it will be elaborated why it is used to model the density waves.

After the principles of the slurry flow have been assessed and the introduction into the 2LM is made, the historical observations of density waves in past projects is explained. First, the explanation of Matoušek (1995, 1996a, 1996b) on the extensive amount of data measured for the construction of the Prins Clausplein intersection is summarised to give an introduction into the alleged physical processes that lead to a density wave in long distance pipeline systems. Secondly, the findings of Talmon (1999, 2002); Talmon, Aanen, and Bakker-Vos (2007) are explained since he came to new conclusions about the origin and physical processes to why certain density waves are self-amplifying. Subsequently a brief explanation on the findings of Miedema, Zhihua, and Matousek (2003) as they applied a numerical method to model concentration fluctuations in a two dimensional space for the Two-Layer model. The latest findings of de Hoog (2016); de Hoog et al. (2017, 2021) are explained at last. From these historical findings the unknown processes become clear, to which an experimental set-up can be designed to test the hypothesis mentioned in section 1.2.

To assess the influence of the sedimentation and erosion balance basic knowledge is required regarding the different pick-up functions, sedimentation flux, settling velocities and erosion regimes. Using the research of van Rhee (2010); van Rijn (1984a) and Bisschop (2018), among others, a clear overview is made for which erosion regimes the pick-up functions have been developed.

2.2 Experimental Study

To test the hypothesis that a transient accumulation effect (de Hoog et al., 2021) is the reason that a density wave is self-exciting, a dedicated flow loop is build. Using an experimental setup makes it possible to observe and measure the physical processes quite accurately, while difficulties such as long computation times, extensive calibration and uncertainties of a large-scale numerical method are not present. To simulate a density wave a mixture is prepared to the desired concentration and when mixed almost homogeneously send through the measurement section. Note should be made that with the use of a physical model, scale effects do occur.

Variations in slurry concentration before and after the measurement section are measured using two Conductance Concentration Meters (CCM). To be able to measure the bed height and stratification an Electrical Resistance Tomograph (ERT) system is used. Besides the mean concentration, the mean flow velocity and pressure gradient are measured as well. Velocity measurements are needed to determine the operational limits and form the input for the physical modelling part as well. The pressure gradient is measured to be able to determine the bed shear stress, which is required for the physical modelling part. However, it should be noted that the study is foremost for transient slurry phenomena. Therefore, these pressure measurement may contain a high degree of uncertainty as the measurement may include e.g. the pressure difference due to the acceleration of the flow. Moreover, these pressure measurements have a better relation to the shear stresses in steady state flow.

2.3 Interpretations of the Experimental Study

Based on the measurements done in the various experiments the interpretations and conclusions are drawn. This is done using the built theoretical framework and applying the theories to the results of the measurements. Then further processing of the measurements results in velocity signals, concentration profiles, near bed concentrations and bed heights. These are used as input for the physical modelling part of the thesis. For the interpretations multiple programs and programming languages are used. The data is acquired via three separate systems, one system is used for the CCM's, differential pressure transducers and flow meter. The second system is used to log the data acquired with the ERT. The third system is used for acquiring the footage of the high-speed camera.

2.4 Physical Modelling of a Sedimentation and Erosion unbalance

Using the conclusions of the results of the measurements a feedback link can be made towards the theoretical framework, thus acknowledging the shortcomings and limits of the experimental set-up.

By implementation of the results of the measurements the unbalance between sedimentation and erosion is explored. The erosion flux is computed using different functions available in the literature. Furthermore, only one grid cell is used to simulate the bed height evolution, using the sedimentation and erosion balance at the location of the plane of the ERT. Using the near bed concentration measured with the ERT and the flow velocity as forcings for the model the bed height evolution is simulated. The calculated bed height from the numerical model is then compared to the measurements from the ERT to validate the applicability of each pick-up function to the experiments.

1

Literature Review

3

Basic Principles of Slurry Flow in Pipelines

In this chapter the principles of slurry flow for different kind of mixtures are elaborated. First some important definitions are given that will be used throughout this thesis. Subsequently, the actual principles for horizontal slurry flow are explained for the different flow regimes. Then the step toward inclined and vertical flow is made, reflecting on the differences and similarities with horizontal flow. Eventually an introduction to the Two-Layer Model is made to explain the principles thereof and explain why it is used for modelling a density wave.

3.1 Definitions for Transition Velocities and Important Parameters

The definitions used for the typical velocities in slurry flow are given below:

Hindered Settling Velocity (w_s)
In highly concentrated mixtures, such as in slurry pipeline flow, the sediment that is subject to the settling process settles significantly slower than a single particle in a fluid. This phenomena is called hindered settling and is of significant importance to the erosion and sedimentation flux in slurry pipeline flow. The hindered settling is due to the flow upwards of liquid as it is displaced by the particles moving down, the liquid exerts increased drag on particles next to each other, thus reducing the settling velocity (Matoušek, 2004). Yet, in case of very low concentrations the settling velocity will actually increase as the particles are able to settle within each others shadow (Miedema, 2016). Richardson and Zaki (1954) derived an equation to determine the influence of the concentration on the settling velocity. The equation of Richardson and Zaki (1954) is given in equation 3.1.

$$w_s = w_0 \left(1 - c_{nb}\right)^m \tag{3.1}$$

Where, w_0 is the terminal settling velocity of the particle, c_{nb} the near bed concentration and the exponent m can be calculated based on the particle Reynolds number. The latter can be determined with $\mathbf{Re}_\mathrm{p} = \frac{w_0 d}{\nu}$. For the exponent m Richardson and Zaki (1954) found the following values:

$$\mathbf{Re}_\mathrm{p} < 0.2 \qquad m = 4.65 \tag{3.2}$$
$$\mathbf{Re}_\mathrm{p} > 0.2 \wedge \mathbf{Re}_\mathrm{p} < 1 \qquad m = 4.35 \cdot \mathbf{Re}_\mathrm{p}^{-0.03} \tag{3.3}$$
$$\mathbf{Re}_\mathrm{p} > 1.0 \wedge \mathbf{Re}_\mathrm{p} < 200 \qquad m = 4.45 \cdot \mathbf{Re}_\mathrm{p}^{-0.1} \tag{3.4}$$
$$\mathbf{Re}_\mathrm{p} > 200 \qquad m = 2.39 \tag{3.5}$$
$$\tag{3.6}$$

This function unfortunately does not result in a smooth continuous curve. Rowe (1987) tried to improve the function for the exponent m and was able find with an equation that was in the order of the original curve of Richardson and Zaki (1954). The resulting equation is given in equation 3.7.

$$m = \frac{4.7 + 0.41\mathbf{Re}_p^{0.75}}{1 + 0.175\mathbf{Re}_p^{0.75}} \tag{3.7}$$

The equation of Rowe (1987) is used in this thesis for the calculations of the exponent of the hindered settling equation as it provides an simple continuous functions that can be used for all particle Reynolds numbers.

Mixture velocity (V_m)
The mixture velocity is defined as the velocity of the flow as a whole, it includes the solids and fluid fraction. Mathematically it is equal to the sum of the solids flow rate and the fluid flow rate divided by the cross-sectional area, see equation 3.22.

Deposit limit velocity (V_{dl})
In literature several different definitions are given for the deposit limit velocity. For this thesis when speaking of the Deposit limit velocity it is meant that when the flow rate reaches below a certain value a stationary deposit will form. Slurry flow beyond the deposition limit is free of a stationary deposit (Matoušek, 2004). According to Miedema (2016) this is defined as the Limit of Stationary Deposit Velocity (LSDV).

Critical velocity (V_{crit})
The minimum velocity at which no solids form a bed at the bottom of the pipeline as given by Kökpınar and Göğüş (2001); Oroskar and Turian (1980); Turian, Hsu, and Ma (1987). All the solids are thus suspended at this velocity. In the book of Miedema (2016) this is defined as the Limit Deposit velocity. van den Berg (1998) defined this velocity as the minimum velocity when the transition between a fully suspended heterogeneous flow regime and a flow with the first solids settling to the bottom occurs. The critical velocity was considered the minimum velocity to ensure a safe and economic operation of the pipeline system.

Minimum velocity (V_{min})
The minimum velocity is defining the flow rate for which the least energy is dissipated. This flow velocity is most energy efficient for a slurry at a given slurry density. However, this velocity is not considered a suitable operation velocity in a pipeline system. This is due to the fact that interaction between the pipeline and a pump the value of V_m is bigger than V_{min} to prevent unstable flow regimes (Matoušek, 2004).

Maximum velocity at the limit of stationary deposition in Wilson model (V_{sm})
V_{sm} is defined by Wilson (1979) as the maximum value for the deposit limit velocity for different solid concentrations in the slurry flow. It can either be determined using the demi-McDonald nomographic chart or by its' empirical approximation, see equation 3.8 (Matoušek, 2004).

$$V_{sm} = \frac{8.8\left[\frac{\mu_s(S_s-S_f)}{0.66}\right]^{0.55} D_{pipe}^{0.7} D_{50}^{1.75}}{D_{50}^2 + 0.11 D_{pipe}^{0.7}} \tag{3.8}$$

In which, μ_s is the coefficient of mechanical friction and assumed to have a value of 0.45, S_s is the relative density of sand, S_f is the relative density of the fluid, D_{pipe} is the pipeline diameter in [m] and D_{50} is the mass median grain size diameter in [mm].

Slip ratio (ξ) and Slip Factor ($1-\xi$)
The slip ratio is based on the slip velocity (v_{sl}), which is defined as the difference in velocity of the solids and the fluid mixture (Miedema, 2015; Vlasák, Chára, Konfršt, & Kysela, 2017) The slip ratio is defined by Miedema (2015, 2016) as given in equation 3.9. This is the ratio of the solids velocity over the mixture velocity. The slip ratio can also be considered as a parameter capable of describing a mechanism of material aggregation in a long pipeline (Matoušek, 1995). Another ratio to be used for the slip ratio is the delivered concentration over the average concentration of solids in a pipeline (van Grunsven & Talmon, 2012).

$$\xi = \frac{v_s}{V_m} = \frac{C_{vd}}{C_{vi}} \tag{3.9}$$

3.2 Slurry Flow Principles

Hydraulic transport can come in many forms. In this section the principles of horizontal coarse slurry flow are explained. The previous mentioned definitions form a support for the different processes that are present in slurry flow.

A slurry can be defined as a two-phase mixture. In a pipeline this flow is governed by the physical laws of conservation of mass, energy and momentum. In this two-phase mixture there is the carrier fluid and the solids,

meaning that inside the pipe the mass of the mixture equals the mass of the liquid added with the mass of the solids (equation 3.10) (Matoušek, 2004).

$$\rho_m U_m = \rho_f U_f + \rho_s U_s \tag{3.10}$$

In the above equation U is the volume of the material and ρ_f the density, the subtext f regards the carrier fluid and s the solids. When speaking of the concentration in the slurry there are different definitions as well. The volumetric concentration (C_v) is defined as U_s/U_m. Using $U_m = U_f + U_s$ equation 3.10 now becomes:

$$\rho_m U_m = \rho_f (U_m - U_s) + \rho_s U_s$$

If one thereafter divides the above equation by U_m and rewrites the expression of C_v for U_s, implements it in the equation one can find the following:

$$\rho_m = \rho_f (1 - C_v) + \rho_s C_v$$

Subsequently rearranging leads to the equation for the volumetric concentration and is given as in equation 3.11. The spatial volumetric concentration represents the fraction of solids present in the pipeline. (Matoušek, 2004).

$$\boxed{C_v = \frac{\rho_m - \rho_f}{\rho_s - \rho_f} = \frac{U_s}{U_m}} \tag{3.11}$$

Due to the fact that the mixture is flowing the physical meaning of the concentration of the solids requires further specification. The volume fraction can be measured at different locations, in a horizontal section of a pipeline and at the outlet of the pipeline. The difference in these two measurements require two distinct volumetric concentrations. The *spatial volumetric concentration* (C_{vi}) and the *delivered volumetric concentration* (C_{vd}). The latter is defined as given in equation 3.12. The delivered volumetric concentration represents the fraction of solids that is delivered from a pipeline (Matoušek, 2004).

$$\boxed{C_{vd} = \frac{Q_s}{Q_m}} \tag{3.12}$$

In which Q_s is defined as the flow rate of the solid and Q_m the flow rate of the mixture.

In the case of flow through pipe segments the flow experiences friction. This is the case for liquid flow and even more for slurry flows. This friction or flow resistance is defined as the amount of mechanical energy that is dissipated in a pipeline. When one applies the Bernoulli equation for two arbitrary points in the segment it can be found that steady slurry flow is characterised by the pressure difference along a horizontal pipeline section of which the diameter is constant (Matoušek, 2004; Miedema, 2016). This pressure difference (ΔP can be divided over the length of the segment to find the pressure gradient ($\frac{\Delta P}{L}$). The head that is lost due to friction per length of pipeline segment is known as the *hydraulic gradient* (I) and is a frequently used term in slurry transport. The hydraulic gradient is dimensionless and is defined as given in equation 3.13.

$$\boxed{I = \frac{\Delta P}{\rho_f g L}} \tag{3.13}$$

When assessing flow through a pipeline consisting only of water the hydraulic gradient can be computed using the equation of Darcy-Weisbach (equation 3.14). However when assessing slurry flow the so-called solids effect needs to be accounted for. This solids effect is defined as the difference between the the mixture pressure gradient and the pressure gradient of the carrier fluid only. This may also be called the excess pressure gradient (Wilson et al., 2006).

$$\Delta P = \frac{\lambda_f}{D} \frac{\rho_f V_f^2}{2} L \tag{3.14}$$

In which λ_f is known as the Darcy-Weisbach friction coefficient, ρ_f is the density of the carrier fluid, D is the diameter of the pipe, V_f the flow velocity of the carrier fluid and L the length of the pipeline section.

Therefore to assess this solids effect, empirical correlations were developed , among others, by Durand and Condolios (1952); Führböter (1961); Jufin and Lopatin (1966); Newitt (1955); Wilson (1976). Each of these are applicable to various types of slurry flow, though note that each of these relations have their own validity range and shortcomings as they have been determined empirically.

3.2.1 *Slurry Flow Regimes*

When talking about flow by a carrying liquid it can either be characterised as turbulent or laminar. Laminar flow occurs at low velocities, characterised by a Reynolds number with a maximum value of 2300 (Matoušek, 2004). In dredging and deep sea mining pipelines velocities will be quite high, therefore causing the flow to be turbulent. A turbulent flow creates eddies that causes solids to remain suspended, provided that the particles are small enough, and makes it possible to transfer mass and momentum within the slurry flow. In the case of slurry flow with coarser grains it is possible that the grains do not become suspended even for very high velocities (de Hoog et al., 2021).

In case of slurry flow several flow patterns can be clearly distinguished. The patterns as described by Matoušek (2004) are summarised below. Ramsdell and Miedema (2013) distinguished 9 patterns, however they made a further distinction for heterogeneous flow in case of no suspended material with the same type of stratification and are therefore deemed too specific for now.

I. Homogeneous flow of non-Newtonian mixtures

II. Pseudo-homogeneous flow of Newtonian mixtures

III. Slightly stratified heterogeneous flow

IV. Very stratified heterogeneous flow

V. Fully stratified flow with an eroded top of the bed

VI. Fully stratified flow

I. Homogeneous flow of non-Newtonian mixtures
Mixture characterised by a high concentration of fines, such as silt and/or clay particles. Also tailings and mineral concentrates can have this regime. The fines in the mixture give it the non-Newtonian properties (Talmon, 2019). In the pipeline a almost uniform concentration across the diameter is present. This flow regime will not be elaborated in a more detailed manner as density wave amplification is not expected for these very fine particles.

II. Pseudo-homogeneous flow of Newtonian mixtures
In the case of coarse silt or fine sand all material can become suspended. However, for the latter this would be at velocities far above the deposit limit velocity. In this flow regime the concentration profile over the cross-section is uniform.

III. Slightly stratified heterogeneous flow
Present in the case of medium or medium to coarse sand mixtures where a great portion of the material is suspended. A small fraction of the material moves within a moving granular bed. In this flow regime the mixture velocity is above the deposit limit velocity.

IV. Very stratified heterogeneous flow
The flow is characterised by a big fraction of the transported material within a granular bed and a small portion due to suspended material. This is for medium to coarse sand and the finer gravels. In cases of gravel the velocity of the mixture should be far above the deposit limit velocity.

V. Fully stratified flow with an eroded top of the bed
For mixtures containing fine to medium gravel material this is the dominant flow regime. In the flow a strong stratification is present where a small part of the material is transported via a shear movements or jumping and rolling. The major part of the material is moved in a sliding granular bed.

VI. Fully Stratified flow
Present in mixtures consisting of medium to coarse gravel or cobbles and boulders. In this flow regime the grains

are too heavy to be lifted by turbulent motion in the pipeline and can therefore only be transported via a sliding granular bed.

3.3 Vertical Slurry Flow

In case of deep sea mining, dredging and oil drilling operations it is not always the case that a system solely consists out of horizontal pipeline segments. In dredging operations the material needs to be transported from the seabed upwards, mostly via an inclined segment and in deep sea mining of poly-metallic nodules the use of vertical pipelines is used to bridge the extreme depths towards the surface.

3.3.1 *Differences with Horizontal Flow*

Due to the fact that the flow is now differently orientated it actually leads to different processes within the pipeline that may lead to different flow regime as well. Newitt, Richardson, and Gliddon (1961) observed in vertical oriented pipeline flow of coarser particles, but smaller than 1 mm, that the slurry behaved as a conveying liquid, with practically no solids effect on the flow friction. For fine slurries they observed that the flow behaved like equivalent liquid flow.
Dependent on the hindered settling velocity of the particles and the flow velocity, the mixture can be characterised as a plug flow or as a homogeneously fluidised mixture flow van Wijk, Talmon, and van Rhee (2016). This difference in flow regime, going from heterogeneous to homogeneous, logically results in different resistance of the mixture along the pipeline.

3.3.2 *Typical Concentration Distribution*

In the case of vertical slurry flow, considering a particle near the pipeline wall. The particle is affected by the pipeline wall due to the steep velocity gradient. This causes a force which tends the particle to rotate and move towards the axis of the pipe cross-section (Miedema, 2016). This is caused by both the force due to the velocity gradient (the Saffman lift force) and the Magnus lift, where the latter is caused by the rotation of the particle. Both these forcec push the particles away from the pipe wall, hence leading to a particle poor or even particle free viscous sub layer. These affects contribute to a higher concentration of solids along the pipeline axis. Matoušek (2009); Wilson and Sellgren (2003); Wilson, Sellgren, and Addie (2000) found that for particles in the range of 0.08 to 0.4 mm the particles are driven away from the wall due to hydrodynamic lift force. Moreover, as proven by Talmon (2013), a watery layer that is present along the pipe wall ensures the inability of particles to fit within the viscous sub layer at similar concentrations as that of in the main flow.

3.4 Introduction to The Two-Layer Model

For the physical modelling part of this thesis a Two-Layer Model (2LM) is used to model the erosion rate and bed height evolution in the horizontal pipeline segment. Therefore the basis and geometry of the 2LM using knowledge of Wilson (1976) and later modifications of Wilson, Addie, Sellgren, and Clift (1992) are elaborated in this section to provide the necessary theoretical foundation.

3.4.1 *Principles of the Wilson et al. (1992) Model*

The model is founded on the assumption of two physical mechanisms for sediment transport (Matoušek, 2004), either by interparticle contact or by suspension in a carrier liquid. Bagnold (1956) stated that suspended particles directly transfer their submerged weight on to the carrier fluid, while for non-suspended particles the suspended weight is transferred via interparticle contacts on to the pipeline wall. In the 2LM there is a bed layer present, which can either be moving or stationary, this bed has a delivered concentration of approximately a loosely poured bed (if the flow is fully-stratified). Above this bed there is a clear water flow in case of the fully-stratified case or a suspended slurry flow in case of heterogeneous flow. A schematisation of the Two-Layer model is shown in figure 3.1. In this schematisation the stratification is clearly visible. The 2LM uses the real slurry stratification, with the concentration distribution over the cross-section, and transforms this profile into a simplified model with two layers (Matoušek, 2004).

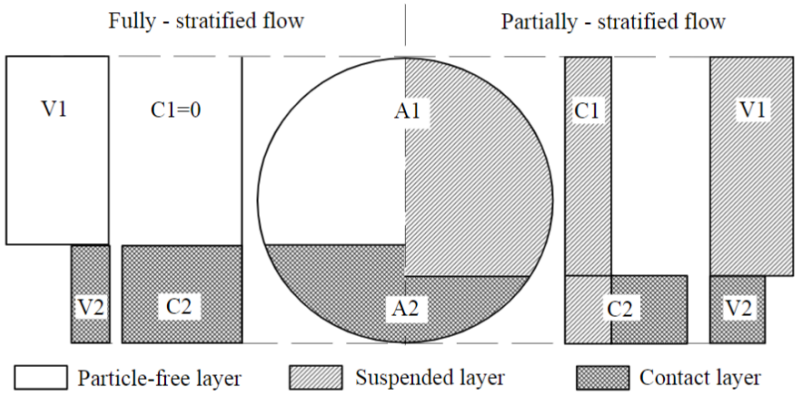

Figure 3.1: Principle of the 2LM with the modifications made by Wilson et al. (1992)

In the 2LM the behaviour of the flow is predominantly characterised by the force balance between driving and resisting forces in the flow in the two layers. The driving force being the pressure gradient due to a pump and the resisting force is represented by the shear stress which is exerted by flowing material at the flow boundary (Matoušek, 2004).

3.4.2 *Geometry of the Model*

For the 2LM some geometrical parameters are necessary to be defined beforehand in order to be able to accurately derive the necessary equations for solving the 2LM with a certain set of given parameters. The mathematical derivation of the 2LM is based on the conservation of mass and momentum within mixture flow. The control volume is defined as the section of a pipeline with length L along which the layer height is constant. In these layers the quantities are described by the mean values, as shown in figure 3.1.

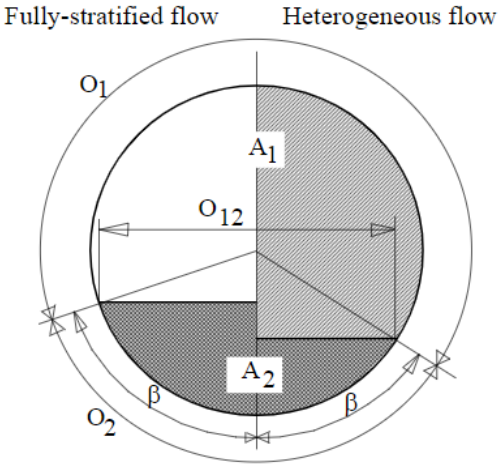

Figure 3.2: Geometry of the 2LM as developed by Wilson (1976)

The geometrical parameters of the 2LM are given in equations 3.15 to 3.21.

$$A = \frac{\pi}{4} D_{pipe}^2 \tag{3.15}$$

$$A_2 = \frac{1}{4} D_{pipe}^2 \left(\beta - \sin\beta \cos\beta\right) \tag{3.16}$$

$$A_1 = A - A_2 \tag{3.17}$$

$$y_{bed} = \frac{D_{pipe}}{2} \left(1 - \cos\beta\right) \tag{3.18}$$

$$O_1 = (\pi - \beta) D_{pipe} \tag{3.19}$$

$$O_2 = D_{pipe}\beta \tag{3.20}$$

$$O_{12} = D_{pipe} \sin\beta \tag{3.21}$$

3.4.3 *Conservation of Mass in the 2LM*

By using the conservation of volume and the geometry from figure 3.1 and 3.2 this results in the equation for the slurry rate defined as in equation 3.22 (Matoušek, 2004).

$$\begin{aligned} Q_m &= Q_{m,1} + Q_{m,2} \\ \boxed{V_m A = V_1 A_1 + V_2 A_2} \end{aligned} \tag{3.22}$$

In which, Q_m is the flow rate of the mixture, and the subscripts 1 and 2 are regarding the upper and lower layer, respectively. V_m is the mean flow velocity of the mixture, and V_1 and V_2 the mean flow velocity of the mixture in the upper and lower layer respectively. The cross-sectional area's of the upper and lower layer are defined by A_1 and A_2, respectively. In the same manner this balance can be made for the flow rate of the solids (equation 3.23) and carrier fluid (equation 3.24), respectively.

$$\begin{aligned} Q_s &= Q_{s,1} + Q_{s,2} \\ A_S V_S &= C_{vi} A V_S \\ &= C_1 A_1 V_1 + C_2 A_2 V_2 \end{aligned} \tag{3.23}$$

$$\begin{aligned} Q_f &= Q_{f,1} + Q_{f,2} \\ A_f V_f &= (1 - C_{vi})\, A V_f \\ &= (1 - C_1)\, A_1 V_1 + (1 - C_2)\, A_2 V_2 \end{aligned} \tag{3.24}$$

The volume balance for the solids part of the cross-section can be written as:

$$\boxed{C_{vi} = C_1 A_1 + C_2 A_2} \tag{3.25}$$

Using the definition for $C_{vd} = Q_s/Q_m$ (as given in equation 3.12) one can rewrite equation 3.23 to equation 3.26.

$$\boxed{C_{vd} A V_m = C_1 A_1 V_1 + C_2 A_2 V_2} \tag{3.26}$$

3.4.4 *Conservation of Momentum for Flow in Two Layers*

The conservation of momentum is used to represent the balance of the forces between the driving and resisting forces acting on the flow boundaries of each layer in a horizontal pipeline of length L. The force equilibrium in the upper layer can be derived as given in equation 3.27.

$$\Delta P A_1 = \tau_1 O_1 L + \tau_{12} O_{12} L \tag{3.27}$$

In which the friction component along the along the upper section of the pipeline wall is denoted as τ_1, the circumference of the top layer as O_1, the friction component over the interface of the upper and lower layer as

τ_{12} and the width of the bed as O_{12}. The length along the pipeline section over which the forces act is denoted as L. Lastly, the pressure drop over this section is given with ΔP. For the lower layer this results in equation 3.28.

$$\Delta P A_2 = \tau_{12} O_{12} L + (\tau_{2,f} + \tau_{2,s})\, O_2 L \tag{3.28}$$

In which, the friction component along the interface of the upper and lower layer is once again denoted as τ_{12}. The friction component of the bed along the pipeline wall is split in two, where the contribution of the fluid is denoted as $\tau_{2,f}$ and the contribution of the solids as $\tau_{2,s}$. The circumference of the bed in the cross-section is given as O_2.

To give the force balance over the whole pipeline cross-section equations 3.27 and 3.28 have to be summed up. Leading to equation 3.29

$$\Delta P A = \tau_1 O_1 L + (\tau_{2,f} + \tau_{2,s})\, O_2 L \tag{3.29}$$

3.5 Concluding Remarks

For the physical modelling part a numerical model of the bed interface is set up. The up- and downward moving interface with a stationary bed can therefore be modelled as a 2LM, the geometry of the 2LM model forms the basis for that. Besides the geometry the volume balance can be used as well to calculate the velocities of the layers. Specifically, if the bed layer is said to be stationary, using the ratios of the layers the velocity above the bed can be computed directly.

4

Density Waves in Pipeline Systems

In this chapter a historical overview of the findings of different researchers is elaborated. This is done to form a basis for the explanation of later findings via the experimental setup for this thesis. In the current available research a lot can be found regarding the observations of density waves. However, the specific origin(s) causing these density waves is (are) still unknown, hence the need for more research on that matter.

In 1981 during the construction of the *Prins Clausplein*, a highway intersection in the Netherlands, a vast amount of sand was needed. The dredged material was transported over ten kilometres, using three booster stations, towards the construction site near The Hague. The transported material consisted of fine to medium sand and was conveyed in a pipeline for which of the most part the diameter was 650 mm. For research purposes a vast amount of data was measured along two of the three booster stations and at the dredge. This data is called "MeaVli" (Matoušek, 1995).

During a dredging operation the slurry density varies in time and space. However, controlled global operational parameters are presumed to be maintained at a consistent level during the whole operational time. Hence, if non-stationary solids flow would be modelled based on the basic hydrodynamic equation, thus accounting for transport and turbulent dispersion, the varying density should be damped due to turbulent mixing processes (Basco, 1977).

4.1 Long Horizontal Slurry Pipelines with Non-Stationary Solids Flow

Based on the measurements of the construction of the *Prins Clausplein* Matoušek (1995, 1996a, 1996b) analysed the data from the dredging operation and found several possible conclusions about the processes causing an amplifying density wave. These outcomes are discussed in this section.

Matoušek (1995, 1996a, 1996b) found a material aggregation phenomenon along the pipeline. This was expressed by the transformation of density waves along the pipeline. It was expected that the influence of the pump performance was imperceptible due to the dimensions of the density waves and the length of the pipeline sections. By reconstruction and comparison of the data Matoušek (1995, 1996a, 1996b) found that this was true and that the density wave was a product of the instability of the solids flow in the pipeline. The variability of the flow induced a variability in the solids flow along the pipeline thus causing a relative material transfer between moving density waves, hence resulting in the transformation thereof.

For determining the internal structure of the slurry flow Matoušek (1995, 1996a, 1996b) assumed a simplified physical model which is capable of approaching integral values of the related quantities. For the pipe cross-section that would be C_{vi}, V_m, and particle settling velocity. These integral parameters are mutually related using the equations of section 3.2.

On the condition that the flow can be modelled using the Two-Layer model, in this case the one of Wilson (1992), simplifications regarding the internal structure the flow are required. Matoušek (1995, 1996a, 1996b) found that the partially stratified slurry flow regime quite correctly approximated the composition of the real internal structure of the flow when compared to the plotted solids velocity profiles of the real slurry flow. He furthermore concluded that a physical two-layer model sufficiently models the data and therefore it should be

possible and accurate enough to estimate the slip in the cross-section of a pipeline, thus coming to the conclusion that due to the variable slip in different pipe cross-sections along the pipeline a highly concentrated density wave can grow. Matoušek (1995, 1996a, 1996b) stated that an increasing slip ratio is due to an increase in slurry density, hence solids flow has to be unstable even when slurry flow rate and other material properties are generally maintained constant during the transport operation. Matoušek (2001b) furthermore observed from the database MeaVli data that the dredged material had a rather wide particle size distribution (PSD). For such a mixture he concluded that the velocity of the solids at the bottom of the pipeline varied for densities that fluctuate over the pipeline cross-section. The particles located at the bottom are accelerated within a denser mixture. Matoušek (2001b) attributes this to the higher impelling force that is exerted on a bed load by a denser mixture stream. He also attributes this to the buoyancy effect that reduces the submerged weight of the bed. So, in conclusion Matoušek attributed the density wave growth to a variable slip as a function of the density.

4.2 Mathematical and Physical Modelling of Density waves

Based on the findings of Matoušek (1995, 1996a, 1996b), Talmon (1999) wanted to prove the hypothesis of the influence of the slip ratio on amplifying the density waves using mathematical and physical modelling techniques. Talmon (1999) investigated the role of the 'force interaction' hypothesis (higher impelling force of high density suspension waves accelerated the moving bed layer) and the mass exchange processes between bed layer and suspension. For the first hypothesis he tested the consequences of variable slip and used a non-linear modified burgers equation to calculate the density wave development in the case of variable slip. For the second hypothesis he carried out a linear stability analysis.

Talmon (1999) fitted the linear variable slip function to the variable slip data of Matoušek (1997), which is only valid for distinct conditions in the laboratory. By decomposing the concentration variation in the density wave for the 1D non-linear cross-sectional averaged mass continuity equation, the time-development of the amplitude and propagation velocity of each harmonic wave component is computed. It appeared that, based on the first model, the initial sinusoidal density wave deforms quickly into a sawtooth wave. The cause thereof is the non-linear advection term in the mass-continuity equation, which appears to generate harmonic wave with shorter wavelength. Hence leading to a sawtooth shape as wave energy is continuously fed into the higher harmonics. Therefore the step-change of the density can occur and this is keeping the form of the sawtooth intact. However, the amplitude of the sawtooth decreases in time, thus Talmon (1999) stated that the variable slip could not explain the density wave amplification phenomenon. However, the unbalance between sedimentation and erosion at high concentrations would be able to explain density wave amplification. Therefore Talmon (1999) carried out a linear stability analysis where the exact role of the mass exchange between the bed layer and suspension was investigated. The combination of advection, dispersion and particles exchanging between the layers was accounted for by the linear stability analysis. Talmon (1999) identified the hindered settling of particles at high concentrations as the cause of the unbalance of erosion and sedimentation. The latter is the cause for density wave amplifications.

Using the findings of Matoušek (2001b), Talmon (2002) expended his linear stability analysis to see whether the unbalance of erosion and sedimentation was still the cause of the amplification of density waves in a sliding bed regime. Talmon (2002) set up the calculations in two model configurations. In the first he considered that the momentum balance of both layers and mass exchange processes are blocked. For the second model configuration all processes were included. The calculations showed that the amplification is somewhat slowed for the suspended load instability compared to the stationary bed conditions. The explanation for this is that the bed layer accelerates when a density wave passes. Subsequently, the difference of the velocity between the two layer decreases, leading to a slower density amplification. During this passing of a high density wave, low momentum mixture is entrained within the suspended flow. Thus leading to slowed down load velocities as the shear-instability mechanism is experiencing more damping (Talmon, 2002). From the calculations it could be concluded that the unbalance of erosion and sedimentation is the cause of density wave amplification in the sliding bed regime as well.

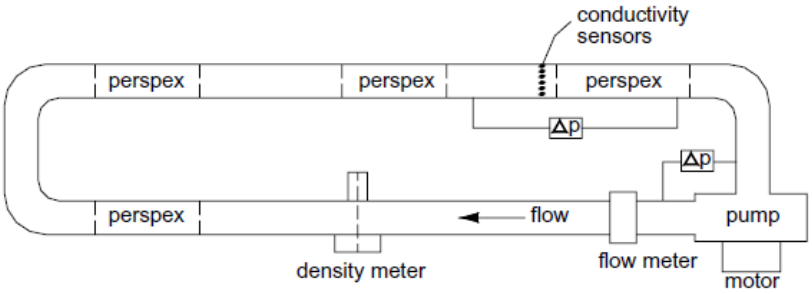

Figure 4.1: Sketch of the test loop for the self-exciting concentration fluctuations, retrieved from Talmon et al. (2007)

The sedimentation and erosion unbalance at high concentrations as cause for density wave amplification was further explored by Talmon et al. (2007) via experiments. By this means he found that the adverse process possibly has a favourable effect on the density wave amplification. In high concentration slurry flow sedimentation and erosion are both affected. Whenever there is more transfer of sand from the bed layer towards the suspension it might be possible that the variety of the density of the slurry is amplified. The laboratory test loop Talmon et al. (2007) set up is shown in figure 4.1. For the test loop a closed circuit was build to mimic long distance pipeline transport, however it is required that the length of the loop is longer than the critical wavelength at which density amplification occurs (Talmon et al., 2007). The foremost conclusions were that the amplifying density waves occur when, at minimum, a thin bed layer is present and that the mixture velocity is around the deposit limit velocity. Furthermore, Talmon et al. (2007) found that harmonic concentration fluctuations were deformed into large amplitude sawtooth-like concentration fluctuations. Linear theory is unable to explain this process, therefore non-linear processes govern the deformation of density waves. These non-linear processes also determine the maximum density fluctuations.

Matoušek and Krupička (2013) researched different types of unsteady solids flow where they focused on density waves and the restratification effect. Both these phenomena appeared to be correlated with secondary currents present in the pipeline system. These secondary currents are interacting with the granular bed in the stratified flow regime, though more specific research is necessary to find the mechanisms that lead to the generation and development of these flows. Matoušek and Krupička (2013) found density waves in their loop at velocities which were around the deposit limit velocity. The amount of density waves appeared to be unlinked to the length of the flow loop. For these experiments Matoušek and Krupička (2013) were unsure how and why these density waves were generated. Though, since an assymetrical shape of the discharge area above the deposit was observed, which caused secondary flow effects to occur, it was proposed to further investigate the influence of secondary flow effects.

4.3 Numerical Modelling of Density Waves in Pipelines

Miedema et al. (2003) conducted numerical simulations to simulate dynamic effects of unsteady solids flow, as for example a density wave. To be able to do this they set up a 2D Two-Layer Model to account for the vertical transfer of solid particles between the bed layer and the suspension layer. For the 2D model, they divided the pipeline into a finite number of elements. In each of this element the flow is split into two layers, a bed layer (lower) and a suspended layer (upper). The bed layer can either be stationary or sliding. As the flow of solids is unsteady, the bed thickness in each of the different elements is different as well. A schematisation of this model is shown in figure 4.2.

Miedema et al. (2003) modelled the mass exchange in the two directions: horizontal and vertical. The horizontal transport of solid particles is defined as given in equation 4.1. Where, Δm is the change of mass, Q the slurry flow rate, t the time step, $C_{v,up}$ the volumetric concentration of solids in the suspended layer and ρ_s the density of the solids.

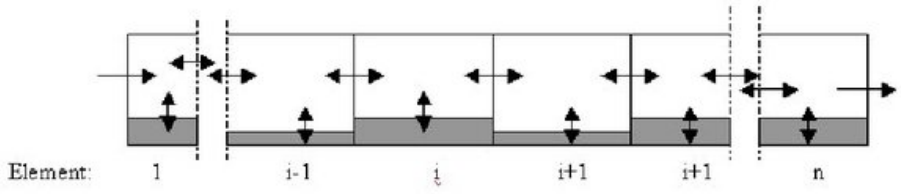

Figure 4.2: Schematisation of the 2D model for a 2LM, retrieved from Miedema et al. (2003)

$$\Delta m = Q \cdot t \cdot C_{v,up} \cdot \rho_s \tag{4.1}$$

Horizontal transport is affected by turbulent longitudinal dispersion in the horizontal direction which can be quite complex. Therefore, in the 2D model it is modelled comparable to molecular diffusion. For vertical transport Miedema et al. (2003) accounted for hindered settling as determined by Richardson and Zaki (1954) and hindered erosion van Rhee and Talmon (2000). By combining these fluxes Miedema et al. (2003) came up with an adjusted erosion-velocity equation to simulate the relative velocity representing the mass exchange between the layers. The so-called sedimentation velocity. This sedimentation flux is defined as the hindered settling flux minus the hindered erosion flux and the vertical velocity of the bed. Due to the unbalance in erosion and settling the bed layer grows or erodes in different segments of the pipeline. At high mixture concentrations the hindered effects of settling compared to erosion were always found larger. Hence, creating a density wave in the process.

The results of the model developed by Miedema et al. (2003) represent the same trends as observed in real life. Note should be made that the inertia component was not accounted for in the analysis of Miedema et al. (2003), while the analytical model of Talmon (2002) did.

4.4 Density Waves in Inclined and Vertical Pipeline Systems

For deep sea mining operations research was conducted for inclined flows and lazy S-wave bends by de Hoog (2016); de Hoog et al. (2017) and for vertical transport by de Hoog et al. (2021); Müller, Mischo, and van Wijk (2018); van Wijk (2016); van Wijk, van Rhee, and Talmon (2014).

The research object of de Hoog (2016); de Hoog et al. (2017) was to find new operational limits for coarse slurry flow in inclined and S-Wave bends. Additionally, density waves were observed in the loop. Though where in previous research the density waves developed at flow velocities near the deposit limit velocity, de Hoog (2016); de Hoog et al. (2017, 2021) observed density waves at velocities far above the deposit limit velocity. This renders the current knowledge quite incomplete, as new limits are therefore needed to be developed. de Hoog et al. (2021) hypothesised that the source of the amplification is due to a transient material accumulation effect between two pipe segments with a significant difference in transport capacity and thus slip ratio. This was thought to be the case for the observed density waves in the Freiberg experiment (de Hoog et al., 2021; Müller et al., 2018).

The main source of transients are due to the centrifugal pumps de Hoog et al. (2021), though these pumps are not the origin of an unstable system nor density wave amplification. A density wave amplification can be started by the centrifugal pump, though the underlying physical processes play a more important role therein. The main mechanism is the unbalance between erosion and sedimentation at high concentrations. Moreover, the amplification is not just a product of differential slip and advection as the amplification is only possible in case there is a buffer of available material for the wave to grow on. These sources are made when in parts of the pipeline the slurry velocity temporarily drops below the deposit limit velocity. This could be seen in the inclined pipe segment (de Hoog, 2016; de Hoog et al., 2017) and the S-wave bend (de Hoog, 2016).

The effects of vertical transport on density waves during a plug flow of material, resembling a density wave, and whether or not a vertical pipe segment can get blocked were investigated by van Wijk (2016). Part of his research consisted of finding the axial dispersion in a vertical pipe which could possibly dampen a passing density

wave (van Wijk et al., 2014). He found that the axial turbulent dispersion is not playing a major role in vertical hydraulic transport with Stokes numbers larger than 0.3. Where the Stokes number represents the behaviour of particle suspended in flow. In his experiments, he did observe the dampening of the initial plug, though as he was working with a closed loop the material was re-used for several laps in the circuit. van Wijk et al. (2014) attributed the dampening to the many bends and pump in his system which lead to dispersion of the material in the loop.

4.5 Concluding Remarks

Based on the current knowledge several causes for density wave amplification can be distinguished. While pumps and the input side of a pipeline system may introduce the gradients in density and therefore concentration within the pipeline. The physical processes play a stronger and more significant role in the amplification of density waves.

The research of Matoušek (1995, 1996a, 1996b) was the first attempt to find the origin of density wave amplification. In his research he found that the variability of the flow was inducing variabilities within the solids flow along the pipeline. This caused a relative material transfer between the moving density waves, consequently transforming these waves. Matoušek (1995, 1996a, 1996b) found that modelling the internal structure of the flow as a 2LM was in sufficient agreement with the measured data. Based on his data interpretation he confirmed his hypothesis that there is a relationship between slip and slurry density.

Later research conducted by Talmon (1999), who tried to mathematically prove the hypothesis of the influence of the slip ratio on the amplifying density waves, actually came to a different conclusion. While using a non-linear one-dimensional model to calculate the density wave development if a variable slip is used, he found that when using the slip data of Matoušek (1997) lead to dampening of the waves, and de Hoog et al. (2021) confirmed this by modelling stronger axial slip, leading to more damping. Talmon (1999) therefore stated that the variable slip could not explain the amplifying behaviour of density waves. New findings of Matoušek (2001b) lead to expansion of his older linear stability analysis by Talmon (2002). He found that for both stationary and sliding bed regime the density wave amplification was to be attributed to the erosion and sedimentation unbalance. By further implementation of new experiments Talmon et al. (2007) tried to prove that the cause for amplifying density waves was actually to be found in the unbalance between sedimentation and erosion at high concentrations. The research of Talmon et al. (2007) found that density waves were occurring at velocities around the deposit limit velocity and whenever at minimum a thin bed layer was present.

However, more recent research by de Hoog et al. (2021); Müller et al. (2018) in inclined and vertical pipeline systems, observed amplifying density waves at velocities far above the deposit limit velocity. They hypothesised that the erosion and sedimentation unbalance is the driving factor for density wave amplification. Moreover, the amplification is not just a product of differential slip and advection as the amplification is only possible in case there is a buffer or source of available material for the wave to grow on. These sources are made when in parts of the pipeline the slurry velocity temporarily drops below the deposit limit velocity, which may be the case after bends in the vertical plane as the transport capacity is different for the horizontal and vertical part. The latter was seen in the experiments of de Hoog (2016) and de Hoog et al. (2017). However, for these experiments the flow velocity was around the deposit limit velocity.

5

Erosion and Sedimentation Unbalance

The fundamentals of erosion of sand grains has been a topic of research for many decades, however still a lot of relations are empirical and therefore may require specific flow conditions. For fluvial flow extensive research has been done by Shields (1936) to explain the bed load transport. He formulated a curve for the critical Shields parameter in relation to the particle Reynolds number to predict the initiation of motion, see equation 5.1. Erosion is started when the flow conditions are such that the critical Shields parameter is exceeded.

$$\theta_b = \frac{\tau_c}{(\rho_s - \rho_w)\, gd} = \frac{u_*^2}{\Delta g d} \tag{5.1}$$

In which τ_c is defined as the critical shear stress that the flow exerts on the bed. The relative density is denoted as $\Delta = \frac{\rho_s - \rho_w}{\rho_w}$. The shear stress is dependent on flow velocity, density and the roughness of the bed as shown in equation 5.2.

$$\tau_c = c_f \rho_f u^2 \tag{5.2}$$

In which c_f is defined as the friction coefficient of the bed, ρ_f as the density of the carrier fluid and u as the average flow velocity over the bed. An example on how to calculate the critical Shields parameter is given in equation 5.3. This equation was derived by Brownlie (1981) to provide a continuous function for the critical Shields parameter.

$$\theta_{cr} = 0.22 \mathbf{R}_\mathrm{p}{}^{-0.6} + 0.06 \exp\left(-17.77 \mathbf{R}_\mathrm{p}{}^{-0.6}\right) \tag{5.3}$$

In which θ_{cr} is defined as the critical Shields parameter and $\mathbf{R}_\mathrm{p}$ is denoted as the particle Reynolds number, which can be calculated using equation 5.4.

$$\mathbf{R}_\mathrm{p} = \frac{d\sqrt{\Delta g d}}{\nu} \tag{5.4}$$

The research of Shields (1936) was extended by van Rijn (1984b, 1984c) to couple the grain size diameter to the Shields number. This to make the curve more usable towards erosion in fluvial flows. While the erosion in pipelines has some similarities, there are a lot of differences as well. Due to the much higher concentration of slurries in pipelines other physical processes such as hindered settling and hindered erosion play a more significant role. Moreover, the fact that a pipe segment is closed at the upper water level and fluvial flow has an open boundary leads to some significant differences as well. The influence of the concentration on the transport of sediment has been researched by Bisschop (2018); van Rhee (2010); van Rhee and Talmon (2000, 2010); van Rijn et al. (2019); Winterwerp, Bakker, Mastbergen, and van Rossum (1992); Winterwerp, Groot, Mastbergen, and Verwoert (1990) among others.

5.1 Sedimentation Flux

In highly concentrated slurry flows erosion and sedimentation takes place constantly and simultaneously. When considering a cross-section, the erosion and sedimentation are exactly in balance if despite the transport of

material the height of the bed is constant. This means that some material may settle, however the same amount of material is eroded in the same time span. To be able to adequately describe the processes due to the hindered effects on sedimentation and on a lesser scale on erosion a good understanding is needed on which parameters have an influence.

The sedimentation of particles is based on an equilibrium of forces of the material in a carrier fluid. In pipeline slurry flow that consists of only sand it may be assumed that the material does not flocculate. The particles therefore do not change in size and due to gravity the grains settle. On the particle two vertical forces are present. One is an upward directional force that is caused by the frictional drag of the fluid on the particle and the other is a downward directed force due to the difference in density of the grain and the carrier fluid (Miedema, 2016). A general formula for the terminal settling velocity is given in the equation below.

$$w_0 = \sqrt{\frac{4 \cdot g \cdot (\rho_s - \rho_f) \cdot d \cdot \psi}{3 \cdot \rho_f \cdot C_D}} \tag{5.5}$$

Where, ψ is defined as the grain shape factor ≈ 0.7 for real sand particles and C_D is defined as the drag coefficient of the particle. Due to the fact that actual sand particles are not round, extensive research has been done for dredging applications to find straightforward empirical equations specifically derived for sand particles (Matoušek, 2004). An example of these equations are those of Stokes, Budryck and Rittinger, however these equations are only valid for specific particle Reynolds numbers ($\mathbf{Re}_p$) and accompanying regimes. For the Stokes equation this is $\mathbf{Re}_p < 0.1$, which holds for grains smaller than 0.1 *mm* and is considered the *laminar regime*. The equation of Stokes is given in equation 5.6.

$$w_0 = 424 \frac{(S_s - S_f)}{S_f} d^2 \tag{5.6}$$

In which, S_s is the specific density of the solids defined as ρ_s/ρ_w and S_f the specific density of the fluid, defined as ρ_f/ρ_w. The Budryck equation requires $0.1 \leq \mathbf{Re}_p \leq 500$, which is the case for grains of a size between 0.1 *mm* and 1 *mm*, this is the *transition regime*. The Budryck equation is given in equation 5.7.

$$w_0 = \frac{8.925}{d} \left[\sqrt{1 + 95 \frac{(S_s - S_f)}{S_f} d^3} - 1 \right] \tag{5.7}$$

Lastly, the Rittinger equation is valid for $\mathbf{Re}_p > 500$, which is typically for sand grains larger than 1 *mm*, this is considered the *turbulent regime*. The Rittinger equation is defined as given in equation 5.8.

$$w_0 = 87 \sqrt{\frac{(S_s - S_f)}{S_f} d} \tag{5.8}$$

Combining these three equations for each regime results in a function that has undesirable discrete jumps on the transition points. Zanke (1977) derived a new empirical equation for the terminal settling velocity that was found to be adequately accurate for grains of a size 10 μm to 10 *mm* according to Miedema (2016). The terminal settling velocity derived by Zanke (1977) is given in equation 5.9.

$$\boxed{w_0 = \frac{10 \cdot \nu}{d} \cdot \left[\sqrt{1 + \frac{0.01 \cdot \Delta \cdot g \cdot d^3}{\nu^2}} - 1 \right]} \tag{5.9}$$

The equation of Zanke (1977) is found to be relatively in the neighbourhood of the combination of the three separate regimes equations. A more recent study was done by Ferguson and Church (2004) to develop a simple universal terminal settling velocity equation. The new equation is a function based on the grain size diameter, fluid viscosity, fluid density and solid density. While the equations of Stokes, Budryck, Rittinger and Zanke (1977) were specifically for sand particles the equation of Ferguson and Church (2004) is not, the new equation can used for spherical grains as well. Therefore, to be able to make a clear distinction in these types of grains two grain specific parameters are used. The equation of Ferguson and Church (2004) was derived using a dimensional analysis and resulted in equation 5.10.

$$w_0 = \frac{\Delta g d^2}{C_I \nu + (0.75 C_{II} \Delta g d^3)^{0.5}} \tag{5.10}$$

In which, C_I and C_{II} are the two grain specific parameters. The above equation was visually compared to earlier settling velocity equations by Ferguson and Church (2004) and plotted against earlier and new data sets assembled by Hallermeier (1981) and Raudkivi (1990). The results were found to be fairly good and the equation seemed to adequately fit the experimental data. For sand the soil parameters C_I and C_{II} can be estimated to be equal to 20 and 1.1, respectively (Ferguson & Church, 2004). van Rhee (2018) gives slightly different values for C_I and C_{II}, which are given as 18 and 1, respectively.

For an overview all earlier mentioned terminal settling velocities have been plotted in figure 5.1 to show how these compare to each other. The lower limit for the grain size is set to 0.01 mm or 100 μm and the upper limit to 10 mm. The laminar regime, Stokes equation, is thus excluded. At 1 mm the discrete jump can be seen for the Budryck and Rittinger function. Comparing the Ferguson and Church (2004) and Zanke (1977) functions, it can be concluded that they overlap reasonably well. For the determination of the terminal settling velocities, the equation of Zanke (1977) is used throughout the rest of this thesis as this equation gives a sufficient assessment for the terminal settling velocity for sands and gravel (Miedema, 2016).

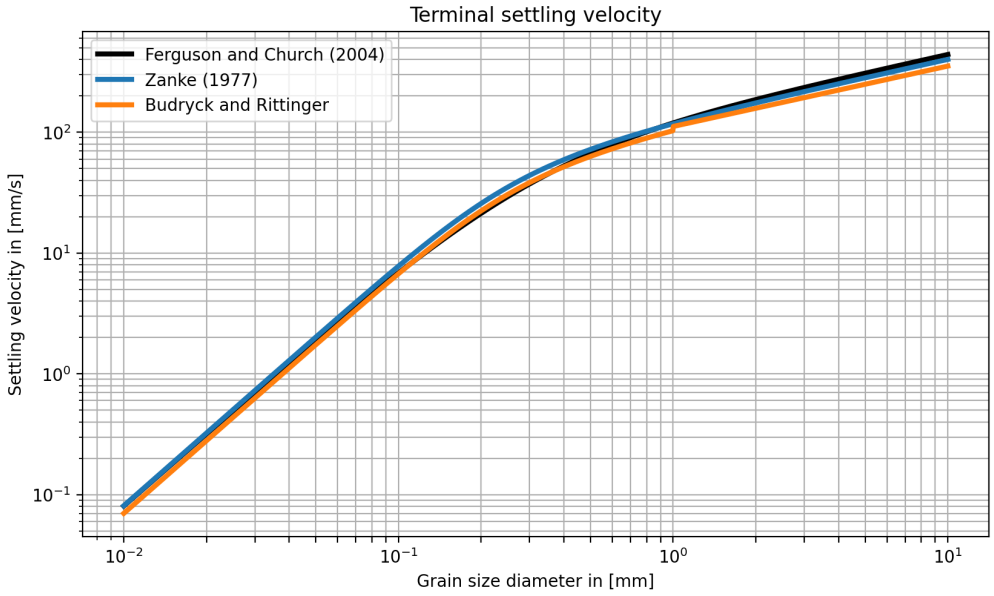

Figure 5.1: The different terminal settling velocities according to Budryck and Rittinger, Zanke (1977) and Ferguson and Church (2004)

As mentioned in section 3.1 hindered settling plays a major role in the sedimentation flux in a pipeline. For the hindered settling equation of Richardson and Zaki (1954) the near bed concentration is deemed to be the influential parameter, which is in compliance with van Rhee and Talmon (2010). The total sedimentation flux can be determined with equation 5.11.

$$S = \rho_s w_s c_{nb} = \rho_s w_0 c_{nb} (1 - c_{nb})^m \tag{5.11}$$

In which S is denoted as the sedimentation flux, ρ_s as the solids density, w_s as the hindered settling velocity, w_0 as the terminal settling velocity determined using the Zanke (1977) equation, c_{nb} as the near bed concentration and m as the exponent in the Richardson and Zaki (1954) equation. The latter can be determined using the equation of Rowe (1987), as given in equation 3.7.

5.2 Erosion and Sedimenation flux in a Control Volume

The ongoing process of sedimentation and erosion takes place simultaneously and can be schematised as shown in figure 5.2. When the sedimentation flux is larger than the erosion flux sedimentation will occur. Considering a control volume near the interface of bed and fluid, the volume of particles moving from the flow through the interface into the bed needs to be the same as the particles stored within the bed. This needs to be true vice

versa. The velocity at which the interface moves up during sedimentation is denoted as v_{sed} and when moving down in the case of erosion as v_e. The general expression for the velocity of the interface when considering net sedimentation is given in equation 5.12.

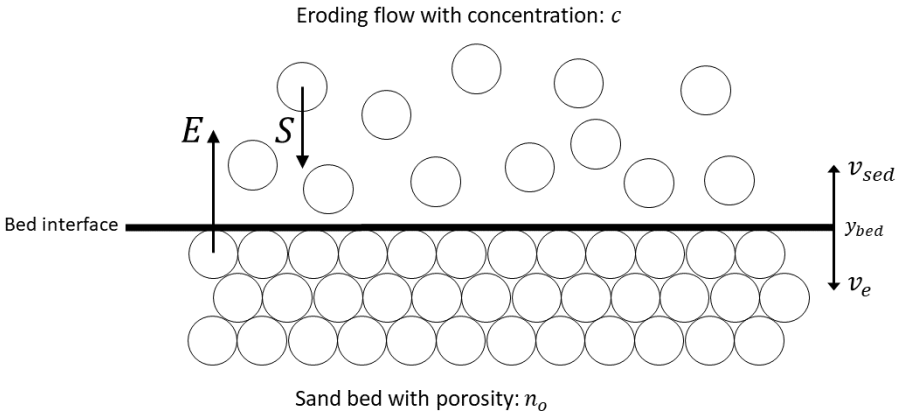

Figure 5.2: Schematisation of the control volume near the bed-fluid interface, based on Bisschop (2018); van Rhee (2010)

$$v_{sed} = \frac{S - E}{\rho_s (1 - n_0 - c_{nb})} \tag{5.12}$$

In which, S is denoted as the sedimentation or settling flux and can be calculated using equation 5.11, E as the erosion flux, n_0 as the porosity of the bed prior to erosion and ρ_s as the density of the sediment. For the erosion several pick-up functions have been derived in the literature over the years, one example of the most well known equations is the empirical function of van Rijn (1984a) for the grain by grain erosion regime. While erosion takes place the erosion flux is higher than the settling flux, thus leading to the bed interface moving down. In this situation the erosion velocity can be computed using the fact that $v_e = -v_{sed}$.

5.3 Erosion of Grains

At very low flow velocities an initially flat bed can be transformed into features that seem some what irregular (Kennedy, 1969). This formation of features is attributed to a systematic sequence of scour and deposition, where the smallest inconsistencies induce small variations in flow velocity. Beyond this flow regime actual erosion takes place. For which, one of the better known erosion pick-up equations was derived by van Rijn (1984a). He made use of a fairly simple procedure where sediment was loaded on to platform attached to a vertical piston supplying material to the flow. This platform was located on a sill like structure to which sediment was glued on. At flow velocities in the range of 0.5-1 m/s and a constant depth of 0.25 m, various grain sizes were moved up into the stream. The grain size used varied from 130 μm to 1.5 mm. Consequently, due to the acting bed shear stress, the lose grains were able to be eroded. The erosion rate was then measured using equation 5.13.

$$E = \frac{M}{A \Delta T} \tag{5.13}$$

In which, E = pick-up rate in $[kg/sm^2]$, M = total sediment mass in $[kg]$, A = area of the moving platform in $[m^2]$ and ΔT = the measuring time in $[s]$. The pick-up rate was measured in equilibrium flow conditions. For the determination of the bed shear velocity an acoustical probe was placed in the middle of the flume. Using the relation of the logarithmic velocity law as given in equation 5.14, the bed-shear velocity was calculated.

$$\frac{u(z)}{u_*} = \frac{1}{\kappa} \ln \left(\frac{z}{z_0} \right) \tag{5.14}$$

In which $u(z)$ = velocity at location z above the origin in $[m/s]$, u_* = the bed-shear velocity, κ = Von Karman constant (=0.4), z_0 = the level at which the velocity is equal to zero; $z_0 = 0.11 \frac{\nu}{u_*} + 0.033 k_s$. k_s is estimated

to be equal to $2D_{50}$. van Rijn found in earlier studies that the pick-up rate can be expressed in terms of a dimensionless grain-size parameter, D_*, and a dimensionless transport-stage parameter T. The equations of aforementioned dimensionless parameters are given in equation 5.15 and 5.16.

$$D_* = D_{50}\sqrt[3]{\frac{\Delta g}{\nu^2}} \tag{5.15}$$

In which Δ = is the relative density $\left(\frac{\rho_s - \rho_w}{\rho_w}\right)$, g = the gravitational acceleration in $[m/s^2]$ and ν is the kinematic viscosity of the fluid.

$$T = \frac{(u_*)^2 - (u_{*,c})^2}{(u_{*,c})^2} \tag{5.16}$$

In which $u_{*,c}$ = the critical bed-shear velocity according to Shields (1936). Using these equations the dimensionless pick-up rate can be found as defined by Einstein (1950), see equation 5.17.

$$\Phi_p = \frac{E}{\rho_s\sqrt{\Delta g D_{50}}} \tag{5.17}$$

The new derived dimensionless pick-up rate defined by van Rijn (1984a), equation 5.18, shows fairly good results when comparing it to the measured pick-up rates in his experiments as van Rijn found a relative standard error of around 30%.

$$\Phi_p = 0.00033 D_*^{0.3} T^{1.5} \tag{5.18}$$

Implementing equation 5.18 in to equation 5.17 results in an equation which is used for the physical modelling part of this research, see chapter 8. The result for the erosion flux is given in equation 5.19.

$$\boxed{E = 0.0033 D_*^{0.3} T^{1.5} \rho_s \sqrt{\Delta g D_{50}}} \tag{5.19}$$

5.4 Influence of the Concentration on the Erosion Rate

While van Rijn (1984a) did not elaborate deeply on the influence of the concentration of sand on the transport capacity of the flow, Winterwerp et al. (1990) hypothesised that the influence was significant. van Rijn (1984a) only carried out experiments with very low concentrations. Hence, the applicability on highly concentrated mixture flow is therefore not without ambiguity when using the van Rijn (1984a) equation to calculate the pick-up rate. The vastly different conditions of highly concentrated mixture flow during the construction of closure dams and the slurry flow in hydraulic transport applications thus required more research into the effects of the concentration on erosion and sediment transport.

Winterwerp et al. (1990) were amongst others interested in the influence of the concentration on the transport capacity of the flow and carried out small-scale and full-scale experiments. The experiments were set up identically for each scale. It consisted out of a mixing tank, where a slurry could be prepared at the desired concentration and a tilting flume, the setup is shown in figure 5.3. When doing a test, a concentration and discharge were set and the slope of the tilting flume was reduced in steps of 0.001 rad until the formation of sand bars was visible. The slope at the previous step, thus before the formation of the sand bars, was defined as the equilibrium slope. A this slope the sedimentation and erosion are perfectly in balance. In their experiments Winterwerp et al. (1990) used sands with a grain size in the range of 120-225 μm. The most relevant conclusions were that the equilibrium slope that in the turbulent flow regime is a function of the flow velocity and the grain size, and at concentrations of below 20% this seemed almost independent of the mean concentration. In the case of increasing concentrations, Winterwerp et al. (1990) found that the near-bed concentration increases at first, this may be due to an increasing shear layer at higher concentrations. The solution to the diffusion equation has two values as a result of the significant effects of hindered settling. Hence, the resulting mean concentration highly depends on the initial conditions in the flow.

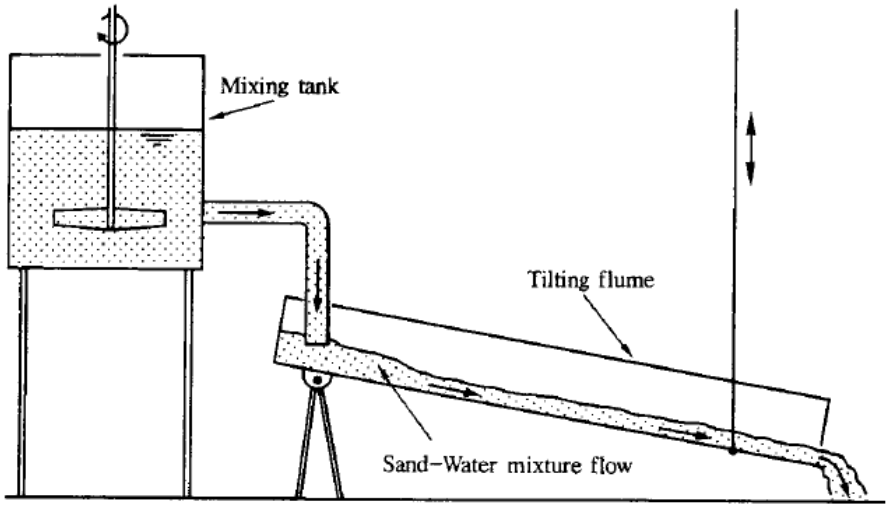

Figure 5.3: Set-up of the experiments used by Winterwerp et al. (1992, 1990)

In later research, Winterwerp et al. (1992) further assessed the influence of the concentration on the transport capacity of the flow. During the new experiments, a focus was put on the erosion on the lee side of a sand bar and on the development of a equation for the pick-up rate including the effects of the concentration. Using the same setup as described in Winterwerp et al. (1990), with the difference that in the new experiments the slope was set to 0.001 rad before the equilibrium slope. At this slope sand bars were visible and seen to migrate upstream. During the experiments the transformation of the sandbars was measured at concentrations of around 10%. At this concentration one main sandbar was visible of which the deformation could be visualised over time. When using higher concentrations Winterwerp et al. (1992) was unable to recreate perceptible measurements as the flow became more and more unstable. Thus leading to a bed that was frequently deformed, with resulting local scouring and extra sandbars on the main sandbar.

Based on these experiments Winterwerp et al. (1992) found a new relation for the pick-up rate which had the same form as former relations such as the one from van Rijn (1984a). In the new relation the effects of the concentration were indirectly accounted for. The pick-up rate as defined by Winterwerp et al. (1992) is given in equation 5.20.

$$\Phi_p = 0.012 D_*^{0.3} \left(\theta_b^{0.5} - 1.3\right) \tag{5.20}$$

Implementing equation 5.20 into equation 5.17 results in a equation that can be used for the physical modelling part. The resulting equation is shown below.

$$\boxed{E = 0.012 \rho_s \sqrt{\Delta g D_{50}} D_*^{0.3} \left(\theta_b^{0.5} - 1.3\right)} \tag{5.21}$$

5.5 Dilatancy Reduced Erosion

During further research on the matter of hindered erosion, van Rhee and Talmon (2000) build a closed circuit with a rectangular measurement section in which the flow velocity could be adjusted using a valve. Resulting in sedimentation in the rectangular section. Parallel to the measurement section a bypass was added, when the valve was closed the mixture velocity in the bypass section would further increase. In the case the valve was opened the mixture was pumped at a velocity above the deposit limit velocity. The sediment used during these experiments had a grain size of 110 μm and 200 μm. By use of this method van Rhee and Talmon (2000) were able to measure the sedimentation at different concentrations and velocities. They concluded that the pick-up functions as defined by van Rijn (1984a), Cao (1997) and Fernandez Luque (1974) were not applicable to high concentrations. Furthermore, van Rhee and Talmon (2000) found that hindered settling appeared to be

dominant over hindered erosion at high concentrations. This subsequently supports the hypothesis of Talmon (2002), stating that the cause of density wave amplification is due to hindered settling, i.e. an unbalance between erosion and sedimentation.

van Rhee (2010) conveyed further research on the pick-up function for highly concentrated mixtures and high flow velocities, since the conventional pick-up functions are not applicable to these conditions. It is found that in case of high flow velocities the way sand erodes changes significantly. Where in relatively low flow velocities the sand is eroded grain by grain, at high velocities this changes to a shearing upper layer. If a granular sediment is sheared the volume will not remain the same, because the porosity of the granular bed has to increase leading to an increase of the total volume. As the sediment is incompressible the change in volume is attributed to the change in the pore water volume. This mechanism is called dilatancy and Reynolds (1885) was the first to describe this phenomenon scientifically.

Due to the shearing of the top layer, the porosity of the top layer increases. Therefore, water has to flow directly into these pores. Hence, this increases the hydraulic gradient over the bed pushing the layer onto the bed and thus hindering the erosion due to the flow. To be able to use the conventional pick-up functions, such as the one from van Rijn (1984a), the critical Shields parameter needs to be modified so that it takes the effects of dilatancy into account. The altered critical Shields parameter is defined as given in equation 5.22.

$$\theta'_{cr} = \theta_{cr}\left(\frac{\sin(\varphi-\beta_s)}{\sin\varphi} + \frac{v_e}{k_l}\cdot\frac{n_l-n_0}{1-n_l}\frac{A}{\Delta}\right) \tag{5.22}$$

In which θ'_{cr} is the altered critical Shields parameter, θ_{cr} is the critical Shields parameter based on the equation of Brownlie (1981), since he provide a continuous function for the critical Shields parameter. The equation of Brownlie (1981) is given in equation 5.3. Moreover, φ is defined as the angle of internal friction of the sediment, β_s is the slope angle, k_l is the permeability of the sediment bed at minimum compaction. The bed porosity n_l is estimated as the maximum porosity n_{max}. Furthermore, n_0 is defined as the bed porosity prior to erosion and A is a coefficient with value 3/4 for single particle erosion and $1/(1-n_0) \approx 1.7$ for a continuum. At last, Δ is the relative sediment density.

Using the altered critical Shields parameter in the van Rijn (1984a) equation, van Rhee (2010) derived a pick-up function that is applicable for high flow velocities and accounts for the dilatant behaviour of the soil during shearing of the top layer. The new pick-up equation is shown in equation 5.23.

$$\Phi'_p = 0.00033 D_*^{0.3}\left(\frac{\theta_b-\theta'_{cr}}{\theta'_{cr}}\right)^{1.5} \tag{5.23}$$

When one is interested in the erosion velocity of the bed, equation 5.24 can be derived using equations 5.12, 5.11 and 5.17.

$$v_e = \frac{1}{1-n_0-c_{nb}}\left(\phi'_p\sqrt{g\Delta D_{50}} - c_{nb}w_s\right) \tag{5.24}$$

Consequently, substituting equation 5.23 in 5.24 results in a implicit relation since v_e is found on both sides of the equation 5.24. When a solution needs to be found, the root of equation 5.25 needs to be solved using a numerical calculation.

$$\boxed{\frac{1}{1-n_0-c_{nb}}\left(\phi'_p\sqrt{g\Delta D_{50}} - c_{nb}w_s\right) - v_e = 0} \tag{5.25}$$

5.6 Recent Developments in Research on Dilatancy Reduced Erosion

Based on the knowledge that at high flow velocities dilatant processes play a major role in the behaviour of the soil during erosion, Bisschop (2018); Bisschop, Miedema, Visser, Keetels, and van Rhee (2016) conducted experiments to find a pick-up function that would explicitly account for these phenomena. The experiments were executed in an adapted closed flume. In the adapted closed flume several conductivity probes were placed at different heights. By using this method the height of the sand bed can be measured and thereafter the erosion velocity. Additionally, a radioactive density meter was used to determine the density of the sand bed at a specific height. By using a flow meter Bisschop (2018); Bisschop et al. (2016) was able to determine the discharge in the measurement section. For the determination of the hydraulic gradient and pore water pressures use was

made of relative and absolute pressure sensors, respectively. The actual circuit set up of the experiments is shown in figure 5.4.

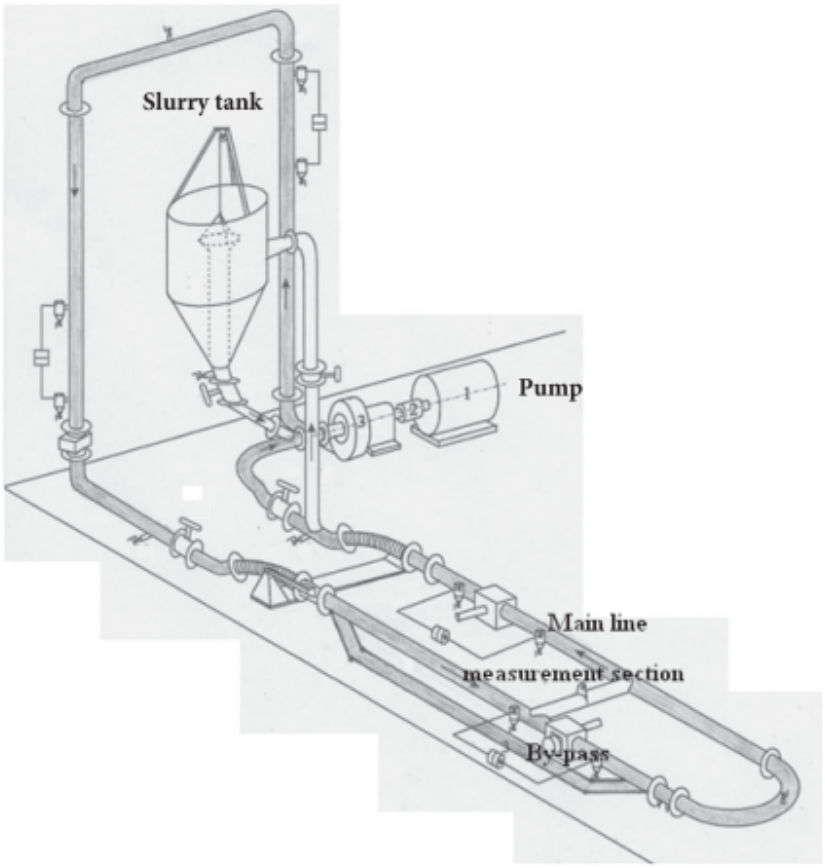

Figure 5.4: Circuit setup used for the experiments of Bisschop (2018); Bisschop et al. (2016), retrieved from Bisschop et al. (2016)

Using the experiments Bisschop (2018) developed a new pick-up function which he based on several driving and resisting mechanisms. As the driving mechanism, he observed turbulent bursts picking up material in the adapted flume during the experiments. This effect was relevant for erosion in two steps. Initially, these turbulent burst results in shearing of lumps of sand within the top of the sand bed and subsequently, these burst cause the entrainment of the sediment into the main flow. Due to the presence of these sweeps it is confirmed that the erosion takes place as a result of a bulk of sand shearing in a plane in the bed, instead of shearing of grain layers. Consequently, the sand bed is locally affected by turbulent normal wall stresses leading to a contracting part in the sand bed and thus relatively higher excess pore water pressures and liquefaction.

The hindering effects of erosion at higher flow velocities and concentration were attributed by Bisschop (2018) to the shear resistance of a plane subjected to vertical stresses, the effect of excess pore water pressures in the dilating plane on shear resistance and inertia effects. The latter since a bulk of eroded sand particles needs to be accelerated to the average flow velocity. The effects of liquefaction were not included in the derivation of the model of Bisschop (2018). The derived pick-up function is given in equation 5.26.

$$\boxed{E = \frac{0.5 \cdot h_s \cdot \lambda_s \cdot (1 - n_i) \cdot \rho_s}{T_B}} \tag{5.26}$$

In which h_s is defined as the thickness of the sheared layer and can be calculated using equation 5.27. n_i is the in-situ porosity, ρ_s the density of the sediment and T_b is defined as the mean bursting period. λ_s is defined as the averaged area of all sweeps per unit of bed area, which can be regarded as $0.5 \cdot \lambda_b$. Where λ_b is the area of

bursts per unit area.

$$h_s = \frac{(p' - \sigma_a) \cdot \tan(\pi/4 + \varphi/2)}{N_\gamma \cdot g \cdot (\rho_i - \rho_f + i \cdot \rho_f)} \tag{5.27}$$

In which p' is defined as the turbulent normal wall stress and can be calculated using equation 5.28. σ_a is the extra stress required to be exerted by a sweep on a sheared mass for it to accelerate to the depth-averaged flow velocity above the bed. φ is the internal friction angle of the sediment. N_γ is a constant related to the soil strength, g is the gravitational acceleration. The hydraulic gradient caused by the flow inward the bed is given as i and can be calculated using equation 5.30 as used by van Rhee (2010). Lastly, ρ_i is defined as the in-situ density, ρ_f as the density of the water.

$$p' = 0.5 \cdot \rho_f \cdot \hat{w}^2 \tag{5.28}$$

Where, $\hat{w}$ is defined as the average vertical velocity due to the turbulent bursts. This velocity is a function of the bed shear velocity and can be estimated with $\hat{w}^2 = 1.0 \cdot u_*$ (de Hoog, 2021). For σ_a equation 5.29 can be used.

$$\sigma_a = h_s \frac{u_*}{2T_B} \rho_s \left(1 - n_i\right) \tag{5.29}$$

The hydraulic gradient as used by van Rhee (2010) is given as:

$$i = \frac{v_e}{k_{\max}} \cdot \frac{n_{\max} - n_i}{1 - n_{\max}} \tag{5.30}$$

In dredging engineering applications the erosion velocity is comparable to the horizontal or active wall velocity (Bisschop, 2018). Hence, the erosion velocity can be estimated to be equal to h_s/T_B. When this estimation is implemented into the above equation it results in equation 5.31.

$$i = \frac{h_s}{T_B k_{\max}} \cdot \frac{n_{\max} - n_i}{1 - n_{\max}} \tag{5.31}$$

The soil strength constant, N_γ, can be calculated using equation 5.32.

$$N_\gamma = 0.5 \cdot \left[\left(\frac{1 + \sin\varphi}{1 - \sin\varphi} \right)^{5/2} - \left(\frac{1 + \sin\varphi}{1 - \sin\varphi} \right)^{1/2} \right] \tag{5.32}$$

While Bisschop (2018) stated that the thickness of the sheared layer, h_s, needs to be solved iteratively due to the presence of h_s in equation 5.31, de Hoog (2021) was able to transform equation 5.27 in to an explicit equation by substituting equations 5.29 and 5.31 in to equation 5.27. This greatly reduces computational time when using numerical solvers as it results in a second order parabolic equation, which can be solved analytically. The result is shown in equation 5.33.

$$h_s = \frac{-C_1 + \left(C_1^2 + C_2\right)^{0.5}}{C_3} \tag{5.33}$$

In which C_1, C_2 and C_3 are representing soil specific and fluid flow acting on the bed surface variables and can be computed as:

$$C_1 = \frac{\rho_s}{2} \cdot (1 - n_i) \cdot \frac{u_*}{T_B} \cdot \tan(\pi/4 + \varphi/2) \tag{5.34}$$

$$C_2 = \frac{4}{T_B k_{\max}} \cdot \left(\frac{n_{\max} - n_i}{1 - n_{\max}} \right) \cdot N_\gamma \cdot g \cdot \rho_f \cdot p' \cdot \tan(\pi/4 + \varphi/2) \tag{5.35}$$

$$C_3 = \frac{2}{T_B k_{\max}} \cdot \left(\frac{n_{\max} - n_i}{1 - n_{\max}} \right) \cdot N_\gamma \cdot g \cdot \rho_f \tag{5.36}$$

The newly derived equation for h_s can be substituted in equation 5.26, which results in a explicit function.

Based on the experiments and the outcomes of Bisschop (2018) the old sediment pick-up function of van Rijn (1984a) was recalibrated by van Rijn et al. (2019). To account for the high flow velocity regime and the dilatant behaviour of the soil at these velocities an additional damping parameter, f_D, is introduced. This factor comprises of the effects that occur in this high velocity range. This includes the most relevant processes of increasing

kinematic viscosity, damping of the turbulent bursts near the bed and the dilatant behaviour of the top of the sand bed. The new pick-up function is given in equation 5.37.

$$\boxed{E = \alpha \rho_s \sqrt{(s-1) g D_{50}} \, (D_*)^{0.3} \, f_D \left[\frac{\theta' - \theta_{cr}}{\theta_{cr}} \right]^{1.5}} \tag{5.37}$$

The damping factor can be calculated with equation 5.38. The parameter α has a value of $0.0033 \pm 30\%$. The above mentioned pick-up function is only valid for clean sediment that is sufficiently densely packed. Furthermore, the sediment should not contain clay particles. The porosity needs to be in the range of 0.37 to 0.43. In the above equation f_D is only related to the grain Shields parameter, while in reality it also has a relation to the porosity, permeability and dilatancy parameters of the sand (van Rijn et al., 2019). If these effects need to be included, the altered Shields parameter of van Rhee (2010) can be used instead. Based on computations using the pick-up function, van Rijn et al. (2019) stated that the damping parameter needs to be improved to come to more accurate results, as the differences using equation 5.37 is in the order of a factor 2 for the high velocity range with the measured values from the experiments of Bisschop (2018). The only exception was for very fine sediment of 51 μm.

$$f_D = \begin{cases} 1/\theta', & \text{if } \theta' > 1 \\ 1, & \text{if } \theta' \leq 1 \end{cases} \tag{5.38}$$

5.7 Hindered Erosion

During flow velocities for which $\theta_b < \theta_{cr}$ the tendency of the sediment is to settle towards the bottom, at this point the concentration profile is not in an equilibrium (van Rhee & Talmon, 2010). In such flow conditions a growing bed is to be expected as the flow is not sufficiently capable of transporting sediment.

Based on turbulent eddy burst over a bed, Cao (1997) derived a pick-up function that essentially could describe the pick-up rate at higher concentrations. However, the calibration of Cao (1997) was done based on the dataset of van Rijn (1984a). The latter experiments were carried out with concentrations up to 5%, making the calibration of the pick-up function of Cao (1997) for higher concentrations ambiguous.

Based on the concept of the turbulent eddy bursts the influence of the near bed-concentration on the sediment pick-up is included (van Rhee & Talmon, 2010). Presuming that the turbulent eddy picks up sediment at the bed with a concentration of $1 - n_0$, the eddy has to transport the same volume of water and sediment back to the bed surface. In case the near bed concentration is low, the returning flow contains sediment. For higher concentrations the eddies will return sediment to the bed. At the upper limit a situation is present where the near bed concentration equals the bed concentration and therefore no net sediment transport as a result of the turbulent eddies. From this reasoning van Rhee and Talmon (2010) created a reduction factor to include the effect of the near-bed concentration on the pick-up flux. This inclusion and further normalisation to the data found using the experiments done by van Rhee and Talmon (2000) leads to the pick-up function as given in equation 5.39.

$$\Phi_p = 0.0025 \, (D_* - 2.4)^{0.3} \left[\frac{1 - n_0 - c_{nb}}{1 - n_0} \right] \theta_b \tag{5.39}$$

Using the same method as for other pick-up functions, the above equation can be substituted in equation 5.17 resulting in equation 5.40.

$$\boxed{E = 0.0025 \, (D_* - 2.4)^{0.3} \left[\frac{1 - n_0 - c_{nb}}{1 - n_0} \right] \theta_b \cdot \rho_s \sqrt{\Delta g D_{50}}} \tag{5.40}$$

5.8 Concluding Remarks

Considering the process of sedimentation and erosion simultaneously results in a bed interface that can be modelled as an upward or downward moving interface. In the specific case that the interface moves downward the velocity thereof can be calculated using equation 5.12.
In this equation the sedimentation flux (S) can be calculated using the principle of hindered settling by Richardson and Zaki (1954). During the experiments the density and the porosity of the sediment are known and the near bed concentration can be measured or estimated. Hence, the remaining unknown in the equation is the erosion flux. Wherefore, several pick-up functions have been described elaborately in this chapter. Between these pick-up equations some major differences can be distinguished, which is touched upon in this section.

Firstly, one of the most known pick-up functions, the one of van Rijn (1984a) was specifically developed for fluvial flow and for low Shields numbers. This made the applicability to slurry flow, with high Shields numbers and high concentrations arbitrary. As showed by multiple studies, such as the ones from van Rhee and Talmon (2000); Winterwerp et al. (1990) and van Rhee (2010), the pick-up function of van Rijn (1984a) overestimates the erosion flux for high flow velocities.

Therefore, new adjusted pick-up functions were desired to be able to adequately estimate the pick-up flux for these conditions. Winterwerp et al. (1990) was one of the first to study the influence of the concentration on the erosion flux. Further assessing the influence of the concentration on the erosion flux Winterwerp et al. (1992) found a new relation that would better estimate the erosion in mixture flow of high concentrations.

van Rhee (2010), conducted research in the dilatancy reduced erosion regime. van Rhee (2010) essentially adjusted the pick-up function of van Rijn (1984a) to account for the dilatant behaviour of the grains. Theretofore, he adapted the critical shields parameter with soil specific parameters such as the permeability and the porosity. This new pick-up flux was able to match the measurements of old data sets more accurately, while also competently matching the results for the pick-up flux in lower flow velocities, so for the grain-by-grain erosion regime. Unfortunately the new derived equation was an implicit function where the dilatant behaviour of the soil was determined by the erosion velocity itself. This requires numerical methods to solve the erosion velocity from the pick-up function.

For the hindered erosion regime van Rhee and Talmon (2010) incorporated additional reduction factors to account for the effects of reduced pick-up due to the near bed concentration. For this they used the theory of turbulent bursts by Cao (1997) as a base. As a result of these bursts, sediment is not only entrained in to the flow, part of the sediment is returned back in to the bed layer as well. This process of returned sedimentation hinders the pick-up of new sediment, hence reducing the pick-up flux.

For the dilatancy reduced erosion regime, Bisschop (2018) integrated sediment bulk properties to adequately agree with the physical processes at high flow velocities. In this regime the sediment is most likely to be sheared away in layers, where not only permeability and porosity play a significant role but the height and strength of the sheared layer are considerable as well. These sheared layers were the result of turbulent bursts picking up material and the entrainment of the picked up material in to the flow. Bisschop (2018) stated that the height of the shear layer was required to be solved iteratively. However, de Hoog (2021) was able to transform the equation for the height of the sheared layer by substitution of equations 5.29 and 5.31 in to equation 5.27. The result was an explicit function which can be solved analytically, hence greatly reducing its computational time in numerical models.

Based on the outcomes of the research of Bisschop (2018), van Rijn et al. (2019) adjusted his older pick-up function (van Rijn, 1984a) to better account for the dilatant behaviour of soil. This to reduce the overestimation of the pick-up flux of van Rijn (1984a) for high flow velocities. Therefore, a damping factor was implemented which depending on the Shields parameter is 1 if $\theta' \leq 1$ or calculated as $1/\theta'$ if the Shields is larger larger than 1. For the new pick-up function to be valid the porosity needs to be in the range of 0.37 to 0.43. If the dilatant behaviour of the soil is to be incorporated the Shields parameter of van Rhee (2010) should be used instead (van Rijn et al., 2019). Furthermore, van Rijn et al. (2019) argued that the damping parameter requires some improvement as the calculations differ substantially from measurements of the experiments of Bisschop (2018).

II

Experimental Study

6

Setup of the Experiments

To be able to answer the research question posed for this thesis an experimental study is carried out. The experiments are designed specifically to be able to assess the erosion sedimentation balance at high concentrations. The loop was originally designed to be able to assess the difference between the transport rate in a vertical and horizontal loop as well. Hence, the loop consists of a vertical part and a horizontal part. In this manner the mismatch in transport capacities could be researched as well as the unbalance of erosion and sedimentation balance at high concentrations behind a bend in the vertical plane. The latter experiments were performed and the setup for that is explained in this chapter.

6.1 General Properties of the Experimental Loop

The setup consists of a loop orientated in the vertical plane with a horizontal measuring section. The choice is made for an open loop design to be able to prevent any closed loop effects. This is done by discharging the slurry in a sedimentation tank and letting the sediment settle, while reusing the water. As it is the intention to send a density wave through the main circuit a secondary loop is constructed to be able to ensure a homogeneous developed slurry with a specific concentration. The actual design and experimental process is explained more deliberately later on in this chapter.

6.1.1 *General Dimensions of the Loop*

The loop is designed to test the hypothesis of the unbalance between erosion and sedimentation at high concentrations, in figure 6.1 the setup is shown without the support frame. In section 6.3 the measuring equipment is indicated to give the complete overview, see figure 6.5. The most important dimensions of the experimental measurement loop are given in table 6.1

Table 6.1: General dimensions of the experimental loop

	Value	Unit
Volume sedimentation tank	125	L
Volume bypass mixing loop	8.3	L
Internal pipe diameter	40	mm
Length Horizontal Measurement Section	2.0	m
ΔL for pressure difference over ERT	0.65	m
ΔL for pressure difference u-tube	0.7	m

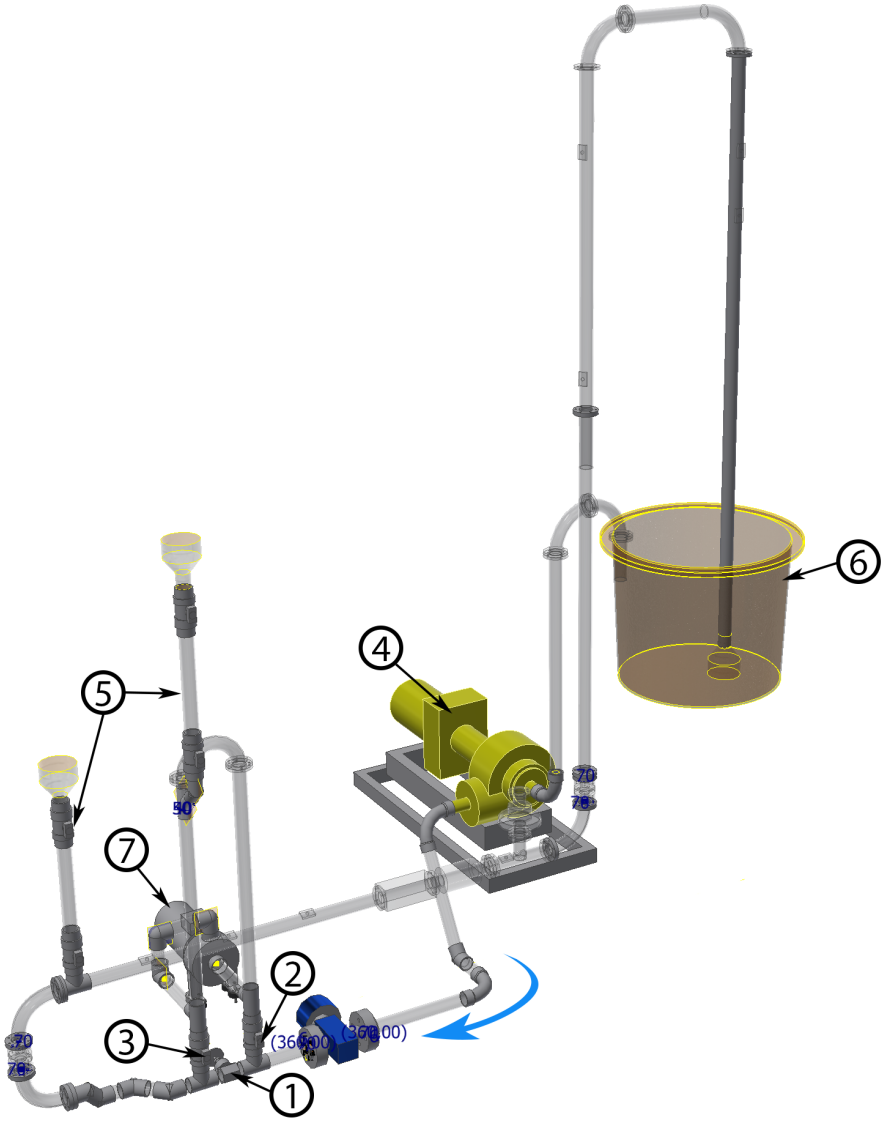

Figure 6.1: The setup of the experimental loop with the important equipment labelled, the support frame is removed from the image. **1.)** Ball valve; **2.)** Gate valve 1; **3.)** Gate valve 2; **4.)** Main pump; **5.)** Filling tubes; **6.)** Sedimentation tank; **7.)** IHC pump;

6.1.2 *Measuring Equipment*

To be able to observe the changes of the bed in the measurement section specific equipment is used to visualise and/or measure these changes. In this section the function of the equipment is described as well as the reasoning behind the usage thereof. For the experiments the data acquisition system includes a *Dewesoft SIRIUS E* unit with accompanying *Dewesoft X* software to initially visualise the results and the *ITS Z8000* system with *ITS Toolsuite* software.

Electrical Resistance Tomography (ERT)
An ERT can be used to visualise the slurry flow through the horizontal measurement section. Making use of the electrical resistance of the carrier fluid and image reconstruction techniques a two dimensional image can be constructed (Giguère, Fradette, Mignon, & Tanguy, 2008). This represents a map of the electrical conductivity of the slurry over the cross-section. One of the applications of the ERT is to construct a concentration profile over the cross-section, which can be used to determine the flow regime (Faraj, Wang, & Jia, 2013; Giguère et

al., 2008). However, Faraj et al. (2013) found that the difference between a sliding bed regime and a stationary bed regime is quite hard to be distinguished based on an ERT image. Yet, in combination with a high speed camera this can be a useful tool to determine the prevailing flow regime. The erosion and sedimentation balance requires the near bed concentration as an input parameter, which can be determined using the ERT.

Besides the near bed concentration the bed height is required for the physical modelling part of this research. Knowing that the ERT measures in a 20x20 grid, with only 316 of these grid cells active, the rows of the grid can be used to find a mean value for the concentration at a specific height from the bottom of the pipeline. The exact process is explained more elaborately in chapter 7. The ERT used for the experiments is an *ITS Z8000*. For the visualisation of the results the associated software *ITS ToolSuite* is used. Further post-processing of the ERT data is done with MATLAB.

Conductance Concentration Meter (CCM)
The volumetric concentration of the slurry is measured in front and behind the measurement section. Since there is a stationary bed in the measurement section the erosion rate at a certain concentration can be measured directly. As the sediment passes the conductivity of the fluid decreases. To be able to determine the concentration over time the characteristic of the sensors when measuring conductivity is required first. The method for this is explained in appendix A.

When using the CCM it should be noted that the conductivity of the fluid is highly dependant on the fluid temperature and the amount of dissolved salts. For the temperature, a reference measurement before the start of each experimental can be done to exclude the effect of the temperature. Since the experiments take place in a circuit with an open end and the fact that the measurements concern transient flow phenomena the influence of the temperature is expected to be small to negligible. This is checked during the experiments nevertheless to be sure.

The salts however are expected to be of greater influence as quite a lot of sediment is needed for each run. During high concentrations more salts are expected to be dissolved in the water. By washing the sediment a lot of these salts may be removed. This is one of the first steps that have been taken to prevent the influence of the salt. Secondly, during mixing in the bypass loop tap water is constantly added until the water flowing out of an overflow valve has the desired conductivity. In this way, the influence of the salts is minimised.

For the calibration of the CCM's regarding the volumetric concentration, two methods can be used. The first method is quite simple, where the CCM units are filled with tap water and a known volume of sediment. The unit is then closed with blind flanges. While the sediment is settled the carrier fluid conductivity is measured, then during shaking of the CCM unit the sediment becomes suspended and the mixture conductivity is logged and measured. Thereafter the ratio of the mixture conductivity and the fluid conductivity can be computed. Since the volumetric concentration is known a plot can be made and the values can be compared to the exponential, Archie et al. (1942) and Maxwell equation, see equation A.9, A.10 and A.11, respectively.

When using the CCM to determine the volumetric for coarse slurry flows with a grain size of $d/D>0.1$ van Wijk and Blok (2015) concluded that extra calibration was necessary. While a whole range of grain sizes is used in the experiments, the condition of $d/D>0.1$ is not exceeded. Therefore the actual value of ζ needs to be derived from the calibration points. For each of the five different sand types the outcomes have been compared to the equations mentioned in appendix A (equations A.9, A.10 and A.11). Using the linear regression fit method on the found data points, the best values for ζ and ζ_2, have been calculated as well. These values are summarised in table 6.2.

Table 6.2: Calibration values for ζ and ζ_2

	CCM1		CCM2	
Sand type	ζ	ζ_2	ζ	ζ_2
Dorsilit nr.5G	0.7713	1.141	-	-
Dorsilit nr.7	0.7738	1.1897	0.8525	1.1226
Dorsilit nr.8	0.9	1.005	-	-
Zilverzand	0.7281	1.2088	-	-
GEBA	1.2729	0.8549	-	-

Note: The empty rows for CCM2 are there due to the fact that a lot of inconsistencies were found for the calibration exponents. This caused a lot of uncertainties and rendered the applicability of the CCM's only as a qualitative tool instead of quantitative. This is explained in more detail in section 7.2.3.

High speed camera

To assess the flow characteristics a high speed camera is used to be able to determine the velocity profile in the horizontal measurement section. In combination with the results from the ERT the prevailing flow regime can be determined. Moreover, other important velocities, such as the deposit limit velocity and critical velocity can be determined via visual observation as well, though the importance thereof might be marginal. The images are made with an *Optronic CR600x2* at a frame rate of 750 frames per second, for the use of this specific camera the *Timebench 2.6.30* software package is required.

Flow meter

The flow meter can be used to measure the mean flow rate, which in combination with the high speed camera can be used to determine the important velocities which are required to be determined using visual observations. The mean flow rate in the loop is measured using a electromagnetic flow meter, specifically the *Endress+Hauser PROMAG 55S*. The settings are chosen so that the reaction time and logging delay are minimal, this ensures a very responsive logging signal that is able to show the current flow velocity with sufficient accuracy. This is required since the experiments regard transient slurry flow phenomena where the importance of fast data logging is key. This provides adequate insight in the actual flow velocity which is subject to influences of the bed. Moreover, switching the gate valves extends the length of the loop and introduces a mixture into the loop, which both increase the resistance of the flow. Putting even more emphasis on the importance of a quickly responsive flow meter. Since the 2LM requires the mean slurry flow as input parameter this can be used for the physical modelling part.

Differential Pressure sensors

For the pick-up functions of van Rhee and Talmon (2010) and Bisschop (2018) the Shields parameter is based on the bed related hydraulic diameter. The latter can be determined using the bed shear stress which is related to the pressure loss over the bed. Therefore the difference in pressure is measured over the bed within the ERT to be able to determine the bed shear stress and subsequently calculate the bed related hydraulic diameter. The differential pressure sensor is a *Rosemount DP3*, with a range of - 1 kPa to 1 kPa.

Both Pugh and Wilson (1999) and Vanoni and Brooks (1957) described methods to acquire the effective bed friction based on a method that takes the total loss of force along the top of the bed and walls of the measurement section into account. This loss of force can be related to the pressure drop over the length of the measurement section. The key difference between these two methods, is how the wall friction coefficient is calculated.

U-tube

By the application of a U-tube section the delivered concentration (C_{vd}) can be determined continuously throughout the experiments. This can be done by determining the pressure difference between two points on the up-going riser pipe segment and two points on the down-going pipe segment. This concept was first suggested by Hagler (1956) to determine the density and thus concentration. When measuring upward flow and downward flow the frictional pressure can assumed to be equal in contribution and independent on the solids concentration. This principle for the experiments is shown in figure 6.2

Applying the equation of Bernoulli and assuming that the wall friction can be eliminated as these are equal for both the ascending and descending section van Grunsven and Talmon (2012). Furthermore, measuring the values

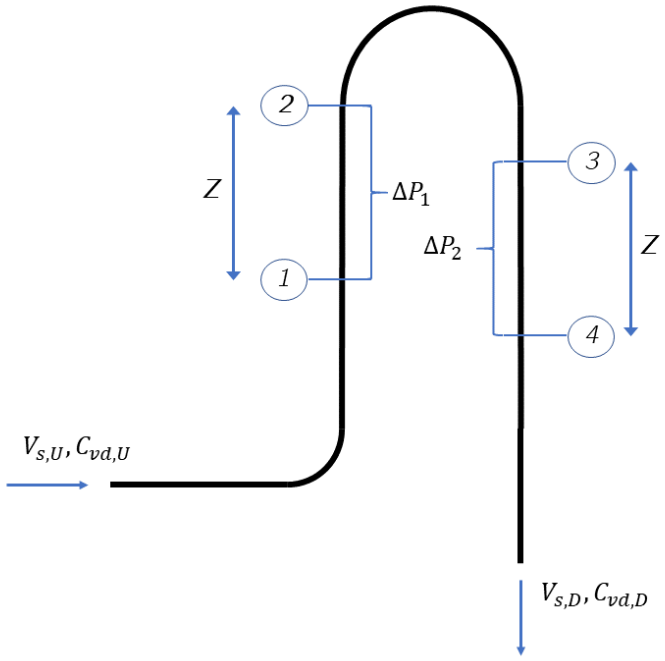

Figure 6.2: Principle of the u-tube section to measure the delivered concentration in the setup for the experiments.

for ΔP_1 and ΔP_2 and using equation 6.1, the mixture density can be calculated. This requires the assumption that the particle settling velocity is equal for the upward and downward section.

$$\rho_m = \frac{\Delta P_1 + \Delta P_2}{2 \cdot g \cdot Z} \cdot \rho_f \tag{6.1}$$

In which, ρ_m is the mixture density, ΔP_1 the pressure loss in the ascending section, ΔP_2 the pressure loss in the descending section, g the gravitational acceleration, Z the distance over which the pressure loss is measured, which is 0.7 m in the experimental setup and ρ_f the fluid density. The pressure loss is measured using a *Rosemount DP3*, with a range of - 0 kPa to 7 kPa in the ascending pipeline section and a *Rosemount DP3*, with a range of - 1 kPa to 6 kPa in the descending pipeline section. Subsequently, equation 3.11 can be used to determine the delivered concentration, equation 3.11 is repeated below for clarification.

$$C_v = \frac{\rho_m - \rho_f}{\rho_s - \rho_f}$$

Due to the influence of hindered settling as found by Richardson and Zaki (1954) the settling velocities in the different segments are not precisely equal, since Leung, Wiles, and Nicklin (1969) proved that the Richardson-Zaki correlation was applicable to vertical hydraulic transport. For the applicability of hindered settling to be valid, the condition was that the volumetric concentration should not exceed 50-55%. Clift and Clift (1981) mathematically determined the error connected to the hindered settling principle for coarser slurry flows for the delivered volumetric concentration when using the u-tube method.

6.1.3 *Deposit Limit Velocity*

During the experiments the erosion is expected to be heavily dependent on the flow velocity. The velocity however needs to be chosen such that the bed is not fully eroded when the mixture passes. It is therefore chosen to keep the velocity as close to the V_{sm} as possible. Note should be made that no flow control is implemented, therefore adequate assessment of the influence of the flow velocity is impossible as a varying flow velocity is to be expected during the experiments. Using equation 3.8 figure 6.3 can be calculated.

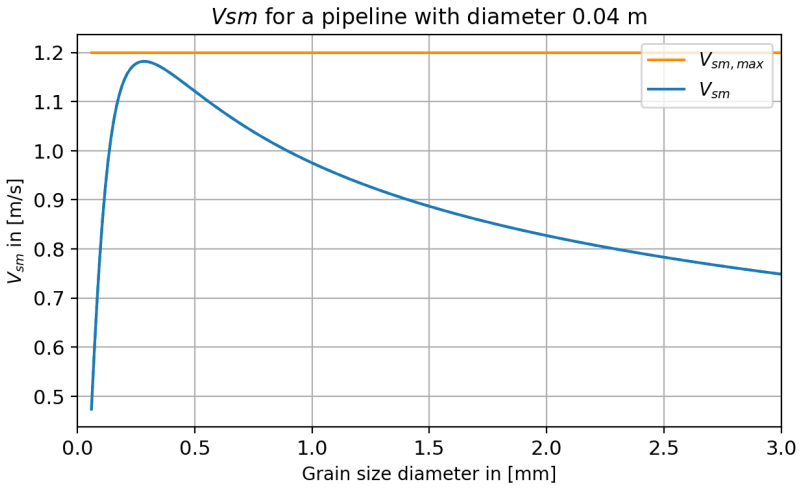

Figure 6.3: The values for V_{sm} at different grain sizes.

Based on the calculation it is aimed to have the mean flow velocity around the blue line drawn in the above mentioned figure. This is the velocity range in which erosion and sedimentation is expected to be heavily present at the same time. This creates the perfect circumstances to investigate the sedimentation and erosion unbalance.

6.2 Sediment Properties

For the experiments several sand types are used to study the influence of the grain size on the erosion rate. Where Bisschop (2018) used mostly really fine sand to investigate the dilatant reduced behaviour of erosion, this thesis tries to study the extent of the applicability of the different pick-up functions for other grain sizes. Therefore, the properties of the sand types used for the experiments are elaborated in this section. The types of sand are listed below in order of coarse to fine:

- Dorsilit nr.5G: 1.6-2.5 mm
- Dorsilit nr.7: 0.6-1.2 mm
- Dorsilit nr.8: 0.3-0.8 mm
- Sibelco Zilverzand
- GEBA FG: 0.06-0.3 mm

All the sand types have been washed thoroughly to remove the fines and salts as much as possible.

First of, the grain size distributions of the types are determined using a sieve tower in the Dredging Laboratory of the TU Delft. Using the method described by NEN-EN:993-1 (2012) the grain size distributions as shown in figure 6.4 are found.

Based on the grain size distribution found as above the most important grain sizes can be quantified. The values thereof are given in table 6.3. These values are of importance for the physical modelling part as the bed roughness and pick-up fluxes are often modelled as a function of the D_{90} and D_{50}, respectively.

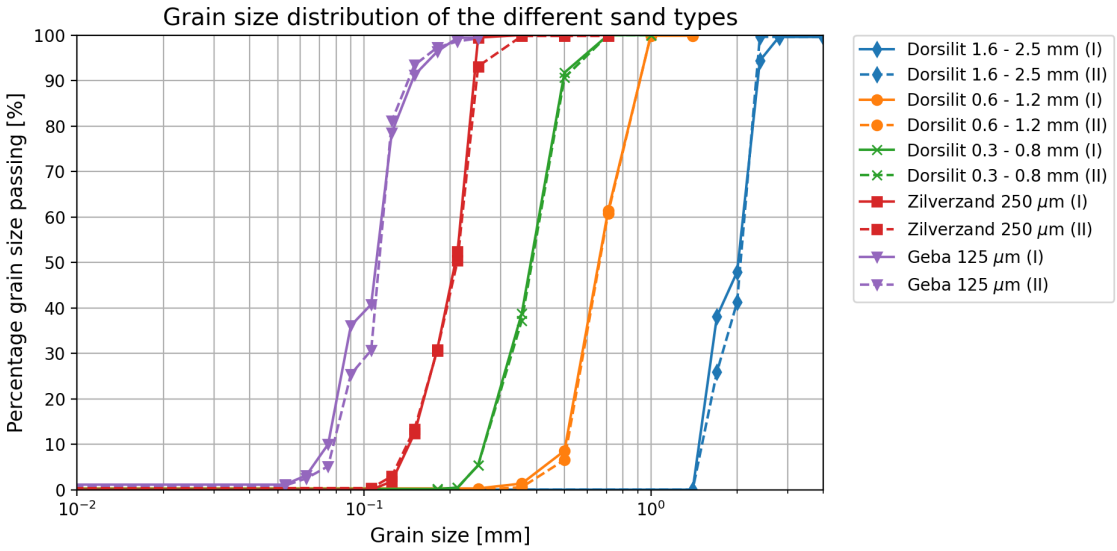

Figure 6.4: Sieve curves of the different sand types.

Table 6.3: Characteristics of the different sand types

Sand type	Grain size in [mm]					Porosity [-]	
	D_{10}	D_{15}	D_{50}	D_{60}	D_{90}	n_{min}	n_{max}
Dorsilit nr.5G	1.500	1.548	2.040	2.120	2.350	0.360***	0.520***
Dorsilit nr.7	0.510	1.530	0.667	0.706	0.927	0.360**	0.520**
Dorsilit nr.8	0.266	0.282	0.388	0.416	0.4975	0.366*	0.475*
Zilverzand	0.144	0.154	0.210	0.220	0.245	0.370*	0.470*
GEBA	0.077	0.080	0.112	0.117	0.146	0.370*	0.560*

*These values have been retrieved from Bisschop (2018)

**These values have been retrieved from Bianco, Higuita, Tosco, Tiraferri, and Sethi (2017)

***These values are assumed to be approximately equal to that of Dorsilit nr.7

Moreover, based on the found values for D_{15} and the porosity the permeability can be calculated using the equation of den Adel (1987). While this equation is quite known in the Dutch engineering sector it is not commonly known outside of the Netherlands, as stated by van Rhee (2010). Though the applicability appears to be quite adequate. van Rhee (2010) showed that based on experiments reported by van Rhee and Bezuijen (1998), equation 6.2 yielded good results.

$$k = \frac{g}{160\nu} D_{15}^2 \frac{n_0^3}{(1-n_0)^2} \tag{6.2}$$

Based on the aforementioned equation the values for the maximum permeability can be calculated if instead of the initial porosity, the maximum porosity is implemented. This is required for the pick-up equations of van Rhee (2010) and Bisschop (2018).

6.3 Erosion and Sedimentation Unbalance at High Concentrations due to a Density Wave

The experiments are an experimental study into the erosion capacity of highly concentrated mixture flows to research the hypothesis of density wave growth due to an unbalance in the erosion and sedimentation flux. The procedure for these experiments consist of a preparation of a mixture in the bypass mixing loop with volumetric concentration C_v. This results in a situation which is able to resemble a passing density wave. In the horizontal measurement section a stationary bed is placed by filling the top tube with identical sand as is used in the bypass

mixing loop. After opening the valves the material within the bypass is sent into the main loop where the first CCM is able to measure the concentration in time over the cross-section. The mixture velocity is around the maximum limit of stationary deposit, which depends on the grain size diameter. In the horizontal section the pressure difference over the ERT is measured to be able to calculate the bed associated hydraulic diameter to estimate a value for the bed shear stress. This is required for the pick-up flux defined by van Rhee (2010) and Bisschop (2018). An overview of the experimental setup is shown in figure 6.5.

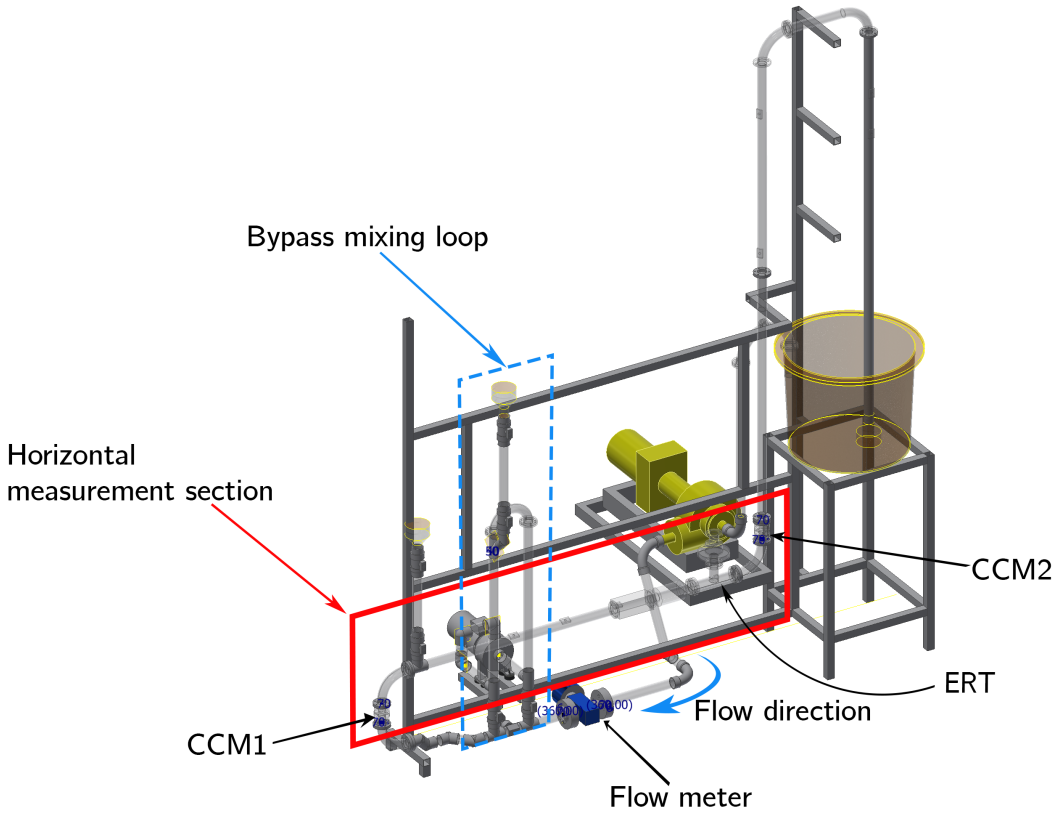

Figure 6.5: Setup of the experimental loop for the erosion experiments with the indications of the measuring equipment

The most important output of the ERT is the near bed concentration and bed height. The measured bed height ($y_{bed,measured}$) is compared to the bed height computed using a numerical model ($y_{bed,computed}$) to verify which pick-up flux is sufficiently accurate to estimate the development of the bed height and thus the pick-up rate. This is done for varying volumetric concentrations between 5% and 30% and each of the sand types mentioned in table 6.3. As mentioned before, the flow velocity is set to be just above the values of V_{sm} as defined by Wilson (1979). However, note that the erosion process regards transient flow phenomena and no flow feedback control is implemented. Therefore, when the mixture is introduced into the main loop a drop in mean flow velocity is expected.

6.3.1 *Experimental Step-by-Step Plan*

To be able to repeat the experiments a detailed step-by-step plan is explained. The valves described in this plan are labelled in figure 6.1.

1. Start by weighing the desired sand type to reach the desired concentration.
2. Close the gate valves of the mixing loop, thus separating the mixing loop and the main loop.
3. Almost fully close the ball valve behind the flow meter, this to ensure that the flow velocity in the horizontal

measurement section is low. That causes the material to be spread as evenly as possible throughout the horizontal measurement section. Subsequently the main pump can be turned on.

4. Depending on the sand type it is preferred to start laying the stationary bed (a) or filling the mixing loop to the desired concentration with the weighted sand (b). While the coarser material is able to quickly mix in the mixing loop it is better to prevent a lot of degradation of the material and opt for placing the stationary bed first. The finer sand however, settles very slow, thus requiring more time for both placing the bed and mixing in the bypass. Moreover, it is more prone to flush with the water when washing, which needs to be prevented as much as possible.

   (a) The horizontal measurement section has to be filled until half of the pipe in the ERT is deposited with sand. This can be visually observed as well as checking the ERT when this is running in the background. Filling of the pipe is done by filling the filling tube of the measurement section with the desired sand type, closing the top gate valve and subsequently closing the lower gate valve. Wait for all the sand to be settled and transported a little more upstream by the flow. No extra compressing measures are taken, hence the bed is likely to be loosely packed ($n_0 \approx 0.4$). Which is desired for the physical modelling part where an assumption is required for the initial porosity of the bed.

   (b) The mixing loop can be filled using the filling tube, while the first material does not require the mixing loop pump to be turned on eventually this will be necessary otherwise the pipeline will be clogged. It is advised to start at low flow velocities, making it easier to wash the sand in the beginning. This can be visually observed by a stratified stationary bed at the u-turn at the top of the mixing loop. Eventually, during adding of the rest of the weighted sand the flow velocity has to be increased to prevent a lot of flushing of the sand.

5. Extra washing of sand in mixing loop such that the conductivity is approximately equal to that of the main loop, which can be measured using a handheld conductivity meter. This to ensure that the measurements by both the CCM's and the ERT are as accurate as possible. Make sure to note the measured conductivity values as these may be needed to correct the values within the *ITS Toolsuite*.

6. When the conductivity of the mixing loop and the main loop are approximately equal, the ball valve needs to be closed fully. Making sure the flow over the bed goes as quickly as possible to zero preventing any premature erosion. Especially the case for the finer material, which erodes very quickly.

7. Shut down the main pump.

8. Close the filling tube of the mixing loop and flushing valve.

9. Ensure the filing tube of the horizontal measurement section is closed as well.

10. Start data acquisition systems and subsequently start main pump

11. Pull on gate valves connecting mixing loop with the main loop and use pedal to shut down the mixing loop pump almost simultaneously

12. When all material is passed though the measurement section, shut down the data acquisition systems. Since some material remained within the mixing loop and the accompanying pump, quick flushing of the loop is required to set up a new experiment.

6.4 Experimental plan

For the experiments different sand types and concentrations are used as input for the experiments. A complete overview of the logged measurements and variables is given in table 6.4.

Table 6.4: Experimental plan with variables and logged measurements during the experiments

Variables		Logged measurements							
Sand type	C_v	V_m	y_{bed}	c_{nb}	$C_{v,in}$ (CCM1)	$C_{v,out}$ (CCM2)	$\frac{\Delta P}{\Delta x}$	C_{vd}	Flow regime
Dorsilit nr.5G	5% 10% 20% 30%								
Dorsilit nr.7	5% 10% 20% 30%								
Dorsilit nr.8	5% 10% 20% 30%								
Zilverzand	5% 10% 20% 30%								
GEBA	5% 10% 20% 30%								

7

Results and Interpretations of the Experiments

In this chapter the results of the experiments are interpreted and elaborated. The results are retrieved via post-processing using both MATLAB and Python. The methods thereof are explained in more detail to provide a complete overview on the process as a whole. The most important results are mentioned in this chapter, though the full data overview is available in the appendix.
To be able to adequately gain insight into the experiments the data retrieved via the different data acquisition systems is required to be processed. Subsequently, the data can be synchronised, and the influences of the volumetric concentration and grain size diameter can be visualised.

7.1 Post-Processing steps for the ERT Data

The concentration profile within the cross-section is determined using two planes measuring the impedance of the mixture with the *ITS z8000* system. The accompanying software *ITS Toolsuite* is used to initially visualise the results. However, for the actual post-processing, the data is exported to *.csv*-files to be able to import the data into MATLAB scripts.

The ERT data is retrieved with a frequency of 64 Hz, which was the maximum possible frequency. While a higher frequency is preferred, especially for transient slurry flow processes, it is expected that the erosion and sedimentation process can be sufficiently reviewed since the maximum flow velocity is around the deposit limit velocity.

7.1.1 *Exporting and Organising the Data*

From the ERT data, the bed height and near bed concentration are the variables which need to be calculated. To be able to do this, one needs to find the concentration profiles over the cross-section first. Regarding the interface of the bed and the subsequent concentration profile data Adler, Sutherland, and Kotze (2019) argued that while more research is needed to prove the validity, their first results showed it may be useful to extract additional information from the data retrieved by the ERT system.

The *ITS z8000* outputs data on a 20x20 grid with only 316 grid cells active. The concentration per grid cell is found in the *ITS Toolsuite* using the Maxwell equation for non-conductive material.

Exporting the concentration data using the *ITS Toolsuite* to a *.csv* file changes the data to a time series of arrays of which the latter have a length of 632 values. So, per time step the length of the array is 632 as two planes were measured. The first 316 values account for the grid cell values of the first measurement plane and the other 316 values account for the grid cell values of the second measurement plane. These two planes can be separated by storing the corresponding values in a new time series array. The indices corresponding to the location of the grid cell in the measurement plane are shown in figure 7.1.

i \ j	1	2	3	4	5	6	7	8	9	10	11	12	13	14	15	16	17	18	19	20
1								1	2	3	4	5	6							
2						7	8	9	10	11	12	13	14	15	16					
3				17	18	19	20	21	22	23	24	25	26	27	28	29	30			
4			31	32	33	34	35	36	37	38	39	40	41	42	43	44	45	46		
5			47	48	49	50	51	52	53	54	55	56	57	58	59	60	61	62		
6		63	64	65	66	67	68	69	70	71	72	73	74	75	76	77	78	79	80	
7		81	82	83	84	85	86	87	88	89	90	91	92	93	94	95	96	97	98	
8	99	100	101	102	103	104	105	106	107	108	109	110	111	112	113	114	115	116	117	118
9	119	120	121	122	123	124	125	126	127	128	129	130	131	132	133	134	135	136	137	138
10	139	140	141	142	143	144	145	146	147	148	149	150	151	152	153	154	155	156	157	158
11	159	160	161	162	163	164	165	166	167	168	169	170	171	172	173	174	175	176	177	178
12	179	180	181	182	183	184	185	186	187	188	189	190	191	192	193	194	195	196	197	198
13	199	200	201	202	203	204	205	206	207	208	209	210	211	212	213	214	215	216	217	218
14		219	220	221	222	223	224	225	226	227	228	229	230	231	232	233	234	235	236	
15		237	238	239	240	241	242	243	244	245	246	247	248	249	250	251	252	253	254	
16			255	256	257	258	259	260	261	262	263	264	265	266	267	268	269	270		
17			271	272	273	274	275	276	277	278	279	280	281	282	283	284	285	286		
18				287	288	289	290	291	292	293	294	295	296	297	298	299	300			
19						301	302	303	304	305	306	307	308	309	310					
20								311	312	313	314	315	316							

Figure 7.1: Grid cell indices and corresponding location in the measurement plane(s) of the ERT, the columns are noted with j and the rows with i

Subsequently, the mean of the concentration values of each row i is computed and stored. So, per time step the concentration profile over the cross-section is now computed. It is assumed that the calculated mean concentration per row is valid at the centre-point of the grid cell. Because the experiments are considering a transient process, the concentration profile are changing significantly over time due to the passing of a mixture and the associated erosion and sedimentation processes. The concentration distribution at different time steps is visualised as shown in figure 7.2.

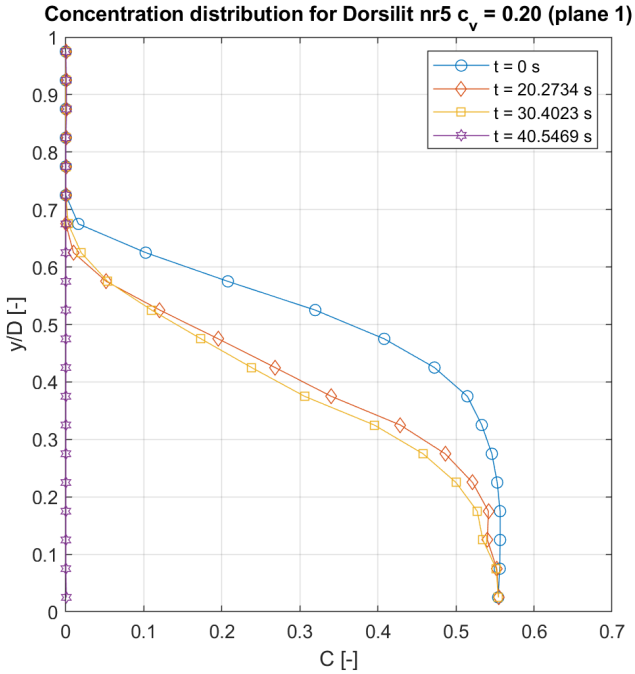

Figure 7.2: Concentration distribution for Dorsilit nr.5G with a passing mixture of $c_v = 20\%$ at different time steps during the sedimentation erosion unbalance experiments. At t = 0 s the ERT starts logging data and at this time, a stationary bed is present within the pipeline with a flow velocity of 0 m/s above the bed.

7.1.2 *Determining the Bed Height*

When the concentration profiles per time step are calculated the bed height can be determined on this basis. First, a value has to be chosen for the concentration to be considered as the bed, here defined as the critical concentration. This is required since at the bottom of the pipeline the concentration appears to be around 55%, though when moving upwards towards the top of the pipeline, the concentration decreases. Even if the flow velocity is zero at t = 0 s, see figure 7.2. This is due to the fact that the grid cells do not exactly match the interface of the bed. Therefore at border cells it is possible that only half of the cells is filled with a concentration of 55%, though when averaging this over the whole cell it results in a value of 22.5% in that specific grid cell.

As a first estimate the critical concentration was set to a of 0.3. Subsequently, a condition to find the first index for which the critical value is exceeded first is programmed. As the diameter of the pipeline is known ($D_{pipe} = 0.04\ [m]$) the height of one grid cell can be computed with: $\Delta y = \frac{0.04}{20} = 0.002\ [m]$. Because MATLAB calculates from left to right the found index indicates the row number from top to bottom. Consequently, the bed height is then calculated using equation 7.1. Once again, it should be noted that it is assumed that the bed height is therefore related to the centre point of the grid cell.

$$y_{bed} = D_{pipe} - i^n \cdot \Delta y + 0.5 \cdot \Delta y \tag{7.1}$$

In which, $\Delta y = 0.002\ [m]$ and i^n is the index of the row at time step n at which the critical concentration value is exceeded first (note that in MATLAB the first index of an array is 1). It is important to note as well that the index calculation will always return an integer. Therefore, this leads to a discrete evolution for the bed height in time. The result of this calculation is shown in figure 7.3, this is done for the experiment using Dorsilit nr.5G with a mixture of volumetric concentration of 20%.

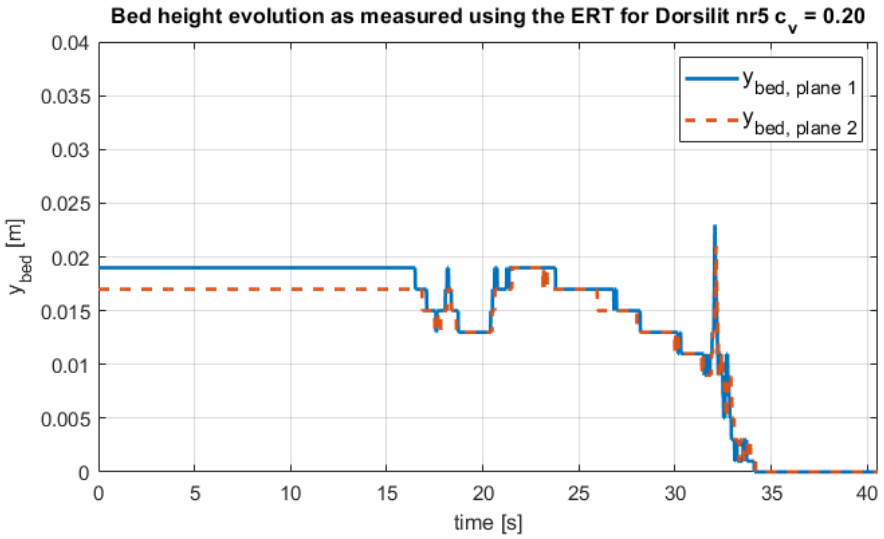

Figure 7.3: Discrete y_{bed} evolution in time due to index integer calculation

Since it is physically impossible to have discrete bed height jumps, adjusting the bed height using linear interpolation between row *i* and *i-1* is required. This linear interpolation is visualised in figure 7.4. Implementing this method the bed height can be calculated more accurately, since the location of the critical concentration is calculated in between the grid cells.

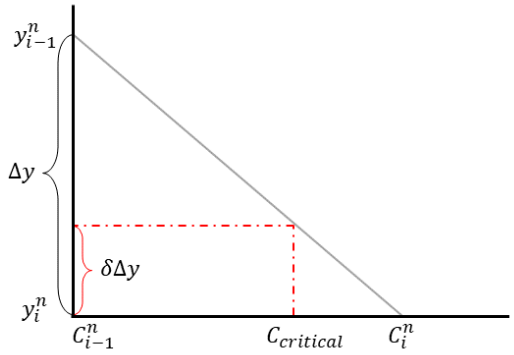

Figure 7.4: Visualisation of the interpolation between the concentration on row *i* and *i-1*

From the interpolation the distance between y_i^n and the y value which corresponds with the critical concentration is calculated. Thus, subtracting this value (denoted as $\delta\Delta y$) from equation 7.1 gives the exact location of the top of the bed, see equation 7.2. Hence, resulting in a smooth evolution of the bed height when this is plotted against the time.

$$y_{bed} = D_{pipe} - i^n \cdot \Delta y + 0.5 \cdot \Delta y - \delta\Delta y \tag{7.2}$$

While doing a more extensive post-processing analysis, the first choice for the critical concentration of 0.3 appeared to be on the low side. This caused fast undesirable changes in the calculated bed height. Therefore, values of 0.35, 0.40, 0.45 and 0.50 were implemented as well to see if this would lead to significant differences. An example of the change in critical concentration is shown in figure 7.5. These figures show the effects for the experiment with Dorsilit nr. 5 with a passing mixture with a volumetric concentration of 30%. Matoušek (2001a) found that for highly concentrated flows, at a local concentration of about 0.35-0.38, the interface of the bed could be found in a sliding bed regime.

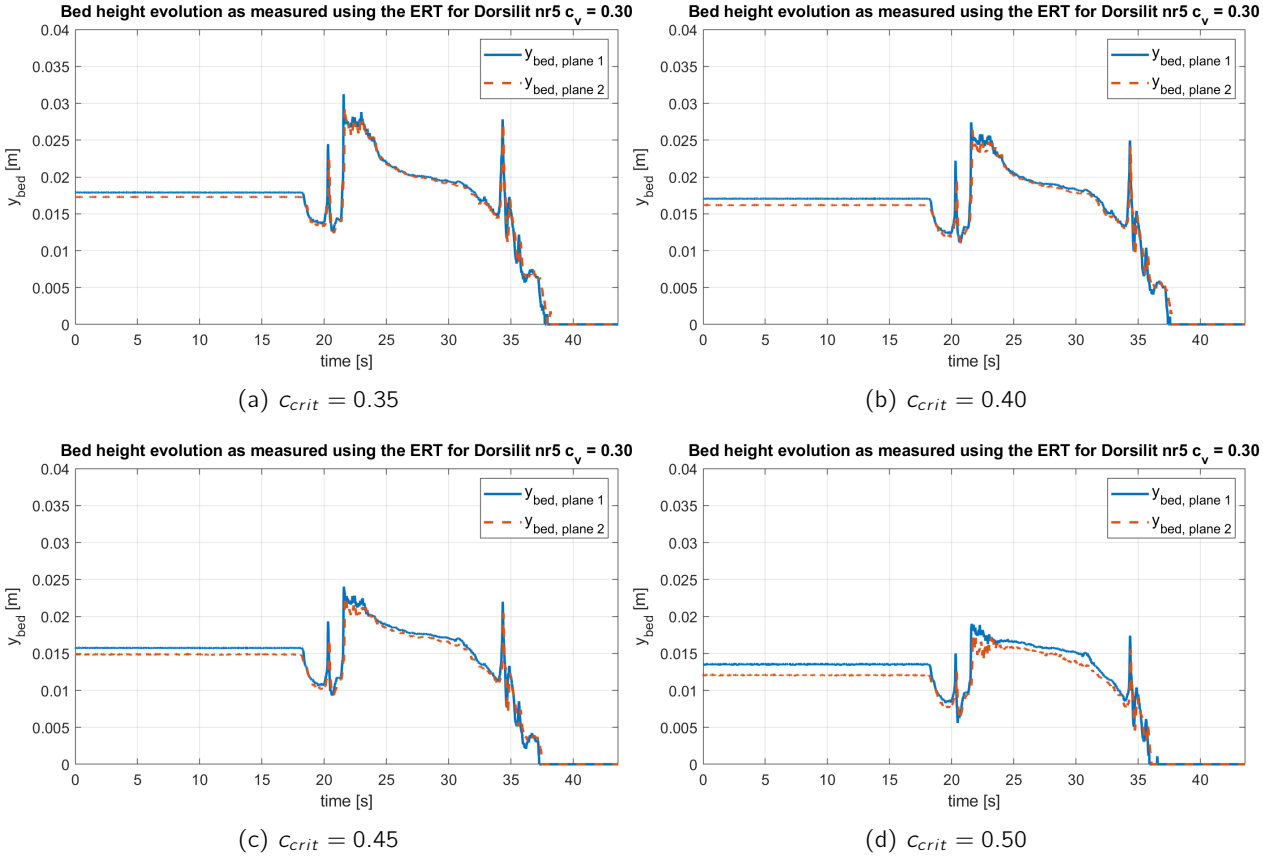

(a) $c_{crit} = 0.35$ (b) $c_{crit} = 0.40$

(c) $c_{crit} = 0.45$ (d) $c_{crit} = 0.50$

Figure 7.5: Effects of different critical values for the bed concentration on the measured bed height by the ERT, using the results of Dorsilit nr.5G with a mixture of a volumetric concentration of 30%

The effects of choosing a different critical concentration are clearly visible and while the most damped results of $c_{crit} = 0.50$ are desirable, the actual bed height does not match the bed heights which were visually observed when preparing the experiments. During the preparations it was opted to fill half of the pipeline cross-section, which was checked by running the ERT system. To have a more damped bed height signal while still remaining close to the original bed height is was opted to set the critical concentration to a value of 0.40. However, inspection for the GEBA experiments showed that a critical concentration of 0.40 resulted in almost no bed at the start of the experiments. This was not in accordance with the visually observed bed height, which was more in compliance with the bed height values when using a critical concentration of 0.30. Therefore, a critical concentration of 0.30 is chosen exclusively for the GEBA experiments.

7.1.3 *Determining the Near Bed Concentration*

The near bed concentration is required for the simulations as the Richardson and Zaki (1954) equation uses the near bed concentration to calculate the sedimentation flux, see equation 5.11. To find the near bed concentration it is chosen to use the concentration values from row *i-1*. However, this results in near bed concentration values very close to the critical concentration values, which may overestimate the near bed concentration. To counter this, while still considering the grid cells close to the bed based on the critical concentration of 40% the mean of rows *i-1* and *i-2* (a height of 0.004 m, which is 10% of the pipeline diameter) is used. This dampens the concentration quite efficiently due to the averaging, which can be considered a positive side effect.

As mentioned before, the ERT returns a somewhat smeared image. At the interface of the bed this can be a problem as it results in a near bed concentration of non-zero, while the flow velocity is zero. A solution would be to consider the ratio of the mean concentration above the bed to near bed concentration, though the correction for hindered settling then requires an extra adjustment in the calculation for the exponent m. Also, at the end of the experiment, when no sand bed remains, the near bed concentration is zero. Thus causing

the aforementioned ratio to go to infinity, resulting in numerical and mathematical problems. For this reason it is opted to use the averaged values of row *i-1* and *i-2* and implementing a condition in the simulation runs to ensure a sedimentation flux of zero at very low flow velocities.

7.1.4 *Upsampling of the Data*

To be able to match the data of the Sirius-E the data has to be upsampled to a common factor. Since the Sirius-E data has been retrieved with a frequency of 100 Hz and upsampling requires a integer multiplication, the first product is found to be 1600 Hz. This higher frequency is achieved by interpolation of the new values upon the old values. In between the old data points new data points are added. Subsequently, the resulting values for the time stamps, measured bed height and near bed concentration are exported to *.txt*-files. These will be imported in a Python script to be able to synchronise the ERT data with the Sirius-E data.

7.2 Post-Processing of the Sirius-E Data

During the experiments the mean flow velocity, pressure difference over the ERT, conductivity of the mixture before and after the horizontal measurement section and the pressure difference in the upward and downward part of a u-turn were measured. These results were logged in a Sirius-E data acquisition system provided by IHC. During the experiments insight in the experiments was visualised by the associated software *Dewesoft X*. In this software the measurement frequency was set to 100 Hz. Also, the logged data can be exported to *.txt*-files for further post-processing. The actual post-processing for the Sirius-E data has been done in Python.

7.2.1 *Mean Flow Velocity*

For the simulations the mean flow velocity is the most important input used from the Sirius-E data, where the *Endress+Hauser PROMAG 55S* measures the mean flow rate at any time at the desired frequency. The flow velocity is calculated within the *Dewesoft X* software using the equation of flow rate, given in equation 7.3 and cross-sectional area of the pipe.

$$V_m = \frac{Q}{A_{pipe}} \tag{7.3}$$

Since A_{pipe} can be easily calculated using the pipeline diameter and the flow rate is measured, the flow velocity is directly calculated thereafter. Therefore, no further processing is required for this signal to be used in the simulations.

7.2.2 *Pressure Difference over the ERT*

During the experiments the pressure difference over the ERT section was measured, in this manner the bed shear stress and subsequently the bed associated hydraulic diameter can be derived. These values could be used in the simulations as directly as input, however they could be indirectly calculated using the flow velocity measurements as well.

When looking into the data acquired by the Sirius-E a lot of high frequency oscillations can be observed. These oscillations are unwanted and can cause (marginal) errors if this data is used in further calculations. Using a Butterworth filter the undesired oscillations in the pressure data are filtered out, remaining is a smooth line that precisely follows the trend of the pressure data.

Where originally the bed shear stress was to be determined using the pressure measurements, the differential pressure transducers over the ERT appeared to exceed their calibrated range quite easily. This lead to a cut off at the maximum pressure for the differential pressure transducers for certain sand types. While the pressure measurement during the experiments with the finer sand types had little to no problems at even the highest concentrations of 30%. The coarser material was subject to exceeding the range of the pressure transducers at lower concentrations as well. An example for Dorsilit nr.5G, the coarsest sand used for the experiments, is shown in figure 7.6.

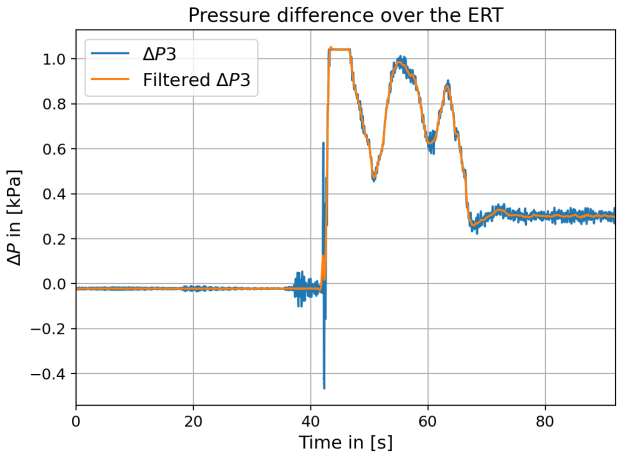

(a) Mixture with $c_v = 0.05$

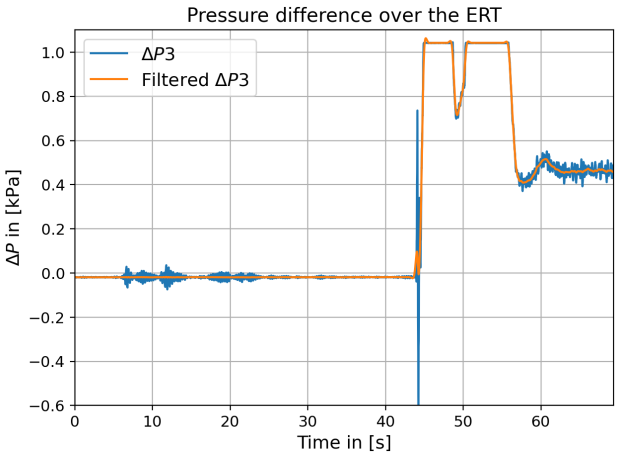

(b) Mixture with $c_v = 0.10$

Figure 7.6: The pressure difference measurements over a length of 0.65 m for Dorsilit nr.5G with a passing mixture with different volumetric concentrations

In figure 7.6a it can be seen that the calibration range is only exceeded at the start of the erosion process. However, the next experiment with a higher concentration (figure 7.6b) already shows a plateau during almost the entire erosion process. Therefore rendering the measurement unusable for further calculations.

As mentioned before, the results for finer sand types are more usable. An example is the measurement for the experiments with GEBA, which is the finest sand used, at the highest concentrations of 20 and 30% is shown in figures 7.7a and 7.7b, respectively.

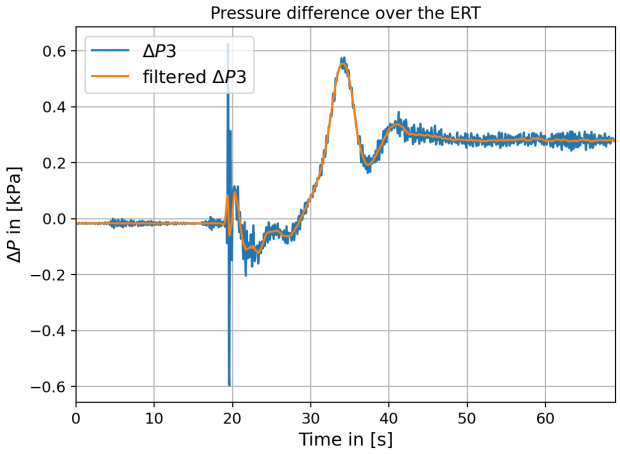

(a) Mixture with $c_v = 0.20$

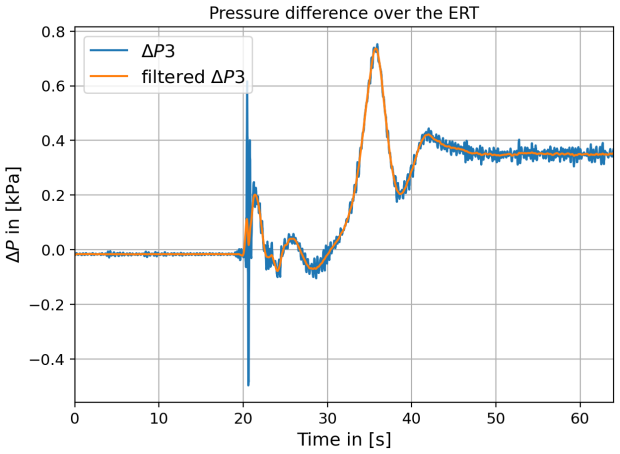

(b) Mixture with $c_v = 0.30$

Figure 7.7: The pressure difference measurements over a length of 0.65 m for GEBA with a passing mixture with different volumetric concentrations

While clearly the results of the finer sand can be used it is however from a consistency point not desirable since only part of the experiments have useful pressure loss data. This would make the direct comparisons between the simulations for different grain sizes and pick-up function incompatible. Therefore, the use of the pressure measurement becomes arbitrary and inconsistent if used during the simulations in the physical modelling part of this thesis. The negative pressure measurements visible in figure 7.6 and figure 7.7 are probably due to the acceleration of the flow when the gate valves are suddenly opened.

7.2.3 *Concentration Measurements*

The measurements regarding the concentration in the pipeline was done at three locations. The first CCM is placed just before the horizontal measurement section, the second CCM is placed right after the horizontal measurement section. Implementing two CCM's means the transformation of the conductivity signal can be studied. The conductivity, if well calibrated, is able to represent the actual volumetric concentration.

While an extensive attempt is made to correctly calibrate the CCM's, it appeared during the calibration runs only one array of conductivity meters is not enough to actually measure the concentration using the mass conservation method as used by van Wijk and Blok (2015). While for one type of sand at a certain flow velocity any exponent of the calibration equations could be changed to fit the data, the exponent had to be alternated for other flow velocities. This made the calibration very inconsistent and unreliable. Therefore, the values found after the calculation serve a indicative purpose. Based on the measurements a qualitative analysis of the transformation of the peaks is still possible, actual quantitative analysis on the other hand is too much of a grey area to be meaningful. The process used to determine the volumetric concentration is explained nonetheless.

The logged data based of the CCM's is returned as conductivity values, the first unit is denoted as k_{CCM1} and k_{CCM2} in the logged data file. The second CCM unit is denoted as the combination of k_{CCM3} and k_{CCM4}. The units are split in two as they are formed by two opposite pairs of conducting sensors in the same cross sectional plane. During the experiments k_{CCM2} appeared to be overestimating the conductivity of the water, the sensors 1,3 and 4 appeared all to be in the same range. The overestimation was found to be relatively constant, thus opting for subtraction of the constant was the most easy method to solve the inconsistency.

The actual method is explained briefly, from all data sets the difference between k_{CCM1} and k_{CCM2} at all time steps is calculated. Then calculating the mean of the difference returns the constant value that needs to be subtracted from the logged k_{CCM2} values. After subtracting that constant value the corrected value is found and these can be used together with the k_{CCM1}. Subsequently, the values for the first CCM unit can be calculated by averaging the signal of k_{CCM1} and the corrected signal k_{CCM2}. Using the same method, this can be done for the second CCM unit as well, however the second unit does not require a correction as the measured values are all in the same order of magnitude. Thereafter, just as the pressure data, a Butterworth filter is applied to reduce the noise in the measured signal. An example of the result for the experiment with Dorsilit nr.5G at a mixture concentration of 10% is shown in figure 7.8.

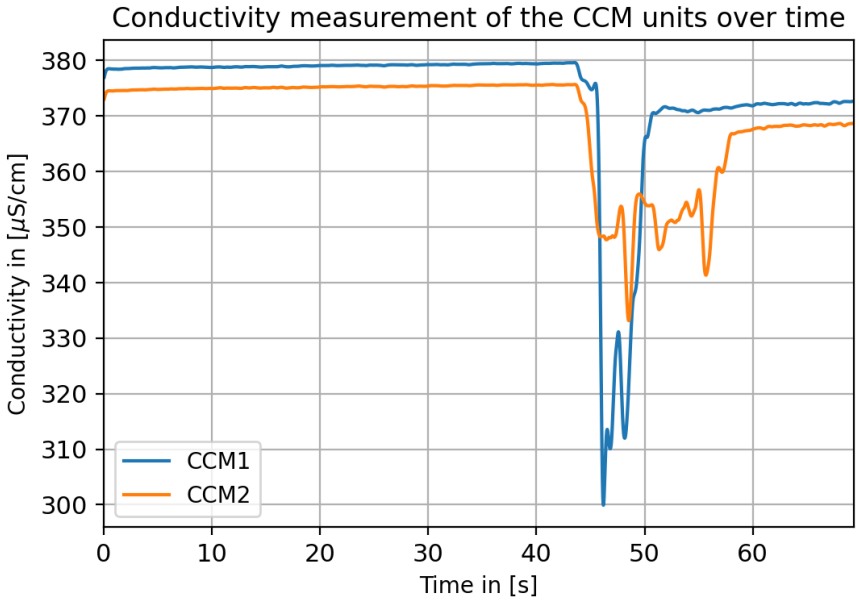

Figure 7.8: Conductiviy measurement retrieved from the Sirius-E data, for the CCM unit before and after the horizontal measurement section, denoted as CCM1 and CCM2 respectively. A Butterworth filter is applied to reduce the noise in the signals

The next step considers a more qualitative inspection of the data. To go from conductivity measurements to

the volumetric concentration, the ratio of the mixture conductivity to fluid conductivity needs to be calculated. By inspecting each data set separately, one can determine whether the fluid conductivity value has to be defined at the start or end of the experiment run.This is done because the conductivity differs slightly before and after the erosion process, as can be seen in figure 7.8. Due to locally charged particles at the probes before the start experiment, and possible remaining salts on the sand particles despite the extensive washing of the material, the conductivity might be higher before the start of the erosion process. When the lowest constant conductivity is observed at the start or end, the average thereof can be calculated to define the value for the fluid conductivity (k_f) of the experiment. When the fluid conductivity is determined, the ratio k_m/k_f is subsequently calculated by dividing all the measured values for each of the CCM unit by the determined value for k_f. Additionally, a condition has to be set to adjust all returned values for $k_m/k_f > 1$. This correction introduces a small error, as part of the signal contributing to the passing mixture, is discarded. Though this error is considered to be marginal.

At last, the concentration calculations are considered. Based on the k_m/k_f ratios and the determined exponent (ζ or ζ_2) for the exponential or Archie et al. (1942) equation, equations A.9 and A.10 respectively, the volumetric concentration is calculated. The result for the experiment run with Dorsilit nr. 5 at a mixture concentration of 20% is shown in figure 7.9.

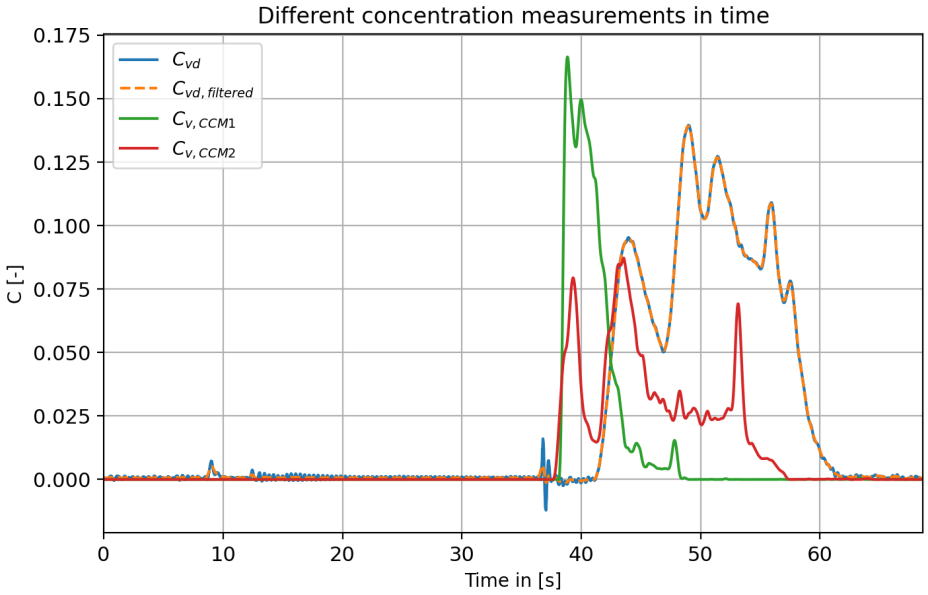

Figure 7.9: Results for the concentration measurements, based on the CCM units and the u-tube. Note that the concentrations based on the CCM measurements are only indicative as the exponents were unable to be determined accurately based on the currently used calibration techniques

The delivered concentration is calculated within the *Dewesoft X* software using equations 6.1 and 3.12. While for steady slurry flow these equations can measure the delivered with high certainty, the application of the u-tube with regards to transient slurry flow phenomena is still unclear. Mostly, due to the fact that the delivered concentration is calculated based on the assumption that both the ascending and descending pipe section are filled with the mixture and this is only the case for part of the erosion process. Due to the fact that the sediment is separated in the sedimentation tank the loop is therefore never completely filled with a mixture.
The beginning of the measurements are therefore a bit arbitrary as only the ascending part is filled with the mixture. The same applies for the end of the experiment, where only the descending part is filled with the mixture.

7.2.4 *Upsampling of the Data Sets*

As mentioned in the previous section where the ERT data was described, the measurements were not retrieved at the same rate. To be able to match and synchronise the data from the ERT and the Sirius-E, the latter

has to be upsampled as well. Since 1600 Hz was the first product with an integer, the Sirius-E data has to be upsampled with a factor 16.

As previously done with the ERT data, the Sirius-E data is also interpolated upon the old data points to reach the desired frequency of 1600 Hz. From the upsampled Sirius-E data the flow velocity and pressure measurements were exported to be used in the simulations.

7.3 Synchronisation of the Data Files

As the ERT data and the Sirius data now have the same frequency, the actual synchronisation of the different data sets is the next step. Looking at the data of the flow velocity one can find that after opening the valves during the experiment an initial dip in velocity is found. While this dip is most likely a numerical error, it can certainly be used to find the time step index of that minimum. It is thought to be a numerical error due to the fact that this dip is only found at a very short time span.

Subsequently, to find the time index at which the valves were opened for the ERT appeared to be a bit harder. Based on the values for the derivative of the bed height, the erosion velocity, not much could be said and it was the same for the near bed concentration. A more qualitative investigation of the bed height data was therefore required. Zooming in on the constant values before triggering the erosion process revealed that only when opening the valves a larger amplitude was exceeded. Defining the amplitude as condition to be exceeded resulted in the time index for the ERT data.

Thereafter, the time indices can be matched for both data sets which by example results in the graph shown in figure 7.10. For the example the data of the experiment with Dorsilit nr. 5 with a mixture concentration of 20% is used.

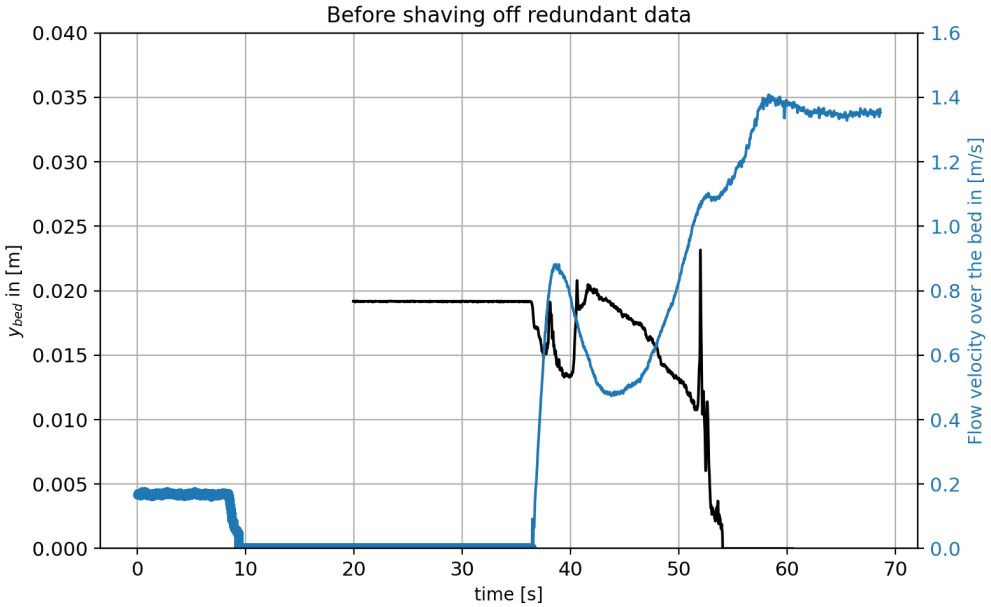

Figure 7.10: Result after the synchronisation of the time indices of both data sets for the experiment with Dorsilit nr. 5 with a volumetric concentration of 20%

From figure 7.10 it can be concluded that the data array of the Sirius-E is quite a lot longer than the ERT data. To match the lengths of the data set for the use in the simulations, the redundant data at the start and end is shaved off. Following, the data of the ERT and Sirius-E can be matched in a data frame, using the time data of the Sirius-E as baseline. In this way the start of both the data sets is now the same. Thenceforth, the values for time, flow velocity, pressure loss, measured bed height for plane 1, near bed concentration for plane 1, measured bed height for plane two and near bed concentration for plane 2 are exported to one *.txt*-file. This file can be used as input for the simulations.

7.4 High speed camera footage

During the experiments the high speed camera was filming 16 seconds, from this footage one is able to easily determine the prevalent mode of transport. The inspection of the footage lead to the conclusion that during the experiments the prevalent mode of transport for the sand types Dorsilit nr.5G, Dorsilit nr.7 and Dorsilit nr.8 was found to be sheet flow over a stationary bed, occasionally the bed moved as a whole. This was mostly due to a sudden increase of bed height, leading to a caterpillar-like movement of the bed. This was easy to be distinguished for the coarser sands using the high speed camera footage.

For GEBA the mode of transport was found to be a pseudo-homogeneous mixture flow over a stationary bed. At last, after inspection of the high speed camera footage of the Zilverzand experiments, it appeared that this sand was mostly transported as a stratified mixture flow over the stationary bed.

7.5 Transport Capacity of a Density Wave

Using the post-processed data, for which the method is described previously in this chapter, the influence of the grain size diameter and the volumetric concentration on the transport capacity is assessed qualitatively. The mass of the sand used within each of the experiment runs and the conductivity are mentioned in table 7.1 and 7.2. Note that the conductivity is given in $\mu S/cm$ and the mass in *grams*.

Table 7.1: Measured input for each of the experiment runs with the different sizes of Dorsilit.

	Dorsilit nr.5G			Dorsilit nr.7			Dorsilit nr.8		
C_v	$k_f[\mu S/cm]$	$m_s[g]$	rpm [−]	$k_f[\mu S/cm]$	$m_s[g]$	rpm [−]	$k_f[\mu S/cm]$	$m_s[g]$	rpm [−]
5%	410	1360	420	388	1246	390	379	1240	390
10%	385	2562	510	401	2492	390	428	2480	390
20%	379	4875	510	384	4638	450	428*	4245	390
30%	382	6877	525	400	6417	510	392**	6414	450

* Bypass and main loop did not have the same order of magnitude for the conductivity

** Missing measurements for conductivity with the handheld conductivity meter

Table 7.2: Measured input for each of the experiment runs with Zilverzand and GEBA.

	Zilverzand			GEBA		
C_v	k_f $[\mu S/cm]$	m_s $[g]$	rpm [−]	k_f $[\mu S/cm]$	m_s $[g]$	rpm [−]
5%	391	1232	330	396	1246	315
10%	413	2464	330	425	2587	405
20%	400*	4723	405	396	4259	405
30%	395	6460	450	400**	6455	450

* Bypass and main loop did not have the same order of magnitude for the conductivity

** Missing measurements for conductivity with the handheld conductivity meter

All the measurements and results of the experiments are shown in appendices B, C, D and E.

7.5.1 *Influence Mean Grain Size Diameter*

To assess the influence of the mean grain size diameter for each concentration, the measurement results shown in appendix D and the high speed camera footage are used to compare the different sand types.

Within the results of the ERT, mostly for the coarser sand types, the bed height measurements show sudden increasing peaks. After studying the high speed camera footage these peaks can be attributed to the caterpillar-like behaviour of a shocking sliding bed, as also described by Matoušek and Krupička (2013). de Hoog et al. (2021) describes the process where erosion becomes more dominant over sedimentation at high concentrations due to the fact that suspended eroded material experiences less friction and is therefore able to travel faster. As this material is transported forward, hence increasing the concentration further along the pipe, again triggering

the unbalance causing the crest of the density wave to move forward. Behind the crest, the bed layer is thinner due to heavy local erosion. This thinner bed experiences less shear stresses causing the bed to stop sliding. Furthermore, de Hoog et al. (2021) states that this movement can be explained using the deposit limit velocity as well. The deposit limit velocity decreases when the concentration increases, this relationship can be calculated using a two-layer model, such as the one of Wilson et al. (2006). The crest within the density wave has a higher local concentration, hence a lower deposit limit velocity. The crest therefore becomes mobile while the tail, with a higher deposition limit velocity is still stationary.

The differences of the sand types per concentration are discussed further on.

Firstly, the mixture concentrations of 5% show some marginal variations, for the majority of the sand types the time it takes for the whole stationary bed to be eroded is approximately 20 seconds. The only difference that is worth mentioning is the sudden increase of the bed height for Dorsilit nr.8 early in the erosion experiments. Based on the inspection of the high speed camera footage this appeared to be the sliding and shocking feature which was described by Matoušek and Krupička (2013) at high concentrations. The finer sand types (Zilverzand and GEBA) show no signs of increasing bed height, both stationary beds are eroded at an almost linear pace in time.

Thereafter, the results for the mixture concentrations of 10% are compared. Where, Dorsilit nr.5G and Dorsilit nr.7 seem to show the same caterpillar-like movement as Dorsilit nr.8. This was confirmed after the footage of the high speed camera was inspected. GEBA however, shows again an almost linear decrease of the bed height in time. Zilverzand shows a small hump of sedimentation after the initial erosion and a somewhat linear decrease of the bed height in time as well.

At higher concentrations the differences between the sand types becomes more and more apparent. For the results of mixture concentrations of 20% intermittently shocking and moving of the bed happens more frequently for the sand types Dorsilit nr.5G and Dorsilit nr.7. Dorsilit nr.8 only shows one peak in bed height, hence one shock that leads to a sliding bed. Using the footage of the high speed camera it is confirmed that immediately after the slide, the bed is stationary again. For of the experiment the bed height decreases almost linearly in time.

At mixture concentrations of 30%, the bed shows even more intermittent sliding and shocking behaviour for Dorsilit nr.5G and Dorsilit nr.7, the latter shows this behaviour the most of these two sand types. Dorsilit nr.8, shows two moments of shocking-sliding bed movements as well. For the experiment with Zilverzand some sedimentation can be distinguished based on the ERT measurements and high speed camera footage, though no actual caterpillar movement is distinguished. The same goes for the experiments conducted with GEBA.

All in all it can be concluded that influence of the mean grain size diameter on the transport capacity of the flow is shown in the ability to form amplifying density waves in the horizontal measurement section. These waves were present for the coarser sand types: Dorsilit nr.5G, Dorsilit nr.7 and Dorsilit nr.8. The waves were visible as caterpillar-like movement of the stationary bed due to the sedimentation and erosion unbalance (de Hoog et al., 2021).

7.5.2 *Influence of the Volumetric Concentration of the Mixture*

To research the influence of the volumetric concentration of the passing mixture, different volumetric concentrations were implemented. To qualitatively study the influence of the volumetric mixture concentration the graphs of appendix D were used. Because these graphs are quite large and there are a vast number of graphs, it is preferred to only show these in the appendix. First of all the difference regarding the flow velocity signal was clearly apparent. It was found that during the experiments the flow velocity signal dropped much steeper at higher concentrations than at lower concentrations. The flattening of the flow velocity signal was clearly visible as well at higher concentrations as well.

Typically, due to the dropping velocity when the mixture passes the horizontal measurement section, a growing bed is expected since the shear strength solely due to the water component of the flow on the bed decreases. The results show that at high mixture concentrations there was an initial growth in the bed. However, shortly after the first sedimentation took place the erosion took over and caused a sharp decrease in the bed height, even though the flow velocity signal showed a steep drop in value. This behaviour strongly suggests a link

between the concentration of the passing mixture and the erosion capacity thereof and confirms the erosion and sedimentation unbalance at high concentrations. It was found that the higher concentrations lead to erosion, while at low concentrations the particles within the mixture tend to settle. This passing of a higher density mixture wave however shows some different effects for each of the sand types.

The effects of the concentration specifically for each sand type is explained in more detail below

- As mentioned before, the velocity signal shows a sharp sudden drop and experiences longer periods of lower flow velocity at higher concentrations, this was clearly visible for the coarsest sand type: Dorsilit nr.5G. Comparing the total duration for the full stationary bed to be eroded it appeared that the total time it took is approximately the same. With differences of almost 5 seconds.
- Dorsilit nr.7 showed steeper drops for each increasing mixture concentration, though the complete time for the stationary bed to be eroded is shorter.
- The flattening of the dropped velocity signal shows an even larger influence for the Dorsilit nr.8 sand. At concentrations of 30%, and much lower flow velocity the bed is eroded in a much shorter time.
- For the Zilverzand the initial sedimentation humps at concentrations above 5% become more and more visible with increasing concentration. At the start of the erosion process the initial drop in bed height is seen more explicitly. Though shortly after an increase of the bed height is shown in the measurements, which is subsequently eroded soon after.
- The experiments with the GEBA sand showed the steep decrease in flow velocity as well. Though since the starting bed height differs a lot as this sediment was a lot harder to spread evenly, it is hard to say anything about the time it took for the bed to be eroded. However, despite the lower initial bed height, initial growth of the bed layer is visible.

The sand types Dorsilit nr.5G, Dorsilit nr.7 and Dorsilit nr.8 were mostly transported as sheet flow. These sand types showed in the ERT measurement sudden increases of the bed height. After complementary inspection of the high speed camera footage these sudden increases were attributed to the caterpillar-like behaviour of a shocking and sliding bed, as similarly described by Matoušek and Krupička (2013). These sudden increases can be found to a greater extent with increasing mixture concentration. Dorsilit nr.7 seems to be most susceptible to these shocking and sliding movements of the bed as the most amount of peaks in bed height are found for this sand type.

7.5.3 *Limitations of the Experimental study*

In this section conclusions regarding the limitation of the experimental study are discussed. These limitations should be mentioned as it is important to check the validity and applicability of the experiments towards different scales. These different scales may concern the grain size or pipeline diameter for example.

First of all, in the current state of the experiments, it is quite hard to the specifically isolate and determine the influence that the volumetric mixture concentration has on the transport capacity. This is mainly due to the heavy fluctuating flow velocity within the experimental flow loop. Because of this, the comparison between different concentrations has an arbitrary nature. The same can be said about the assessment regarding the influence of the mean grain size diameter. While concentrations are approximately the same. The flow velocity, again, is not. Leading to the same kind of arbitrary causes of the influences of the mean grain size parameter on the transport capacity.

It should be noted however that it is possible to take conclusions with sufficient certainty regarding the density wave growth both based on the mixture concentration and the mean grain size diameter. As de Hoog et al. (2021) noted, these caterpillar-like movements are the cause of the erosion and sedimentation unbalance and were found more often at higher mixture concentrations where the unbalance in sedimentation and erosion was expected to show more explicitly during the experiments.

During the experiments the bed height decreases over time. The measurement of the near bed concentration however, show a nearly sawtooth-like evolution in time. These sawtooth-like signals are least present in the finest material, though seem to develop independently of the volumetric concentration of the mixture. These sawtooth-like features may suggest growth of density waves at much smaller wave lengths than previously perceived by

Talmon et al. (2007). It is therefore more likely that these are the result of the discrete measurements by the ERT and the discrete method for determining the bed height and subsequently, the near bed concentration. Furthermore, it may also be affected by the interpolation of the ERT data to determine the bed height.

During the design of the loop it is opted for to not explicitly account for dimensionless numbers, the validity of the experiments for other pipe and/or grain sizes therefore requires that the flow regime is similar to what is found and measured during these experiments.

III

Physical Modelling

8

Physical Modelling of the Sediment Transport Capacity of a Density Wave

The physical modelling part of this thesis regards the erosion capacity of highly concentrated slurry flow. Using a control volume around the bed interface in a pipeline the upward or downward moving interface can be modelled using a sedimentation and erosion balance. This schematisation of the control volume has been described in section 5.2. The discretisation of this control volume is elaborated in the second section of this chapter. Furthermore, for the pick-up functions, of which the theoretical background is described in chapter 5, the actual mathematical applications of the pick-up functions are elaborated in section 8.3.

8.1 Schematisation of the Control volume

In chapter 5 it is described how van Rhee (2010) modelled the bed interface. Using this implementation on the planes of the ERT, a fairly simply model can be created which is able to resemble the evolution of the sand bed during the erosion and sedimentation process. This simulation is done based on the output of measurements of the ERT and Sirius-E, such as the near bed concentration and the mean flow velocity, respectively. These measurements form the initial conditions for the simulation. The extra simplification is shown in figure 8.1.

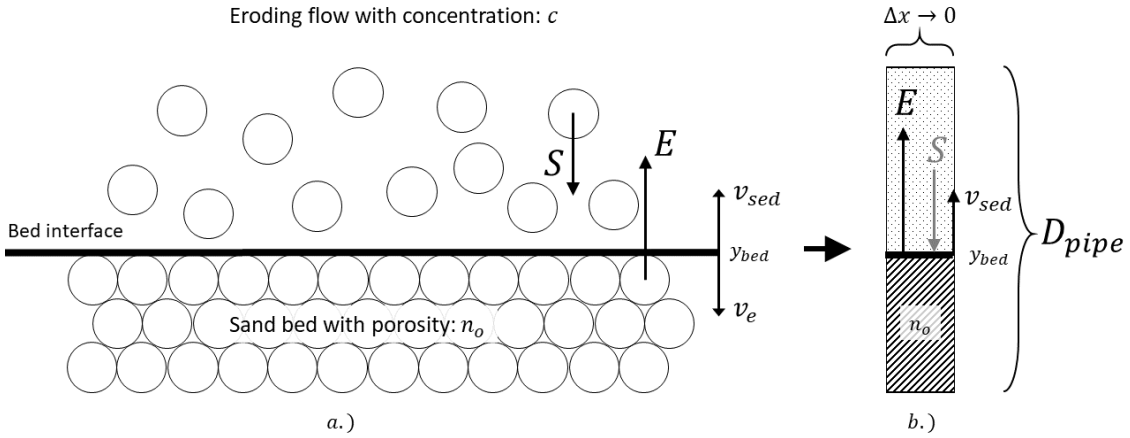

Figure 8.1: *a.)* Schematised bed interface according to van Rhee (2010) and Bisschop (2018). *b.)* The model used in the simulation

Note that the model in the simulation assumes a width that is infinitesimal to be able to adequately compare the discretised erosion and sedimentation balance with the measurements. This assumption however requires extra conditions to assure the physical laws of conservation for mass and momentum. The conditions are listed below.

- The bed does not move as a whole, meaning that a stationary bed is present, over which a stratified slurry flow moves, this can also be a sheet flow. The latter was quite often observed using the high speed camera footage.
- The top and bottom of the pipeline are fixed and can not be eroded. Since the flow goes through a pipeline the flow is spatially confined and the bed height is not able to grow infinitely large. Therefore, if the bed height is as large as the pipe diameter the pipe is clogged. On the other hand, if the bed height is zero this means that there is no stationary bed remaining.
- To prevent clogging of the pipe at the start of the simulations a condition has to be set to ensure a sedimentation flux of zero when the mean flow velocity is very low. Since at very low flow velocities no sediment is picked up it is impossible to have a sedimentation flux in clear water. This condition is necessary since the current method of determining the near bed concentration gives non-zero values during stagnant water. Due to the fact that the hindered settling velocity and sedimentation flux calculation do not require a flow velocity this can result in physically impossible values. These inconsistencies are now forestalled.
- For the simulations it is assumed that the bed is loosely packed. Due to the fact that by means of the filling tube the bed is deposited by settling of the sand particles over time. Furthermore, no soil compacting measures are taken before the experiments are started, a loose packed bed is therefore highly likely. The values for n_0 or n_i (depending on the pick-up function) are set to 0.4.

8.2 Computational Setup of the Model

Based on the schematisation of the bed interface a method is chosen to resemble the evolution of the bed height based on different pick-up equations defined in the literature.

8.2.1 *Mathematical Model used for the Calculations*

To be able to model the bed level of the moving bed in the pipeline the equation for the sedimentation velocity needs to be discretised. van Rhee (2010) described the sedimentation velocity as given in equation 8.1.

$$v_{sed} = \frac{S - E}{\rho_s (1 - n_0 - c_{nb})} \tag{8.1}$$

Where, S is defined as the sedimentation flux which is dependent on the concentration and solids diameter (Richardson & Zaki, 1954). E is the erosion flux, for this parameter different pick-up functions are chosen. ρ_s is the density of the solids, n_0 is the initial porosity and c_{nb} is the near bed concentration.

The sedimentation velocity is defined as the velocity of the bed perpendicular to the flow direction. Therefore, this can be seen as the change of the bed height per time step. The equation thereof is given below:

$$v_{sed} = \frac{\Delta y_{bed}}{\Delta t} \tag{8.2}$$

Implementing equation 8.2 into equation 8.1 leads to a equation that can be easily discretised using the Explicit Euler method, which is also known as the Forward Euler method. The derivation of the discretisation is shown below in equations 8.3 to 8.5. In the discretised form, n is noted as the time step indication.

$$\frac{\Delta y_{bed}}{\Delta t} = \frac{S - E}{\rho_s (1 - n_0 - c_{nb})} \tag{8.3}$$

$$\frac{y_{bed}^{n+1} - y_{bed}^{n}}{\Delta t} = \frac{S^n - E^n}{\rho_s \left(1 - n_0 - c_{nb}^n\right)} \tag{8.4}$$

$$y_{bed}^{n+1} = y_{bed}^{n} + \Delta t \frac{S^n - E^n}{\rho_s \left(1 - n_0 - c_{nb}^n\right)} \tag{8.5}$$

When at an arbitrary time step n, the erosion flux E^n is larger than the sedimentation flux S^n, the sedimentation velocity will be negative. This means that the bed interface is moving down, thus indicating an erosion process.

8.2.2 *Hindered Settling Velocity and Sedimentation Flux*

The sedimentation flux is calculated using the equation of Richardson and Zaki (1954). The equation is already mentioned in section 3.1, see equation 3.1. In this equation the near bed concentration is also time dependent for the simulation as it is an input variable retrieved from the experiments. The discretised result is shown in equation 8.6. Note that both the terminal settling velocity and the exponent m are not time dependent. The terminal settling velocity as defined by Zanke (1977) is dependent on the grain size, kinematic viscosity and relative density as shown in equation 5.9.

$$w_s^n = w_0 \left(1 - c_{nb}^n\right)^m \tag{8.6}$$

The exponent m is calculated using the equation of Rowe (1987) as given in equation 3.7. Based on the hindered settling velocity the sedimentation flux follows from equation 5.11. This leads to equation 8.7 for an arbitrary time step n.

$$S^n = \rho_s w_s^n c_{nb}^n \tag{8.7}$$

The above calculated sedimentation flux can be substituted in to the derived discretised equation for the bed height.

8.2.3 *Initial Conditions and Forcing*

For the model the initial conditions have to be set such that the experiments can be validated. Based on the outcomes of the experiments the initial condition can be bound quite easily. Using the measured bed height at the start of each corresponding experiment as the initial condition, the evolution of the bed height than follows based on difference in the erosion and sedimentation flux. These fluxes are depend on the forcing of the flow and the near bed concentration, conditional of the chosen pick-up function.

The erosion flux is mainly dependent on the flow velocity, which directly influences the Shields parameter. Since the flow velocity is measured this can be used to accurately simulate the bed height evolution based on different pick-up fluxes.

For the sedimentation flux the near bed concentration is required to be able to calculate the hindered settling velocity. Considering the near bed concentration has been determined based on the bed height from the ERT measurements, these values are therefore used.

8.3 Comparison with Erosion Model Variations

In equation 8.5 the only remaining unknown is the erosion flux, for which over the years a lot of different erosion models have been developed. The theoretical background is of each of these models is explained in chapter 5. In this section only the mathematical implementation in to equation 8.5 is elaborated. Furthermore, in this section the applicability of several pick-up functions on the experiments is compared, using the output of the experiments to verify the results.

The geometry of the 2LM has been described in section 3.4. However, for conspectus the schematisation used in the model is shown in figure 8.2. Based on the 2LM some general equations are used to compute the area of the bed (8.8), the wet perimeter of the pipe (equation 8.9) and the wet perimeter of the bed (equation 8.10). The latter is equal to the width of the bed.

$$A_2^n = 0.25 \cdot D_{pipe}^2 \cdot (\beta^n - \sin\beta^n \cos\beta^n) \tag{8.8}$$
$$O_1^n = (\pi - \beta^n) \cdot D_{pipe} \tag{8.9}$$
$$O_{12}^n = D_{pipe} \cdot \sin\beta^n \tag{8.10}$$

In which D_{pipe} is the pipe diameter and β^n is the angle of the bed interface and the middle lower point of the pipe. From the geometry of the 2LM 8.11 can be used to calculate the angle of the top of the bed layer.

$$\beta^n = \arccos\left(1 - \frac{2 \cdot y_{bed}^n}{D_{pipe}}\right) \tag{8.11}$$

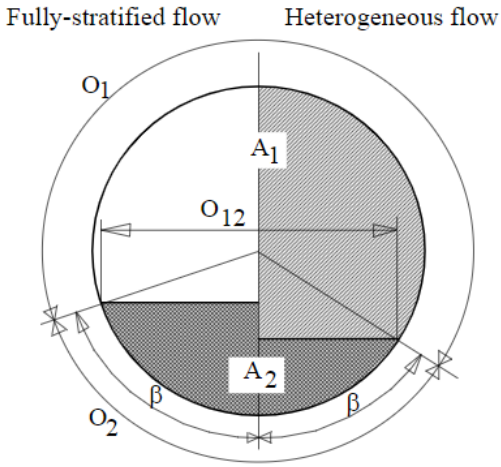

Figure 8.2: Schematisation of the 2LM used in the simulation, retrieved from Wilson (1976)

During the erosion-sedimentation process, the bed height changes, thus requiring this angle to be calculated again and again for each time step in the model. This calculation forms the basis of the model.

8.3.1 *van Rijn (1984a)*

The mathematical implementation of the van Rijn (1984a) pick-up function is explained in this section. In equation 8.5 the unknown erosion flux can be expressed as:

$$E^n = 0.0033 D_*^{0.3} T^{n1.5} \rho_s \sqrt{\Delta g D_{50}} \tag{8.12}$$

In which T^n is the transport factor at time step n and is defined as given in equation 8.13. Furthermore, D_* is the dimensionless grain size parameter for which equation 5.15 can be used.

$$T^n = \frac{(u_*^n)^2 - (u_{*,c})^2}{(u_{*,c})^2} \tag{8.13}$$

Where, u_*^n is the bed shear velocity at time step n, equation 8.15 is used to calculate the bed shear velocity and $u_{*,c}$ is the critical bed shear velocity. The latter is calculated using equation 8.14.

$$u_{*,c} = \sqrt{\theta_{cr} \Delta g D_{50}} \tag{8.14}$$

The critical Shields parameter θ_{cr} is calculated based on the findings of van Rijn (1984b). Who approximated the Shields curve using the below given values.

$$\begin{aligned}
D_* \leq 4 \quad & \theta_{cr} = 0.24\,(D_*)^{-1} \\
4 < D_* \leq 10 \quad & \theta_{cr} = 0.14\,(D_*)^{-0.64} \\
10 < D_* \leq 20 \quad & \theta_{cr} = 0.04\,(D_*)^{-0.10} \\
20 < D_* \leq 150 \quad & \theta_{cr} = 0.013\,(D_*)^{0.29} \\
D_* > 150 \quad & \theta_{cr} = 0.055
\end{aligned}$$

$$u_*^n = \sqrt{\frac{g u_2^n}{C'^n}} \tag{8.15}$$

in which g is the gravitational acceleration, u_2^n is the flow velocity over the bed at time step n and C'^n is the bed related Chézy coefficient at time step n. The assumption that the bed does not move as a whole leads to

the following expression for u_2^n, using equation 3.22 this results in:

$$u_2^n = \frac{A_{pipe}}{A_{pipe} - A_2^n} \cdot u^n \tag{8.16}$$

$$C'^n = 18 \log\left(\frac{12 D_b^n}{3 D_{90}}\right) \tag{8.17}$$

In which D_{hb}^n is the bed related hydraulic diameter and D_{90} is the grain size diameter at which 90% is smaller, the latter can be found from the measured sieve curve. The values of D_{90} for the different sand types are shown in table 6.3. Due to the fact that the pressure measurement were not usable for all simulations it is assumed that D_h is approximately equal to the bed related hydraulic diameter, D_{hb}. Therefore, the hydraulic diameter above the bed can be computed in the same manner as Matoušek (2009) and Miedema and Ramsdell (2014) did, see equation 8.18.

$$D_h^n = \frac{4\,(A_{pipe} - A_2^n)}{O_1^n + O_{12}^n} \tag{8.18}$$

In which A_2^n is the area of the bed in the cross-section and can be calculated using equation 8.8. The wet perimeter of the pipe is denoted as O_1^n for which equation 8.9 can be used. Lastly, O_{12}^n is the wet perimeter of the bed (width of the bed), which can be calculated using equation 8.10. All variables that are calculated for each time step are denoted with time step indication n. An example of the outcomes of the simulation using the van Rijn (1984a) function is shown in figure 8.3. In this example a mixture concentration of 20% with Dorsilit nr.8 is used.

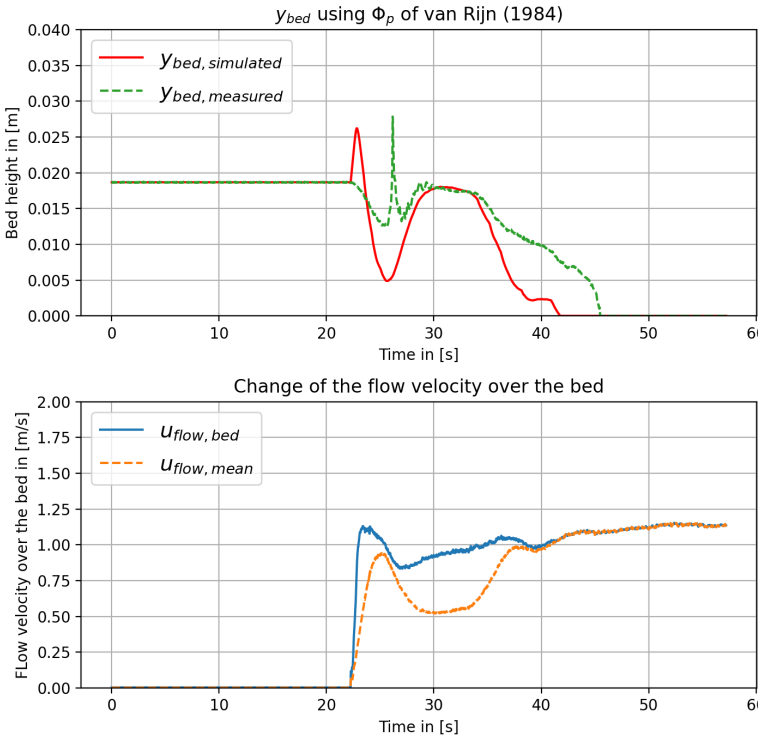

Figure 8.3: Outcomes of simulation using the van Rijn (1984a) pick-up function for Dorsilit nr.8 with a mixture concentration of 20%

8.3.2 *Winterwerp et al. (1992)*

The model that uses the Winterwerp et al. (1992) pick-up flux the exponent m is set to a constant value of 4. Furthermore, the actual model differs slightly as well. Where most models are accounting for the near bed concentration in the model, this term is dropped out of equation 8.5 for the Winterwerp et al. (1992) model. The new discretised model then becomes:

$$y_{bed}^{n+1} = y_{bed}^{n} + \Delta t \frac{S^n - E^n}{\rho_s (1 - n_0)} \tag{8.19}$$

In discretised form, the erosion flux of Winterwerp et al. (1992) is denoted as given in equation 8.20.

$$E^n = 0.012 \rho_s \sqrt{\Delta g D_{50}} D_*^{0.3} \left(\theta_b^{n0.5} - 1.3\right) \tag{8.20}$$

In which, θ_b is the mobility parameter, calculated as in equation 8.21.

$$\theta_b = \frac{f_b}{8} \cdot (1 + \Delta c_{1992}^n) \cdot \left[\frac{u_2^n}{\sqrt{\Delta g D_{50}}}\right]^2 \tag{8.21}$$

In this equation f_b is defined as the Darcy-Weisbach bed friction factor, with a typical value of 0.05-0.06 (Winterwerp et al., 1990). The average concentration above the bed, c_{1992}^n, is assumed to be approximately equal to the near bed concentration as measured with the ERT. Equations 8.8, 8.11 and 8.16 are used to calculate the flow velocity above the bed, which is required for the mobility parameter. Substituting equation 8.20 in equation 8.19 results in a model that can be used to calculate the bed height based on the pick-up function of Winterwerp et al. (1992).

During the simulations it appeared that when the typical values for the Darcy-Weisbach bed friction factor was used, the erosion flux was extremely underestimated. Using the bed friction factor as a calibration parameter, different values were implemented to get to the most suitable results when compared to the measurements. This however, lead to illogical large values for the coarser sand types, such as Dorsilit nr.5G and Dorsilit nr.7. The used values for f_b are given in table 8.1 for a clear overview.

8.3.3 *van Rhee (2010)*

The pick-up equation of van Rhee (2010) is an implicit function which if calculated numerically, directly results in the erosion velocity. Therefore, equation 8.5 can not be used.

The discretised form of the van Rhee (2010) pick-up function is given in equation 8.22.

$$\frac{1}{1 - n_0 - c_{nb}^n} \left(\phi_p'^{\,n} \sqrt{g \Delta D_{50}} - c_{nb}^n w_s^n\right) - v_e = 0 \tag{8.22}$$

In which, the adjusted pick-up flux is defined as:

$$\phi_p'^{\,n} = 0.00033 D_*^{0.3} \left(\frac{\theta^n - \theta_{cr}'}{\theta_{cr}'}\right)^{1.5} \tag{8.23}$$

As mentioned in chapter 5 the value for $n_l = n_{max}$ is assumed and for $k_l = k_{max}$ can be used. The latter can be calculated using the den Adel (1987) equation to compute the maximum permeability, see equation 6.2. The Shield parameter at time step n was calculated using equation 8.24.

$$\theta^n = \frac{f_0}{8} \frac{u_2^{n2}}{\Delta g D_{50}} \tag{8.24}$$

In which f_0 is defined as the friction factor of the bed, van Rhee (2010) used a value of 0.02. The velocity over the bed, u_2^n, is calculated using equation 8.16. From equation 8.23 the adjusted critical Shields parameter can be calculated using equation 8.25.

$$\theta_{cr}' = \theta_{cr} \left(\frac{\sin(\varphi - \beta_s)}{\sin \varphi} + \frac{v_e}{k_{max}} \cdot \frac{n_{max} - n_0}{1 - n_{max}} \frac{A}{\Delta}\right) \tag{8.25}$$

Since the slope of the bed at the start of the erosion experiments was flat ($\beta_s = 0$) the first factor between brackets is equal to one. To solve equation 8.22 an estimate for the erosion velocity is required. For all simulations a value of 0.0001 [m/s] was used as first estimation. Within Python this can be solved numerically, without writing an iterative process. The critical Shields parameter θ_{cr} is calculated using equation 5.3.

Based on the bed friction factor value of 0.02 the results were not within the desired accuracy. Using the same process as for the pick-up flux of Winterwerp et al. (1992) different values of f_0 were implemented. The best results for each of the sand types were found when values of 0.2, 0.06, 0.035, 0.035 and 0.035 for Dorsilit nr.5G, Dorsilit nr.7, Dorsilit nr.8, Zilverzand, and GEBA, respectively were used. The values of f_0 are given in table 8.1 for a clear overview.

As mentioned the equation of van Rhee (2010) calculates the erosion velocity, therefore implementing the outcomes in to the model described by equation 8.5 is redundant. Instead using the relation given in equation 8.2 can be used. Though instead of using v_{sed}, v_{er} is used. This results in equation 8.26 to calculate the bed height at each time step.

$$y_{bed}^{n+1} = y_{bed}^{n} - \Delta t \cdot v_{er}^{n} \tag{8.26}$$

In which, v_{er}^{n} is the erosion velocity calculated at time step n.

8.3.4 *van Rhee and Talmon (2010)*

The pick-up function of van Rhee and Talmon (2010) was developed to better account for the influence of high concentrations in slurry flow. By introducing a mitigating factor in the pick-up flux, dependent on the bed concentration.

$$E^{n} = 0.0025\,(D_* - 2.4)^{0.3} \left[\frac{1 - n_0 - c_{nb}^{n}}{1 - n_0}\right] \theta_b^{n} \cdot \rho_s \sqrt{\Delta g D_{50}} \tag{8.27}$$

The Shields parameter is calculated using equation 8.28. Note that due to fitting of the pick-up flux to available data, the factor $(D_* - 2.4)^{0.3}$ van Rhee and Talmon (2010) introduced a condition for a minimum grain size.

$$\theta_b = \frac{\tau_{bed}}{g\,(\rho_s - \rho_w)\,D_{50}} \tag{8.28}$$

In which the bed shear stress, τ_{bed} can be estimated using equation 8.29.

$$\tau_{bed}^{n} = -\frac{A_b^{n}}{B}\left[\frac{\partial \tilde{p}}{\partial x}\right]^{n} \tag{8.29}$$

In which, A_b is the bed related cross-sectional area, assumed to be $0.4 \cdot (A_{pipe} - A_2^{n})$. B is defined as the width of the cross-section. The latter is assumed to be equal to the diameter of the pipeline. $\left[\frac{\partial \tilde{p}}{\partial x}\right]^{n}$ is the adjusted pressure loss for which equation 8.30 can be used.

$$\left[\frac{\partial \tilde{p}}{\partial x}\right]^{n} = -\frac{f}{D_h^{n}}\frac{1}{2}\rho_w u_2^{n2} \tag{8.30}$$

In which, the friction coefficient f can be estimated using the equation of R. W. Miller (1983). The equation is given in equation 8.31. Once again, since not all pressure measurements are usable for the simulations to compute the bed shear stress, a general implementation to subsequently calculate the bed associated hydraulic diameter was impossible. Therefore, the bed related hydraulic diameter is assumed to be approximately equal to the hydraulic diameter above bed. The hydraulic diameter above the bed is denoted as D_h^{n} and is calculated using equation 8.18. The velocity above the bed is computed using equation 8.16.

$$f = 0.25\left[\log\left(\frac{e/D_h^{n}}{3.7} + \frac{5.74}{\mathrm{Re}^{0.9}}\right)\right]^{-2} \tag{8.31}$$

In which e is the surface roughness, estimated as $3 \cdot D_{90}$, D_h^{n} is the hydraulic diameter at time step n and Re the Reynolds number calculated as $u_2 D_h/\nu$.

Substituting equation 8.30 into equation 8.29 the Shields parameter can be computed for each time step. Subsequently, the erosion flux can be substituted in equation 8.5 and the bed height for each new time step can be calculated directly.

As mentioned before there is a limitation to the minimal grain size. The measured median grain size for the smallest sand type, GEBA, was 112 μm. This consequently lead to a negative value for $D_* - 2.4$, hence the pick-up function was unusable. Though, assuming a value of 125 μm for this sand type assured that no numerical problems remained, while still being in the same order of magnitude for the grain size.

8.3.5 *Bisschop (2018)*

One of the newer erosion equation which accounts for the dilatancy reduced erosion regime is the one of Bisschop (2018). The discretised equation of Bisschop (2018) is given in equation 8.32.

$$E^n = \frac{0.5 \cdot h_s^n \cdot \lambda_s \cdot (1 - n_i) \cdot \rho_s}{T_B^n} \tag{8.32}$$

In which, h_s^n is the height of the sheared layer at time step n, for which equation 8.33 can be used. The averaged area of all sweeps per unit of bed area can be calculated using the relation $\lambda_s = 0.5 \cdot \lambda_b$, where the latter is assumed to have a value of 1 (Bisschop, 2018).

$$h_s^n = \frac{-C_1^n + \left(C_1^{n2} + C_2^n\right)^{0.5}}{C_3^n} \tag{8.33}$$

In the equation above C_1^n, C_2^n and C_3^n are soil specific coefficients at time step n. For the coefficients, equations 8.35, 8.36 and 8.37, respectively, can be used. Furthermore in equation 8.32, T_B^n is defined as the dimensionless mean period of turbulent bursts ($T_B \cdot u_2/h_f$), for which Bisschop (2018) assumed a value of 1.5. Where, h_f is defined as the flow depth, which for the cross-section in a pipeline with a bed can be written as: $h_f = D_{pipe} - y_{bed}$. Rewriting the relation for the dimensionless period of turbulent bursts results in equation 8.34.

$$T_B^n = \frac{1.5 \cdot \left(D_{pipe} - y_{bed}^n\right)}{u_2^n} \tag{8.34}$$

The calculated values for the mean period of turbulent bursts can be substituted in to the equations for the soil specific coefficients:

$$C_1^n = \frac{\rho_s}{2} \cdot (1 - n_i) \cdot \frac{u_*^n}{T_B^n} \cdot \tan(\pi/4 + \varphi/2) \tag{8.35}$$

$$C_2^n = \frac{4}{T_B^n k_{\max}} \cdot \left(\frac{n_{\max} - n_i}{1 - n_{\max}}\right) \cdot N_\gamma \cdot g \cdot \rho_f \cdot p'^n \cdot \tan(\pi/4 + \varphi/2) \tag{8.36}$$

$$C_3^n = \frac{2}{T_B^n k_{\max}} \cdot \left(\frac{n_{\max} - n_i}{1 - n_{\max}}\right) \cdot N_\gamma \cdot g \cdot \rho_f \tag{8.37}$$

In equation 8.35, the bed shear velocity is calculated using equation 8.15. For C_2^n and C_3^n, the maximum permeability is calculated using the equation of den Adel (1987). The soil strength parameter, N_γ is calculated using equation 5.32 using an internal angle of friction of 30°. Lastly, p'^n is computed with the use of equation 8.38.

$$p'^n = 0.5 \rho_f \hat{w}^2 \tag{8.38}$$

In which $\hat{w}^2 = 1.0 \cdot u_*^n$, where u_*^n is the bed shear velocity (de Hoog, 2021). With all the variables calculated, the erosion flux as described by equation 8.32 can now be substituted in equation 8.5. The bed height for each new time step is then calculated for the duration of the experiment.

During the simulations several values for the initial porosity were implemented to research the effects thereof. It became apparent that the effect was actually significant and the value of the initial porosity could be changed such that the simulations would resemble the measurements quite accurately. Thus the variable n_0 could be used as a calibration parameter for the simulations. An example of the effects for the choice of n_0 is shown in figure 8.4. This example shows the results for the simulations using the input from Dorsilit nr.7 at a mixture concentration of 20%.

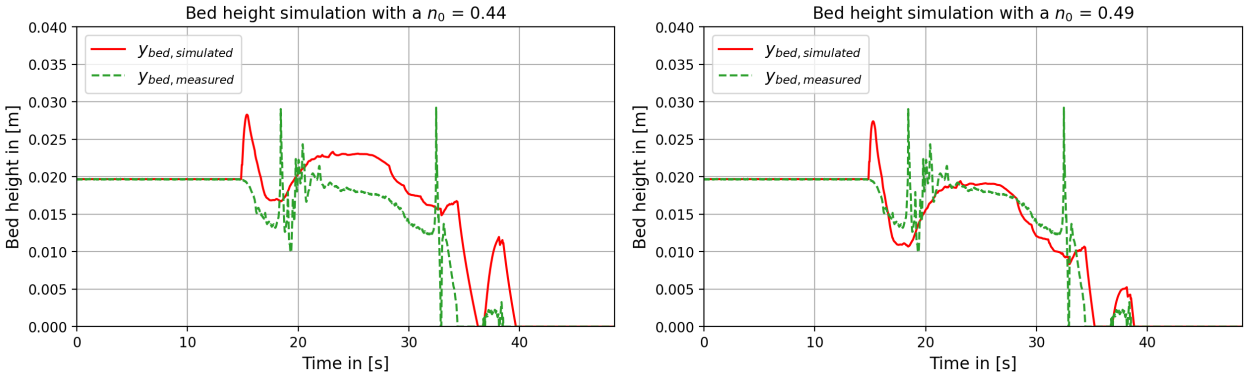

(a) Mixture with $c_v = 0.20$ and $n_0 = 0.44$

(b) Mixture with $c_v = 0.20$ and $n_0 = 0.49$

Figure 8.4: Effects of different values for n_0 for the simulations of the erosion using Dorsilit nr.7 with a mixture concentration of 20%, using the pick-up flux of Bisschop (2018).

From figure 8.4 the effects of the choice of the initial porosity are clearly visible can be seen to have a a big influence on whether the measurements can be estimated accurately. However, with the knowledge that the initial porosity of the sediment can be used as a calibration parameter, the accuracy of the results can be optimised as well. The values for n_0 are given in table 8.1 for a clear overview. An example of the outcomes of the simulation using the Bisschop (2018) pick-up function is shown in figure 8.5.

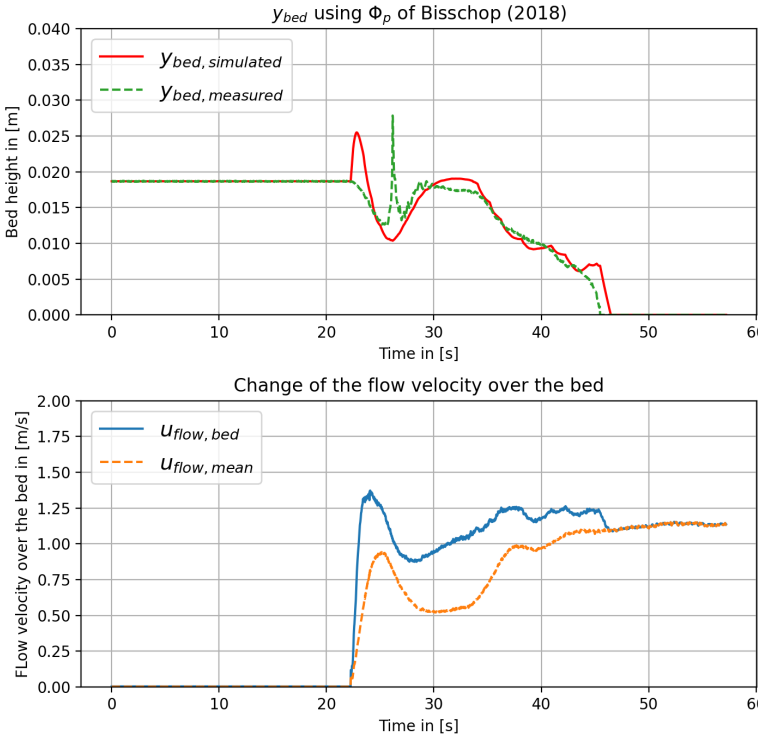

Figure 8.5: Outcomes of simulation using the Bisschop (2018) pick-up function for Dorsilit nr.8 with a mixture concentration of 20%

From the graphs it can be seen that the erosion flux is quite well estimated with the pick-up function of Bisschop (2018). Initially, a steep growth of the bed is calculated this however is deemed to be a numerical error related to the values for the near bed concentration. Within model the sedimentation flux is non-zero for very low flow velocities, resulting in a growing bed.

8.3.6 *van Rijn et al. (2019)*

The adjusted discretised pick-up flux of van Rijn et al. (2019) is given in equation 8.39.

$$E^n = 0.0033\rho_s\sqrt{(s-1)gD_{50}}\,(D_*)^{0.3}\,f_D^n\left[\frac{\theta'^n - \theta_{cr}}{\theta_{cr}}\right]^{1.5} \tag{8.39}$$

In which, the damping factor f_D^n at time step n can be calculated using equation 8.40.

$$f_D^n = \begin{cases} 1/\theta'^n, & \text{if } \theta'^n > 1 \\ 1, & \text{if } \theta'^n \leq 1 \end{cases} \tag{8.40}$$

In which the Shields parameter at time step n, θ'^n, is calculated using equation 8.41.

$$\theta'^n = \frac{\tau_{bed}^n}{(\rho_s - \rho_f)gD_{50}} \tag{8.41}$$

Where the bed shear stress is computed using equation 8.42.

$$\tau_{bed}^n = \rho_f g \cdot \left[\frac{u_2^n}{C'^n}\right]^2 \tag{8.42}$$

For the bed related Chézy coefficient, C'^n, equation 8.17 is used. For the flow velocity above the bed, equation 8.16 is used. Based on these parameters the discretised pick-up flux of van Rijn et al. (2019) can be substituted in equation 8.5. While the adjusted function is adapted to high flow velocities and the dilatant reduced erosion range, the outcomes did not differ a lot from the original van Rijn (1984a) function. The differences were marginal, therefore the improvement of the new pick-up function was not so apparent based on the experiments. An example of the outcomes is shown in figure 8.6. The similarities between the adjusted and the old van Rijn (1984a) equation can be clearly seen for the coarser sand types.

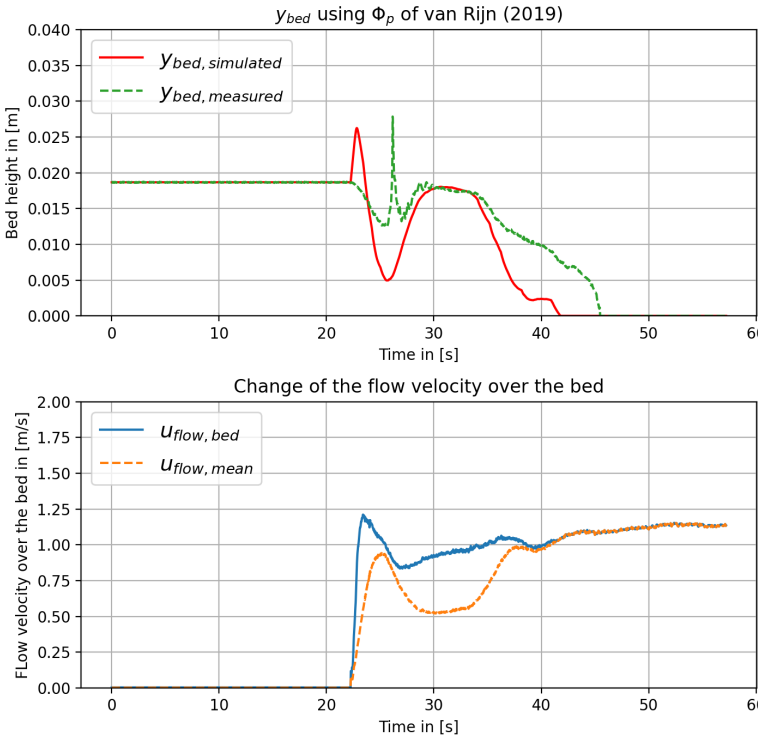

Figure 8.6: Outcomes of simulation using the van Rijn et al. (2019) pick-up function for Dorsilit nr.8 with a mixture concentration of 20%

Supposedly, the flow regime during the experiments was not in the dilatant reduced erosion range. Moreover, it was possible that the dilatant behaviour of the soil was not triggered due to the loose packing of the bed and the fact that quite a lot of coarse sand types were used. Coarse sand types are much less prone to dilatant behaviour as the water is able to penetrate the soil much easier than is the case with fine sand. Therefore, the new form, with the damping factor f_D, actually transforms back in to the old version of van Rijn (1984a).

8.4 Concluding Remarks

Using a two layered model to model the interaction of the sedimentation and erosion of the flow at the interface of the bed an easy model is created, which is able to quite accurately resemble the measurements. Though depending on the sand type the best pick-up function may be different. The rest of the results of the simulations per sand type and per pick-up function are shown in appendix F. For every simulation the outcomes have been qualitatively compared to the measurements. Using a parity graph where on the y-axis the measured bed height is plotted and on the x-axis the simulated values. An example of the parity graphs for Dorsilit nr.7 with mixture concentrations of 10 and 20% can be found in figure 8.7. This ensures an easy comparison between measured and simulated values as both the arrays are synchronised in time. Ideally, the simulations are almost equal to the measured bed heights. As some pick-up functions required additional calibration, the values which retrieved the best results are mentioned in table 8.1.

Table 8.1: Calibration input used in the simulations using the pick-up function of Bisschop (2018); van Rhee (2010); Winterwerp et al. (1992), respectively.

	Bisschop (2018)	van Rhee (2010)	Winterwerp et al. (1992)
Sand type	n_0	f_0	f_b
Dorsilit nr.5G	0.44*	0.2	1.25
Dorsilit nr.7	0.49	0.06	0.6
Dorsilit nr.8	0.455	0.035	0.35
Zilverzand	0.4525**	0.035	0.175
GEBA	0.49***	0.035	0.06

* For C_v = 0.05, n_0 = 0.48

** For C_v = 0.20 and C_v = 0.30, n_0 = 0.44

*** For C_v = 0.05 n_0 = 0.52

The best results are found for the erosion equation of Bisschop (2018), requiring solely a little calibration. Most of the sand types with different mixture concentrations conform really well with the measurements. The higher mixture concentration do have a lot of variation when the measurements are compared to the simulations. Though generally speaking, the trend for every sand type is followed really adequately. Furthermore, the values used for the initial porosity are within the values mentioned in table 6.3. Therefore no illogical values have to be used to competently fit the measurements.

In contrast to the aforementioned pick-up function, the pick-up function of Winterwerp et al. (1992), required really high illogical values for the friction coefficient to fit the pick-up function with sufficient accuracy to the measurements. This rendered the applicability of this pick-up function to these specific experiments unsuitable.

The applicability of the van Rijn (1984a) and van Rijn et al. (2019) equations in the simulations was surprisingly satisfactory. As mentioned before the adjusted pick-up function returned mostly to the old form, though at times the peaks in the simulations were somewhat more damped. The similarities were mostly surprising as the van Rijn (1984a) equation was developed for fluvial flows with very low concentrations. Based on the outcomes however, it appears that the equation is an adequate fit for sheet flow during the experiments as well. Moreover, the results for higher mixture concentrations were satisfactory as well.

The results of the simulation using pick-up function of van Rhee (2010) are decent too. For both the larger and smaller grain sizes. The latter are more prone to the dilatant behaviour, for which this pick-up function was specifically designed. However, the values for the friction coefficient to find these fits is larger than van Rhee (2010) used for his experiments for all sand types. This introduces some notions on the applicability of this pick-up function on these experiments, foremost that the need to properly determine the value for the bed

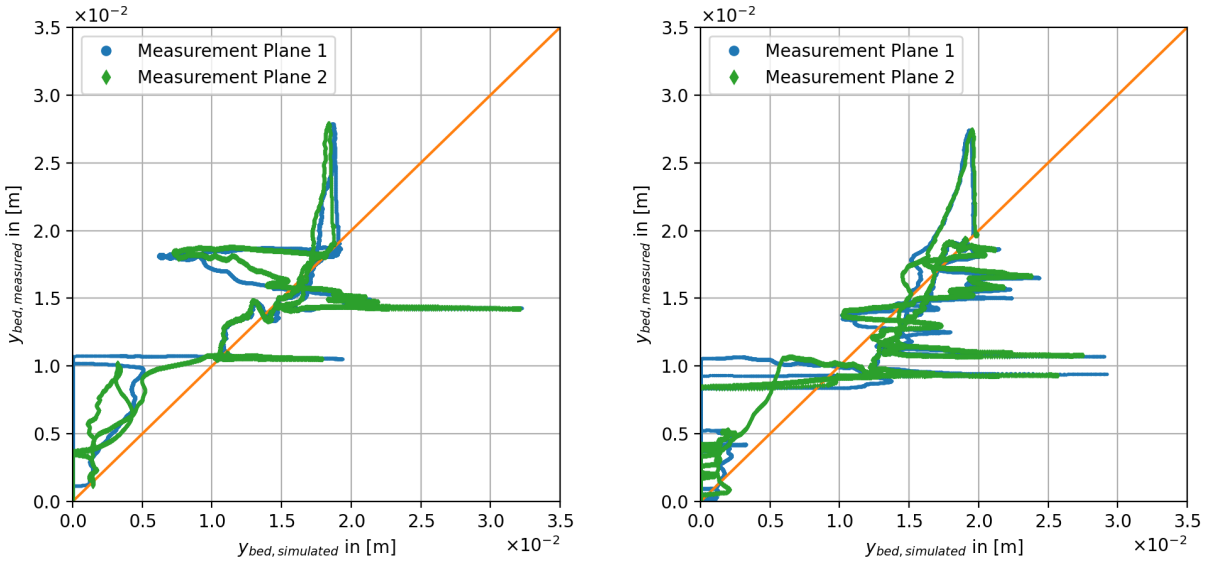

(a) Mixture with $c_v = 0.10$ and $n_0 = 0.49$

(b) Mixture with $c_v = 0.20$ and $n_0 = 0.49$

Figure 8.7: Parity graphs of the simulations for Dorsilit nr.7 with a mixture concentration of 10 and 20% using the pick-up flux of Bisschop (2018).

friction coefficient is quite significant. The equation of van Rhee and Talmon (2010), developed for the hindered erosion regime, consistently underestimates the erosion flux. This is especially apparent for the coarsest sand types. In contrast to earlier mentioned pick-up fluxes, the pick-up equation of van Rhee and Talmon (2010) uses a relatively sophisticated method to calculate the bed friction coefficient. However, this method does require an assumption for the bed roughness, which may be considered arbitrary was well.

IV

Conclusions

9 Conclusion

In this chapter the research questions, as mentioned in section 1.2.3, are answered using the obtained results and measurements. Based on the answers to these research questions, the objective of this thesis is reflected upon. For good measure the main research objective is repeated below.

Investigate whether an unbalance between erosion and sedimentation at high concentration, causes density wave amplification and determine whether the erosion process in a pipeline can be modelled numerically as a 2LM based on the sedimentation-erosion balance using different pick-up functions for the erosion flux

9.1 Theory

In this first section the research questions regarding the literature review and theory are resolved. Since these questions have been answered elaborately in their corresponding chapters as well, see sections 4.5 and 5.8, a summary thereof is given here.

9.1.1 *What are the current described hypothesis in the literature for density wave amplification?*

- The research of Matoušek (1995, 1996a, 1996b) found that the variability of the flow was inducing variations within the solids flow along the pipe line. This caused a relative material transfer between the moving density waves, what resulted in the transformation of these density waves. Matoušek (1995, 1996a, 1996b) found that modelling the internal structure of the flow as a 2LM showed sufficient similarities with the measured data. Within his data interpretation he confirmed his hypothesis that there is a relationship between slip and slurry density and thus the relation of slip ratio and transforming density waves
- Thereafter, Talmon (1999) tried to mathematically prove the hypothesis of the influence of the slip ratio on the amplifying density waves, though he came to a different conclusion. He used a non-linear one-dimensional model to calculate the density wave development under the condition of variable slip. Talmon (1999) found that when applying the slip data of Matoušek (1997) to his model this actually lead to dampening of the waves. Talmon (1999) therefore stated that the variable slip could not explain the amplifying behaviour of density waves.
- Talmon (2002) expanded his previous linear stability analysis using the new findings of Matoušek (2001b). Where, Talmon (2002) found that for both stationary and sliding bed regime the density wave amplification was to be attributed to the erosion and sedimentation unbalance. Furthermore, by implementation of new experiments Talmon et al. (2007) tried to prove that the cause for amplifying density waves was actually to be found in the unbalance between sedimentation and erosion at high concentrations. Talmon et al. (2007) found that density waves were occurring at velocities around the deposit limit velocity and whenever, at minimum, a thin bed layer was present for the wave to grow on.
- de Hoog (2016) and de Hoog et al. (2017) saw that the amplification is not only a product of differential slip and advection since the amplification is only possible whenever there is a buffer of available material for the wave to grow on. These buffers are made when in parts of the pipeline the slurry velocity temporarily

drops below the deposit limit velocity. This may be the case after bends in the vertical plane, as the transport capacity is different for the horizontal and vertical part.

- More recent research conducted by de Hoog et al. (2021); Müller et al. (2018) in inclined and vertical pipeline systems, observed amplifying density waves at velocities far above the deposit limit velocity. They hypothesised that the difference in transport capacity between the horizontal and vertical section lead to temporary sedimentation of material which could lead to density wave amplification.

9.1.2 *What are the main differences between the various chosen pick-up functions?*

- One of the most known pick-up functions, the one of van Rijn (1984a) was specifically developed for fluvial flow and for low Shields numbers. This made the applicability to slurry flow, with high Shields numbers and high concentrations arbitrary. As showed by multiple studies, such as the ones from van Rhee and Talmon (2000); Winterwerp et al. (1990) and van Rhee (2010), the pick-up function of van Rijn (1984a) overestimates the erosion flux for high flow velocities.
- Therefore, new adjusted pick-up functions were desired to be able to adequately estimate the pick-up flux for these conditions. Winterwerp et al. (1990) was one of the first to study the influence of the concentration on the erosion flux. Further assessing the influence of the concentration on the erosion flux Winterwerp et al. (1992) found a new relation that would better estimate the erosion in mixture flow of high concentrations.
- van Rhee (2010) conducted research in the dilatancy reduced erosion regime. van Rhee (2010) essentially adjusted the pick-up function of van Rijn (1984a) to account for the dilatant behaviour of the grains. Theretofore, he adapted the critical Shields parameter with soil specific parameters such as the permeability and the porosity. This new pick-up flux was able to match the measurements of old data sets more accurately, while also competently matching the results for the pick-up flux in lower flow velocities, so for the grain-by-grain erosion regime. Unfortunately the new derived equation was an implicit function where the dilatant behaviour of the soil was determined by the erosion velocity itself. This requires numerical methods to solve the erosion velocity from the pick-up function.
- For the hindered erosion regime van Rhee and Talmon (2010) incorporated additional reduction factors to account for the effects of reduced pick-up due to the near bed concentration. For this they used the theory of turbulent bursts by Cao (1997) as a base. As a result of these bursts, sediment is not only entrained in to the flow, part of the sediment is returned back in to the bed layer as well. This process of returned sedimentation hinders the pick-up of new sediment, hence reducing the pick-up flux.
- For the dilatancy reduced erosion regime, Bisschop (2018) integrated sediment bulk properties to adequately agree with the physical processes at high flow velocities. In this regime the sediment is most likely to be sheared away in layers, where not only permeability and porosity play a significant role but the height and strength of the sheared layer are considerable as well. These sheared layers were the result of turbulent bursts picking up material and the entrainment of the picked up material in to the flow. Bisschop (2018) stated that the height of the shear layer was required to be solved iteratively. However, de Hoog (2021) was able to transform the equation for the height of the sheared layer. The result was an explicit function which can be solved analytically, hence greatly reducing its computational time in numerical models.
- Based on the outcomes of the research of Bisschop (2018), van Rijn et al. (2019) adjusted his older pick-up function (van Rijn, 1984a) to better account for the dilatant behaviour of soil. This to reduce the overestimation of the pick-up flux of van Rijn (1984a) for high flow velocities. Therefor, a damping factor was implemented which depending on the Shields parameter has differen values. The new pick-up function is valid the porosity of the sediment is in the range of 0.37 to 0.43. Though, if the dilatant behaviour of the soil is to be incorporated, the Shields parameter of van Rhee (2010) should be used. Furthermore, van Rijn et al. (2019) argued that the damping parameter requires some improvement as the calculations differ substantially from measurements of the experiments of Bisschop (2018).

9.2 Experimental Study

In this section the research questions regarding the experimental study are answered. Because these research questions have already been discussed in depth in section 7.5, hence a short summary thereof is given in this section.

9.2.1 *What is the influence of the mean grain size diameter on the transport capacity of the slurry in the pipeline system?*

- The influence of the mean grain size diameter on the transport capacity of the flow is characterised by the ability of the mixture to trigger amplifying density waves in the horizontal measurement section. These waves were present for the coarser sand types: Dorsilit nr.5G, Dorsilit nr.7 and Dorsilit nr.8. and could be seen as caterpillar-like movement of the stationary bed due to the sedimentation and erosion unbalance as described by de Hoog et al. (2021).

9.2.2 *What is the influence of the mixture concentration on the transport capacity of the slurry?*

- Generally, the higher mixture concentration leads to a sharper and longer drop of the mean flow velocity in the flow loop. As this sharp drop in flow velocity was not expected, the influence of the higher mixture concentration became a little more arbitrary. While one may expect that due to this drop the total time for the bed to be eroded was longer, this was generally not the case. The total time for the bed to be fully eroded was more or less the same.
- Besides that, the influence of the mixture concentration could be found in the ability of the mixture to trigger amplifying density waves in the horizontal measurement section. As described in the previous section these were seen during the experiments using Dorslit nr.5G, Dorsilit nr.7 and Dorsilit nr.8. With increasing mixture concentration, the catterpillar-like movements of the bed were observed more and more frequently.

9.2.3 *What are the limitations of the experimental study?*

- In the current setup of the experiments, it is quite hard to the specifically isolate and determine the influence that the volumetric mixture concentration has on the erosion velocity. This is mainly due to the heavy fluctuating flow velocity within the experimental flow loop. Therefore, the comparison between different concentrations has an arbitrary nature. The same goes for the assessment of the influence of the mean grain size diameter. While concentrations are approximately the same. The flow velocity, again, is not. Leading to the same kind of arbitrary causes of the influences of the mean grain size parameter on the erosion velocity.
- However, it is possible to take conclusions with sufficient certainty regarding the density wave growth both based on the mixture concentration and the mean grain size diameter. As de Hoog et al. (2021) stated, these caterpillar-like movements are the cause of the erosion and sedimentation unbalance and were found more often at higher mixture concentrations where the unbalance in sedimentation and erosion was expected to show more explicitly during the experiments.
- The design of the loop does not explicitly account for dimensionless scaling numbers, the validity of the experiments for other pipe and/or grain sizes therefore requires that the flow regime is similar to what is found and measured during these experiments.

9.3 Physical Modelling

In this section the research questions regarding the physical modelling part are resolved. Since these questions have been answered elaborately in the corresponding chapter as well, see section 8.4, a summary thereof is given here.

9.3.1 *How can the erosion transport of a density wave be modelled using an erosion and sedimentation balances in a two layer model structure?*

- The bed height evolution in time can be closely approximated using a two-layered model that models the sedimentation and erosion unbalance at the interface of the bed. Depending on the sand type the choice for the pick-up function can be varied to better match the measurements.
- For the physical modelling part it is assumed that the bed does not move as a whole, meaning that a stationary bed is present, over which a stratified slurry flow or sheet flow moves.
- The top and bottom of the pipeline are fixed and can not be eroded. Since the flow goes through a pipeline the flow is spatially confined and the bed height is not able to grow infinitely large. Therefore, if the bed height is as large as the pipe diameter the pipe is clogged. On the other hand, if the bed height is zero this means that there is no stationary bed remaining.
- To prevent clogging of the pipe at the start of the simulations a condition has to be set to ensure a sedimentation flux of zero when the mean flow velocity is almost zero. Since at these low flow velocities no sediment is picked up it is impossible to have a sedimentation flux in clear water. This condition is necessary since the current method of determining the near bed concentration gives non-zero values during stagnant water. Due to the fact that the hindered settling velocity and sedimentation flux calculation do not require a flow velocity this can result in physically impossible values. These inconsistencies are now forestalled.
- Furthermore, it is assumed that the bed is loosely packed since by means of the filling tube the bed is deposited in a settling nature. Furthermore, no soil compacting measures are taken before the experiments are started, a loose packed bed is therefore highly likely. The values for n_0 or n_i (depending on the pick-up function) are set to 0.4. Although for the pick-up function of Bisschop (2018) the value for n_i is used as a calibration parameter.
- The forcing components within the model for the erosion and sedimentation flux consists out of the measurements of the mean flow velocity and the near bed concentration, respectively.
- The initial conditions are set to the first measurement of the bed height.

9.3.2 *Which pick-up function agrees best with the experimental results?*

To answer this research question the parity graphs have been created and the resemblance of each simulation compared to the measurements have been visually compared. The latter is done using the graphs shown in appendix F. Based on these graphs the following conclusions have been drawn.

- The pick-up function of Bisschop (2018) shows the best fit for Dorsilit nr.5G, and for Dorslit nr.7 for the higher mixture concentrations, 20 and 30%.
- The pick-up function of van Rhee (2010) shows good results for the experiments with Dorsilit nr.7. This was mostly for the experiments with mixture concentrations of 5 and 10%.
- For Dorsilit nr.8, the best fits to the results were the pick-up functions of Bisschop (2018) and van Rhee (2010).
- The experiments using Zilverzand showed good resemblance with the pick-up functions of Bisschop (2018); van Rhee (2010) and van Rhee and Talmon (2010).
- Lastly, based on the measurements of GEBA, it appeared that the van Rijn (1984a) equation was able to adequately simulate the bed height evolution, however for higher concentrations (20 and 30%) the pick-up functions of van Rhee (2010) or Bisschop (2018) were much more in correspondence.

9.4 Research objective

The research objective was two-fold, the first question regards the investigation in to the density wave amplification at high concentrations due to an erosion and sedimentation unbalance. Based on the results from the ERT and the high speed camera footage it can be concluded that at higher concentrations the caterpillar-like movement of the bed was observed more frequently. Since these movements are attributed by de Hoog et al. (2021) to the erosion and sedimentation unbalance at high concentrations it is deemed proven that density wave amplification at high concentration is caused by an unbalance in erosion and sedimentation. de Hoog et al. (2021) describes the process where erosion becomes more dominant over sedimentation at high concentrations due to the fact that suspended eroded material experiences less friction and is therefore able to travel faster. As this material is transported forward, hence increasing the concentration further along the pipe, again triggering the unbalance causing the crest of the density wave to move forward. Behind the crest, the bed layer is thinner due to heavy local erosion. This thinner bed experiences less shear stresses causing the bed to stop sliding. Furthermore, de Hoog et al. (2021) states that this movement can be explained using the deposit limit velocity as well. The deposit limit velocity decreases when the concentration increases, this relationship can be calculated using a two-layer model, such as the one of Wilson et al. (2006). The crest within the density wave has a higher local concentration, hence a lower deposit limit velocity. The crest therefore becomes mobile while the tail, with a higher deposition limit velocity is still stationary.

The second objective was to determine whether the erosion and sedimentation process in slurry pipelines could be numerically modelled using a 2LM which was based on the erosion and sedimentation unbalance using different pick-up functions for the erosion flux. While some pick-up functions were much more applicable to the conditions measured during the experiments it is deemed that the developed model is able to simulate the measurements with the sufficient accuracy.

10

Recommendations

During this thesis points of improvements were found at different stages. In this chapter it is discussed, for each of these parts, where future research and/or improvement is possible to increase the quality of this study and for future research.

10.1 Literature Review

Literature regarding basic slurry flow and erosion processes is abundantly available. Therefore a choice was required to include and exclude material. To better understand the physical processes the literature review could be extended regarding several subjects. The most noteworthy topics are mentioned below.

- For now the sedimentation flux has been calculated using the hindered settling principle of Richardson and Zaki (1954), Bisschop (2018) noted however that for values where the average concentration is equal to the near bed concentration the sedimentation flux should be zero, which is mathematically not the case in the original equation of Richardson and Zaki (1954). The influence of this ratio is not accounted for in the literature review, though it is recommended to include this in further research.
- In literature, more pick-up functions describing different modes of erosion are available. For now, the ones that are most interesting and deemed most applicable to the expected flow regime during the experiments are described. It is recommended to extent the current literature review to pick-up functions for other erosion regimes as well.

10.2 Experimental Study

While conducting the experiments several issues were found, which due to time and space restrictions were not improved. These issues are mentioned below to note the importance and to overcome these issues in later research.

- It is desired to have a stable flow condition during the experiments. In this manner the influences of concentration and mean grain size diameter can be better isolated. For this the use of for example flow control can prevent the dip in the flow velocity over time.
- During the filling of the mixture bypass loop it was found that quite some sediment was lost when washing the sand to get to the desired conductivity. It is necessary to have the conductivity of the water in the bypass loop and in the main loop approximately the same as this minimises the probability of measurement errors. Therefore, to provide a bigger outflow option on the mixture bypass loop, for example two filling tubes, it can be assured that out wash of sediment is less likely.
- During the experiments it was found that some finer sediments were unable to settle efficiently, this is desired to make sure that the mixture is the only passing density wave. To efficiently and sufficiently separate the sediment and water in the sedimentation tank, it is advised to choose a larger sedimentation tank. For the finest material it appeared that the tank was not big enough to ensure clean water when

an experiment run was completed. Moreover, it was found that the sedimentation tank had to be cleaned quite often since a lot of sediment was required for each experimental run.

- The u-tube was implemented with the notion that the results may be unusable since the mixture only passes this section once. Since the u-tube requires that both the ascending and descending part of the pipelines are filled with the mixture the results are a bit arbitrary to be actually used in a quantitative or qualitative manner. If the measurement of the delivered volumetric concentration is desired a different measurement technique is recommended. Otherwise, a closed loop design instead of an open loop design could be chosen. This however may result in other difficulties regarding the measurements of the transient processes.
- Since the experiments were conducted in relatively small pipeline diameters, other physical processes play a more significant role, turbulent stresses are less able to lift coarser material in a small pipeline diameter. Therefore, it is recommended to see whether the same results may be found in pipeline diameters closer to what is used in practical dredging and/or deep sea mining applications.
- The sieve curves have been acquired using different sets of sieves, with depending on the grain size not a lot of steps in between. It is recommended to improve the current sieve curves by re-doing the sieve curve method and implementing more sieves in between the current ones. This results in a sieve curve with more detail.

10.3 Post-Processing and Results from the Experiments

Based on the results of the experiments some issues were found that could be related to the measurement equipment. The recommendations on how to improve these issues are discussed in this section.

- Based on the results retrieved by the current method a smeared image of the bed height at the interface of bed and flow was found. It may be interesting to see whether the use of EIDORS could improve this image. EIDORS implements an the interpolation method of the ERT values, this may increase the sharpness of the interface between the bed and flow layer. This can lead to a near bed concentration of zero when the flow velocity is not strong enough to be able to erode the bed.
- From the measurements and subsequent post-processing, sawtooth-like features are visible for the results of the near-bed concentration. These may be contribute to erosion sedimentation unbalance, however this may also be contributed due to the discrete grid of the ERT as well. Since the bed height is measured using a discrete method, the jumps in near bed concentration can be explained by the fact that after a certain time, a new grid row is calculated for the bed height. This can cause a jump of the near-bed concentration towards the values above these rows.
- After the experiments were conducted it was found that for some sand types, the maximum range of the pressure transducers was exceeded. Due to time restrictions other methods to estimate the bed friction were therefore chosen. Recalibration of the pressure transducers to extend the maximum values for the pressure over the ERT or changing to different pressure transducers over the ERT is thus recommended.
- During the calibration procedure of the Conductance Concentration Meters it was found that the single layered configuration of the CCM's appeared to be unable to measure the volumetric concentration with sufficient accuracy. This could be due to the effects of the vertical bend after the measurement section. It could also be because of the fact that measuring the solids particle velocity was not possible with sufficient accuracy. Therefore, it is recommended to implement a multiple layered CCM from which the particle velocity can be determined using the known distance between the planes and the difference in time between the peaks. This method is explained by van Wijk and Blok (2015) and uses a mass balance.
- Since the measurements regard transient slurry flow phenomena, it is interesting to see if the measurement frequency has a significant influence on the results, thus increasing the measurement frequency of the *Sirius-E* data inquisition system is recommended in future experiments.
- While the measurements using the ERT are perfectly adequate, it is interesting to see if a higher measurement frequency may influence the results significantly. The maximum measurement rate of the *ITS z8000* system however is unfortunately 64 Hz. Newer systems of ITOMS and the newer accompanying

software may introduce new insights in the transient processes occurring when investigating the density wave development as a result of the sedimentation and erosion unbalance.

- Standard sand types were used, the influence of the particle size distribution is therefore not studied. It is recommended to see whether the particle size distribution has a significant effect on the density wave amplification as noted by Matoušek (2001b).

10.4 Simulations

For the simulations assumptions and conditions were required to set up the model. In this section these limitations are mentioned and the recommendations to improve the sedimentation-erosion unbalance model are summarised.

- In literature a lot more pick-up functions are described, for this thesis only six have been chosen to be implemented in to the simulations. However, it is recommended to see if any other pick-up functions, such as for example the one of Matoušek (2011) , may be better at resembling the measurement data for certain sand types.
- In the current model it is chosen to model the bed interface at an infinitesimal width, this however is never present in real slurry flow applications. It is therefore recommended to validate this sedimentation and erosion unbalance model using multiple grid cells with a width. Thereto, the axial dispersion and mass and momentum balance have to be implemented for each grid cell.
- Currently, within the model using the pick-up flux of Bisschop (2018) the dimensionless turbulent bursts are calculated based on constant values. Though it is recommended to see whether the influence of these bursts is significant, this can be done with acquiring own values using an extended analysis of the high speed camera footage.
- Assumption of 125 μm for the van Rhee and Talmon (2010) pick-up function required in the simulations for GEBA. While this is not a big difference from the values quantified from the sieve curve, it is recommended to check these values.
- Friction coefficient determined in an arbitrary method, recommended to use relations found in literature to better estimate the fiction coefficient, one may use e.g. Matoušek (2007) or Miedema (2016) to determine the values thereof directly. The friction coefficient can also be determined using the pressure measurements, provided that the measurements are usable.
- Accounting for the influence of the inertia, van Rhee (2010) stated that in (high) flow velocities the mass of the particles has to be accelerated within a relatively short time towards the flow velocity above the bed. This acceleration is dependent on the shear layer and the bulk velocity. The influence of this inertia component is recommended to include when the current model is extended.
- As discussed by van Rhee (2010) the collisional stresses at the current flow regime for the coarser sand types may be of importance for the shear rate and concentration in the top layer. Hence, interparticle stresses may play a more significant role and have an effect on the mobility mechanism. It is therefore recommended to study if these interparticle stresses play a significant role in the flow regime in these small pipeline diameters.
- In case of sheet flow the roughness height of the bed is dependent on the Shields parameter (Wilson, 1989). Since sheet flow was observed, the values for the roughness height within the simulations including the ones using the van Rijn (1984a) pick-up function may need to be determined otherwise. It is recommended to study the influence of the choice for the value of the roughness height of the bed within the simulations more explicitly.
- Within the current simulations some pick-up functions required a little calibration, either based on the friction coefficient or the initial bed porosity. Using a more quantitative optimisation script, one may be able to better estimate the measurements. It is recommended to study the possibilities whether this can be implemented in the simulations for the Bisschop (2018) and van Rhee (2010) pick-up functions, as these functions show the best results.

References

Adler, A., Sutherland, A., & Kotze, R. (2019). Location of bed interface in settling slurry pipe flow using ert. In *19th international conference on transport and sedimentation of solid particles*.

Archie, G. E., et al. (1942). The electrical resistivity log as an aid in determining some reservoir characteristics. *Transactions of the AIME*, *146*(01), 54–62.

Bagnold, R. A. (1956). The flow of cohesionless grains in fluids. *Philosophical Transactions of the Royal Society of London. Series A, Mathematical and Physical Sciences*, *249*(964), 235-297. Retrieved from `https://royalsocietypublishing.org/doi/abs/10.1098/rsta.1956.0020` doi: 10.1098/rsta.1956.0020

Basco, D. R. (1977, 06). Computational methods to model unsteady variable density flows in hydraulic dredging. In *Proc. 2nd int. symp. on dredging technology* (p. 47-58).

Bianco, C., Higuita, J. E. P., Tosco, T., Tiraferri, A., & Sethi, R. (2017). Controlled deposition of particles in porous media for effective aquifer nanoremediation. *Scientific reports*, *7*(1), 1–10.

Bischoff, J. L., & Piper, D. Z. (1979). *Marine geology and oceanography of the pacific manganese nodule province*. Springer Science & Business Media.

Bisschop, F. (2018). *Erosion of sand at high flow velocities: An experimental study* (Unpublished doctoral dissertation). Delft University of Technology.

Bisschop, F., Miedema, S. A., Visser, P. J., Keetels, G. H., & van Rhee, C. (2016). Experiments on the pickup flux of sand at high flow velocities. *Journal of Hydraulic Engineering*, *142*(7), 04016013. doi: 10.1061/(ASCE)HY.1943-7900.0001142

Blöthe, M., Wegorzewski, A., Müller, C., Simon, F., Kuhn, T., & Schippers, A. (2015). Manganese-cycling microbial communities inside deep-sea manganese nodules. *Environmental Science & Technology*, *49*(13), 7692-7700. doi: 10.1021/es504930v

Brownlie, W. R. (1981). *Prediction of flow depth and sediment discharge in open channels* (Tech. Rep. No. 43A). California Institute of Technology , Pasadena, CA: W. M. Keck Laboratory of Hydraulics and Water Resources Report.

Buitendijk, M. (2020). *Royal IHC develops six-kilometre riser system for deepsea mining.* (`https://www.swzmaritime.nl/news/2020/01/23/royal-ihc-develops-six-kilometre-riser-system-for-deepsea-mining/`)

Cao, Z. (1997). Turbulent bursting-based sediment entrainment function. *Journal of Hydraulic Engineering*, *123*(3), 233-236. Retrieved from `https://ascelibrary.org/doi/abs/10.1061/%28ASCE%290733-9429%281997%29123%3A3%28233%29` doi: 10.1061/(ASCE)0733-9429(1997)123:3(233)

Clift, R., & Clift, D. H. M. (1981). Continuous measurement of the density of flowing slurries. *International Journal of Multiphase Flow*, *7*(5), 555 - 561. Retrieved from `http://www.sciencedirect.com/science/article/pii/0301932281900586` doi: https://doi.org/10.1016/0301-9322(81)90058-6

de Hoog, E. (2016). *Coarse particle slurry flow in inclined pipes and vertical s-bends* (Unpublished master's thesis). TU Delft, the Netherlands.

de Hoog, E. (2021). *An explicit method for computing the Bisschop (2018) erosion model.* Internal memo. (M21-001, Royal IHC)

de Hoog, E., in 't Veld, M., van Wijk, J. M., & Talmon, A. M. (2017). An experimental study into flow assurance of coarse inclined slurries. In *Proceedings 18th international conference on transport and sedimentation of solid particles (t&s 2017)* (pp. 113–120). Wroclaw University of Environmental and Life Sciences.

de Hoog, E., Talmon, A. M., & van Rhee, C. (2021). Unstable transients affecting flow assurance during hydraulic transportation of granular two phase slurries. *Journal of Hydraulic Engineering*. doi: 10.1061/(ASCE)HY.1943-7900.0001913

den Adel, H. (1987). Heranalyse doorlatendheidsmetingen door middel van de forchheimer relatie. *Techical Rep. No. CO-272550/56, GeoDelft/Deltares, Delft, Netherlands*.

Durand, R., & Condolios, E. (1952). Experimental investigation of the transport of solids in pipes. *Deuxieme Journée de l'hydraulique, Societé Hydrotechnique de France*.

Einstein, H. A. (1950). *The bed-load function for sediment transportation in open channel flows* (No. 1026). US Government Printing Office.

Faraj, Y., Wang, M., & Jia, J. (2013, 09). Application of the ert for slurry flow regime characterisation. In *7th world congress on industrial process tomography.*

Ferguson, R., & Church, M. (2004). A simple universal equation for grain settling velocity. *Journal of sedimentary Research*, *74*(6), 933–937.

Fernandez Luque, R. (1974). *Erosion and transport of bed-load sediment* (Unpublished doctoral dissertation). Delft University of Technology.

Führböter, A. (1961). *Über die förderung von sand-wasser-gemischen in rohrleitungen*. Mitteilungen des Franzius-Instituts für Grund- und Wasserbau der Technischen Hochschule Hannover.

Giguère, R., Fradette, L., Mignon, D., & Tanguy, P. (2008). Characterization of slurry flow regime transitions by ert. *Chemical Engineering Research and Design*, *86*(9), 989 - 996. Retrieved from http://www.sciencedirect.com/science/article/pii/S0263876208000932 doi: https://doi.org/10.1016/j.cherd.2008.03.014

Glasby, G. P. (2000). Lessons learned from deep-sea mining. *Science*, *289*(5479), 551–553. Retrieved from https://science.sciencemag.org/content/289/5479/551 doi: 10.1126/science.289.5479.551

Hagler, S. T. W. (1956, October 30). *Means for determining specific gravity of fluids and slurries in motion.* Google Patents. (US Patent 2,768,529)

Halfar, J., & Fujita, R. M. (2007). Danger of deep-sea mining. *Science*, *316*(5827), 987–987. Retrieved from https://science.sciencemag.org/content/316/5827/987 doi: 10.1126/science.1138289

Hallermeier, R. J. (1981). Terminal settling velocity of commonly occurring sand grains. *Sedimentology*, *28*(6), 859-865. Retrieved from https://onlinelibrary.wiley.com/doi/abs/10.1111/j.1365-3091.1981.tb01948.x doi: https://doi.org/10.1111/j.1365-3091.1981.tb01948.x

Hein, J. R., Koschinsky, A., & Kuhn, T. (2020, February). Deep-ocean polymetallic nodules as a resource for critical materials. *Nature Reviews Earth and Environment*, *1*(3), 158-169. doi: 10.1038/s43017-020-0027-0

Hoagland, P., Beaulieu, S., Tivey, M. A., Eggert, R. G., German, C., Glowka, L., & Lin, J. (2010). Deep-sea mining of seafloor massive sulfides. *Marine Policy*, *34*(3), 728 - 732. Retrieved from http://www.sciencedirect.com/science/article/pii/S0308597X09001870 doi: https://doi.org/10.1016/j.marpol.2009.12.001

International Seabed Authority. (2013). *Decision of the council of the international seabed authority relating to amendments to the regulations on prospecting and exploration for polymetallic nodules in the area and related matters ISBA/19/c/17.* (https://ran-s3.s3.amazonaws.com/isa.org.jm/s3fs-public/files/documents/isba-19c-17_0.pdf)

Jufin, A., & Lopatin, N. (1966). O projekte tuin na gidrotransport zernistych materialov po stalnym trubo-provodam. *Gidrotechniceskoe Strojitelstvo*, *9*, 49–52.

Kennedy, J. F. (1969). The formation of sediment ripples, dunes, and antidunes. *Annual review of fluid mechanics*, *1*(1), 147–168.

Kökpınar, M. A., & Göğüş, M. (2001). Critical flow velocity in slurry transporting horizontal pipelines. *Journal of Hydraulic Engineering*, *127*(9), 763-771. Retrieved from https://ascelibrary.org/doi/abs/10.1061/%28ASCE%290733-9429%282001%29127%3A9%28763%29 doi: 10.1061/(ASCE)0733-9429(2001)127:9(763)

Leung, L., Wiles, R., & Nicklin, D. (1969). Transition from fluidised to packed bed flow in vertical hydraulic conveying. *Trans Inst Chem Eng*, *47*(8), t271-t278. Retrieved from https://www.scopus.com/inward/record.uri?eid=2-s2.0-0014649728&partnerID=40&md5=dd2164f60d625e00d6c1d2ce679c0b1e

Matoušek, V. (1995). Non-stationary solids flow in a long slurry pipeline with pumps in series - process of material aggregation. In *Proceedings of the 8th conference on transport and sedimentation of solid particles* (p. 1-10).

Matoušek, V. (1996a, 01). Solids transportation in a long pipeline connected with a dredge. *Terra et Aqua*, 3-11.

Matoušek, V. (1996b, 01). Unsteady solids flow in a long slurry pipeline with pumps in series - process of material aggregation. *Journal of Hydrology and Hydromechanics*, *44*, 396-409.

Matoušek, V. (1997). *Flow mechanism of sand-water mixtures* (Unpublished doctoral dissertation). Technische Universiteit Delft.

Matoušek, V. (2001a). Distribution and friction of particles in pipeline flow of sand-water mixtures. In *Handbook of powder technology* (Vol. 10, pp. 465–471). Elsevier.

Matoušek, V. (2001b). On the amplification of density waves in long pipelines connected with a dredge. In *Proceedings 16th world dredging congress.*

Matoušek, V. (2004, September). *Dredge pumps and slurry transport OE4625.* (lecture notes)

Matoušek, V. (2007, 06). Interaction of slurry pipe flow with a stationary bed. *Journal of the Southern African Institute of Mining and Metallurgy*, *107*, 365-372.

Matoušek, V. (2009). Predictive model for frictional pressure drop in settling-slurry pipe with stationary deposit. *Powder Technology*, *192*(3), 367-374. doi: https://doi.org/10.1016/j.powtec.2009.01.017

Matoušek, V. (2011). Solids transport formula in predictive model for pipe flow of slurry above deposit. *Particulate Science and Technology*, *29*(1), 89-106. doi: 10.1080/02726351.2010.510549

Matoušek, V., & Krupička, J. (2011). Unified model for coarse-slurry flow with stationary and sliding bed. In *Proceedings of the 15th international conference on transport and sedimentation of solid particles, wroclaw, poland* (pp. 6–9).

Matoušek, V., & Krupička, J. (2013, September). Different types of unsteady flow of solids generated in laboratory slurry pipe loop. In *16th international conference on transport and sedimentation of solid particles.*

Miedema, S. A. (2015, 06). The slip ratio or holdup function in slurry transport. In *Proceedings of Western Dredging Association and Texas A&M University Center for Dredging Studies - Dredging Summit and Expo 2015.*

Miedema, S. A. (2016). *Slurry transport: Fundamentals, a historical overview and the delft head loss & limit deposit velocity framework.* TU Delft Open.

Miedema, S. A., & Ramsdell, R. C. (2014). An analysis of the hydrostatic approach of wilson for the friction of a sliding bed. In *Weda xxxiv technical conference & tamu 45 dredging seminar.*

Miedema, S. A., Zhihua, L., & Matousek, V. (2003). Numerical simulation of the development of density waves in a long pipeline and the dynamic system behaviour. *Terra et Aqua*, 11–23.

Miller, K. A., Thompson, K. F., Johnston, P., & Santillo, D. (2018). An overview of seabed mining including the current state of development, environmental impacts, and knowledge gaps. *Frontiers in Marine Science*, *4*, 418. Retrieved from `https://www.frontiersin.org/article/10.3389/fmars.2017.00418` doi: 10.3389/fmars.2017.00418

Miller, R. W. (1983). *Flow measurement engineering handbook*. McGraw-Hill.

Monhemius, A. J. (1980). The extractive metallurgy of deep-sea manganese nodules. In *Topics in non-ferrous extractive metallurgy* (pp. 42–69). SCI London.

Müller, T., Mischo, H., & van Wijk, J. M. (2018, 02). Blue mining test facility. In *Sme annual conference & expo.*

NEN-EN:993-1. (2012, December). *Tests for geometrical properties of aggregates - part 1: Determination of particle size distribution - sieving method* (Vol. 2011; Standard). Delft: Stichting Nederlandse Normalisatie Instituut.

Newitt, D. (1955). Hydraulic conveying of solids in horizontal pipes. *Trans. Instn Chem. Engrs*.

Newitt, D., Richardson, J., & Gliddon, B. (1961). Hydraulic conveying of solids in vertical pipes. *Trans. Instn. Chem. Engrs*, *39*, 93–100.

NOAA Office of Ocean Exploration and Research. (2019). *2019 southeastern u.s. deep-sea exploration - dive 07: Habitat response 01.* `https://oceanexplorer.noaa.gov/okeanos/explorations/ex1907/dailyupdates/nov7/nov7.html`.

Oroskar, A. R., & Turian, R. M. (1980). The critical velocity in pipeline flow of slurries. *AIChE Journal*, *26*(4), 550-558. Retrieved from `https://aiche.onlinelibrary.wiley.com/doi/abs/10.1002/aic.690260405` doi: 10.1002/aic.690260405

Pugh, F. J., & Wilson, K. C. (1999). Velocity and concentration distributions in sheet flow above plane beds. *Journal of Hydraulic Engineering*, *125*(2), 117-125. Retrieved from `https://ascelibrary.org/doi/abs/10.1061/%28ASCE%290733-9429%281999%29125%3A2%28117%29` doi: 10.1061/(ASCE)0733-9429(1999)125:2(117)

Ramsdell, R. C., & Miedema, S. A. (2013). An overview of flow regimes describing slurry transport. *WODCON XX*, 15.

Raudkivi, A. (1990). *Loose boundary hydraulics*. Pergamon Press.

Reynolds, O. (1885). Lvii. on the dilatancy of media composed of rigid particles in contact, with experimental illustrations. *The London, Edinburgh, and Dublin Philosophical Magazine and Journal of Science*, *20*(127), 469-481. Retrieved from https://doi.org/10.1080/14786448508627791 doi: 10.1080/14786448508627791

Richardson, J. F., & Zaki, W. N. (1954). Sedimentation and fluidisation: Part i. *Transactions of the Institution of Chemical Engineers*, *32*, 35–53.

Rowe, P. N. (1987). A convenient empirical equation for estimation of the richardson-zaki exponent. *Chemical Engineering Science*, *42*, 2795-2796.

Shields, A. (1936). Anwendung der aehnlichkeitsmechanik und der turbulenzforschung auf die geschiebebewegung. *PhD Thesis Technical University Berlin*.

Steele, J. H., Thorpe, S. A., & Turekian, K. K. (2009). *Elements of physical oceanography: A derivative of the encyclopedia of ocean sciences - marine chemistry and geochemistry*. Elsevier Science. Retrieved from https://books.google.nl/books?id=F0HstDk_cgYC

Talmon, A. M. (1999). Mathematical analysis of the amplification of density variations in long distance sand transport pipelines. In *14th international conference on slurry handling and pipeline transport* (p. 3-20).

Talmon, A. M. (2002). Solids transport instability in the sliding bed regime. In *11th international conference on transport and sedimentation of solid particles. ghent* (pp. 9–12).

Talmon, A. M. (2013). Analytical model for pipe wall friction of pseudo-homogenous sand slurries. *Particulate Science and Technology*, *31*(3), 264-270. doi: 10.1080/02726351.2012.717588

Talmon, A. M. (2019). *OE44035 - SNNS2-2019- Rheology.* University Lecture.

Talmon, A. M., Aanen, L., & Bakker-Vos, R. (2007). Laboratory tests on self-excitation of concentration fluctuations in slurry pipelines. *Journal of Hydraulic Research*, *45*(5), 653-660. Retrieved from https://doi.org/10.1080/00221686.2007.9521801 doi: 10.1080/00221686.2007.9521801

Turian, R., Hsu, F.-L., & Ma, T.-W. (1987). Estimation of the critical velocity in pipeline flow of slurries. *Powder Technology*, *51*(1), 35 - 47. Retrieved from http://www.sciencedirect.com/science/article/pii/0032591087800384 doi: https://doi.org/10.1016/0032-5910(87)80038-4

van Wijk, J. M. (2016). *Vertical hydraulic transport for deep sea mining: A study into flow assurance* (Doctoral dissertation, Delft University of Technology). doi: 10.4233/uuid:2e493b95-486a-4c2f-a8ae-749990b06a5e

van Wijk, J. M., & Blok, B. (2015). The influence of grain size on the performance of conductivity concentration meters. *Flow Measurement and Instrumentation*, *45*, 384 - 390. Retrieved from http://www.sciencedirect.com/science/article/pii/S0955598615300042 doi: https://doi.org/10.1016/j.flowmeasinst.2015.08.005

van Wijk, J. M., Talmon, A. M., & van Rhee, C. (2016). Stability of vertical hydraulic transport processes for deep ocean mining: An experimental study. *Ocean Engineering*, *125*, 203 - 213. Retrieved from http://www.sciencedirect.com/science/article/pii/S002980181630347X doi: https://doi.org/10.1016/j.oceaneng.2016.08.018

van den Berg, C. (1998). Pipelines as transportation systems. *Proceedings of the European Mining Course. IHC-MTI, Kinderdijk, the Netherlands*.

van Grunsven, F., & Talmon, A. M. (2012). Local anomalies in slip for slurry flow within pipes near the deposit limit velocity. In *Proc. ceda dredging days 2012.*

Vanoni, V., & Brooks, N. (1957). *Laboratory studies of the roughness and suspended load of alluvial streams*. U.S. Army Engineer Division, Missouri River. Retrieved from https://books.google.nl/books?id=6wiFYTW-8nkC

van Rhee, C. (2010). Sediment entrainment at high flow velocity. *Journal of Hydraulic Engineering*, *136*(9), 572-582. Retrieved from https://ascelibrary.org/doi/abs/10.1061/%28ASCE%29HY.1943-7900.0000214 doi: 10.1061/(ASCE)HY.1943-7900.0000214

van Rhee, C. (2018, April). *Lecture notes oe44045.* (lecture notes)

van Rhee, C., & Bezuijen, A. (1998). The breaching of sand investigated in large-scale model tests. In *Proc. coastal engineering 1998* (p. 2509-2519). Retrieved from https://ascelibrary.org/doi/abs/10.1061/9780784404119.189 doi: 10.1061/9780784404119.189

van Rhee, C., & Talmon, A. M. (2000, 9). Entrainment of sediment (or reduction of sedimentation) at high concentration. In *Proc., 10th int. symp. on transport and sedimentation of solid particles.*

van Rhee, C., & Talmon, A. M. (2010, 09). Sedimentation and erosion of sediment at high solids concentration. In *18th international conference on hydrotransport.*

van Rijn, L. C. (1984a). Sediment pick-up functions. *Journal of Hydraulic Engineering*, *110*(10), 1494-1502. Retrieved from https://ascelibrary.org/doi/abs/10.1061/%28ASCE%290733-9429%281984%29110%3A10%281494%29 doi: 10.1061/(ASCE)0733-9429(1984)110:10(1494)

van Rijn, L. C. (1984b). Sediment transport, part I: Bed load transport. *Journal of Hydraulic Engineering*, *110*(10), 1431-1456. Retrieved from https://ascelibrary.org/doi/abs/10.1061/%28ASCE%290733-9429%281984%29110%3A10%281431%29 doi: 10.1061/(ASCE)0733-9429(1984)110:10(1431)

van Rijn, L. C. (1984c). Sediment transport, part II: Suspended load transport. *Journal of Hydraulic Engineering*, *110*(11), 1613-1641. Retrieved from https://ascelibrary.org/doi/abs/10.1061/%28ASCE%290733-9429%281984%29110%3A11%281613%29 doi: 10.1061/(ASCE)0733-9429(1984)110:11(1613)

van Rijn, L. C., Bisschop, R., & van Rhee, C. (2019). Modified sediment pick-up function. *Journal of Hydraulic Engineering*, *145*(1), 06018017. Retrieved from https://ascelibrary.org/doi/abs/10.1061/%28ASCE%29HY.1943-7900.0001549 doi: 10.1061/(ASCE)HY.1943-7900.0001549

van Wijk, J. M., van Rhee, C., & Talmon, A. M. (2014). Axial dispersion of suspended sediments in vertical upward pipe flow. *Ocean Engineering*, *92*, 20 - 30. Retrieved from http://www.sciencedirect.com/science/article/pii/S0029801814003758 doi: https://doi.org/10.1016/j.oceaneng.2014.09.041

Vlasák, P., Chára, Z., Konfršt, J., & Kysela, B. (2017). Flow of heterogeneous slurry in horizontal and inclined pipes. In *Proceedings of the 18th international conference on transport & sedimentation of solid particles, prague (czech republic), 369* (Vol. 376).

Vlasák, P., Chára, Z., Krupička, J., & Konfršt, J. (2014). Experimental investigation of coarse particles-water mixture flow in horizontal and inclined pipes. *Journal of Hydrology and Hydromechanics*, *62*(3), 241–247.

Wedding, L., Reiter, S., Smith, C., Gjerde, K., Kittinger, J., Friedlander, A., ... Crowder, L. (2015, 07). Oceans. managing mining of the deep seabed. *Science (New York, N.Y.)*, *349*, 144-5. doi: 10.1126/science.aac6647

Wilson, K. C. (1976). A unified physically-based analysis of solid-liquid pipeline flow. In *Proc. hydrotransport* (Vol. 4, pp. 1–16).

Wilson, K. C. (1979). Deposition limit nomograms for particles of various densities in pipeline flow. In *Proc. hydrotransport* (Vol. 6, pp. 1–12).

Wilson, K. C. (1989). Friction of wave-induced sheet flow. *Coastal Engineering*, *12*(4), 371-379. Retrieved from https://www.sciencedirect.com/science/article/pii/0378383989900136 doi: https://doi.org/10.1016/0378-3839(89)90013-6

Wilson, K. C. (1992). Influence of particle properties on solid effects. In *Proceedings of the 10th international kol. massenguttransport druch rohrleitungen* (Vol. 4, pp. 1–16).

Wilson, K. C., Addie, G. R., Sellgren, A., & Clift, R. (1992). *Slurry transport using centrifugal pumps*. New York: Elsevier Applied Sciences.

Wilson, K. C., Addie, G. R., Sellgren, A., & Clift, R. (2006). *Slurry transport using centrifugal pumps*. Springer Science & Business Media.

Wilson, K. C., & Sellgren, A. (2003). Interaction of particles and near-wall lift in slurry pipelines. *Journal of Hydraulic Engineering*, *129*(1), 73-76. doi: 10.1061/(ASCE)0733-9429(2003)129:1(73)

Wilson, K. C., Sellgren, A., & Addie, G. (2000). Near-wall fluid lift of particles in slurry pipelines. In *Proceedings of the 10th international conference on transport and sedimentation of solid particles* (p. 435–444).

Winterwerp, J. C., Bakker, W. T., Mastbergen, D. R., & van Rossum, H. (1992). Hyperconcentrated sand-water mixture flows over erodible bed. *Journal of Hydraulic Engineering*, *118*(11), 1508-1525. doi: 10.1061/(ASCE)0733-9429(1992)118:11(1508)

Winterwerp, J. C., Groot, M., Mastbergen, D. R., & Verwoert, H. (1990, 01). Hyperconcentrated sand-water mixture flows over a flat bed. *Journal of Hydraulic Engineering*, *116*, 36-54. doi: 10.1061/(ASCE)0733-9429(1990)116:1(36)

Zanke, U. (1977). Berechnung der sinkgeschwindigkeiten von sedimenten. *Mitt. Franzius Inst. Grund-Wasserbau*, *46*, 230-245.

V

Appendices

A

Calibration Methods for Various Measuring Equipment

For the use of various instruments in the loop, either a brand new calibration or revision of the current calibration curve was required. In this appendix the methods are described briefly. Furthermore, the actual curves and equations are given as well.

A.1 Pressure difference over the ERT

For determining the pressure loss over the ERT, which can be used to determine the bed friction coefficient, a *Rosemount DP3*, with a range of - 1 kPa to 1 kPa is used. The bed friction coefficient is required for the pick-up functions of van Rhee and Talmon (2010) and Bisschop (2018). The values of the data points found for the calibration are given in table A.1.

Table A.1: Values of the data points found for the calibration of the pressure sensor in the horizontal measurement section

Voltage in [V]	1.3	1.58	1.85	2.31	2.75	3.0533	3.87	4.2	4.72	5.1
Pressure in [kPa]	-0.83	-0.7	-0.55	-0.32	-0.11	-0.04	0.4	0.56	0.82	1.02

The resulting line through these points as shown in figure A.1 is found by a linear regression method using Python.

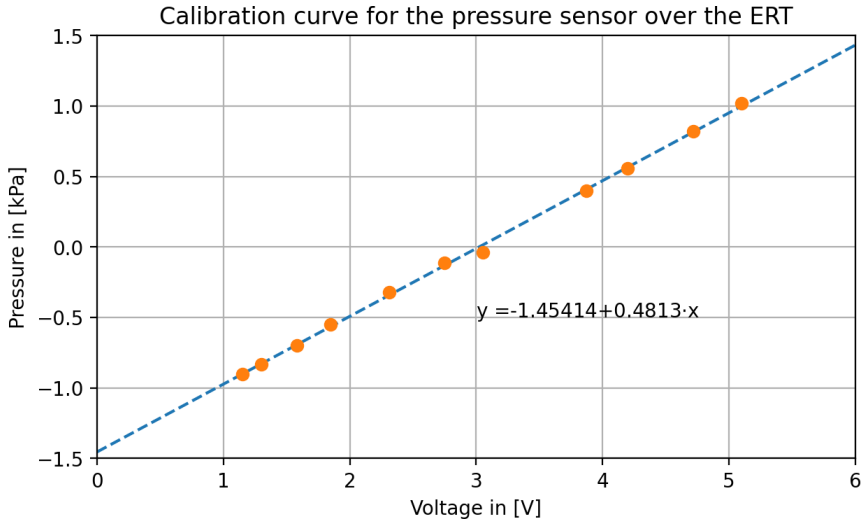

Figure A.1: Calibration curve for the pressure sensor in the horizontal measurement section

The equation for this line is mentioned explicitly in equation A.1 for clarity.

$$\Delta P = -1.45414 + 0.4813 \cdot V \tag{A.1}$$

After all the experiments were done and the measurements were inspected, it was found that most of the experiments exceeded the maximum measuring range. Due to time constraints it was unfortunately not possible to redo all the experiments with an adjusted pressure measuring range.

A.2 Pressure Transducers in the U-tube

Similarly as the pressure transducer in the ERT section the calibration curve for the pressure transducers in the U-tube can be found. In the ascending pipeline section a *Rosemount DP3*, with a range of - 0 kPa to 7 kPa is implemented and a *Rosemount DP3*, with a range of - 1 kPa to 6 kPa, is implemented in the descending pipeline section. For the ascending pipe section:

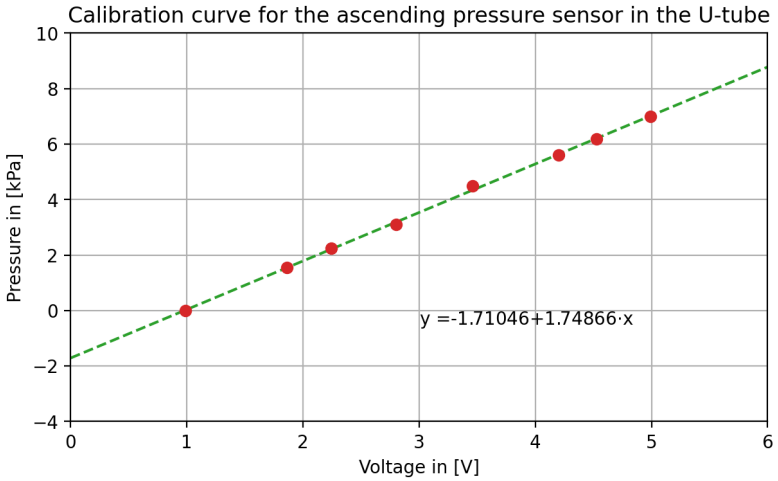

Figure A.2: Calibration curve for the pressure sensor ascending pipeline section in the u-tube

The equation for this line is mentioned explicitly in equation A.2 for clarity again.

$$\Delta P = -1.71046 + 1.74866 \cdot V \tag{A.2}$$

For the descending pipe section:

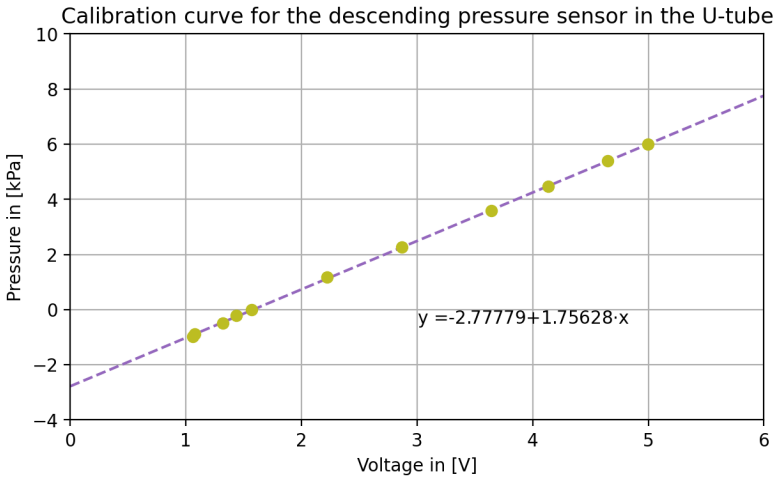

Figure A.3: Calibration curve for the pressure sensor descending pipeline section in the u-tube

The equation for this line is mentioned explicitly in equation A.3 for clarity once more.

$$\Delta P = -2.77779 + 1.75628 \cdot V \tag{A.3}$$

A.3 Flow Meter

During the first measurements it appeared that the flow meter reported different results through *Dewesoft X* and the accompanying screen on the flow meter. Therefore, it was opted to redo the calibration for the *Endress+Hauser PROMAG 55S*. The main loop pump was set at different frequencies, such that different flow rates were measured. Subsequently, after the desired flow rate was stable, the flow rates were written down and the data was logged. Thereafter, the mean voltages over the time series were calculated and coupled to the flow rates. The resulting calibration line is shown in figure A.4.

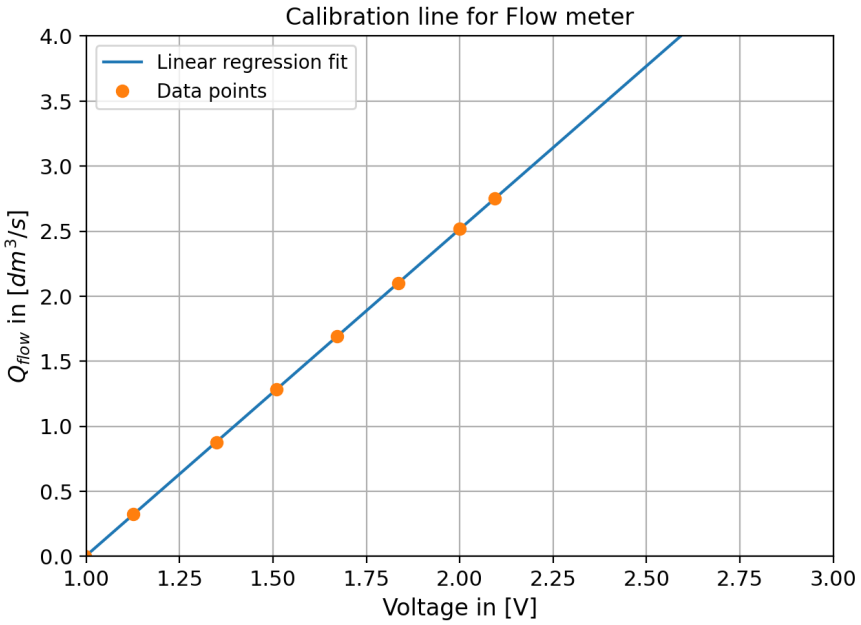

Figure A.4: Calibration line regression fit for the *Endress+Hauser PROMAG 55S*

The corresponding equation for the line is given in equation A.4

$$Q_{flow} = -2.50343 + 2.50932 \cdot V \tag{A.4}$$

A.4 Conductance Concentration Meter

To determine the sensitivity and characteristic of the sensors different mixtures of tap water and demineralized water are used to fill the CCM units. Measuring the conductivity with a handheld meter and then logging the output signal of the CCM units in voltages leads to a set of data points. Using linear regression one can plot a line through these data points, thus ensuring for each individual sensor that a unique $k_f - U$ characteristic can be used for the data processing. The results for the calibration of water resulted in the following graph. The graph is shown in figure A.5. The sensors are denoted as CCM1 to CCM4 in the data logging software. Where CCM1 and CCM2 are considered the first CCM unit located in front of the measurement section and CCM3 and CCM4 are the second unit located behind the measurement section.

The associated equations for the lines are as follows:

$$k_{f,CCM1} = 21.098743 + 161.411323 \cdot V \tag{A.5}$$
$$k_{f,CCM2} = 10.826761 + 197.180144 \cdot V \tag{A.6}$$
$$k_{f,CCM3} = 57.904947 + 130.650480 \cdot V \tag{A.7}$$
$$k_{f,CCM4} = 51.294015 + 151.126426 \cdot V \tag{A.8}$$

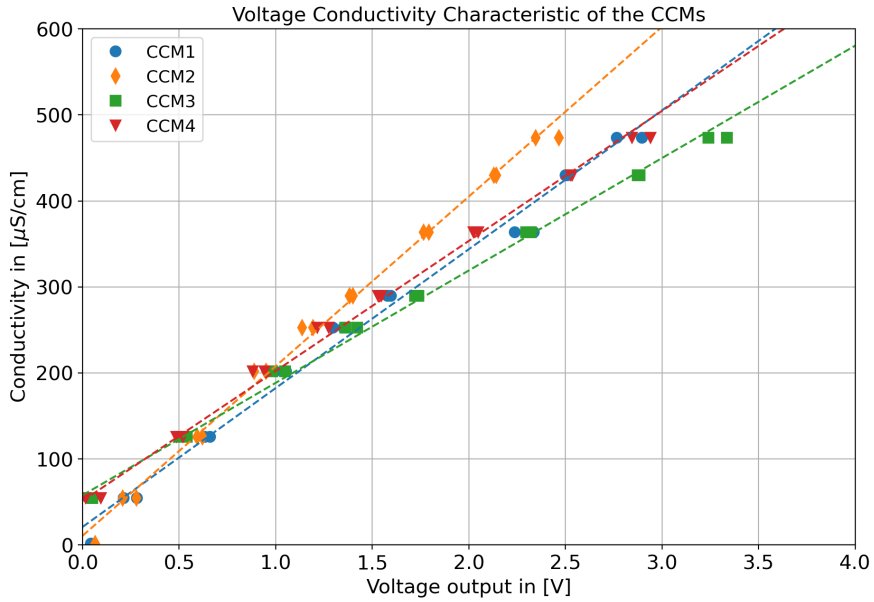

Figure A.5: Conductivity against voltage characteristic for each of the four sensors

For the calibration of the CCM's regarding the volumetric concentration, two methods can be used. The first method is quite simple, where the CCM units are filled with tap water and a known volume of sediment. The unit is then closed with blind flanges. While the sediment is settled the carrier fluid conductivity is measured, then during shaking of the CCM unit the sediment becomes suspended and the mixture conductivity is logged and measured. Thereafter the ratio of the mixture conductivity and the fluid conductivity can be computed. Since the volumetric concentration is known a plot can be made and the values can be compared to equation A.9, A.10 and A.11.

$$\frac{k_m}{k_f} = 1 - C_v^{\zeta} \tag{A.9}$$

In this relation k_f and k_m are the conductivity of the carrier fluid and mixture respectively. ζ is defined as the calibration parameter for the CCM and C_v is the volumetric concentration. When using the CCM to determine the volumetric for coarse slurry flows with a grain size of d/D>0.1 van Wijk and Blok (2015) concluded that extra calibration was necessary. While a whole range of grain sizes is used in the experiments, the condition of d/D>0.1 is not exceeded. Therefore the actual value of ζ needs to be derived from the calibration points. The second equation to which the outcomes of the calibration are compared is the Archie et al. (1942) equation and is given as:

$$\frac{k_m}{k_f} = (1 - C_v)^{\zeta_2} \tag{A.10}$$

In which ζ_2 is the calibration parameter for the Archie et al. (1942) equation. The last equation is known as the Maxwell equation and is denoted as:

$$\frac{k_m}{k_f} = \frac{2 - 2 \cdot C_v}{2 + C_v} \tag{A.11}$$

For each of the five different sand types the outcomes have been compared to the above equations. Using the linear regression fit method on the found data points, the best values for ζ and ζ_2, have been calculated as well.

The results of the calibrations for the k_m/k_f-ratio versus the volumetric concentration are shown in figures A.6 to A.8. The values of the calibration zetas are summarised in table 6.2.

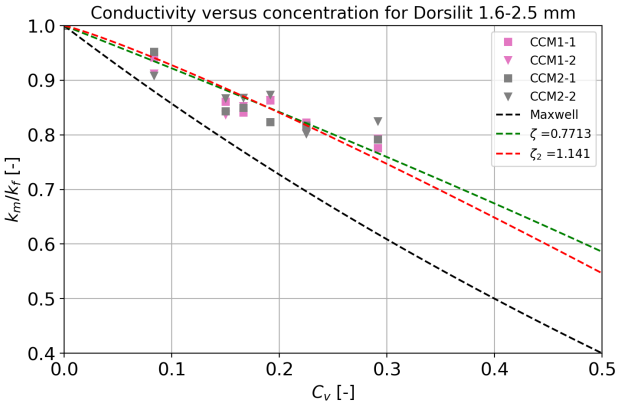

(a) Dorsilit nr.5G

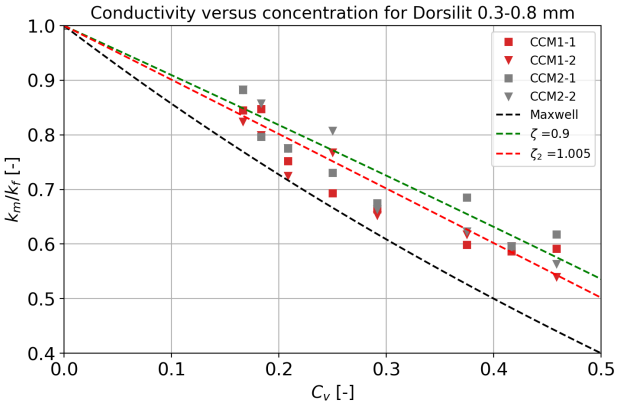

(b) Dorsilit nr.8

Figure A.6: Calibration curves for both the first CCM units for two sand types

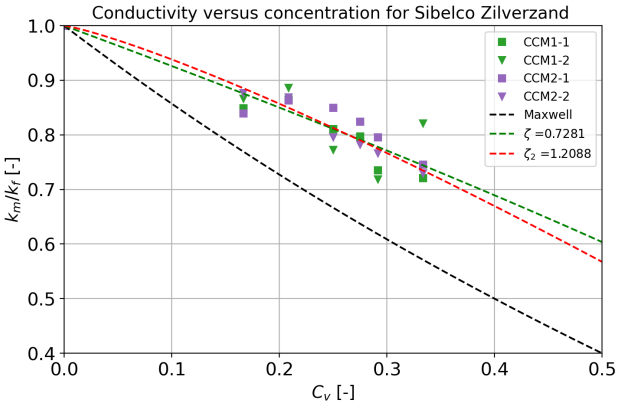

(a) Zilverzand

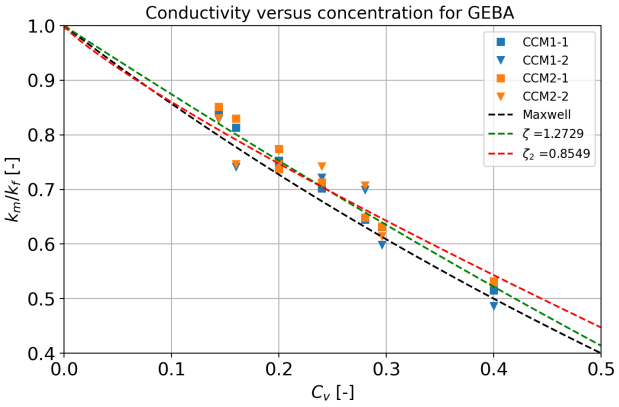

(b) GEBA

Figure A.7: Calibration curves for both the first CCM units for two sand types

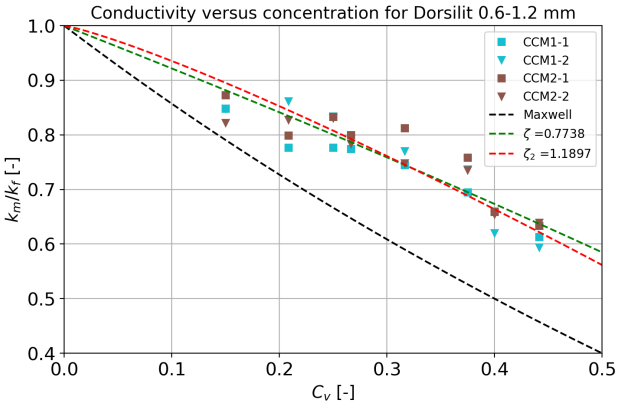

(a) First CCM unit

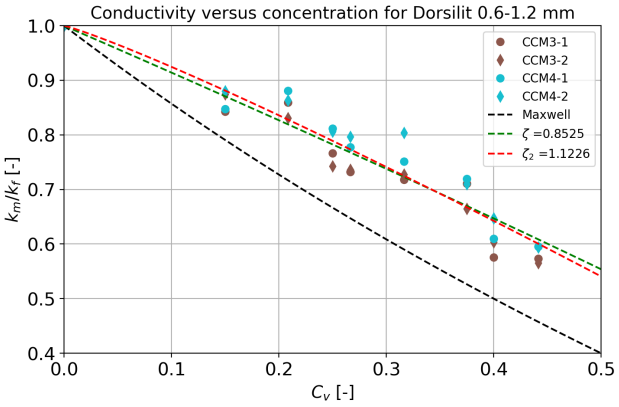

(b) Second CCM unit

Figure A.8: Calibration curves for both the CCM units for Dorsilit nr.7

B

Pressure Measurements from the Experiments

B.1 Dorsilit nr.5G

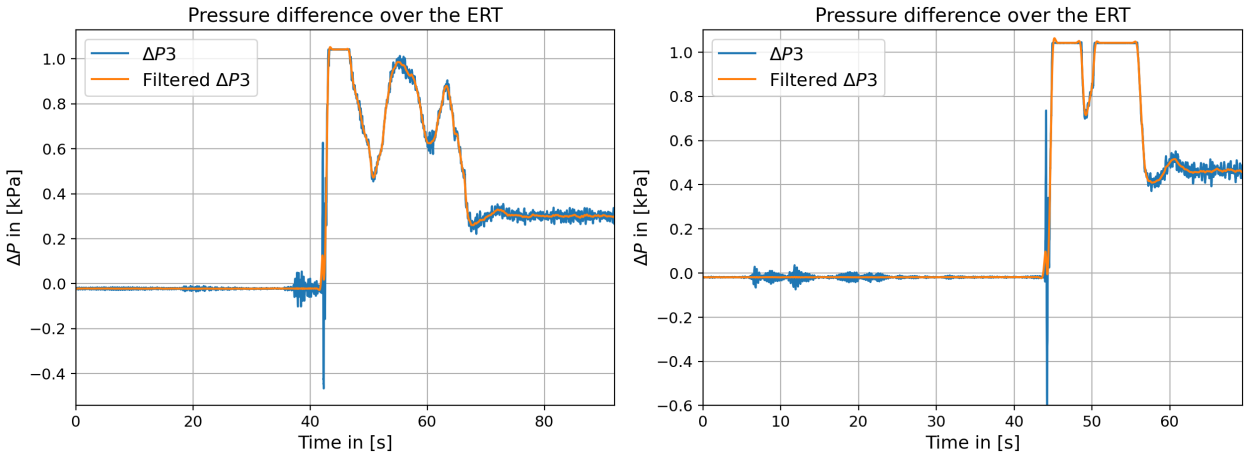

(a) Mixture with $c_v = 0.05$

(b) Mixture with $c_v = 0.10$

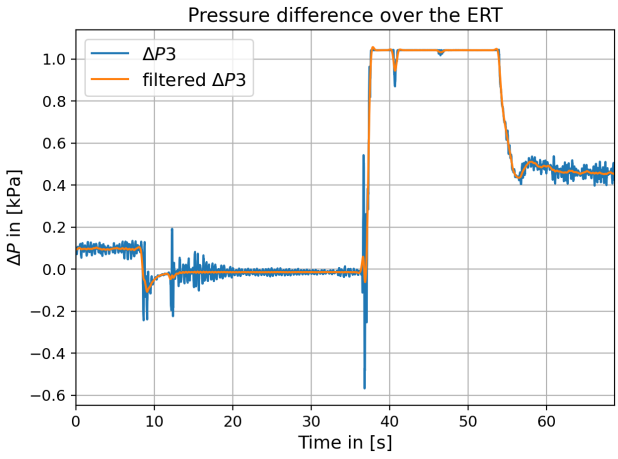

(c) Mixture with $c_v = 0.20$

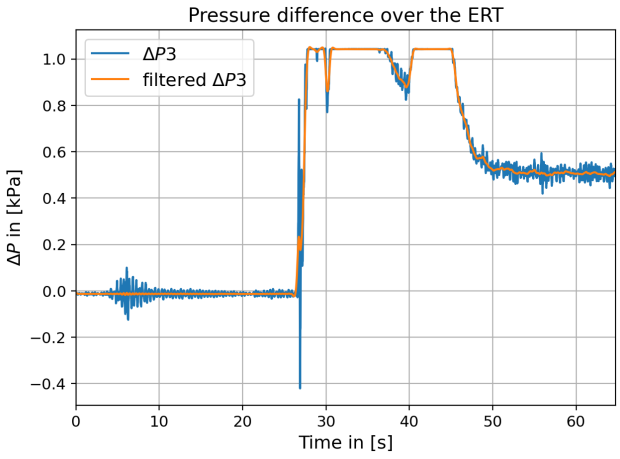

(d) Mixture with $c_v = 0.30$

Figure B.1

B.2 Dorsilit nr.7

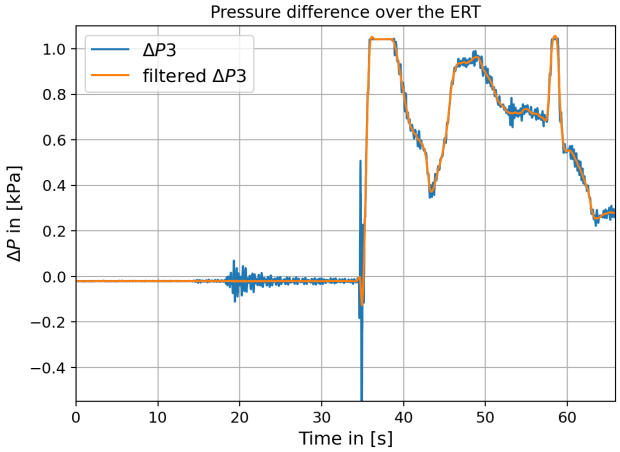

(a) Mixture with $c_v = 0.05$

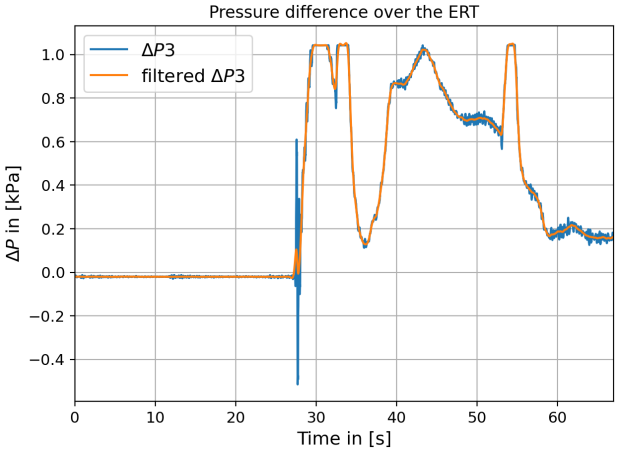

(b) Mixture with $c_v = 0.10$

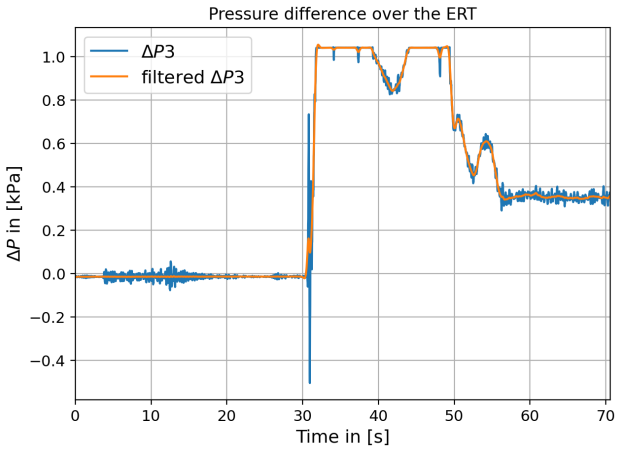

(c) Mixture with $c_v = 0.20$

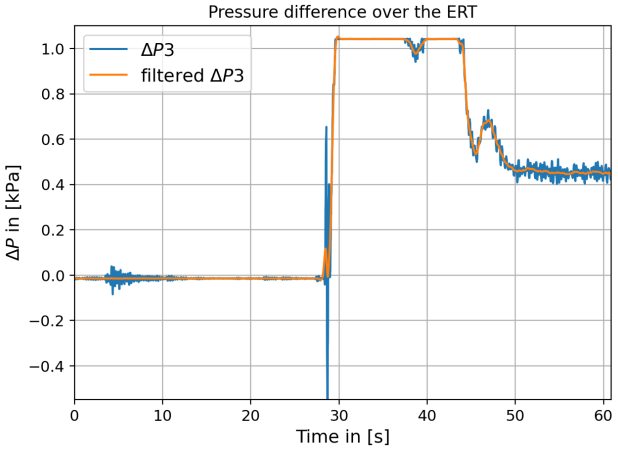

(d) Mixture with $c_v = 0.30$

Figure B.2

B.3 Dorsilit nr.8

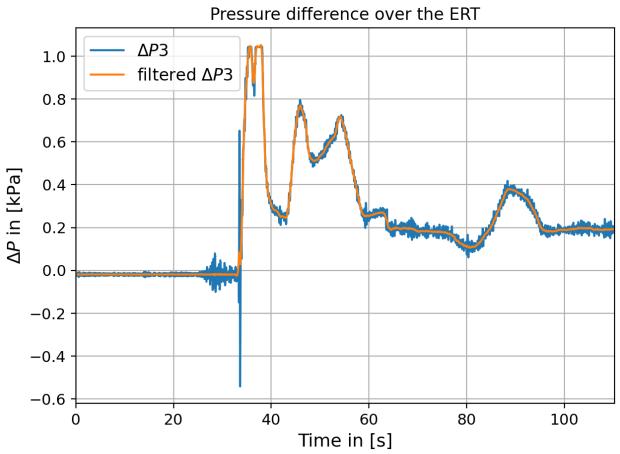

(a) Mixture with $c_v = 0.05$

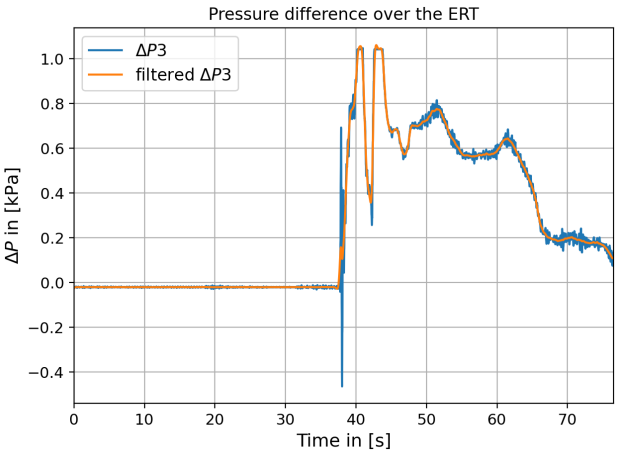

(b) Mixture with $c_v = 0.10$

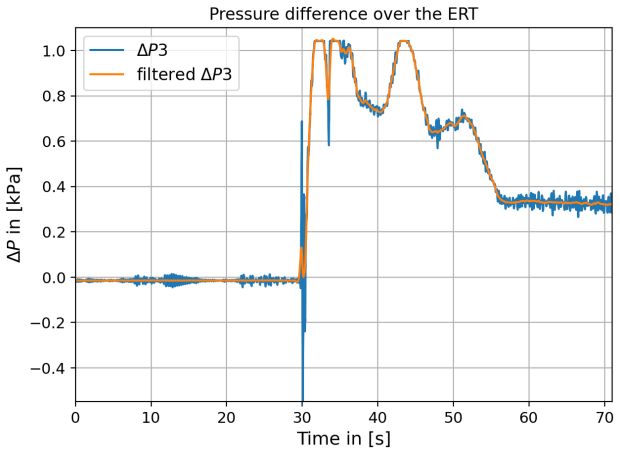

(c) Mixture with $c_v = 0.20$

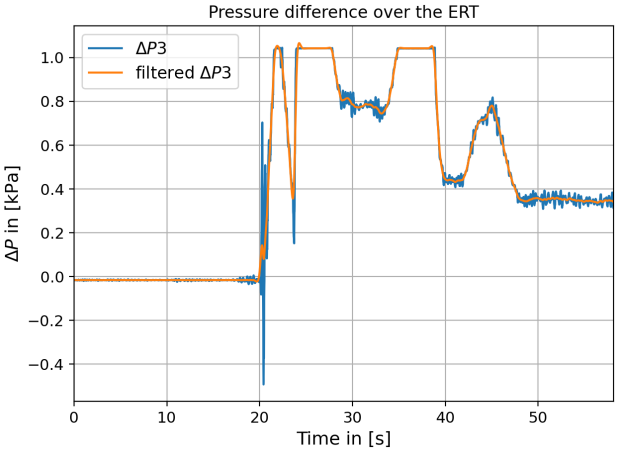

(d) Mixture with $c_v = 0.30$

Figure B.3

B.4 Zilverzand

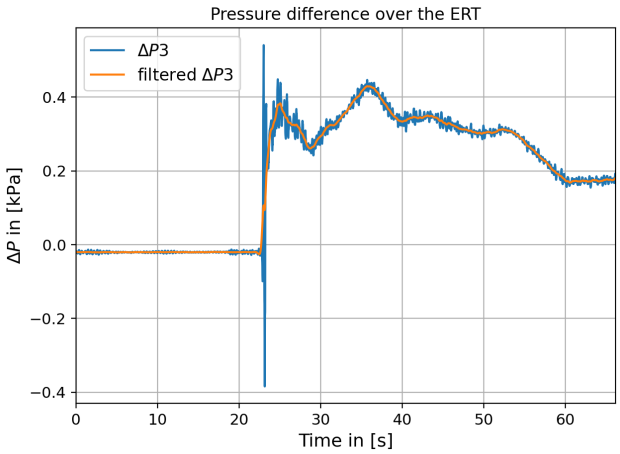

(a) Mixture with $c_v = 0.05$

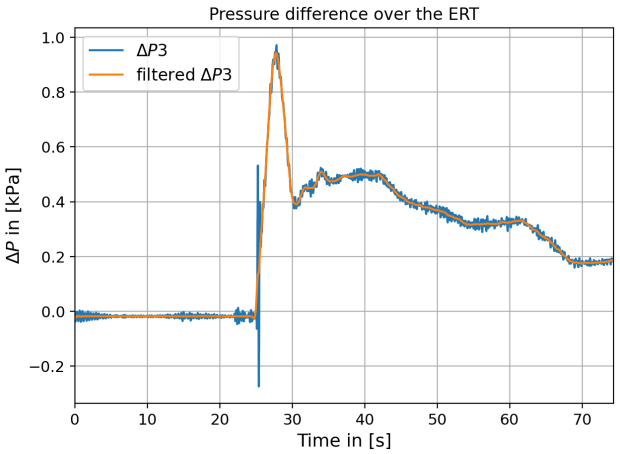

(b) Mixture with $c_v = 0.10$

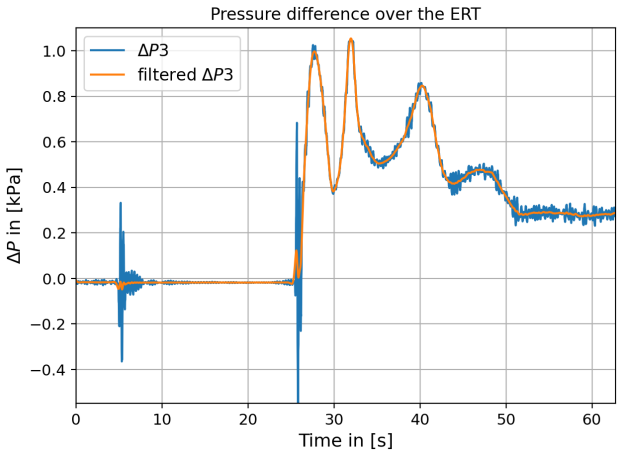

(c) Mixture with $c_v = 0.20$

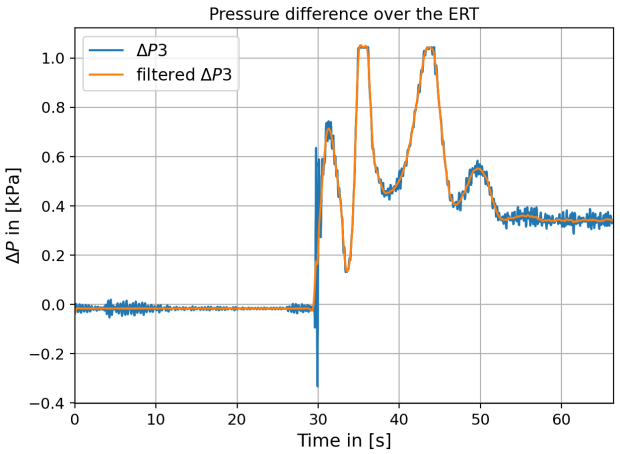

(d) Mixture with $c_v = 0.30$

Figure B.4

B.5 GEBA

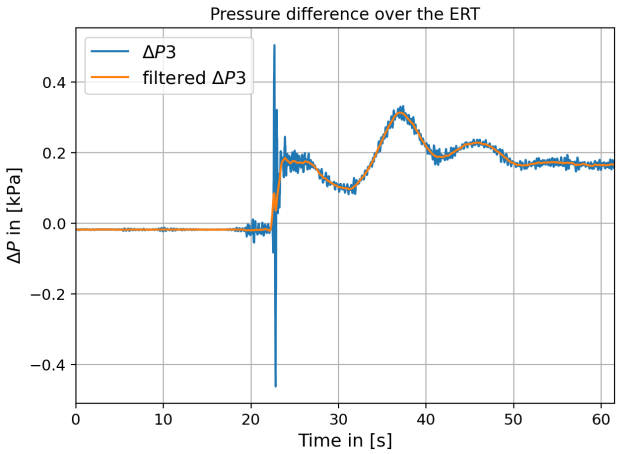

(a) Mixture with $c_v = 0.05$

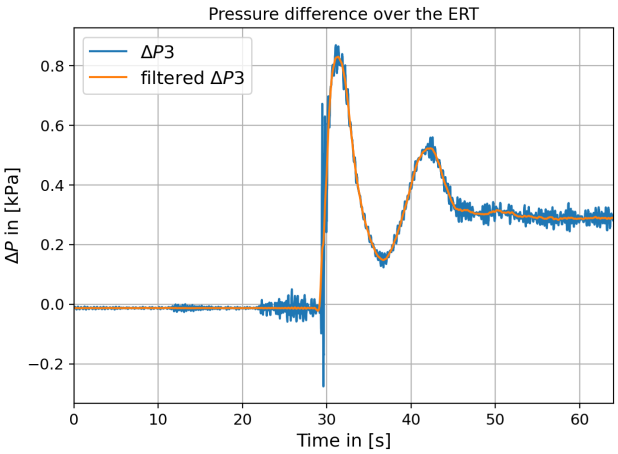

(b) Mixture with $c_v = 0.10$

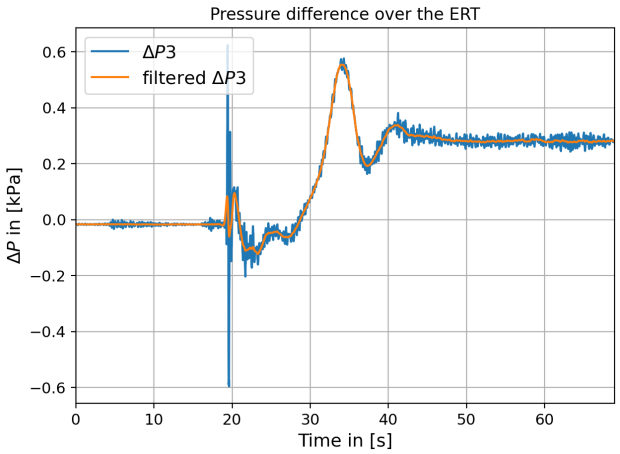

(c) Mixture with $c_v = 0.20$

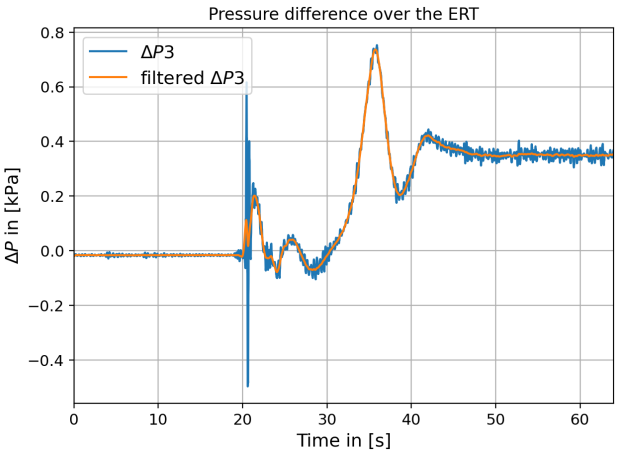

(d) Mixture with $c_v = 0.30$

Figure B.5: Measurements for GEBA

C

CCM Measurements from the Experiments

In this appendix the CCM measurements are shown. This is done per sand type to provide a clear overview.

C.1 Dorsilit nr.5G

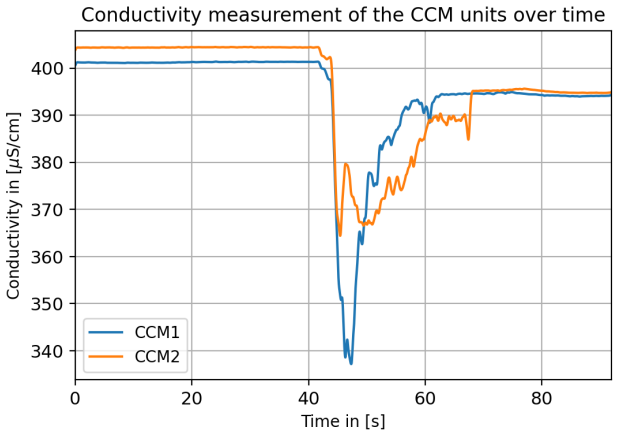

(a) Mixture with $c_v = 0.05$

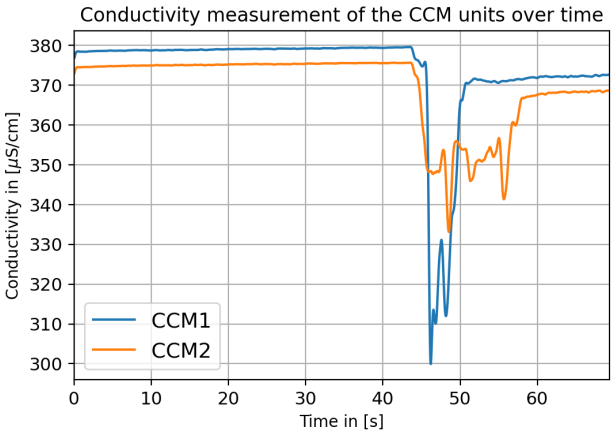

(b) Mixture with $c_v = 0.10$

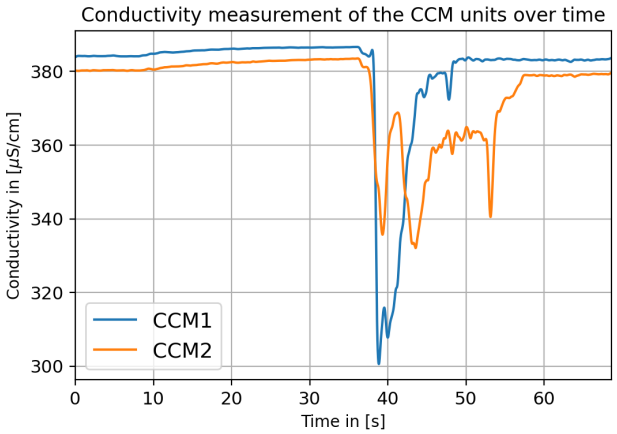

(c) Mixture with $c_v = 0.20$

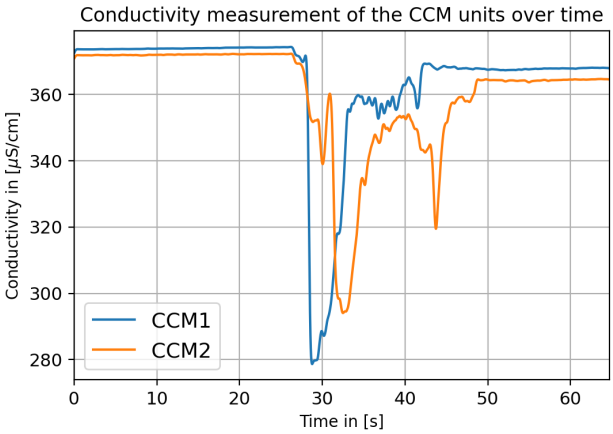

(d) Mixture with $c_v = 0.30$

Figure C.1

C.2 Dorsilit nr.7

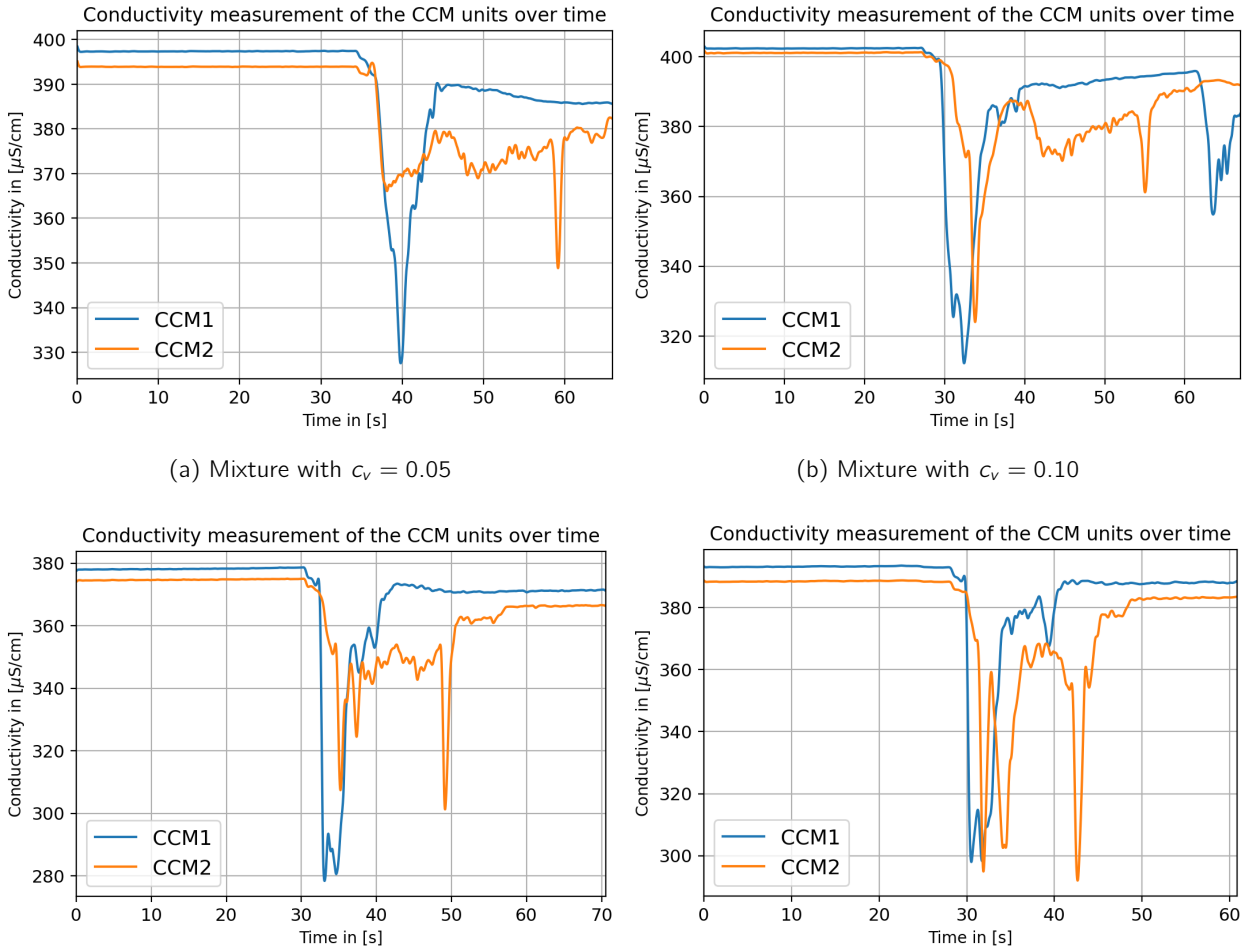

(a) Mixture with $c_v = 0.05$

(b) Mixture with $c_v = 0.10$

(c) Mixture with $c_v = 0.20$

(d) Mixture with $c_v = 0.30$

Figure C.2

C.3 Dorsilit nr.8

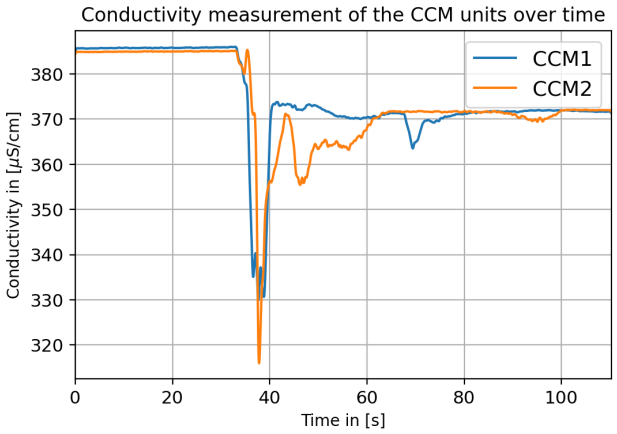

(a) Mixture with $c_v = 0.05$

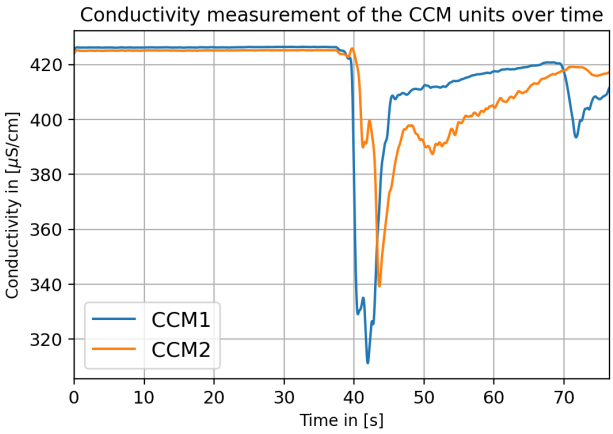

(b) Mixture with $c_v = 0.10$

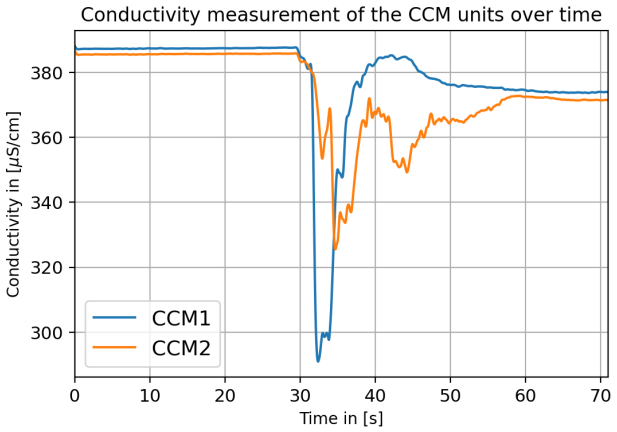

(c) Mixture with $c_v = 0.20$

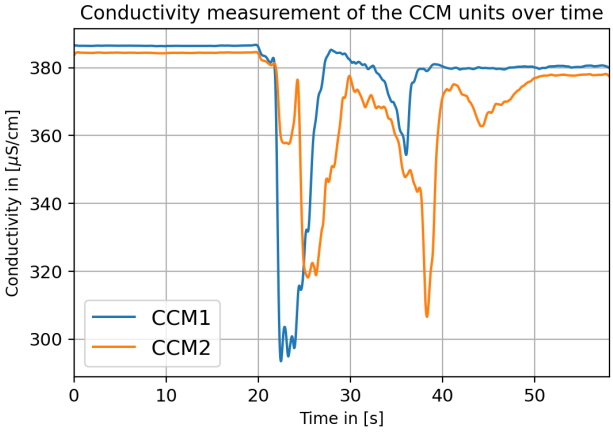

(d) Mixture with $c_v = 0.30$

Figure C.3

C.4 Zilverzand

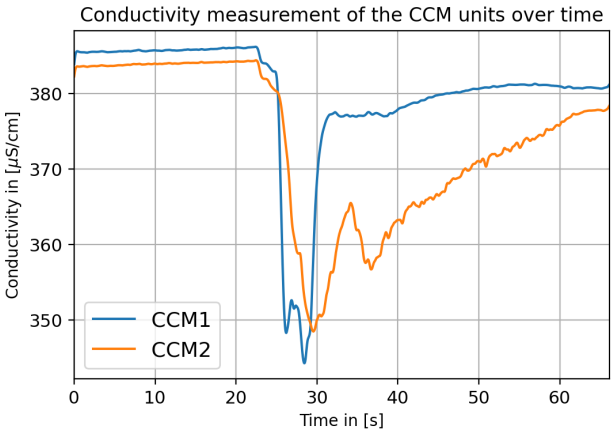

(a) Mixture with $c_v = 0.05$

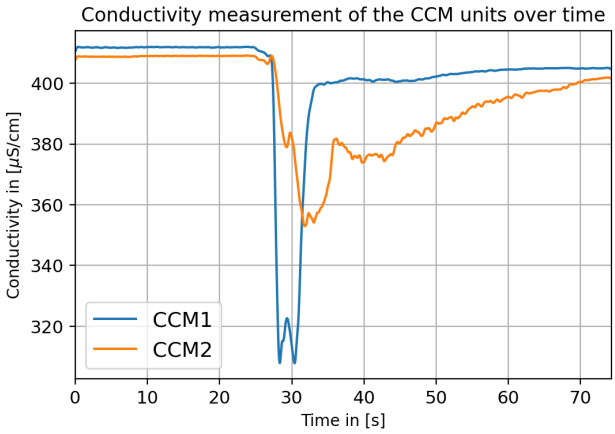

(b) Mixture with $c_v = 0.10$

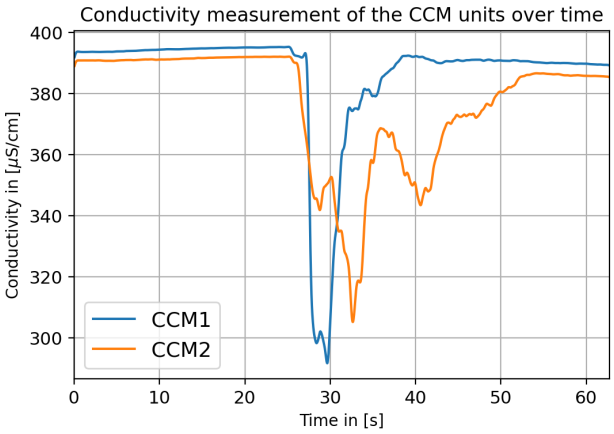

(c) Mixture with $c_v = 0.20$

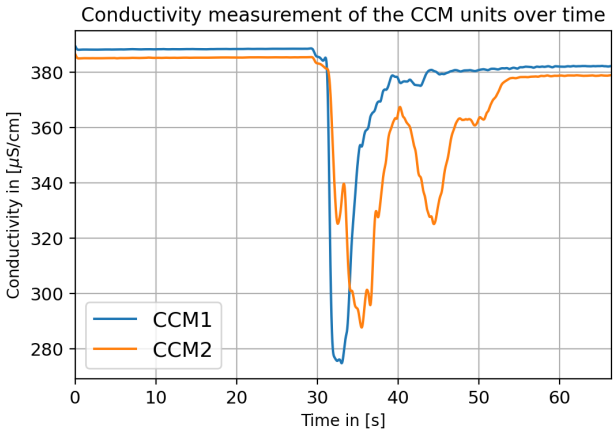

(d) Mixture with $c_v = 0.30$

Figure C.4

C.5 GEBA

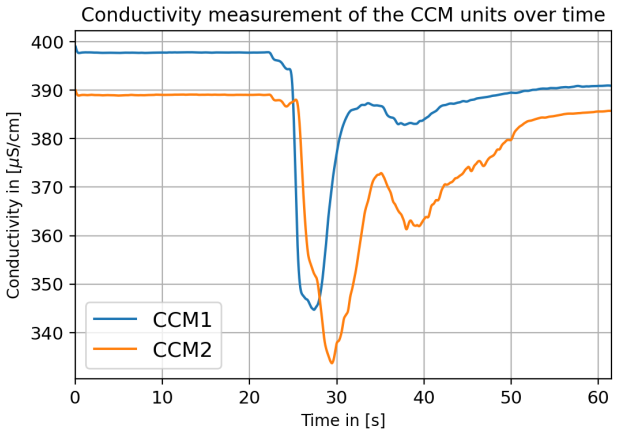

(a) Mixture with $c_v = 0.05$

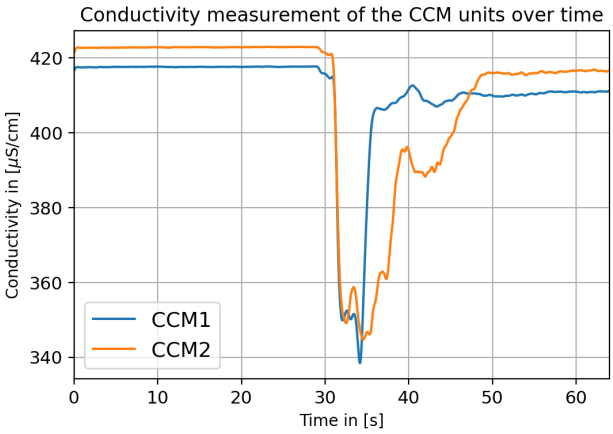

(b) Mixture with $c_v = 0.10$

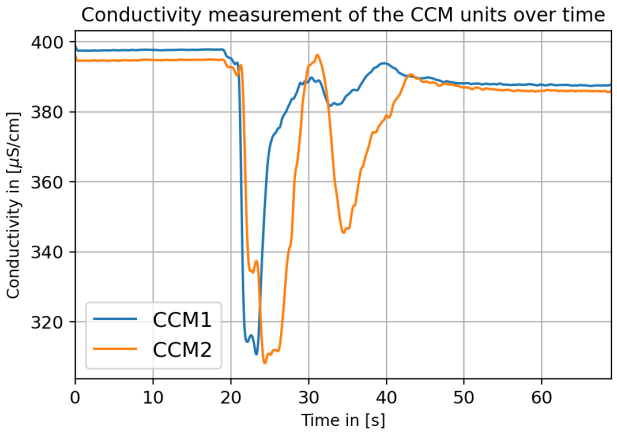

(c) Mixture with $c_v = 0.20$

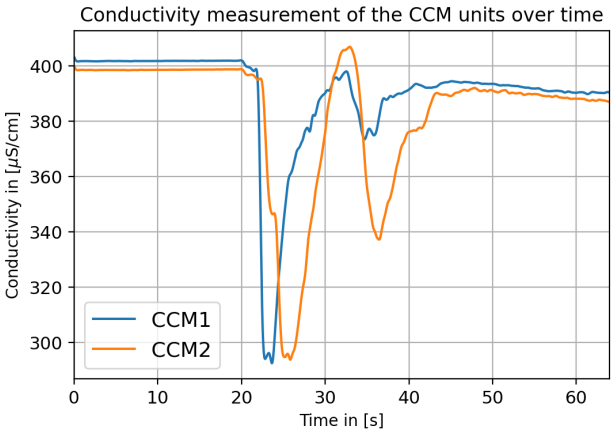

(d) Mixture with $c_v = 0.30$

Figure C.5: Measurements for GEBA

D

Results from the ERT Data

In this appendix the results from the ERT data is shown and visualised. This is done per sand type.

D.1 Dorsilit nr.5G

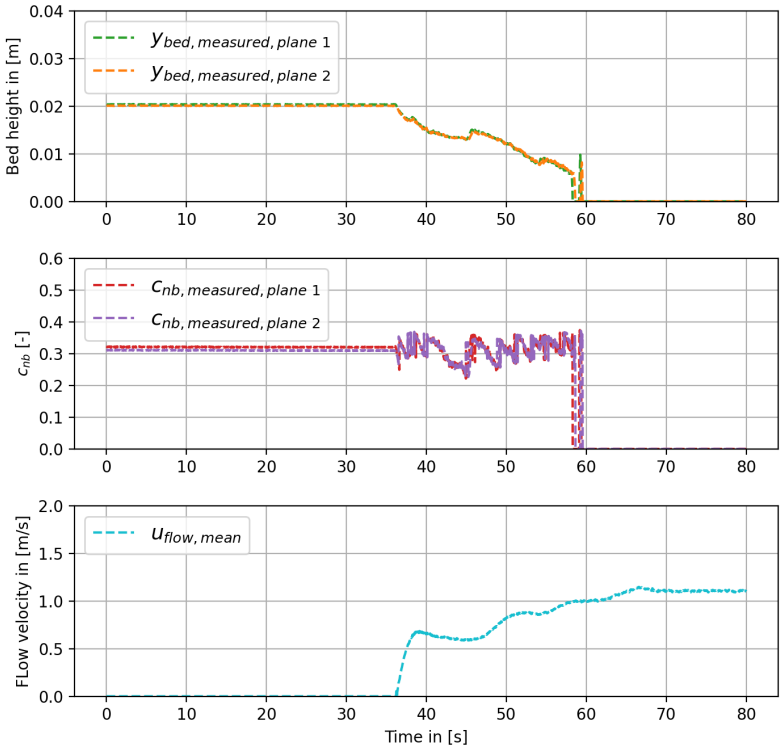

Figure D.1: Dorsilit nr.5G $C_v = 0.05$

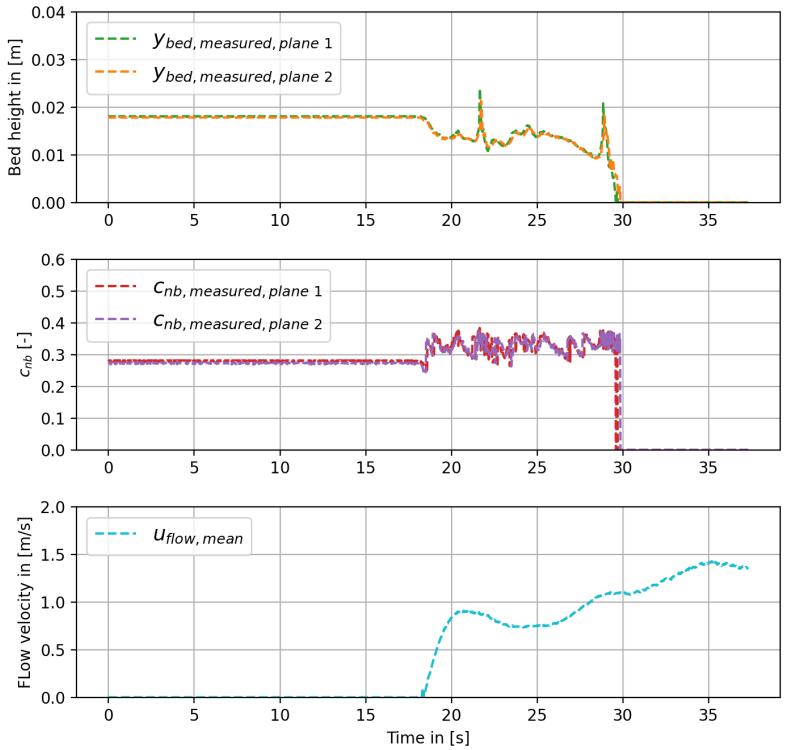

Figure D.2: Dorsilit nr.5G $C_v = 0.10$

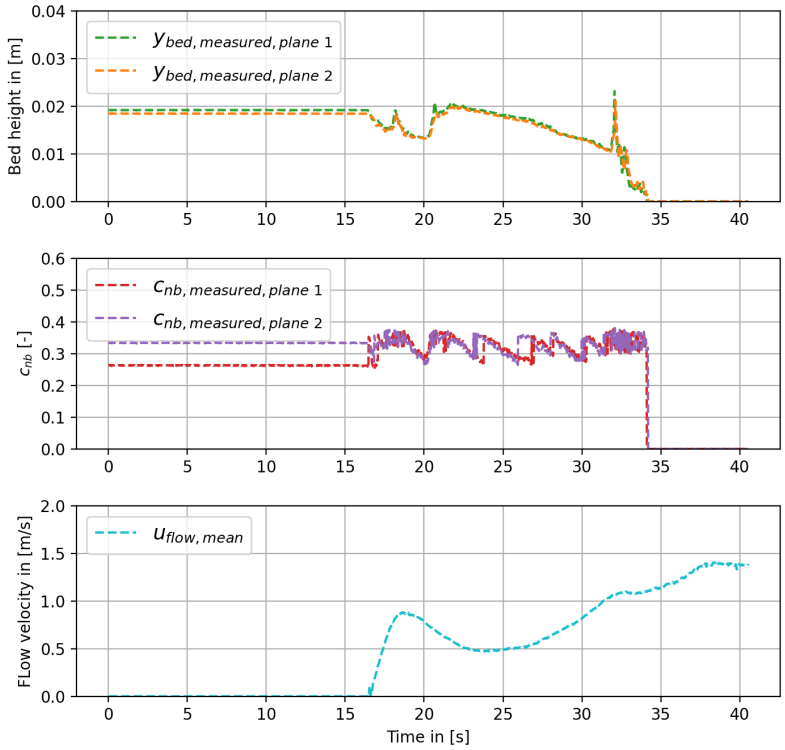

Figure D.3: Dorsilit nr.5G $C_v = 0.20$

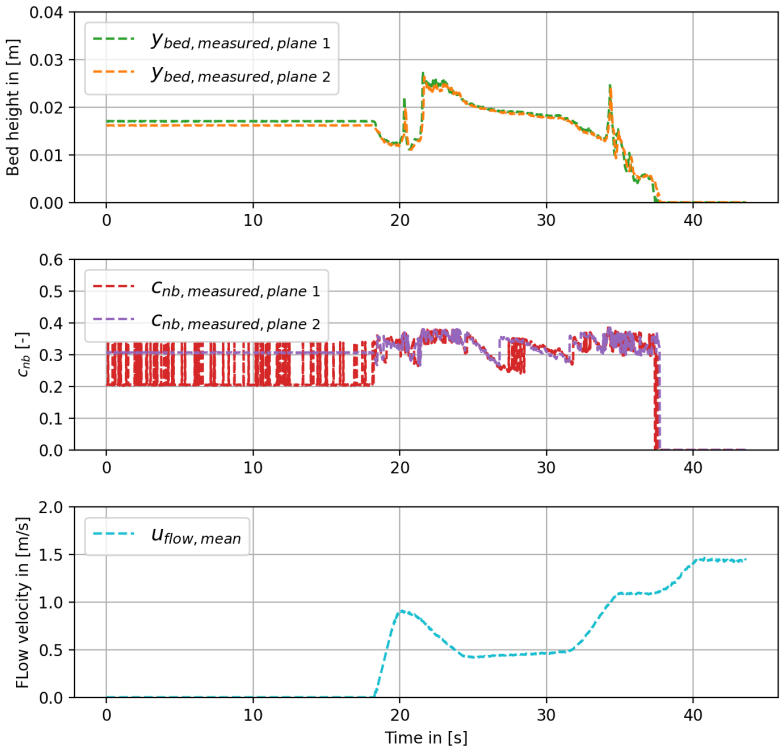

Figure D.4: Dorsilit nr.5G $C_v = 0.30$

D.2 Dorsilit nr.7

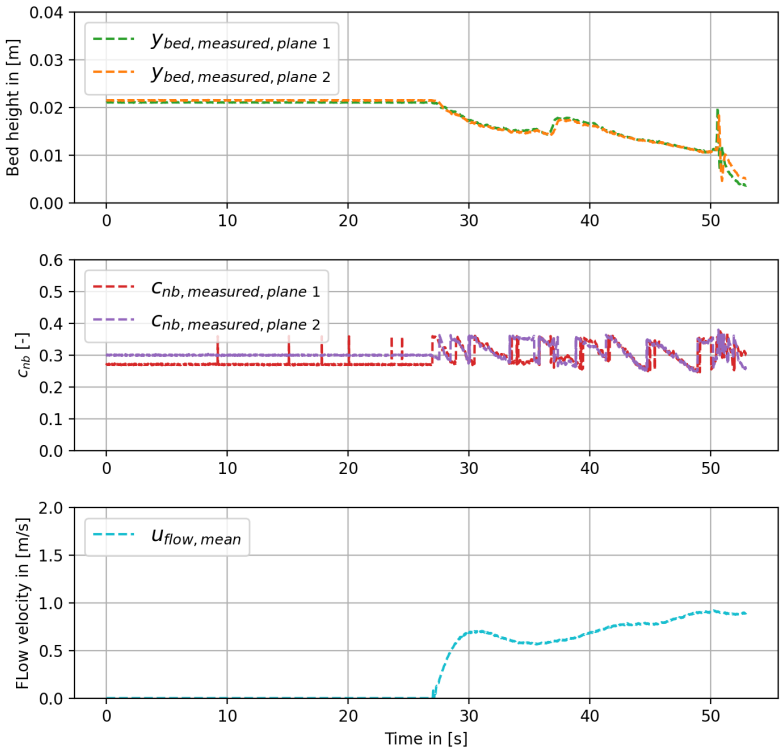

Figure D.5: Dorsilit nr.7 $C_v = 0.05$

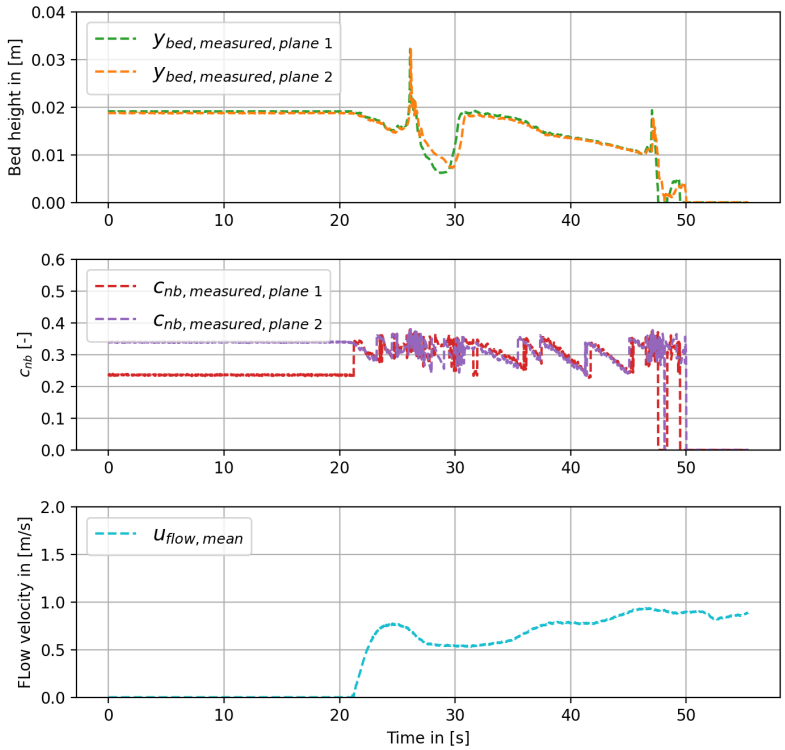

Figure D.6: Dorsilit nr.7 $C_v = 0.10$

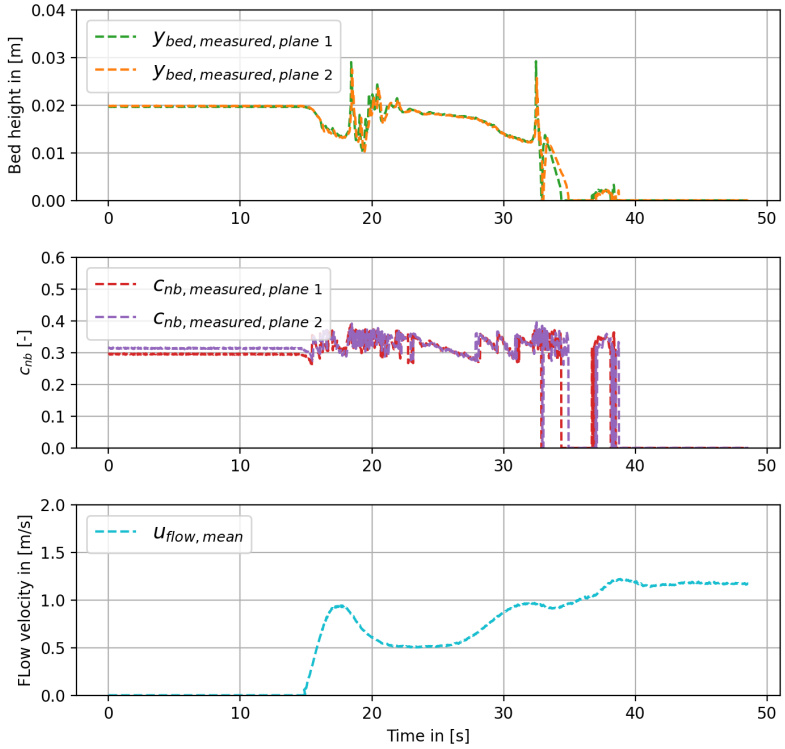

Figure D.7: Dorsilit nr.7 $C_v = 0.20$

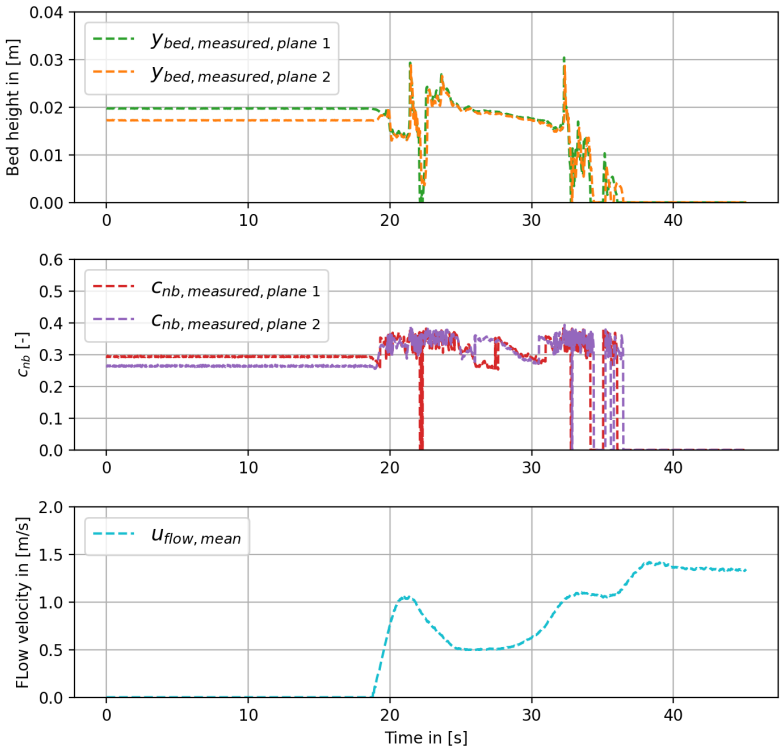

Figure D.8: Dorsilit nr.7 $C_v = 0.30$

D.3 Dorsilit nr.8

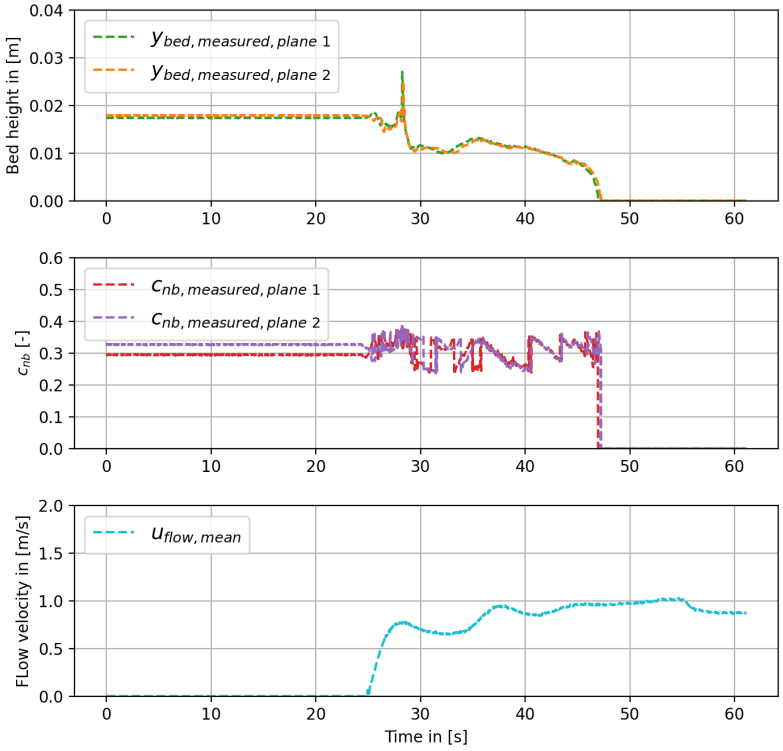

Figure D.9: Dorsilit nr.8 $C_v = 0.05$

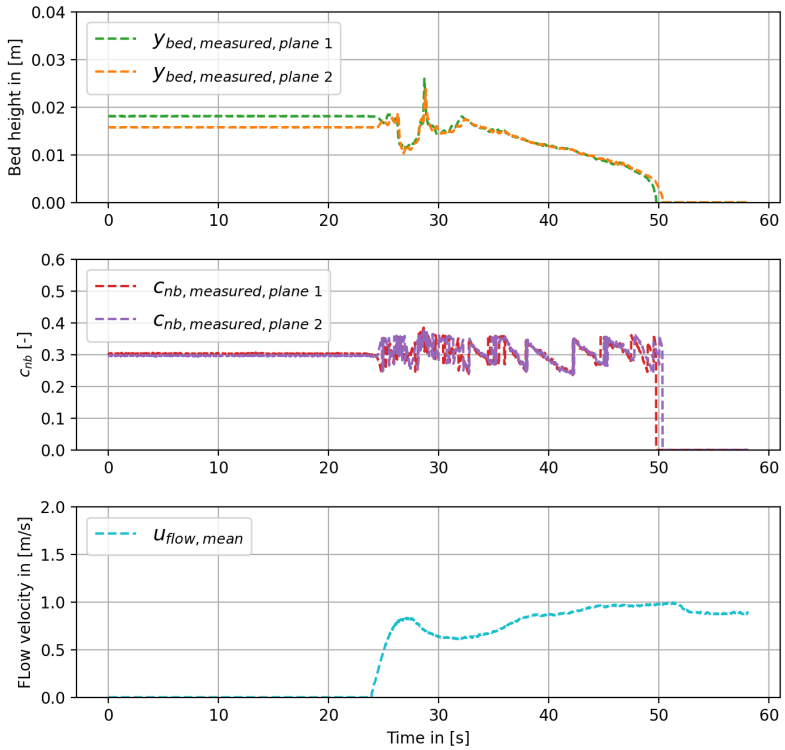

Figure D.10: Dorsilit nr.8 $C_v = 0.10$

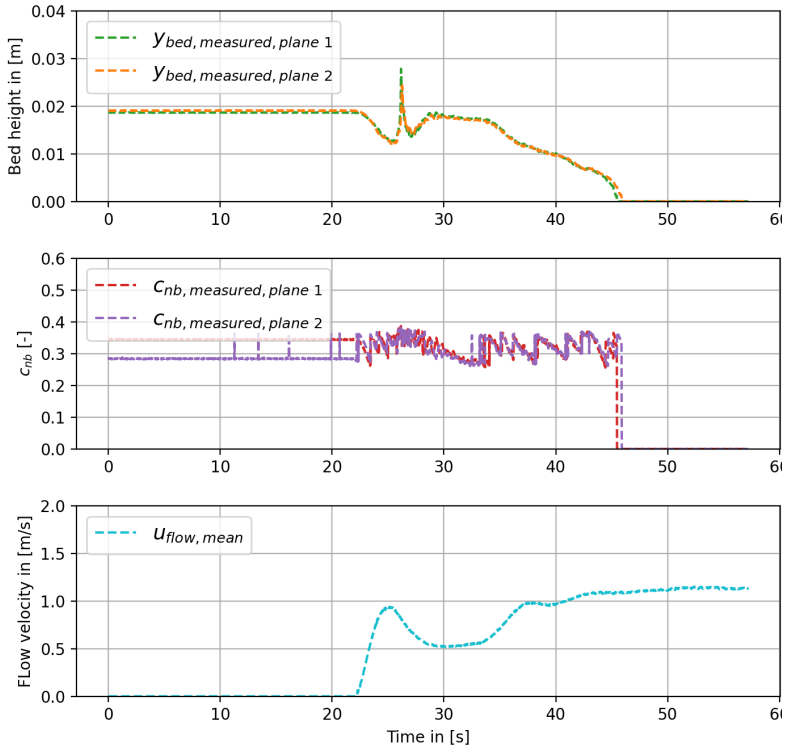

Figure D.11: Dorsilit nr.8 $C_v = 0.20$

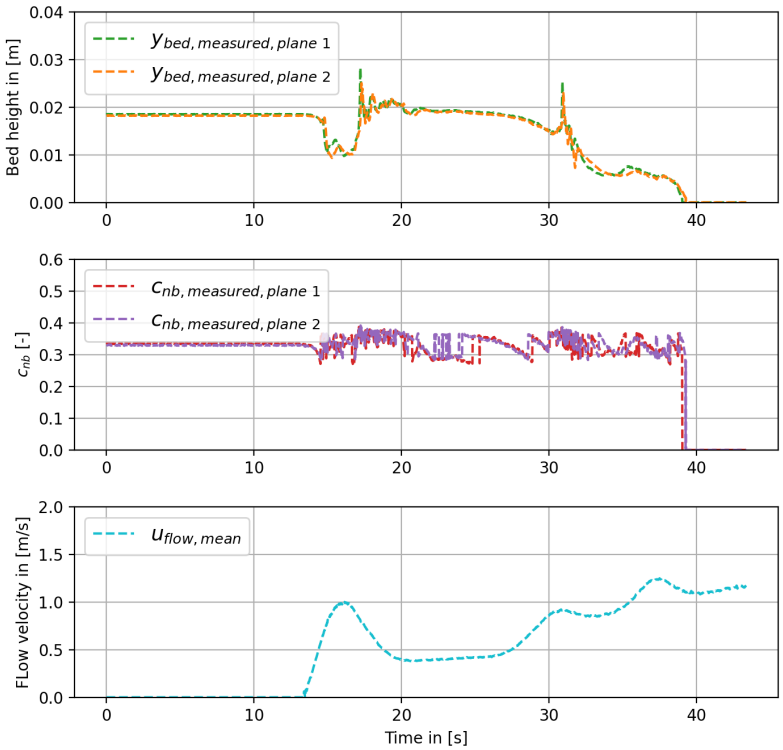

Figure D.12: Dorsilit nr.8 $C_v = 0.30$

D.4 Zilverzand

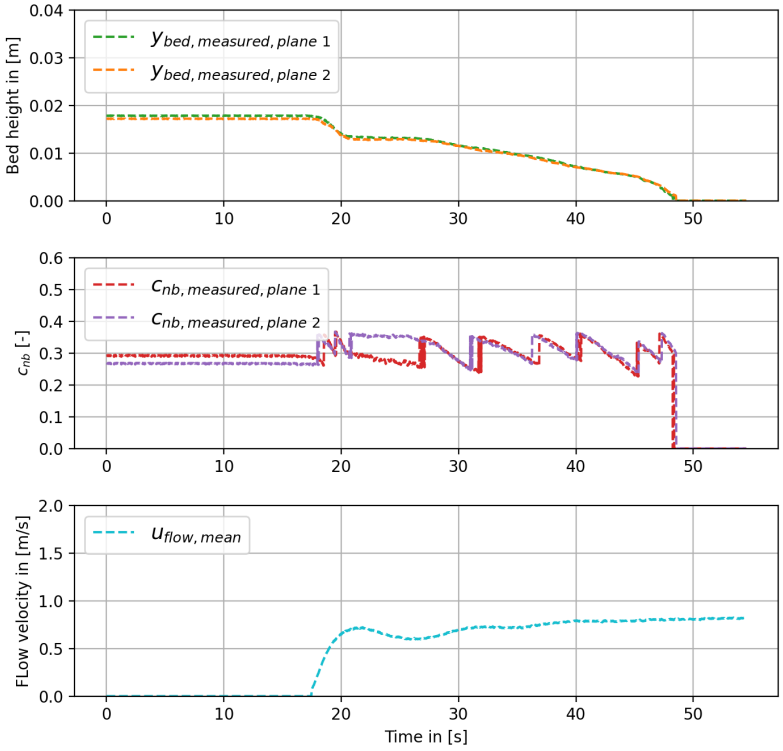

Figure D.13: Zilverzand $C_v = 0.05$

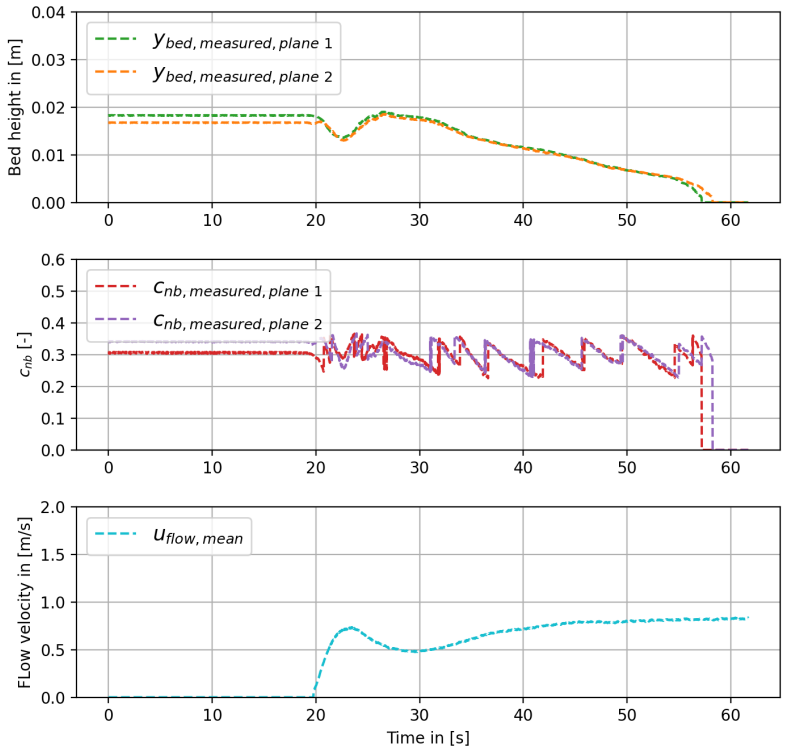

Figure D.14: Zilverzand $C_v = 0.10$

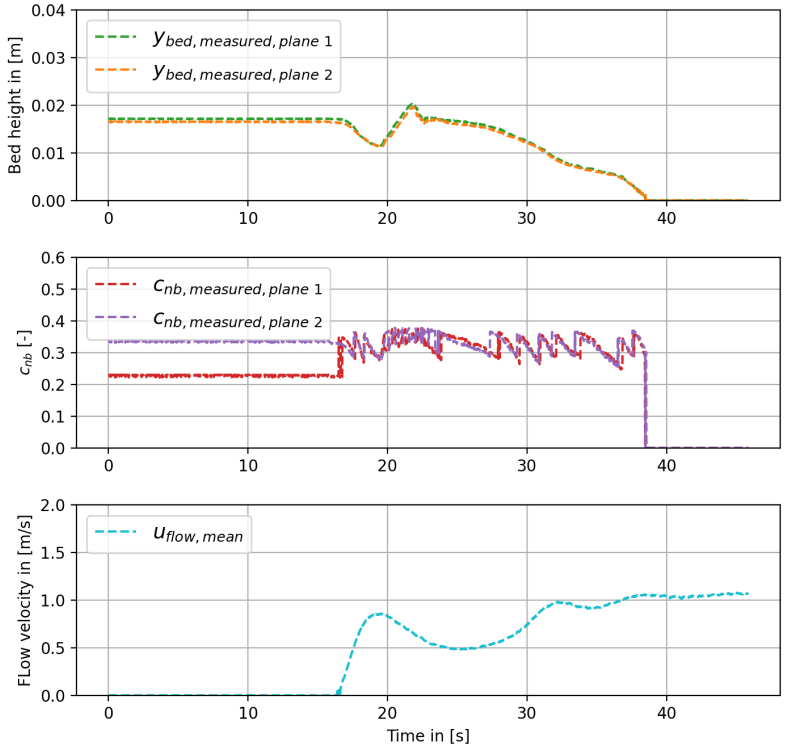

Figure D.15: Zilverzand $C_v = 0.20$

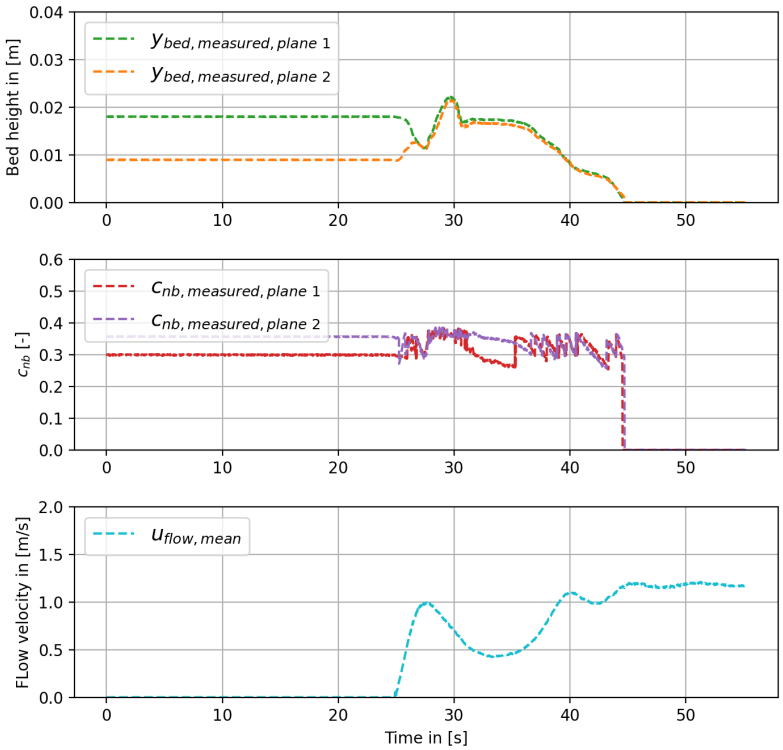

Figure D.16: Zilverzand $C_v = 0.30$

D.5 GEBA

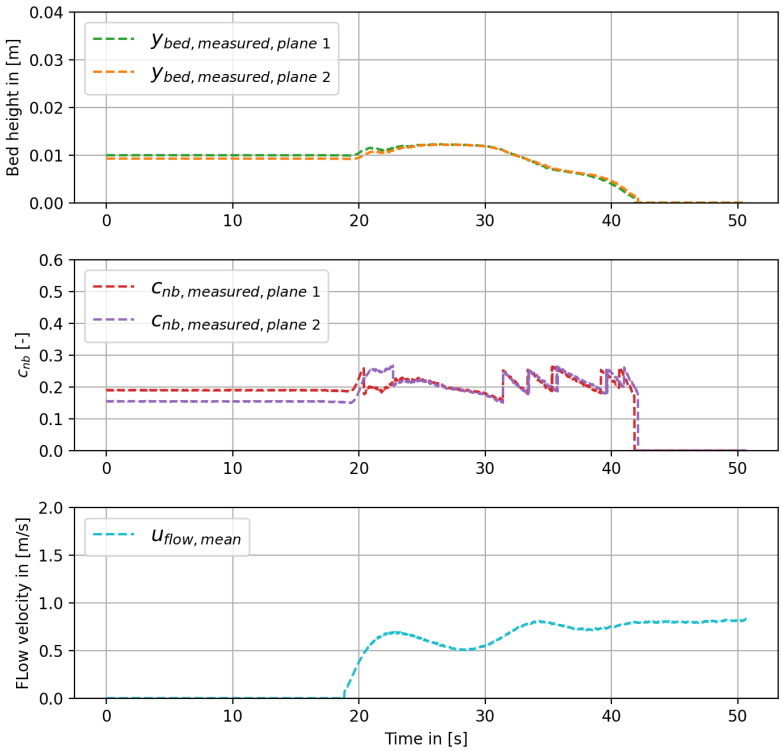

Figure D.17: GEBA $C_v = 0.05$

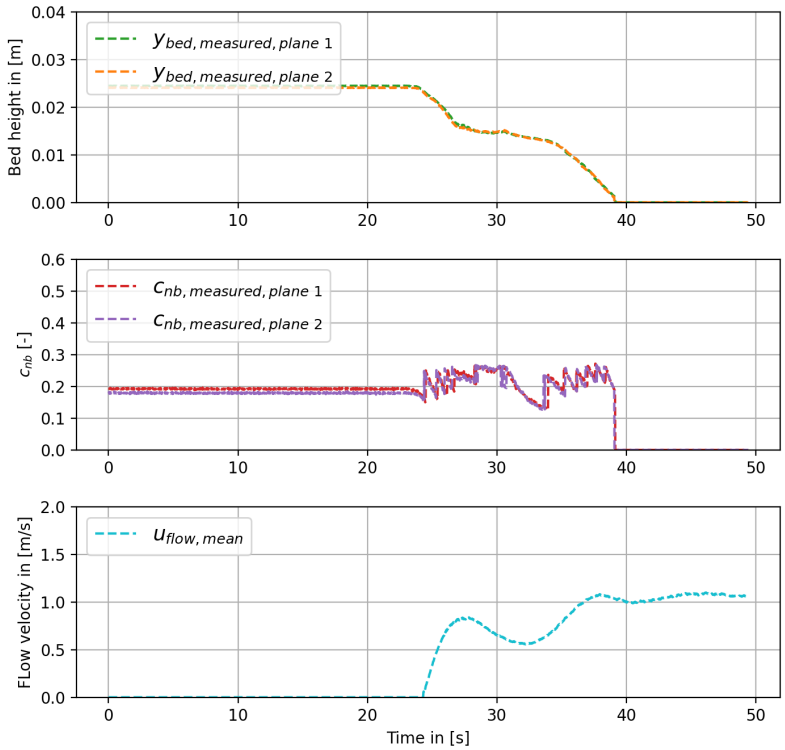

Figure D.18: GEBA $C_v = 0.10$

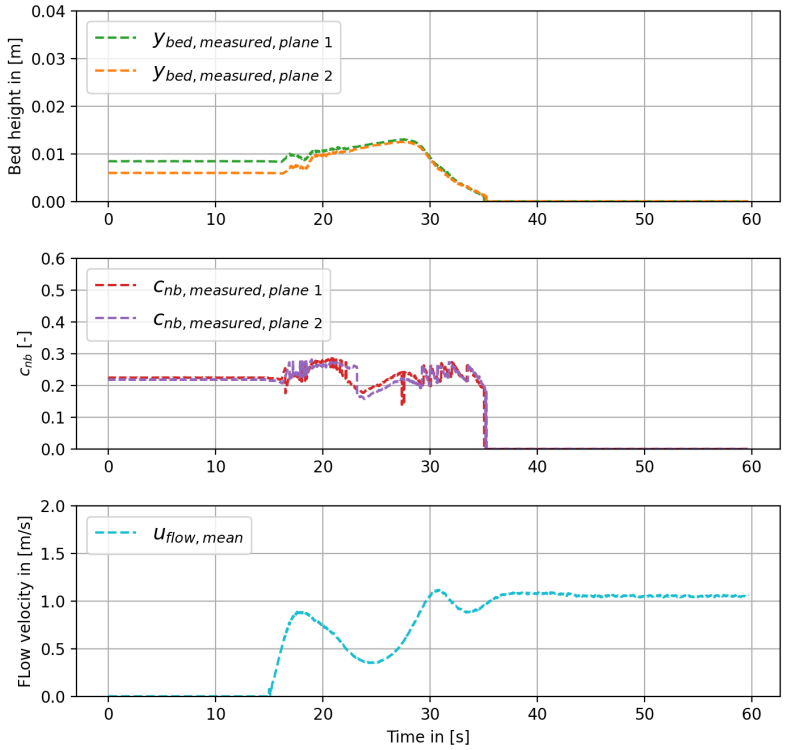

Figure D.19: GEBA $C_v = 0.20$

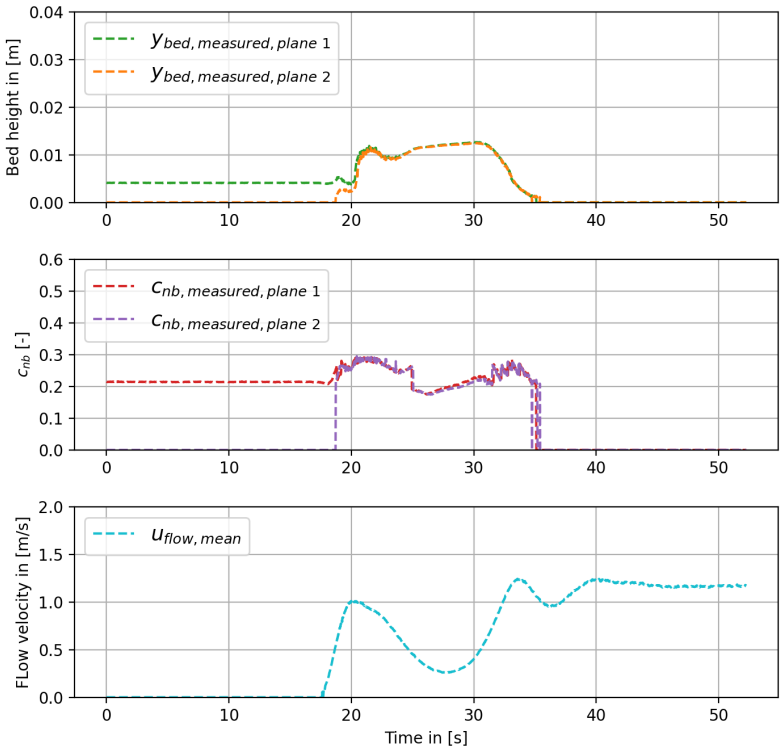

Figure D.20: GEBA $C_v = 0.30$

E

Results from the Sirius-E Data

To see the influence of the concentration

E.1 Dorsilit nr.5G

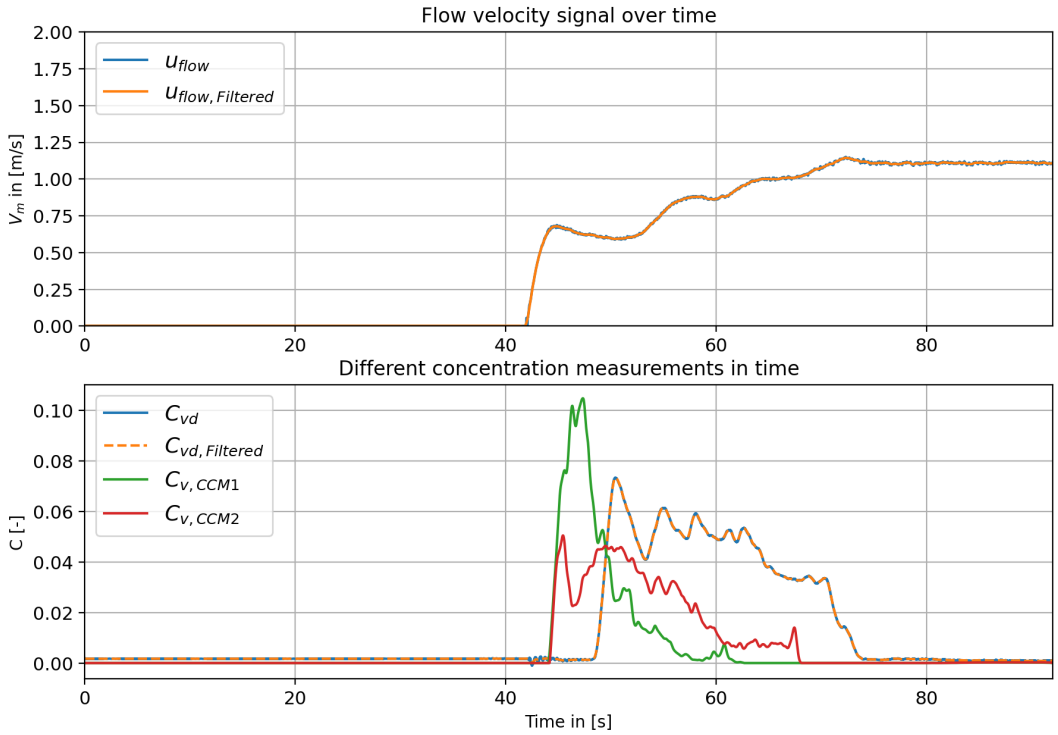

Figure E.1: Dorsilit nr.5G $C_v = 0.05$

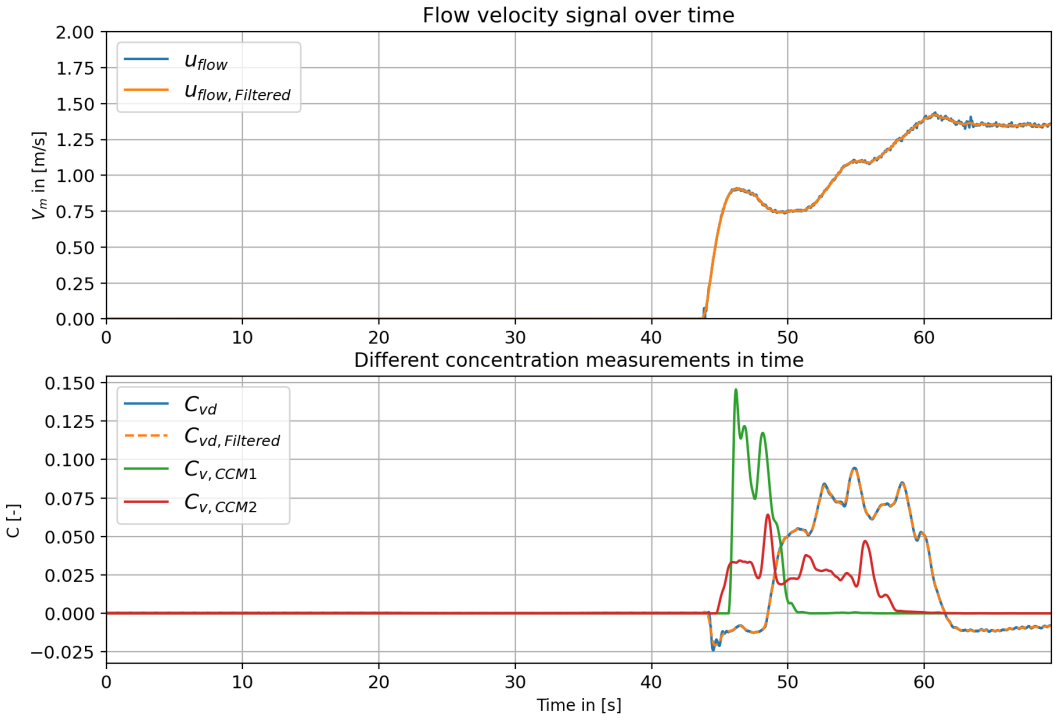

Figure E.2: Dorsilit nr.5G $C_v = 0.10$

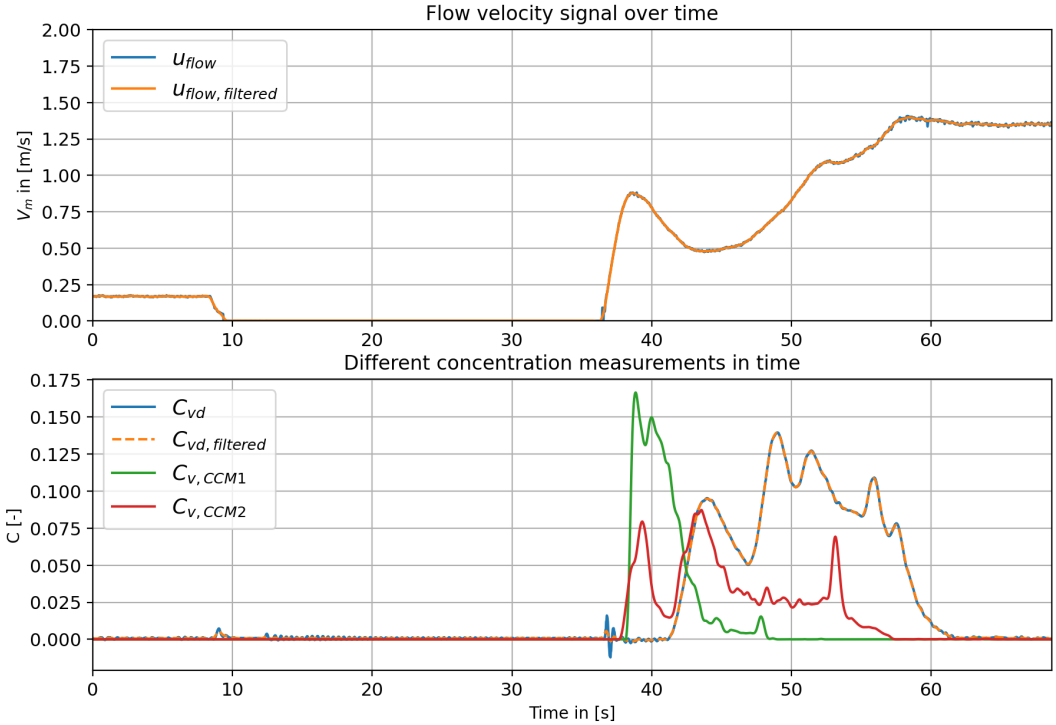

Figure E.3: Dorsilit nr.5G $C_v = 0.20$

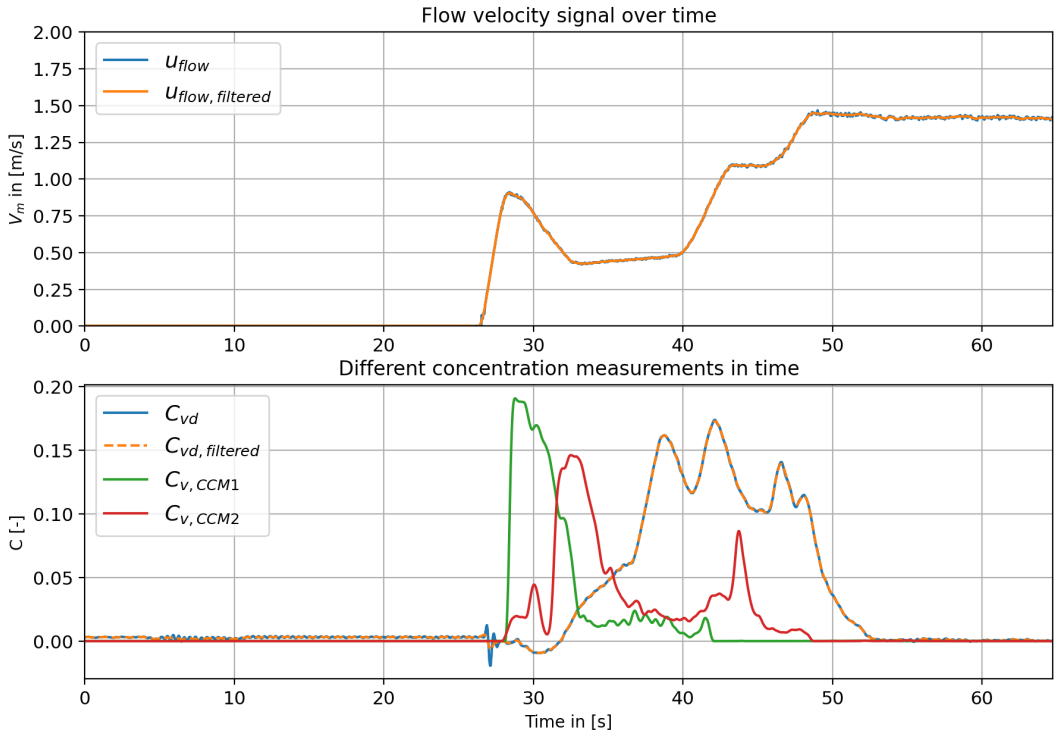

Figure E.4: Dorsilit nr.5G $C_v = 0.30$

E.2 Dorsilit nr.7

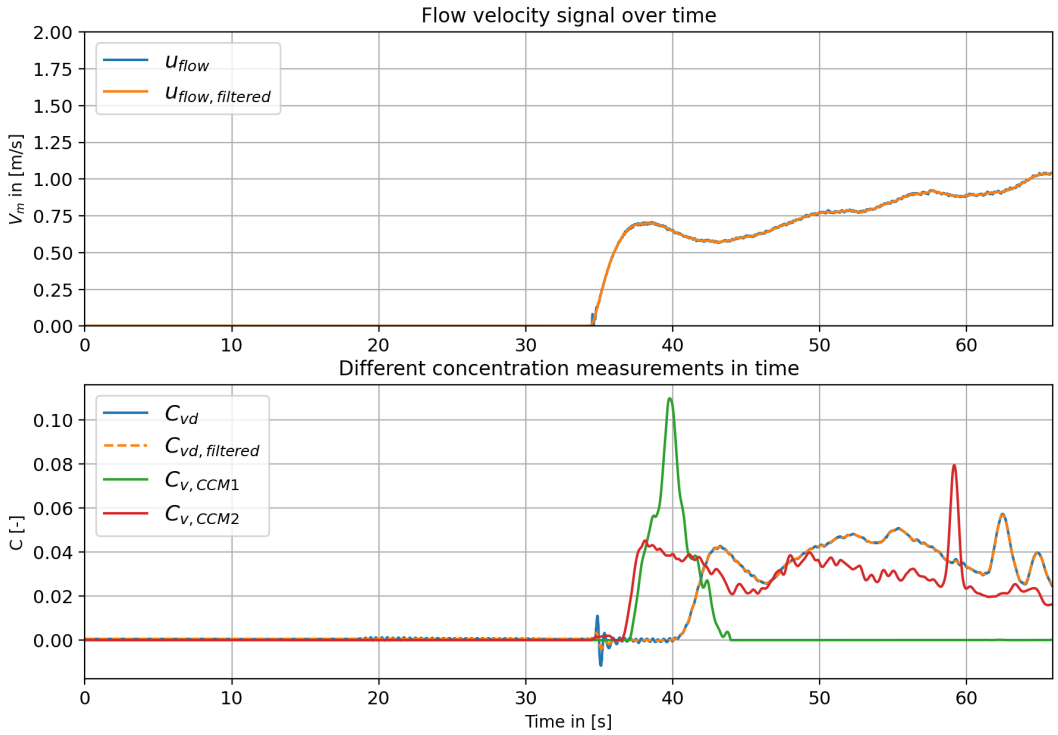

Figure E.5: Dorsilit nr.7 $C_v = 0.05$

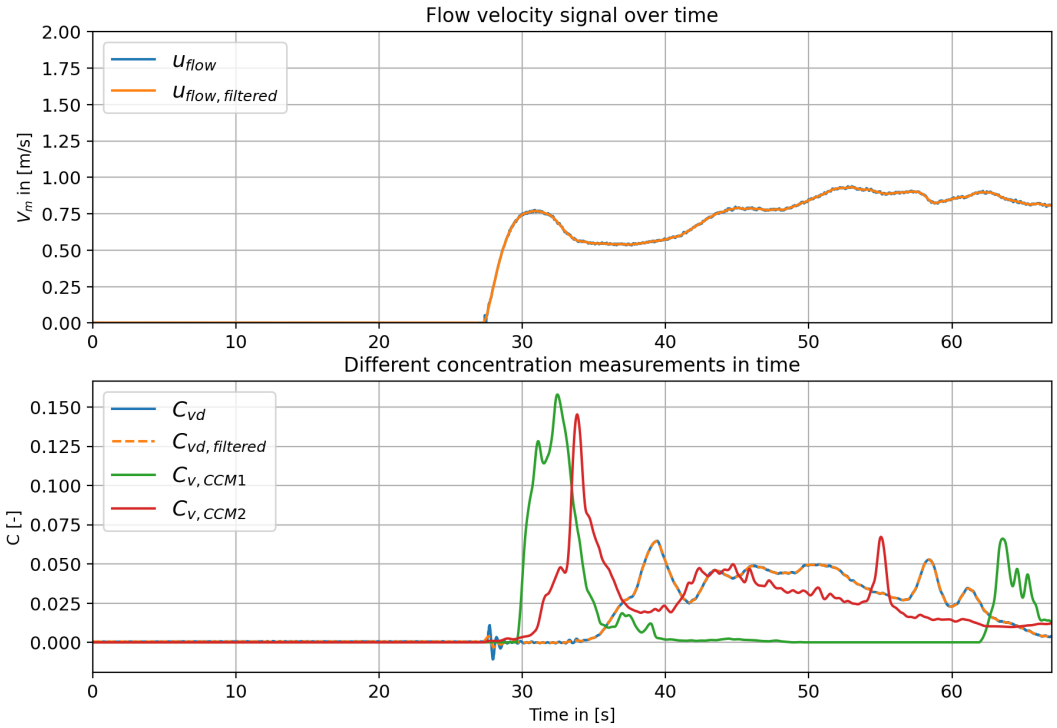

Figure E.6: Dorsilit nr.7 $C_v = 0.10$

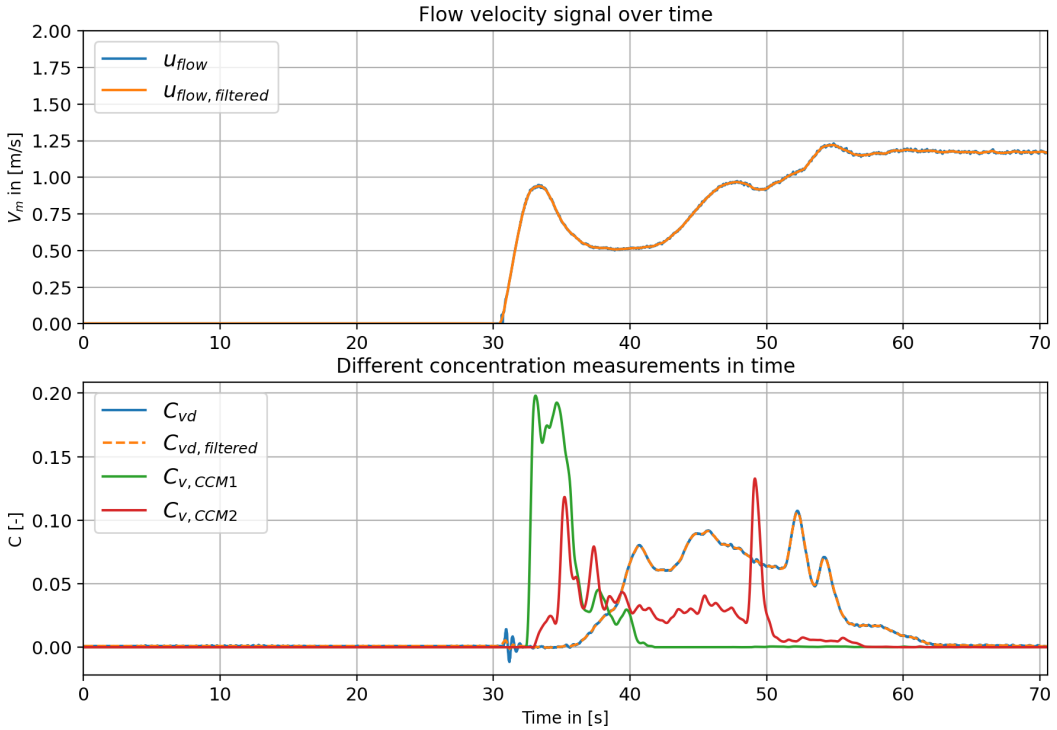

Figure E.7: Dorsilit nr.7 $C_v = 0.20$

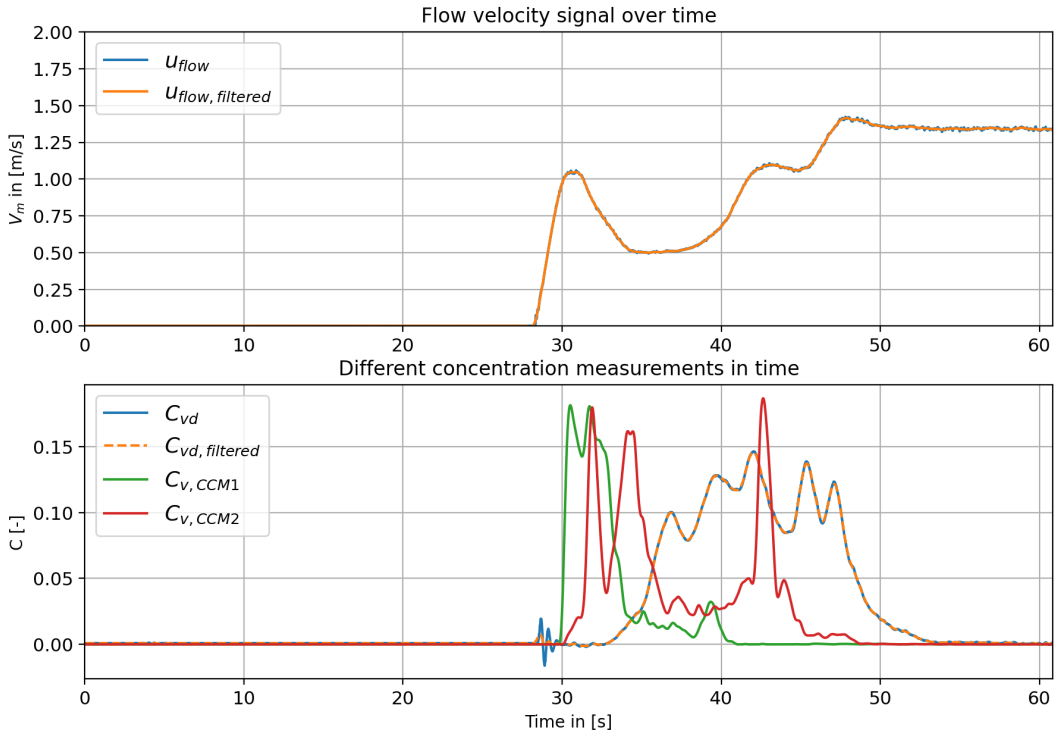

Figure E.8: Dorsilit nr.7 $C_v = 0.30$

E.3 Dorsilit nr.8

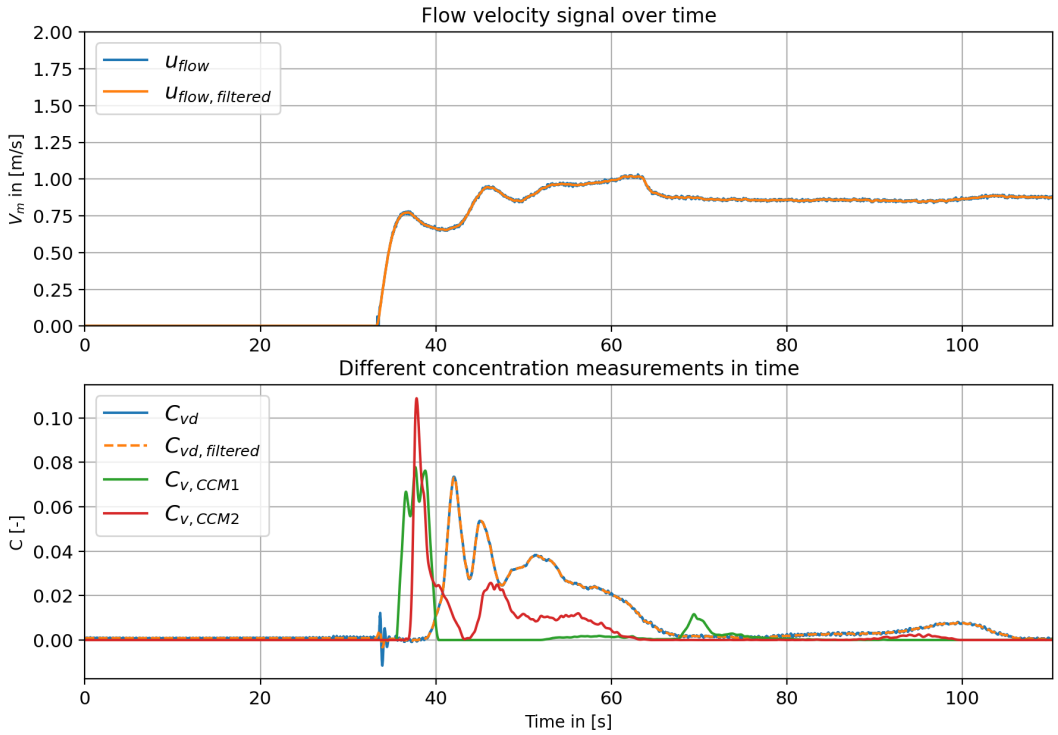

Figure E.9: Dorsilit nr.8 $C_v = 0.05$

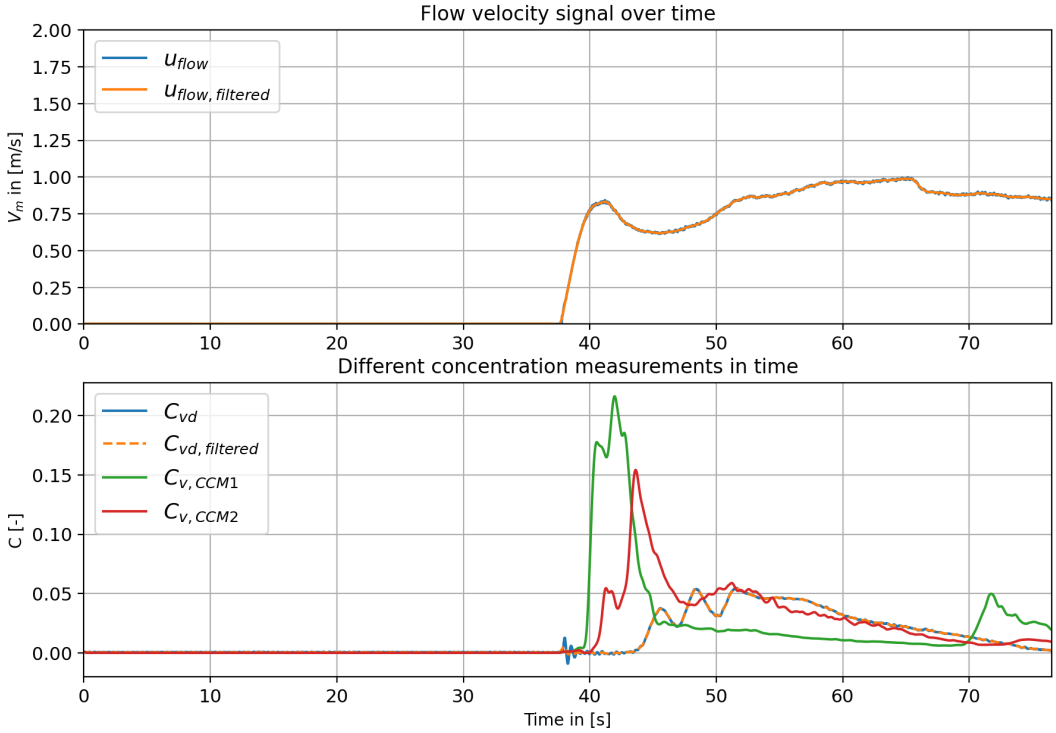

Figure E.10: Dorsilit nr.8 $C_v = 0.10$

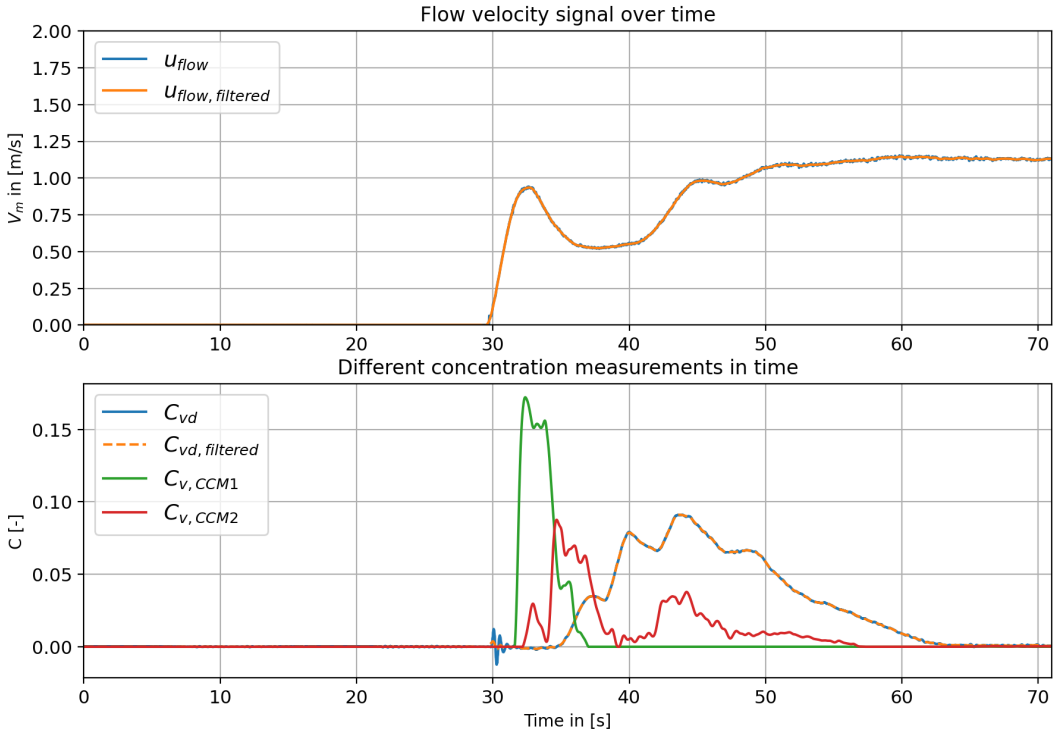

Figure E.11: Dorsilit nr.8 $C_v = 0.20$

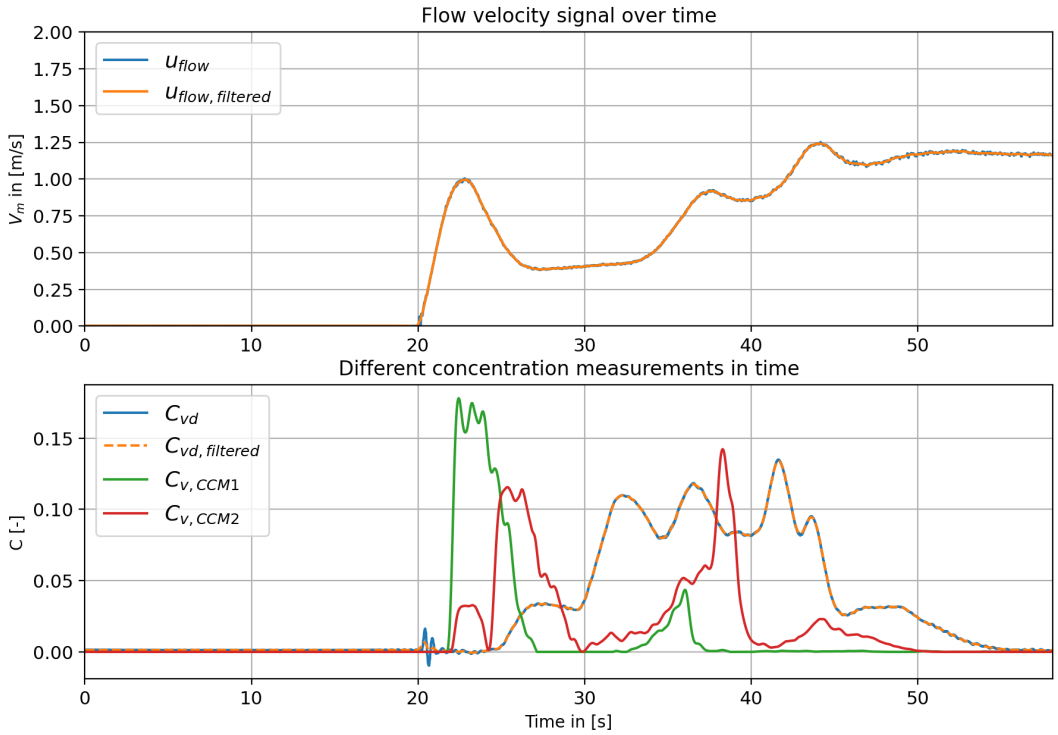

Figure E.12: Dorsilit nr.8 $C_v = 0.30$

E.4 Zilverzand

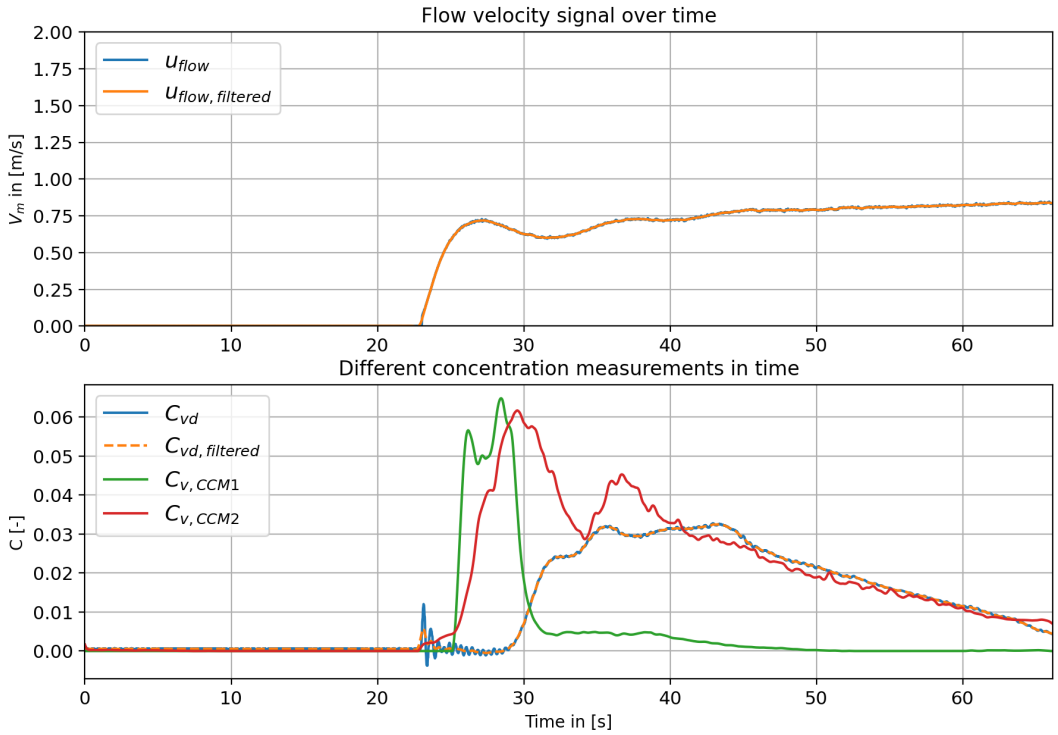

Figure E.13: Zilverzand $C_v = 0.05$

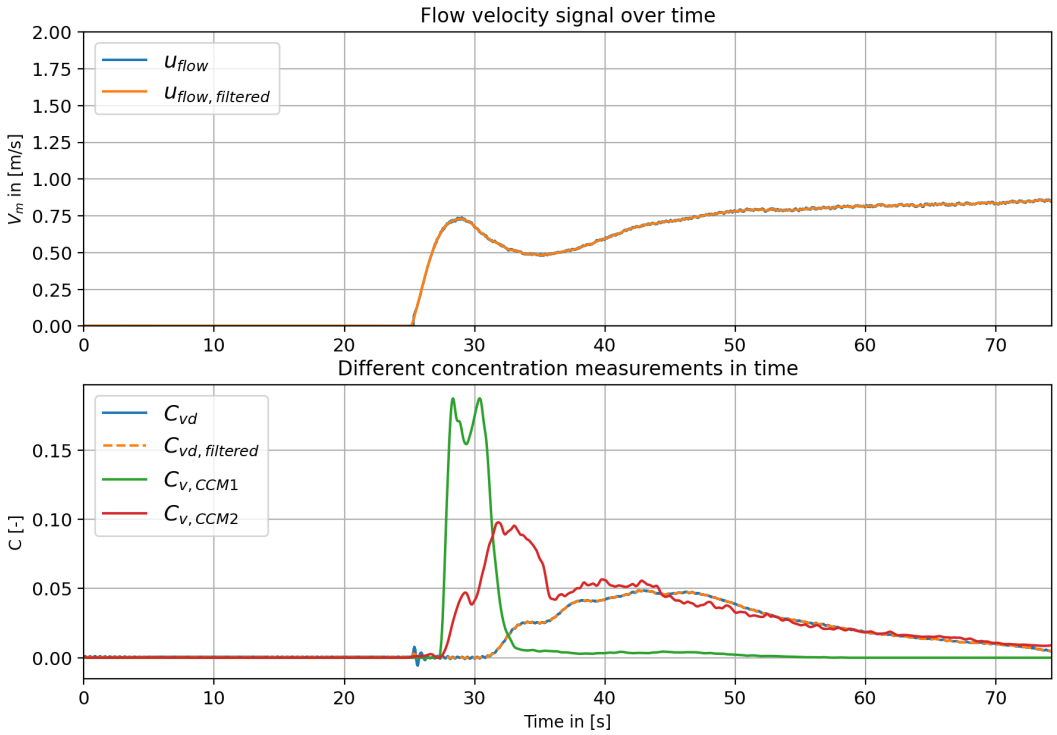

Figure E.14: Zilverzand $C_v = 0.10$

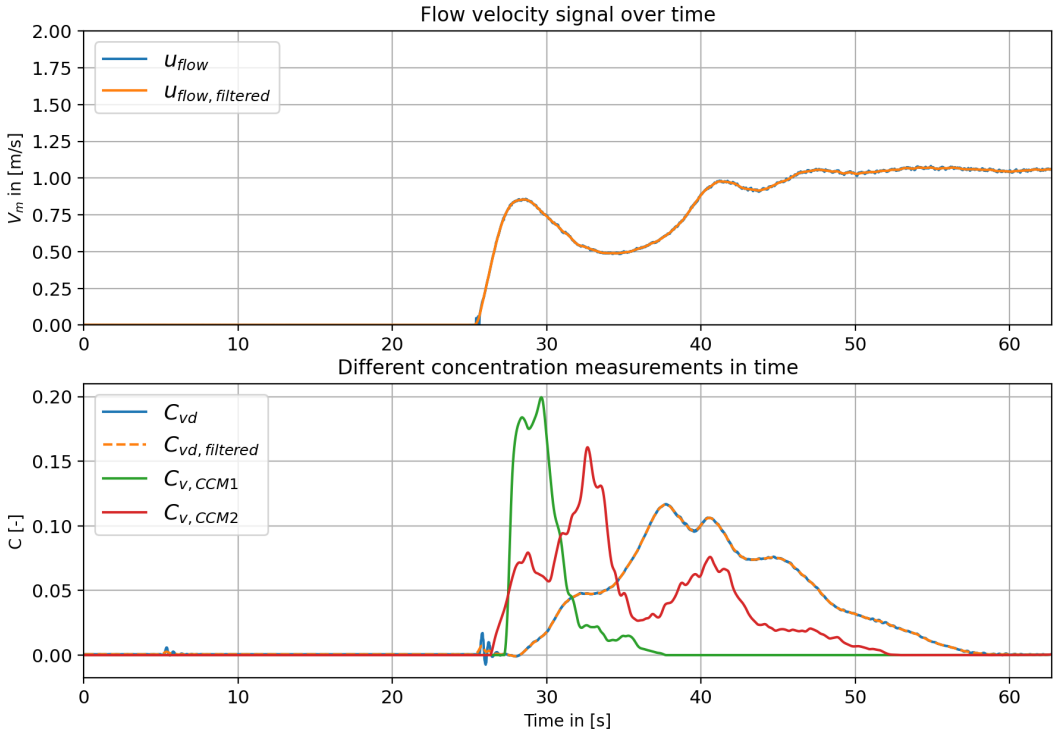

Figure E.15: Zilverzand $C_v = 0.20$

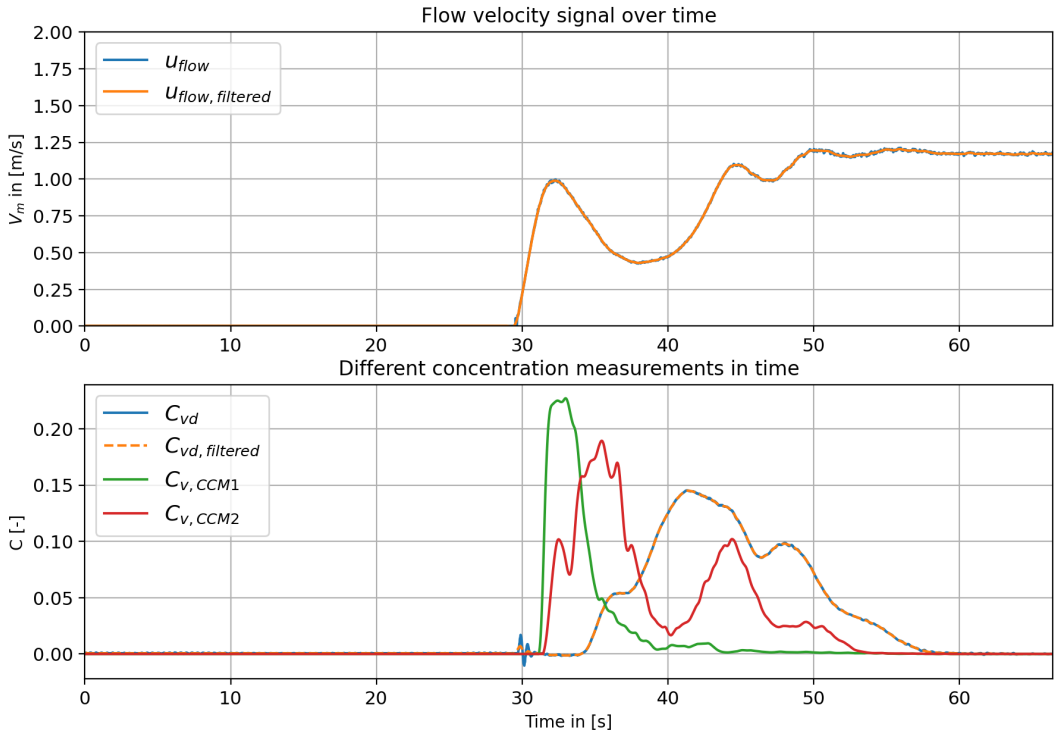

Figure E.16: Zilverzand $C_v = 0.30$

E.5 GEBA

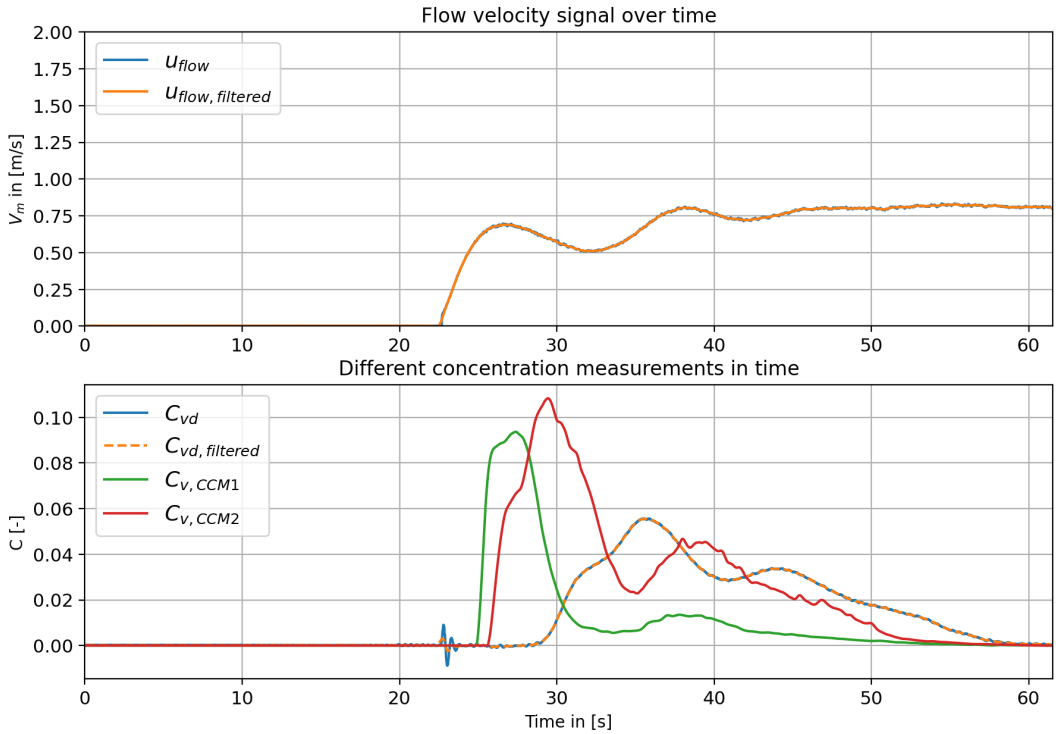

Figure E.17: GEBA $C_v = 0.05$

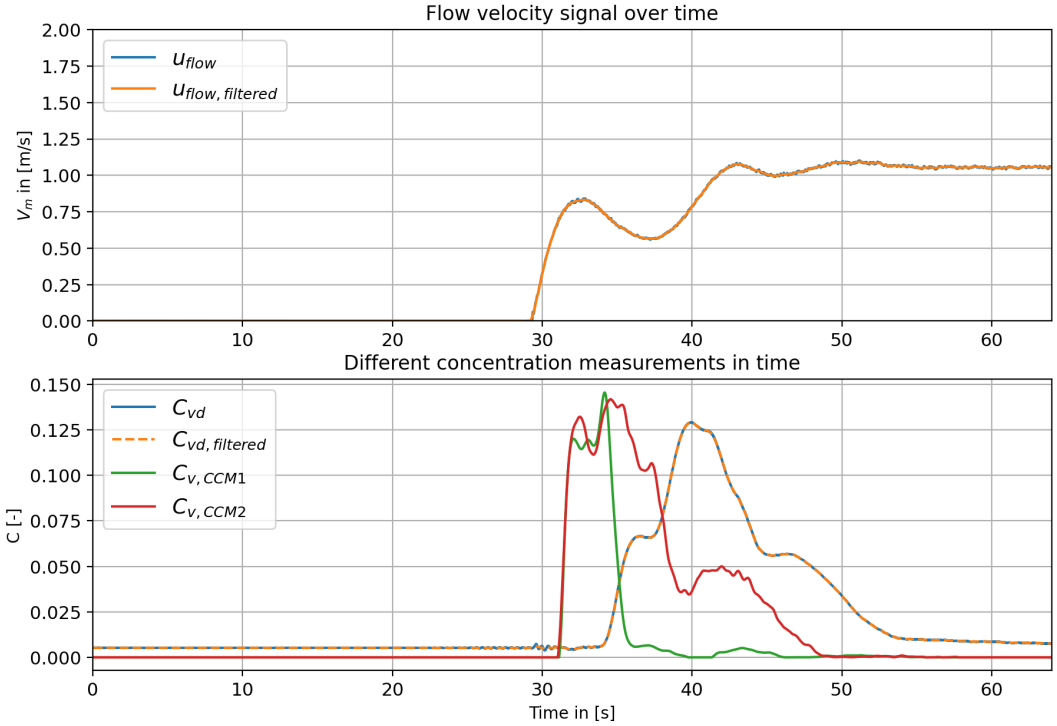

Figure E.18: GEBA $C_v = 0.10$

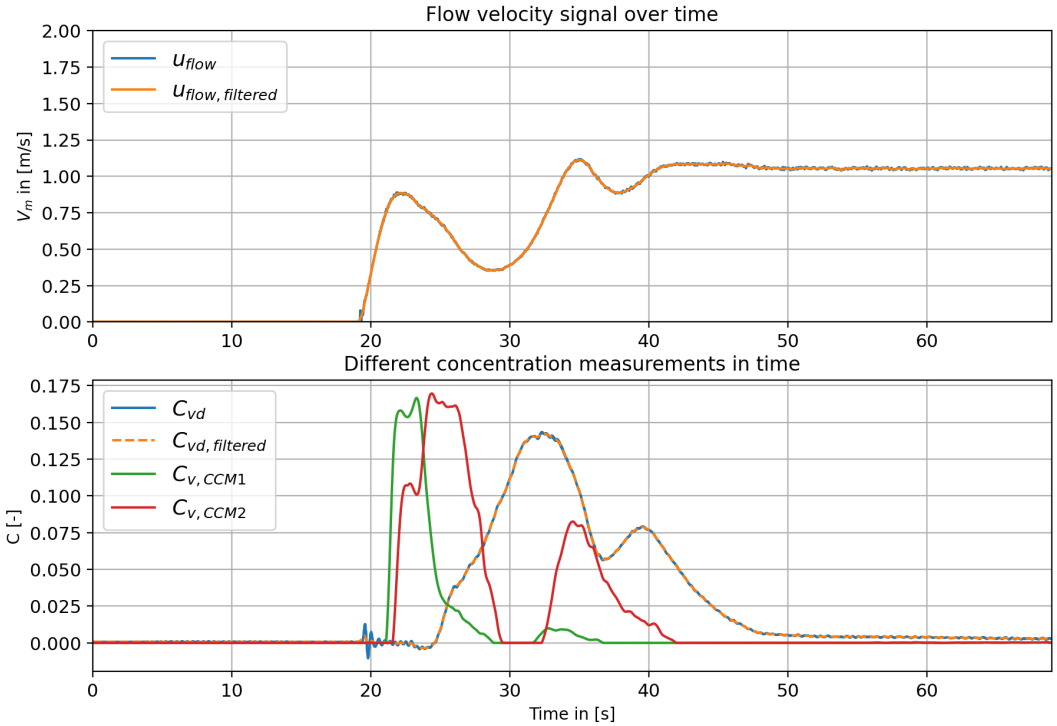

Figure E.19: GEBA $C_v = 0.20$

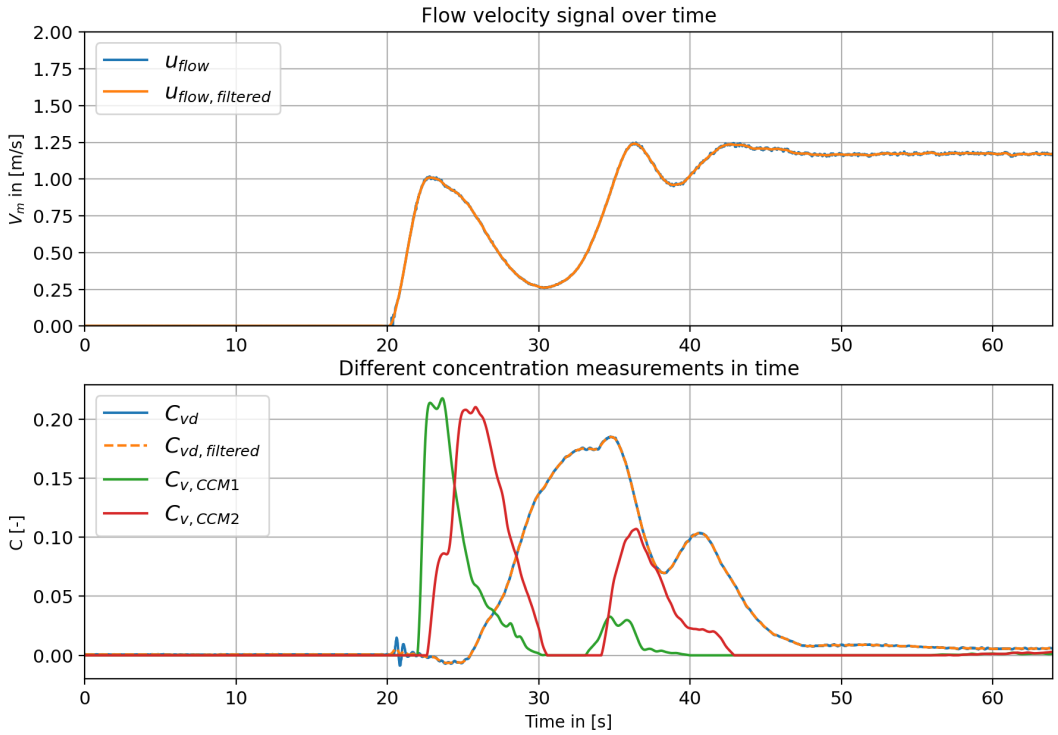

Figure E.20: GEBA $C_v = 0.30$

F

Results of the Sedimentation and Erosion Unbalance Simulations

In this appendix the results of the simulations are shown per pick-up function and per sand type.

F.1 Pick-up Function of van Rijn (1984a)

F.1.1 *Dorsilit nr.5G*

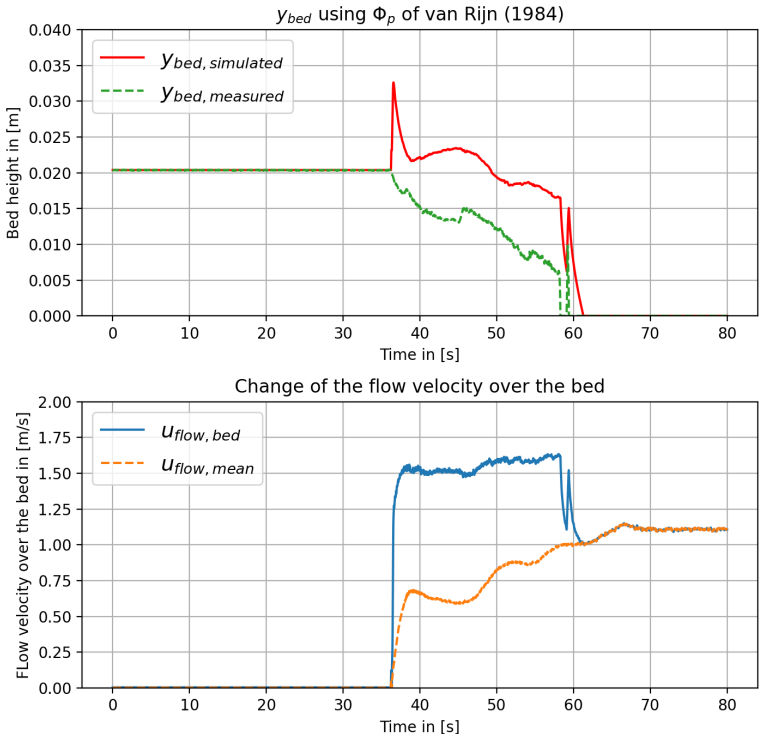

Figure F.1: Outcomes of simulation using the van Rijn (1984a) pick-up function for Dorsilit nr.5G with a mixture concentration of 5%

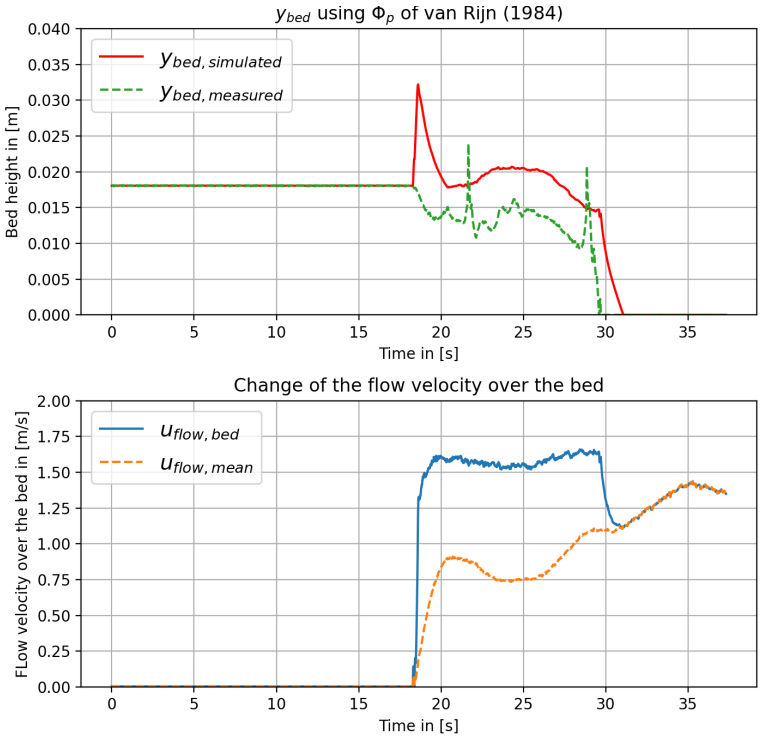

Figure F.2: Outcomes of simulation using the van Rijn (1984a) pick-up function for Dorsilit nr.5G with a mixture concentration of 10%

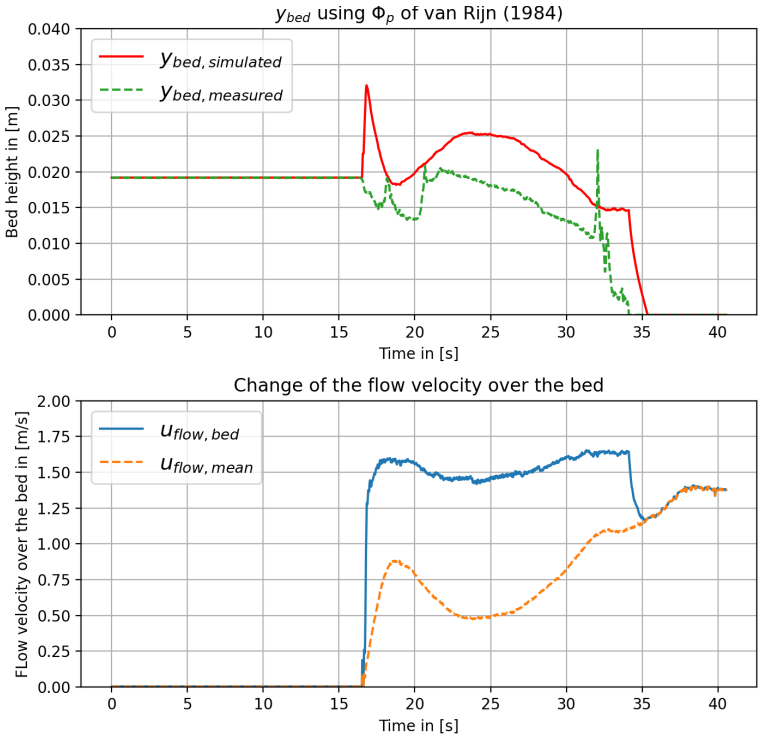

Figure F.3: Outcomes of simulation using the van Rijn (1984a) pick-up function for Dorsilit nr.5G with a mixture concentration of 20%

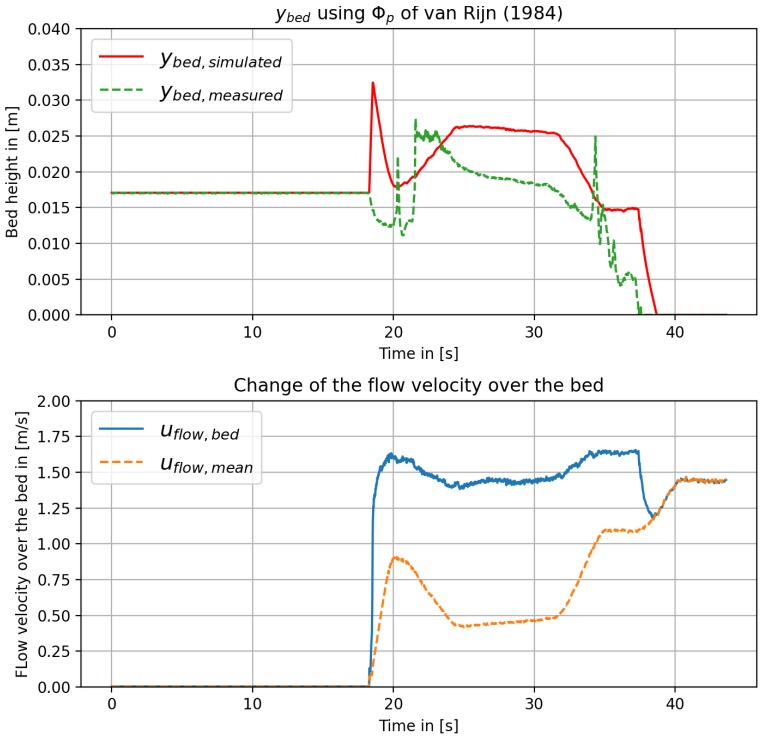

Figure F.4: Outcomes of simulation using the van Rijn (1984a) pick-up function for Dorsilit nr.5G with a mixture concentration of 30%

F.1.2 *Dorsilit nr.7*

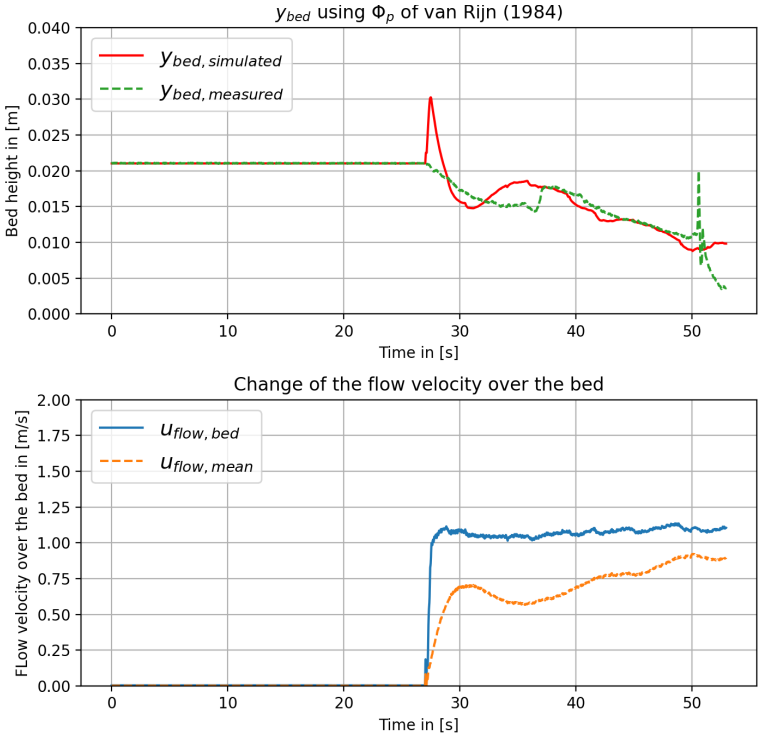

Figure F.5: Outcomes of simulation using the van Rijn (1984a) pick-up function for Dorsilit nr.7 with a mixture concentration of 5%

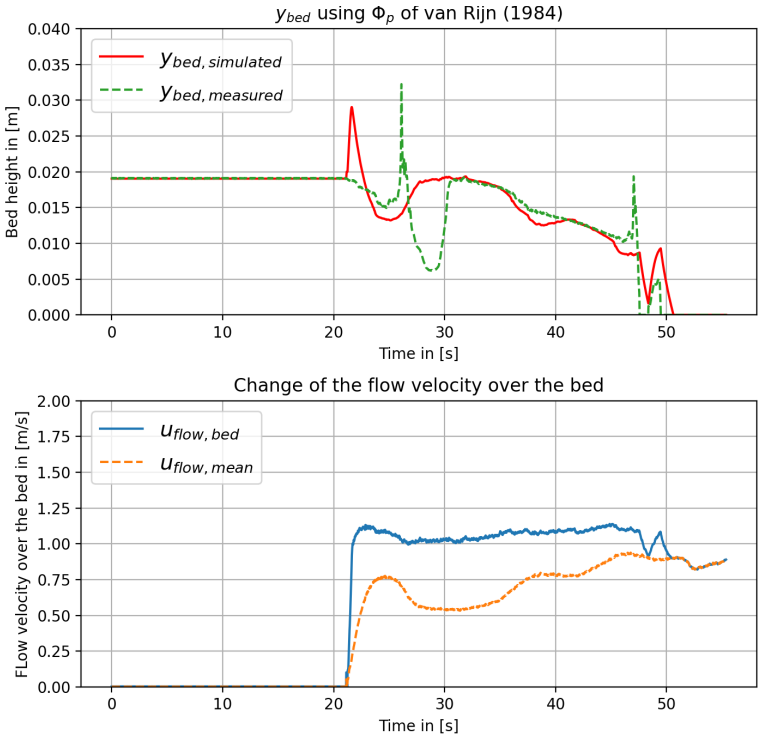

Figure F.6: Outcomes of simulation using the van Rijn (1984a) pick-up function for Dorsilit nr.7 with a mixture concentration of 10%

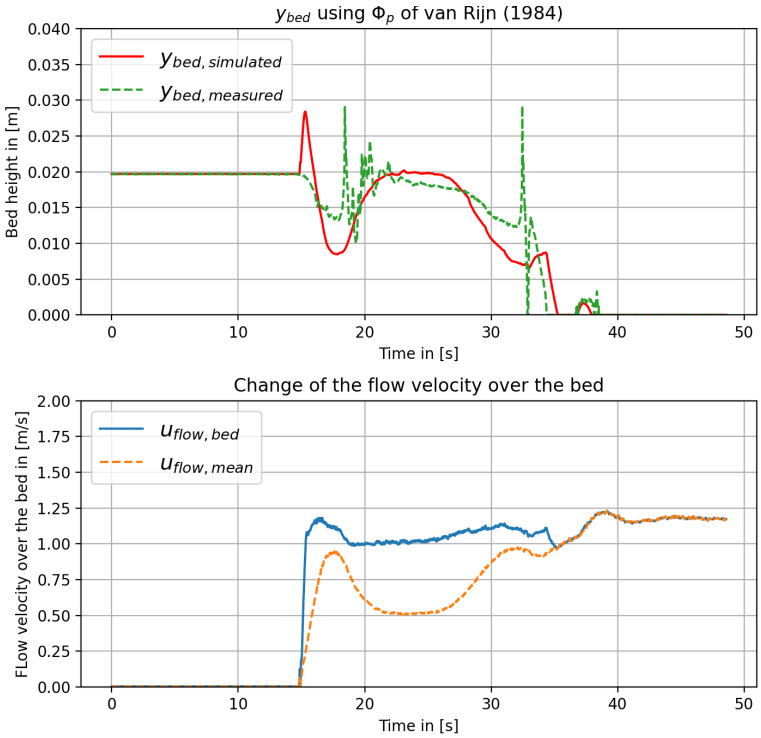

Figure F.7: Outcomes of simulation using the van Rijn (1984a) pick-up function for Dorsilit nr.7 with a mixture concentration of 20%

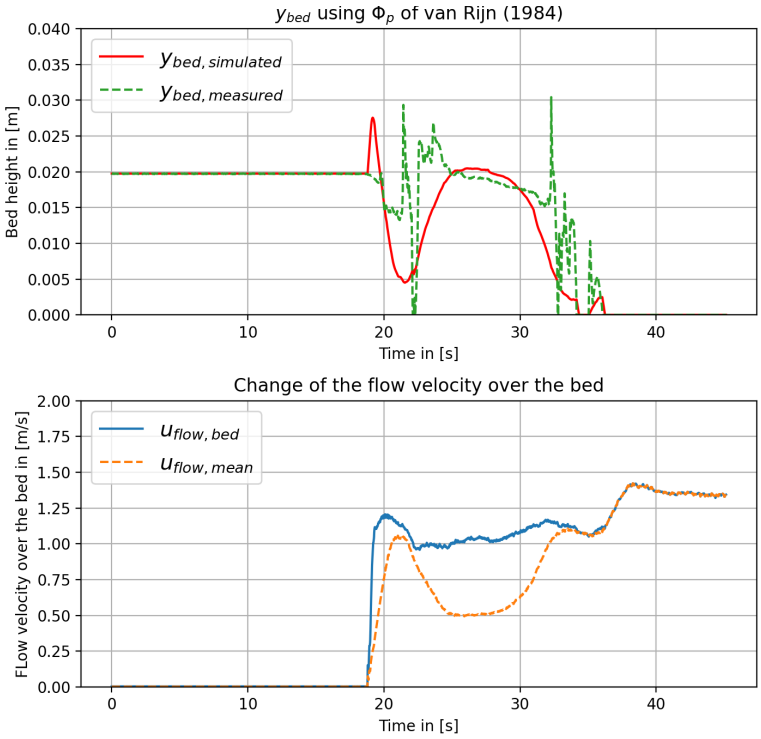

Figure F.8: Outcomes of simulation using the van Rijn (1984a) pick-up function for Dorsilit nr.7 with a mixture concentration of 30%

F.1.3 *Dorsilit nr.8*

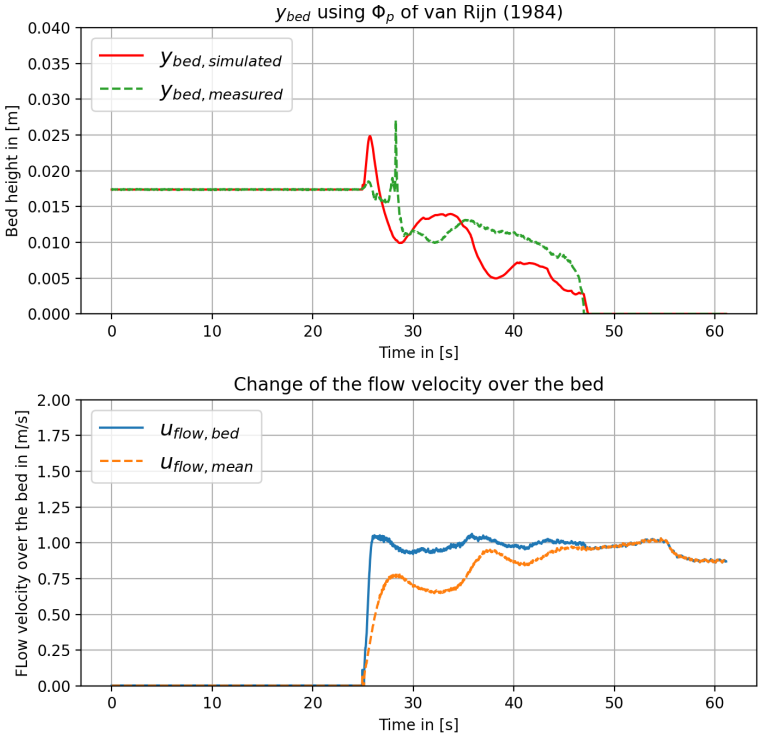

Figure F.9: Outcomes of simulation using the van Rijn (1984a) pick-up function for Dorsilit nr.8 with a mixture concentration of 5%

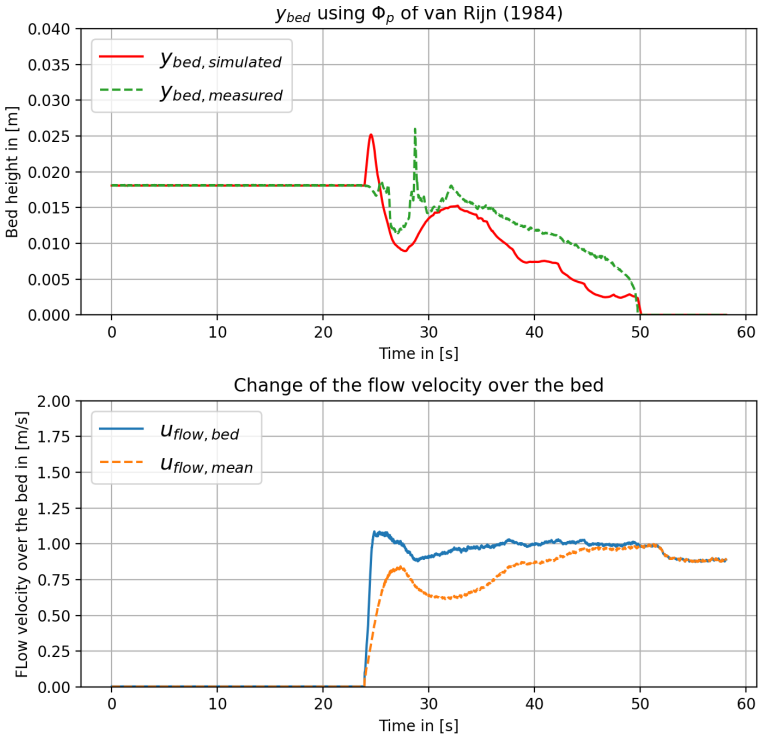

Figure F.10: Outcomes of simulation using the van Rijn (1984a) pick-up function for Dorsilit nr.8 with a mixture concentration of 10%

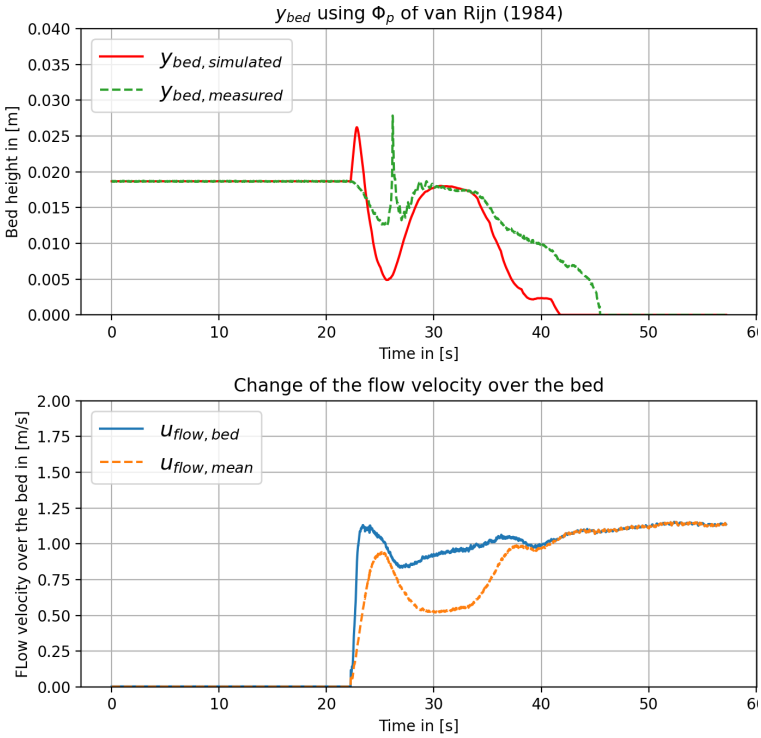

Figure F.11: Outcomes of simulation using the van Rijn (1984a) pick-up function for Dorsilit nr.8 with a mixture concentration of 20%

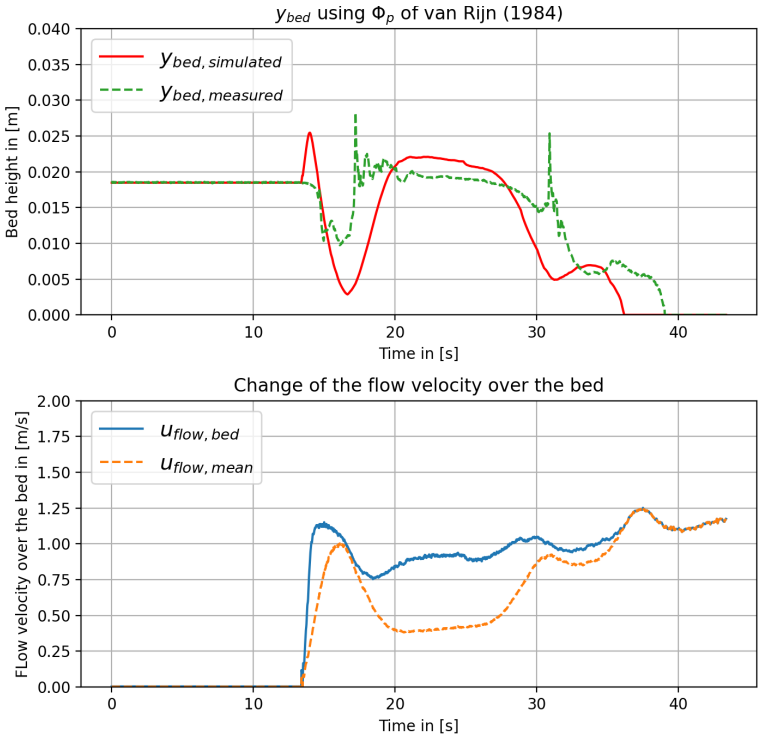

Figure F.12: Outcomes of simulation using the van Rijn (1984a) pick-up function for Dorsilit nr.8 with a mixture concentration of 30%

F.1.4 *Zilverzand*

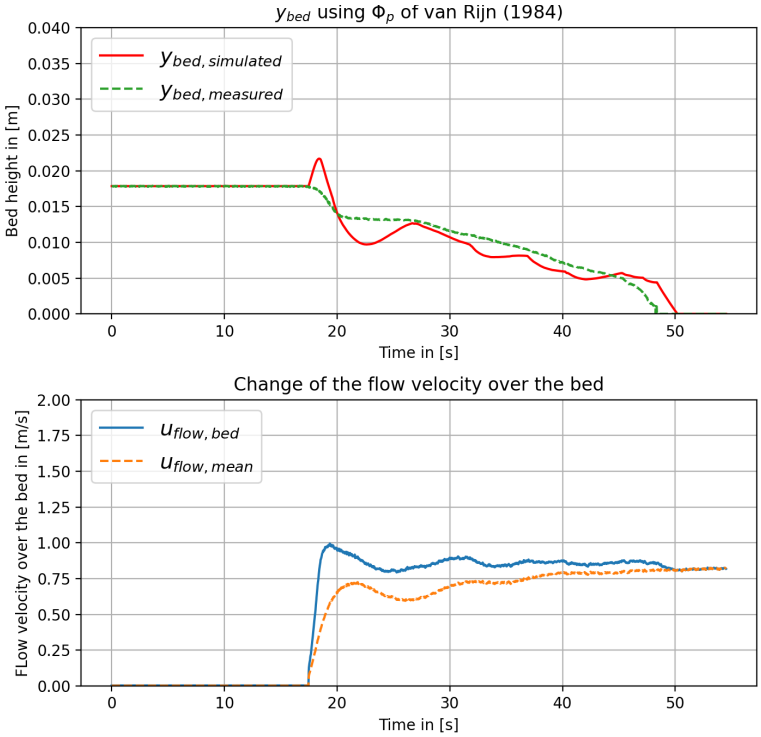

Figure F.13: Outcomes of simulation using the van Rijn (1984a) pick-up function for Zilverzand with a mixture concentration of 5%

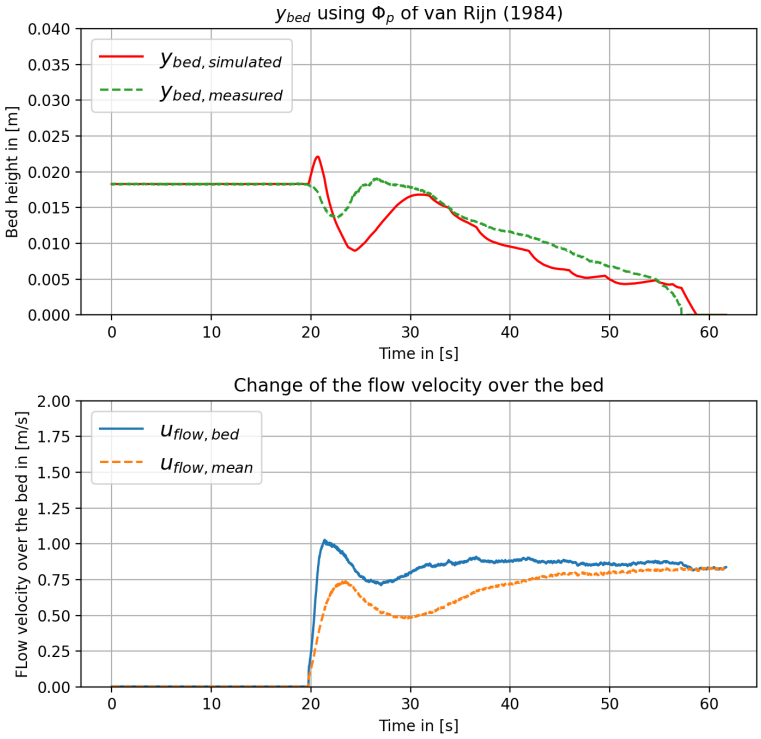

Figure F.14: Outcomes of simulation using the van Rijn (1984a) pick-up function for Zilverzand with a mixture concentration of 10%

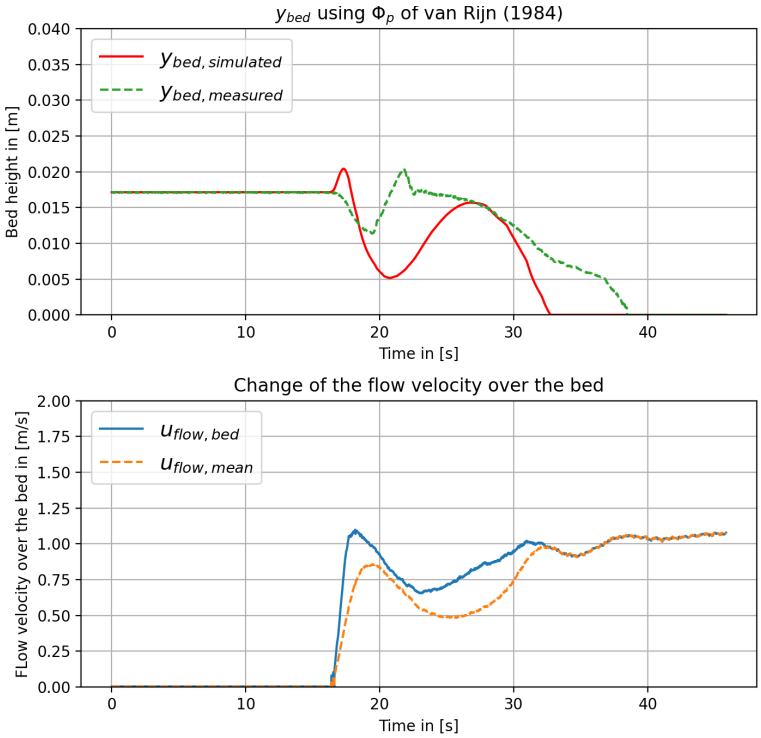

Figure F.15: Outcomes of simulation using the van Rijn (1984a) pick-up function for Zilverzand with a mixture concentration of 20%

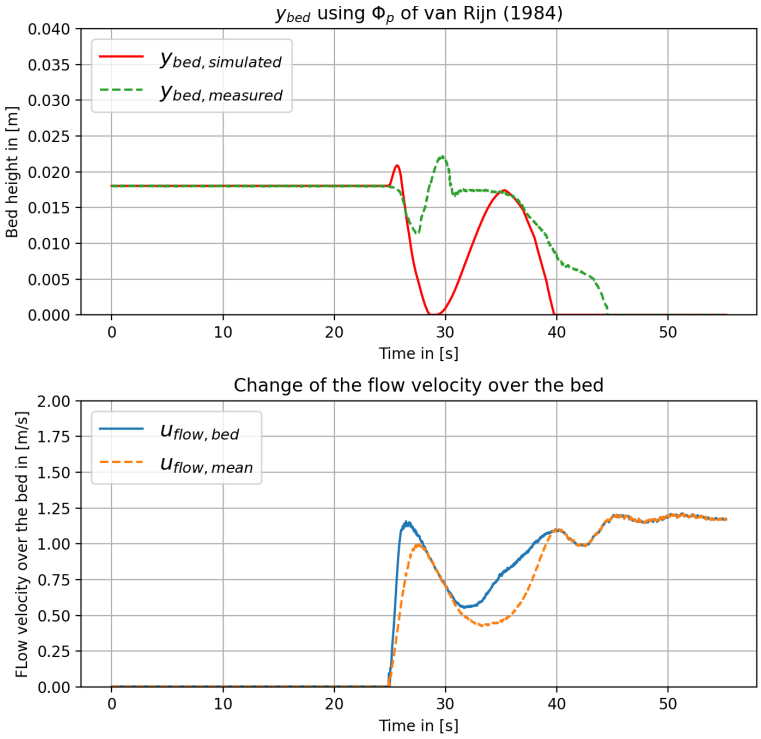

Figure F.16: Outcomes of simulation using the van Rijn (1984a) pick-up function for Zilverzand with a mixture concentration of 30%

F.1.5 *GEBA*

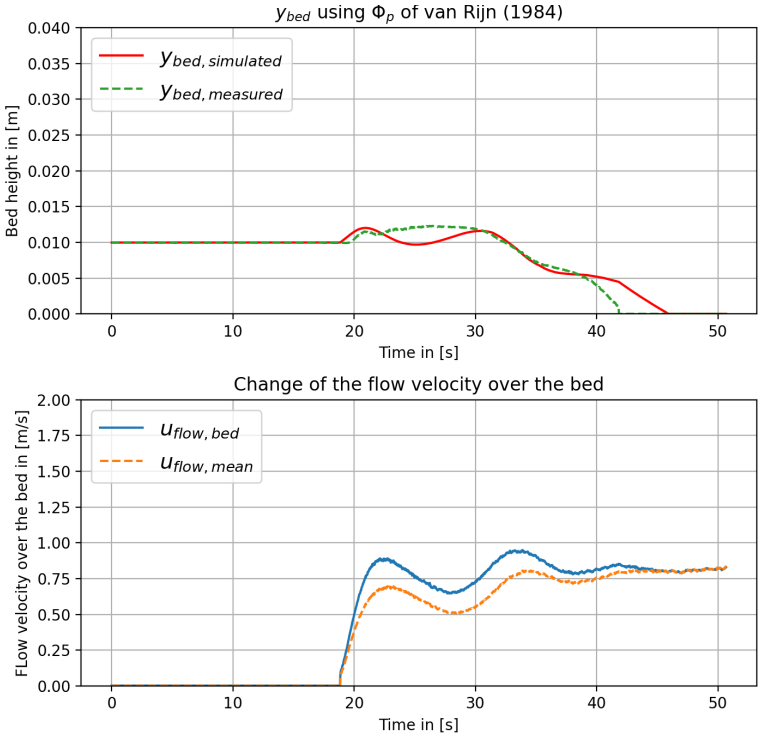

Figure F.17: Outcomes of simulation using the van Rijn (1984a) pick-up function for GEBA with a mixture concentration of 5%

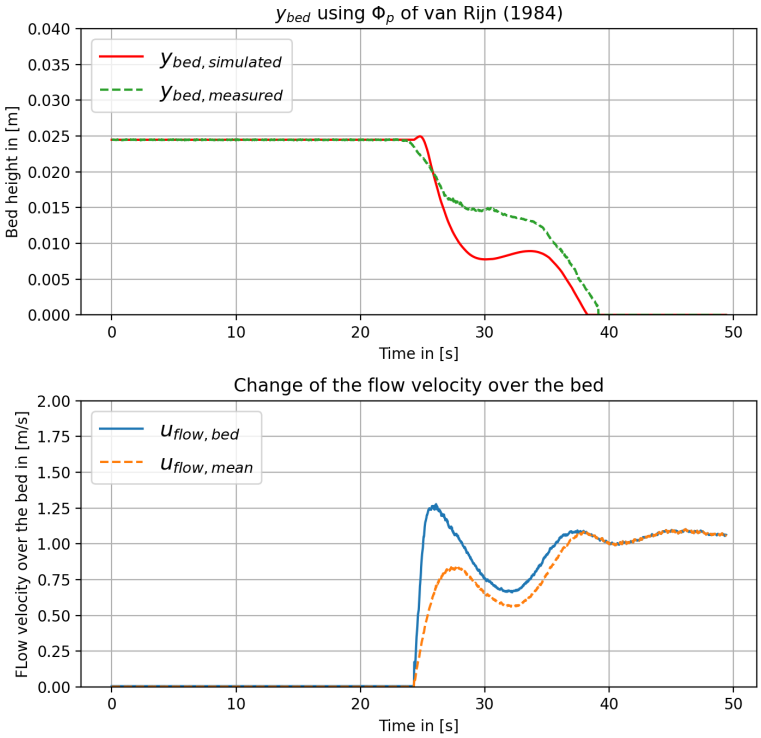

Figure F.18: Outcomes of simulation using the van Rijn (1984a) pick-up function for GEBA with a mixture concentration of 10%

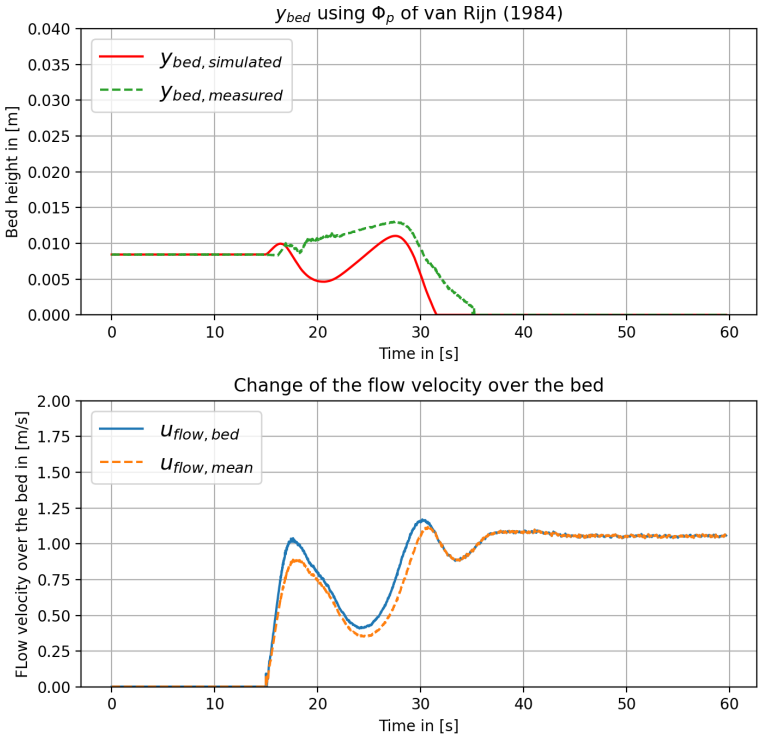

Figure F.19: Outcomes of simulation using the van Rijn (1984a) pick-up function for GEBA with a mixture concentration of 20%

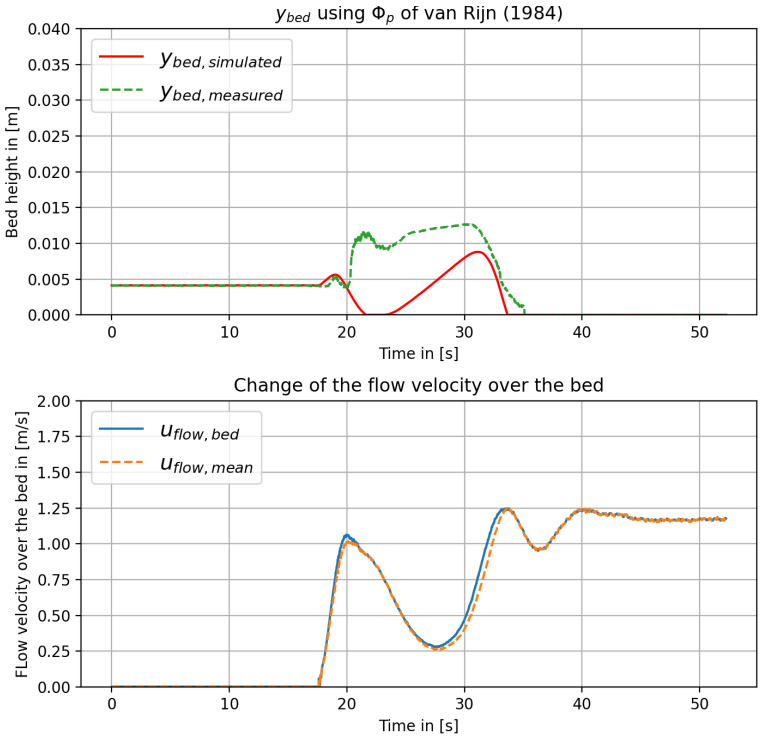

Figure F.20: Outcomes of simulation using the van Rijn (1984a) pick-up function for GEBA with a mixture concentration of 30%

F.2 Pick-up Function of Winterwerp (1992)

F.2.1 *Dorsilit nr.5G*

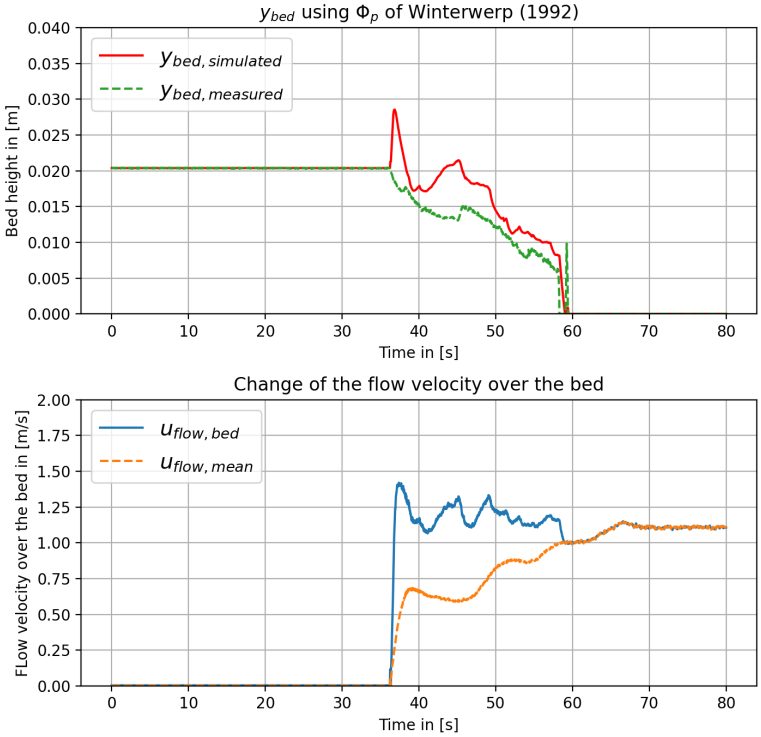

Figure F.21: Outcomes of simulation using the Winterwerp et al. (1992) pick-up function for Dorsilit nr.5G with a mixture concentration of 5%

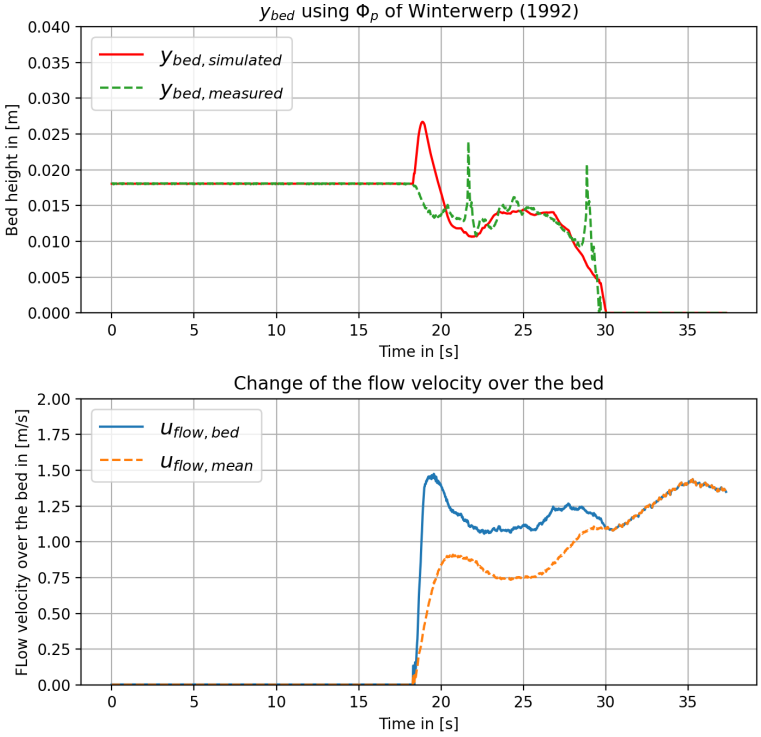

Figure F.22: Outcomes of simulation using the Winterwerp et al. (1992) pick-up function for Dorsilit nr.5G with a mixture concentration of 10%

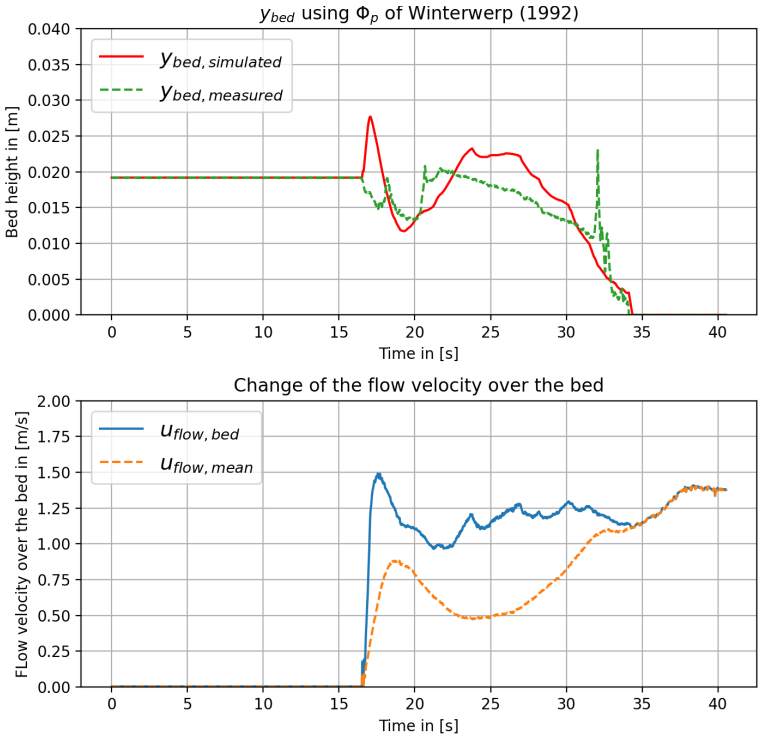

Figure F.23: Outcomes of simulation using the Winterwerp et al. (1992) pick-up function for Dorsilit nr.5G with a mixture concentration of 20%

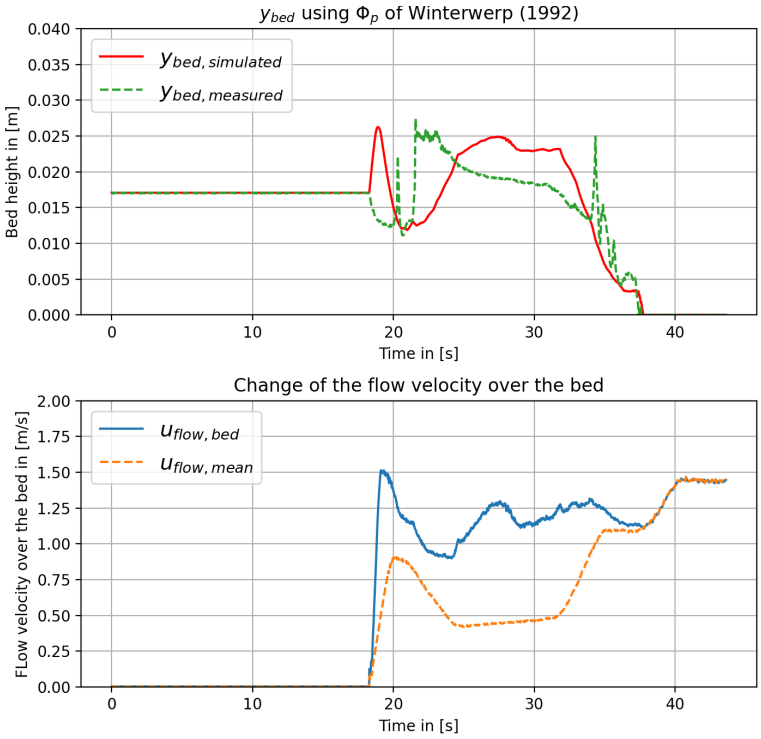

Figure F.24: Outcomes of simulation using the Winterwerp et al. (1992) pick-up function for Dorsilit nr.5G with a mixture concentration of 30%

F.2.2 *Dorsilit nr.7*

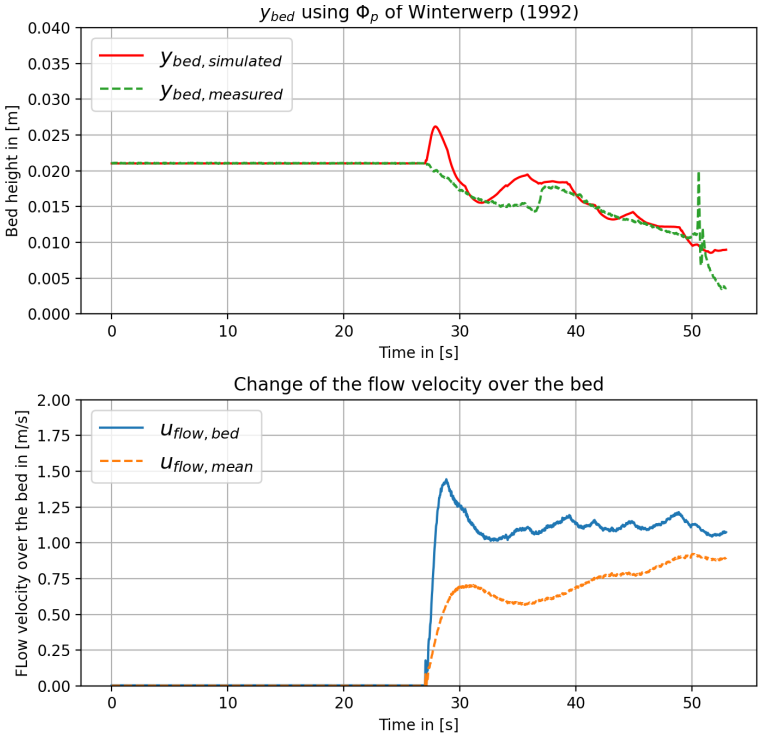

Figure F.25: Outcomes of simulation using the Winterwerp et al. (1992) pick-up function for Dorsilit nr.7 with a mixture concentration of 5%

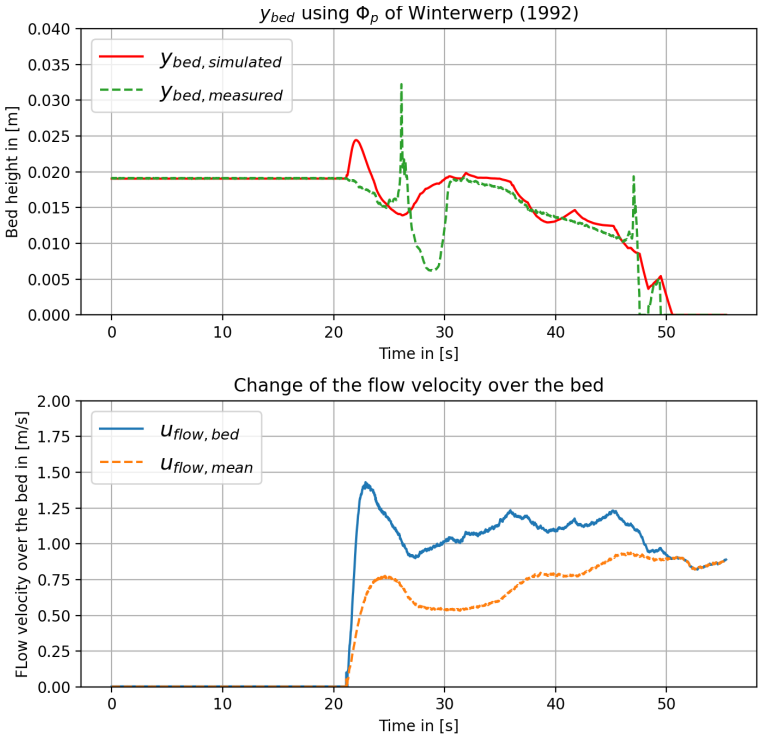

Figure F.26: Outcomes of simulation using the Winterwerp et al. (1992) pick-up function for Dorsilit nr.7 with a mixture concentration of 10%

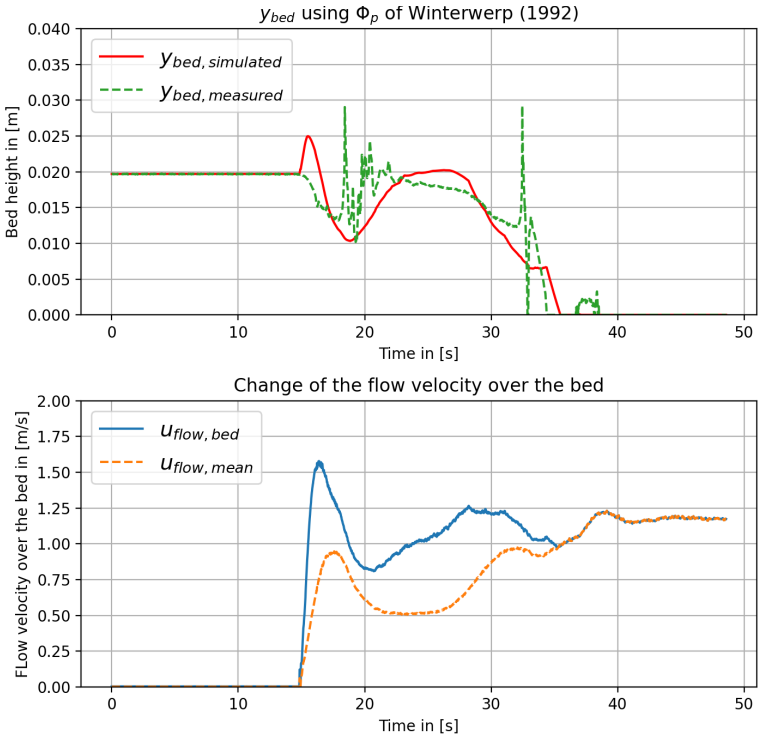

Figure F.27: Outcomes of simulation using the Winterwerp et al. (1992) pick-up function for Dorsilit nr.7 with a mixture concentration of 20%

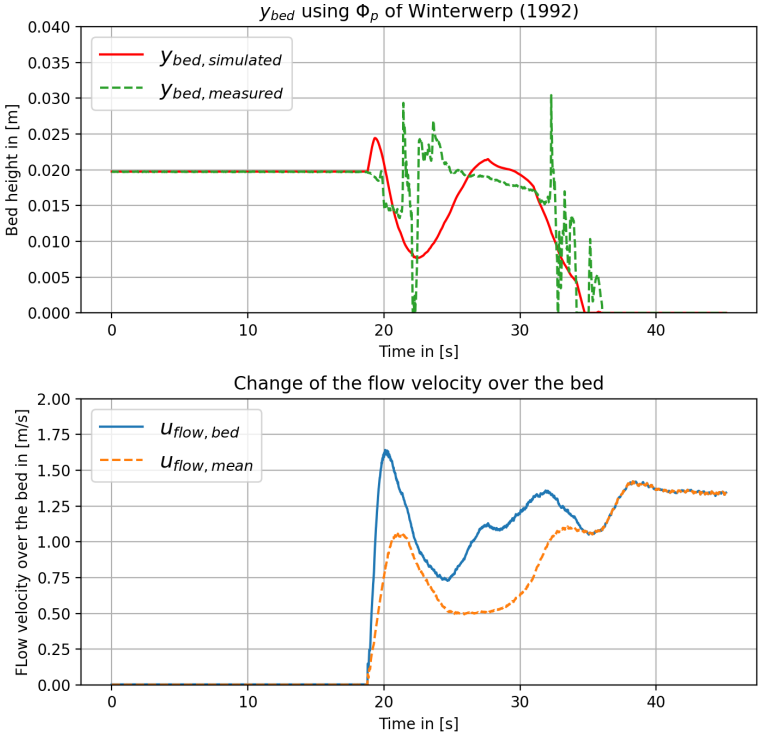

Figure F.28: Outcomes of simulation using the Winterwerp et al. (1992) pick-up function for Dorsilit nr.7 with a mixture concentration of 30%

F.2.3 *Dorsilit nr.8*

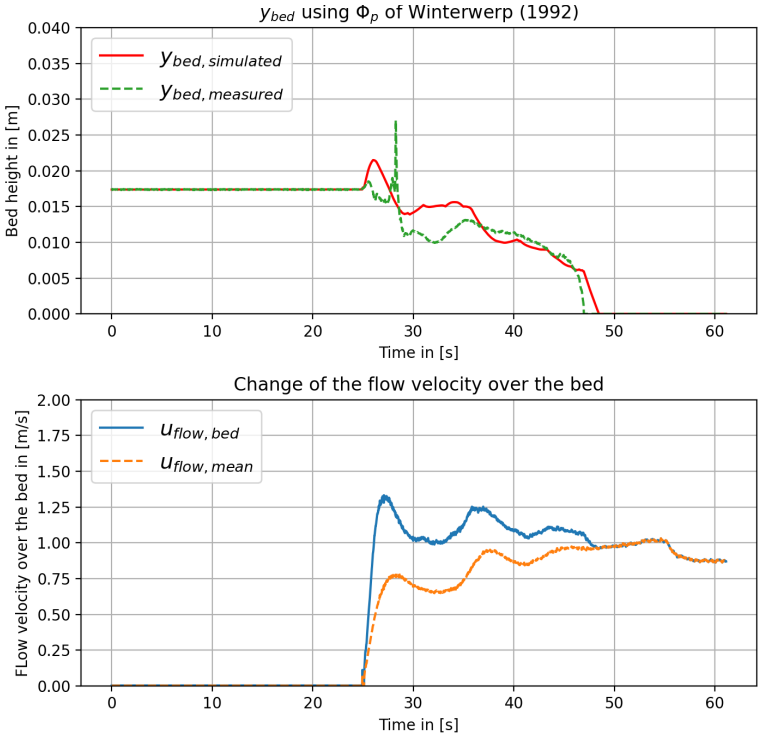

Figure F.29: Outcomes of simulation using the Winterwerp et al. (1992) pick-up function for Dorsilit nr.8 with a mixture concentration of 5%

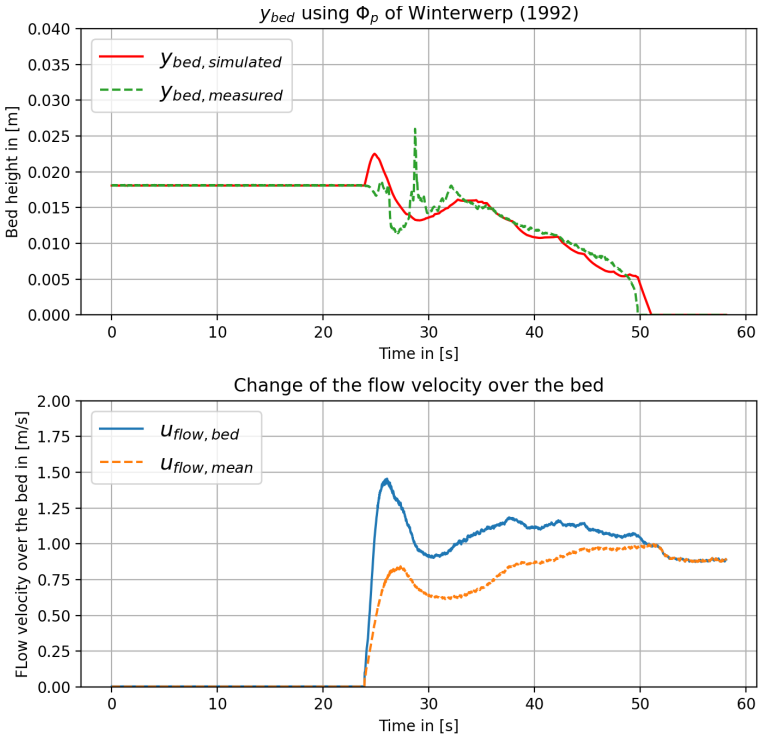

Figure F.30: Outcomes of simulation using the Winterwerp et al. (1992) pick-up function for Dorsilit nr.8 with a mixture concentration of 10%

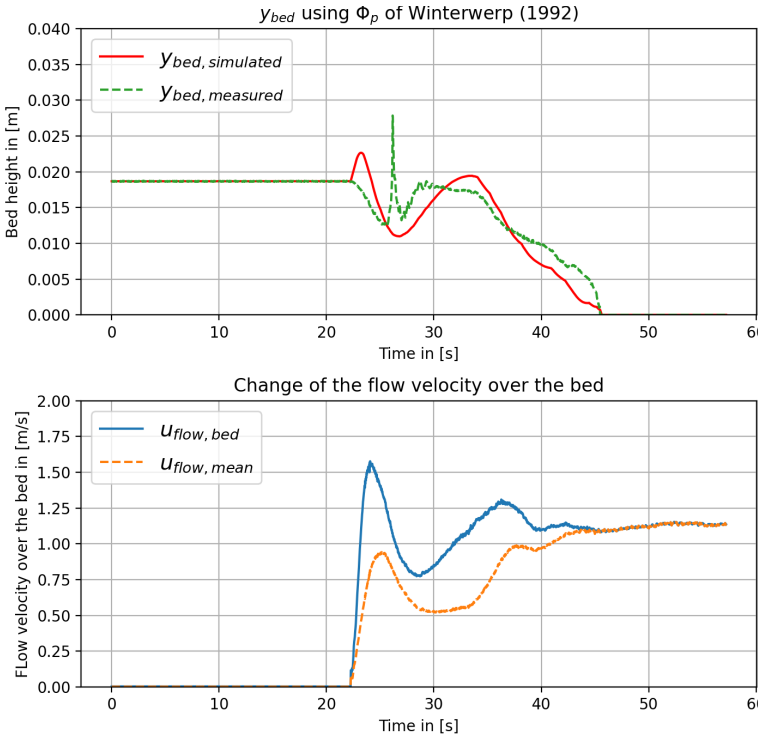

Figure F.31: Outcomes of simulation using the Winterwerp et al. (1992) pick-up function for Dorsilit nr.8 with a mixture concentration of 20%

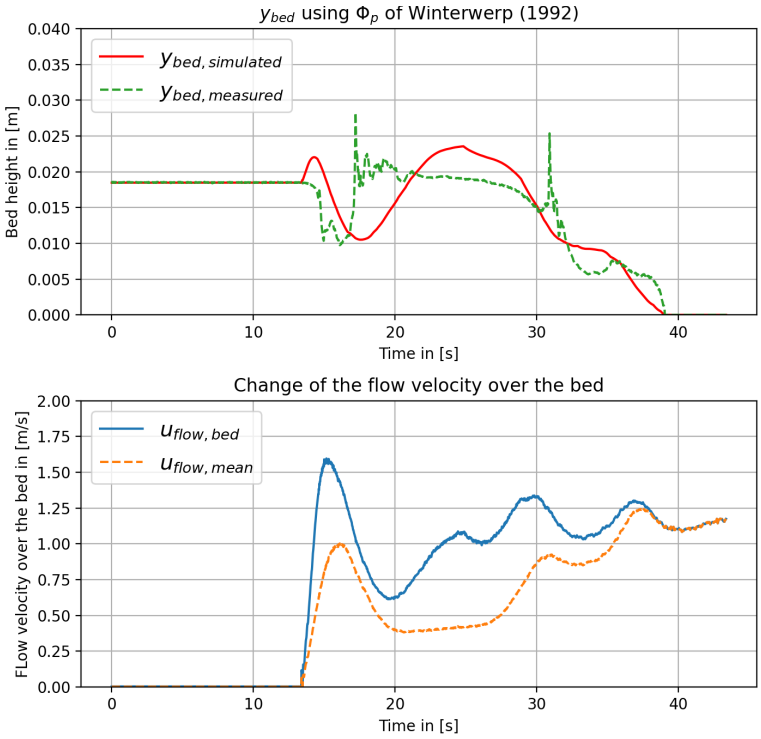

Figure F.32: Outcomes of simulation using the Winterwerp et al. (1992) pick-up function for Dorsilit nr.8 with a mixture concentration of 30%

F.2.4 *Zilverzand*

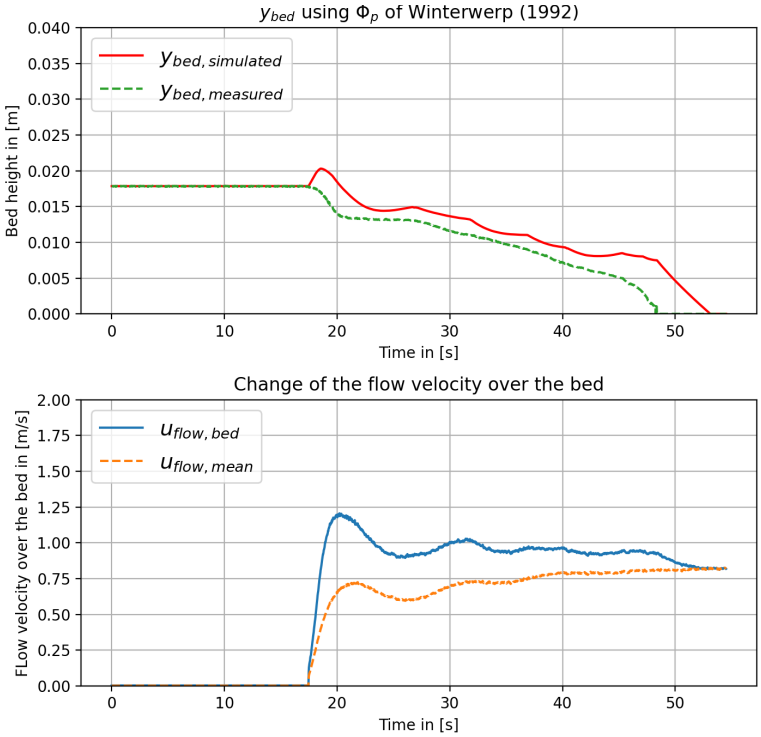

Figure F.33: Outcomes of simulation using the Winterwerp et al. (1992) pick-up function for Zilverzand with a mixture concentration of 5%

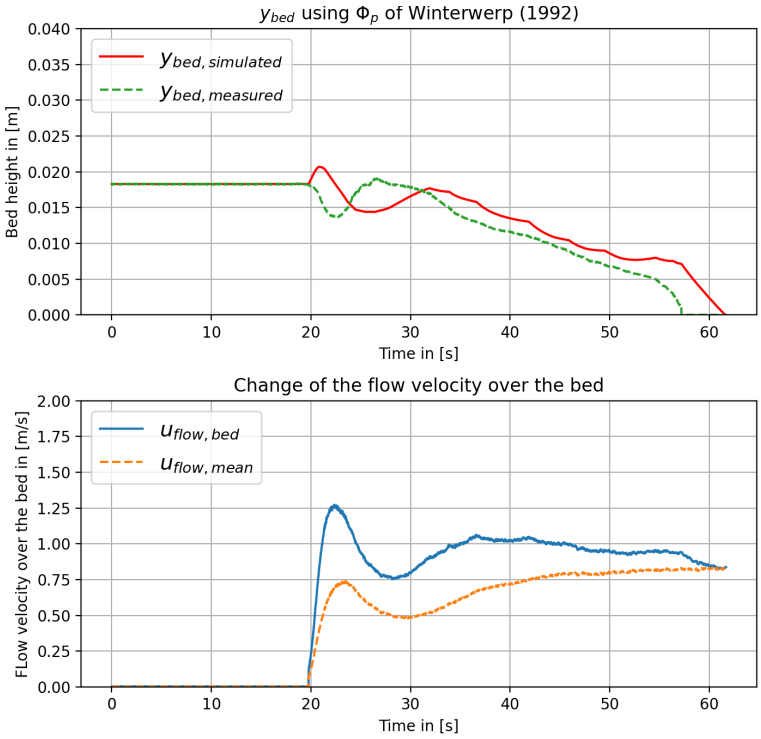

Figure F.34: Outcomes of simulation using the Winterwerp et al. (1992) pick-up function for Zilverzand with a mixture concentration of 10%

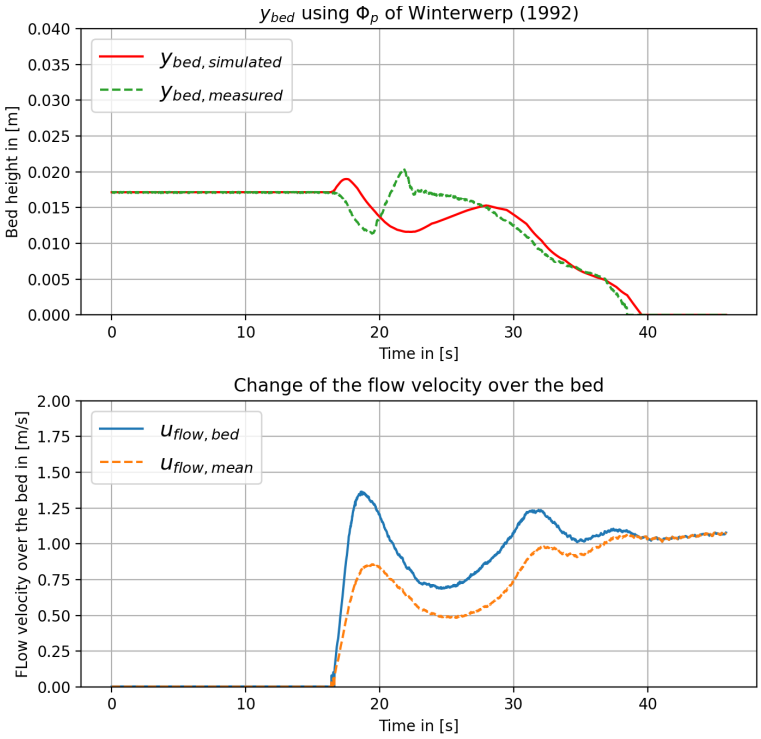

Figure F.35: Outcomes of simulation using the Winterwerp et al. (1992) pick-up function for Zilverzand with a mixture concentration of 20%

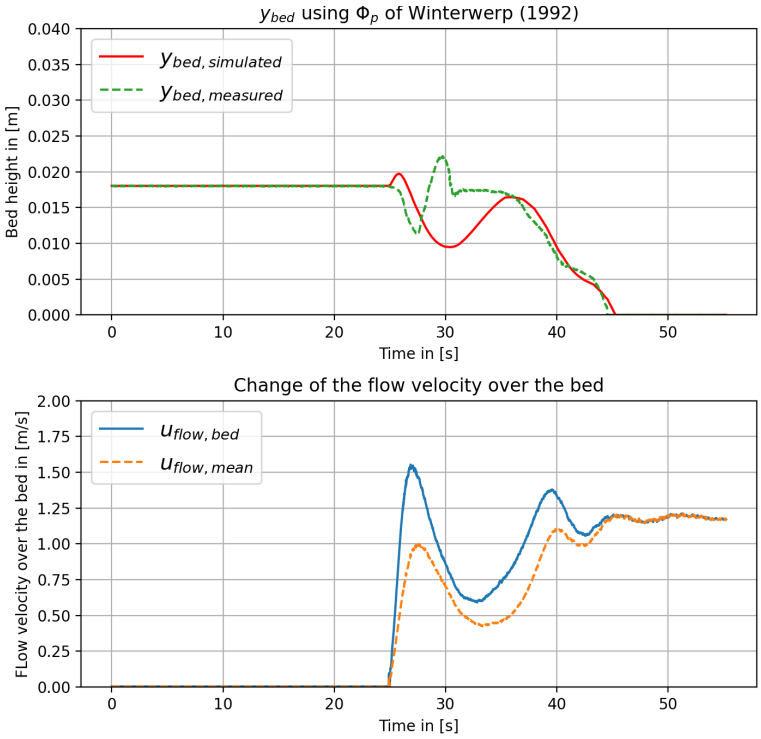

Figure F.36: Outcomes of simulation using the Winterwerp et al. (1992) pick-up function for Zilverzand with a mixture concentration of 30%

F.2.5 *GEBA*

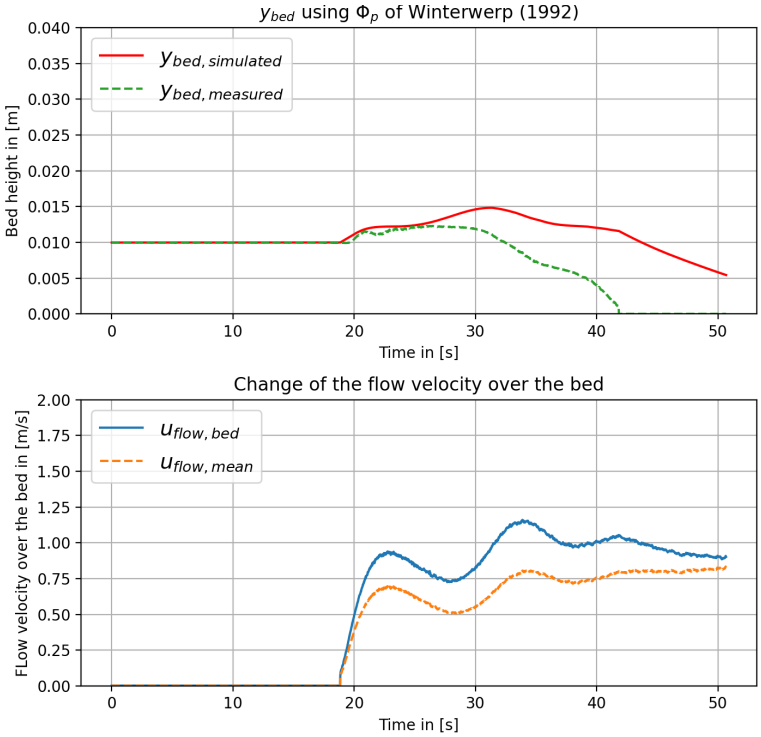

Figure F.37: Outcomes of simulation using the Winterwerp et al. (1992) pick-up function for GEBA with a mixture concentration of 5%

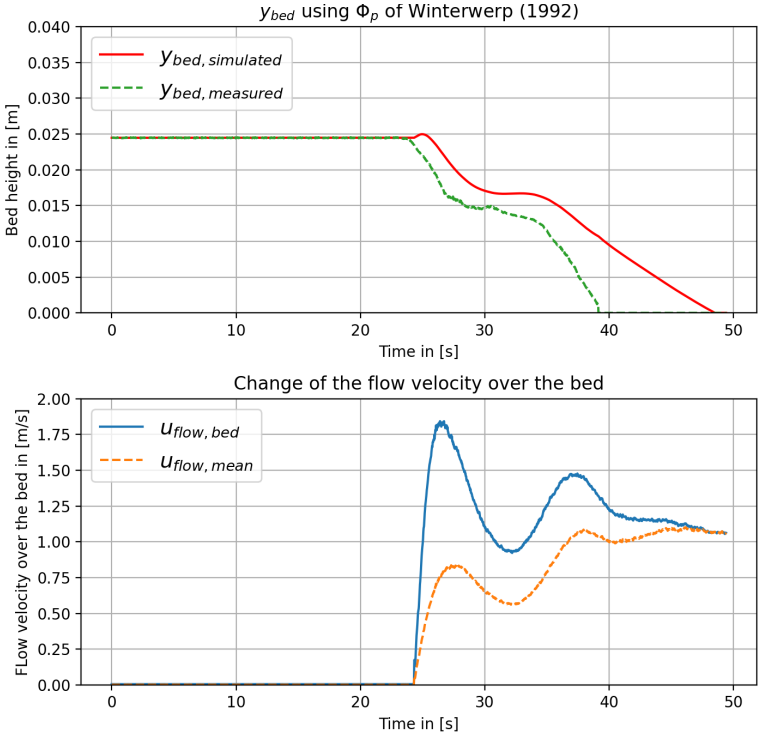

Figure F.38: Outcomes of simulation using the Winterwerp et al. (1992) pick-up function for GEBA with a mixture concentration of 10%

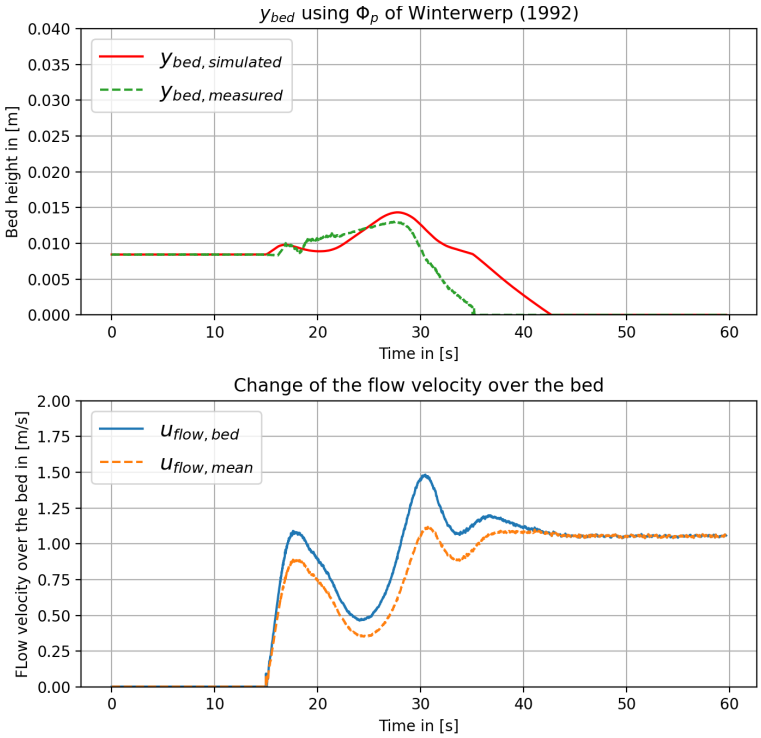

Figure F.39: Outcomes of simulation using the Winterwerp et al. (1992) pick-up function for GEBA with a mixture concentration of 20%

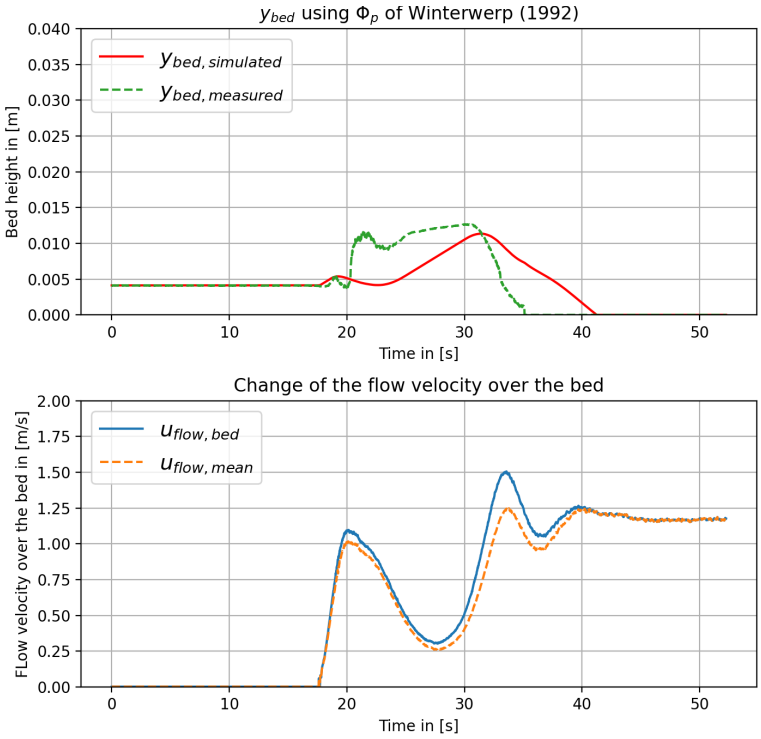

Figure F.40: Outcomes of simulation using the Winterwerp et al. (1992) pick-up function for GEBA with a mixture concentration of 30%

F.3 Pick-up Function of van Rhee (2010)

F.3.1 *Dorsilit nr.5G*

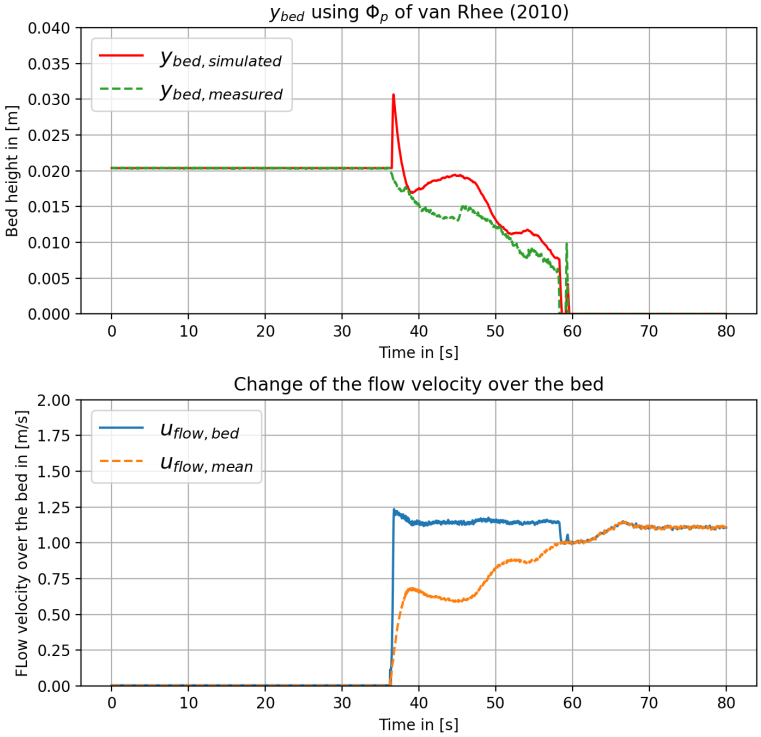

Figure F.41: Outcomes of simulation using the van Rhee (2010) pick-up function for Dorsilit nr.5G with a mixture concentration of 5%

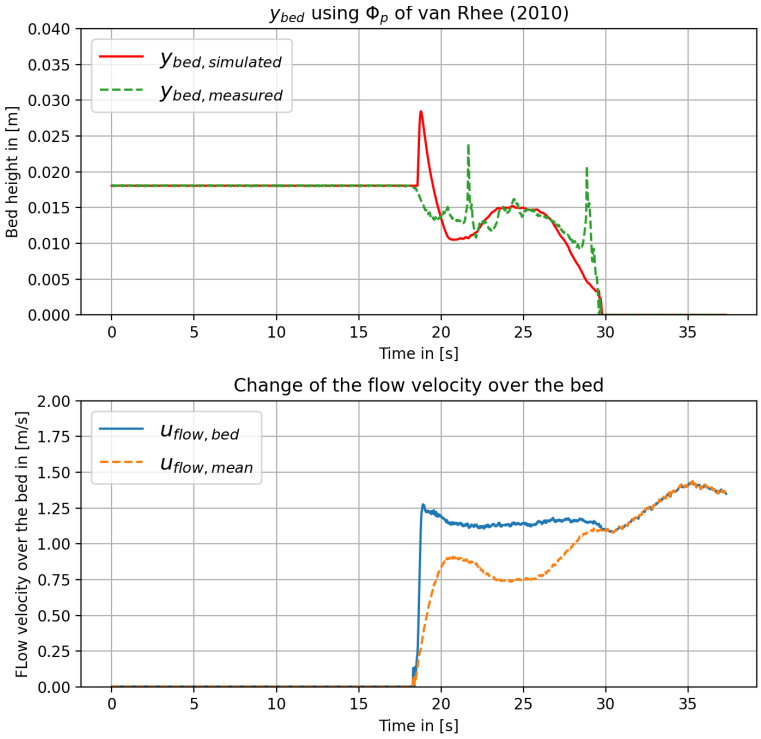

Figure F.42: Outcomes of simulation using the van Rhee (2010) pick-up function for Dorsilit nr.5G with a mixture concentration of 10%

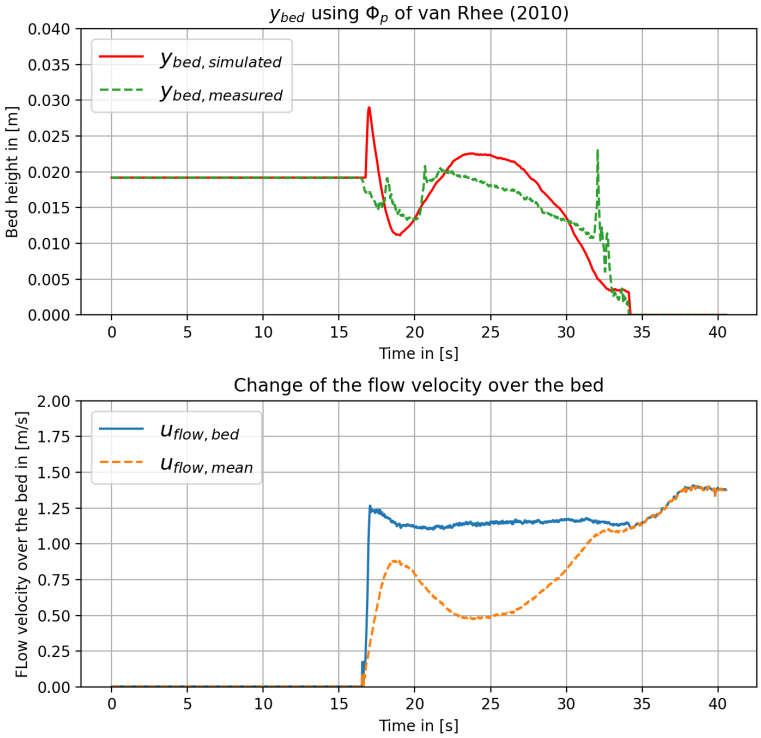

Figure F.43: Outcomes of simulation using the van Rhee (2010) pick-up function for Dorsilit nr.5G with a mixture concentration of 20%

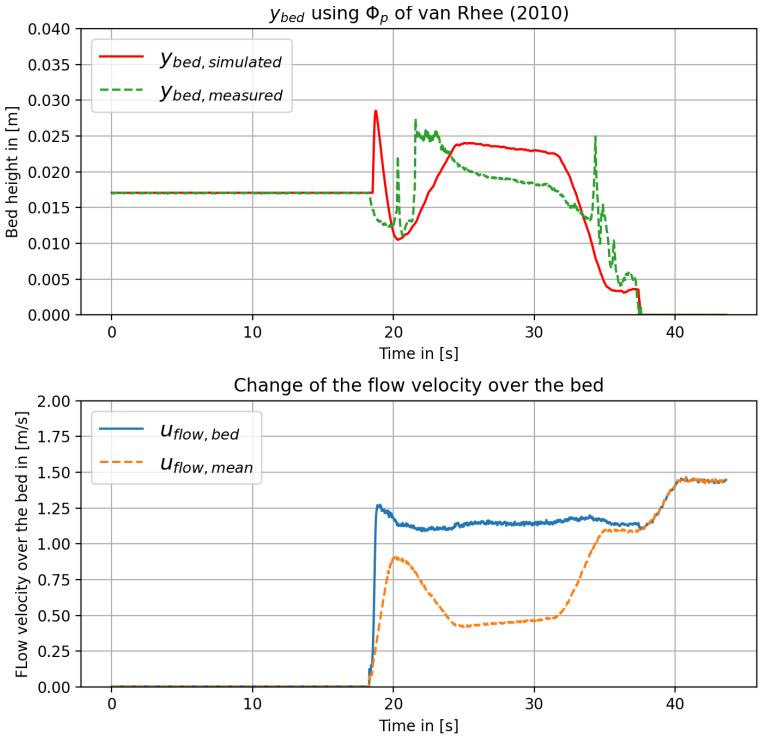

Figure F.44: Outcomes of simulation using the van Rhee (2010) pick-up function for Dorsilit nr.5G with a mixture concentration of 30%

F.3.2 *Dorsilit nr.7*

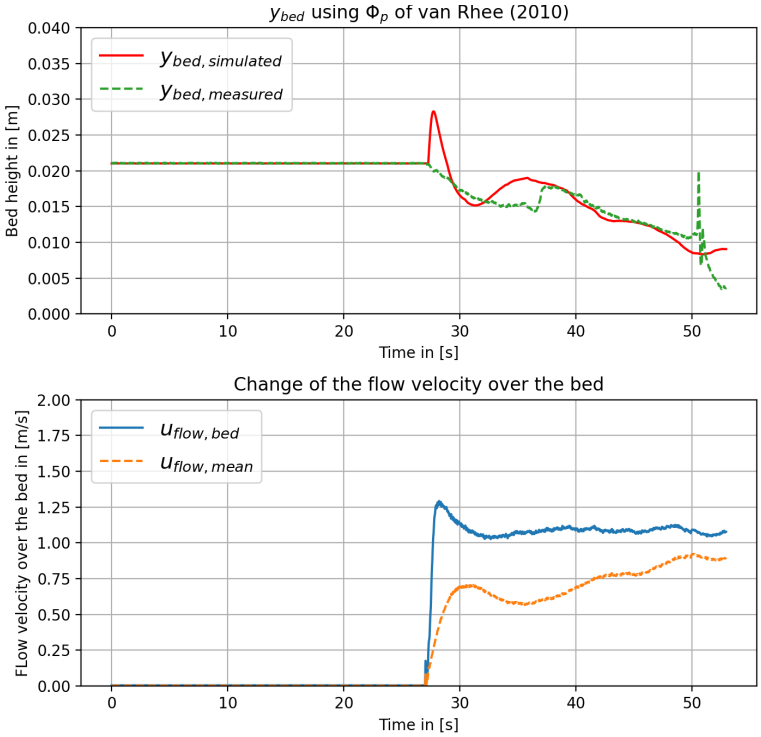

Figure F.45: Outcomes of simulation using the van Rhee (2010) pick-up function for Dorsilit nr.7 with a mixture concentration of 5%

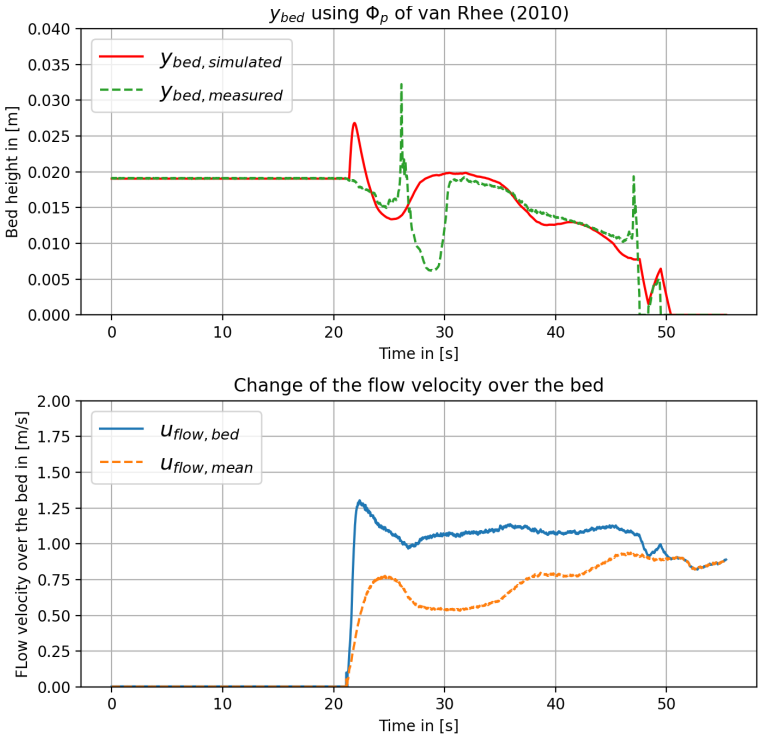

Figure F.46: Outcomes of simulation using the van Rhee (2010) pick-up function for Dorsilit nr.7 with a mixture concentration of 10%

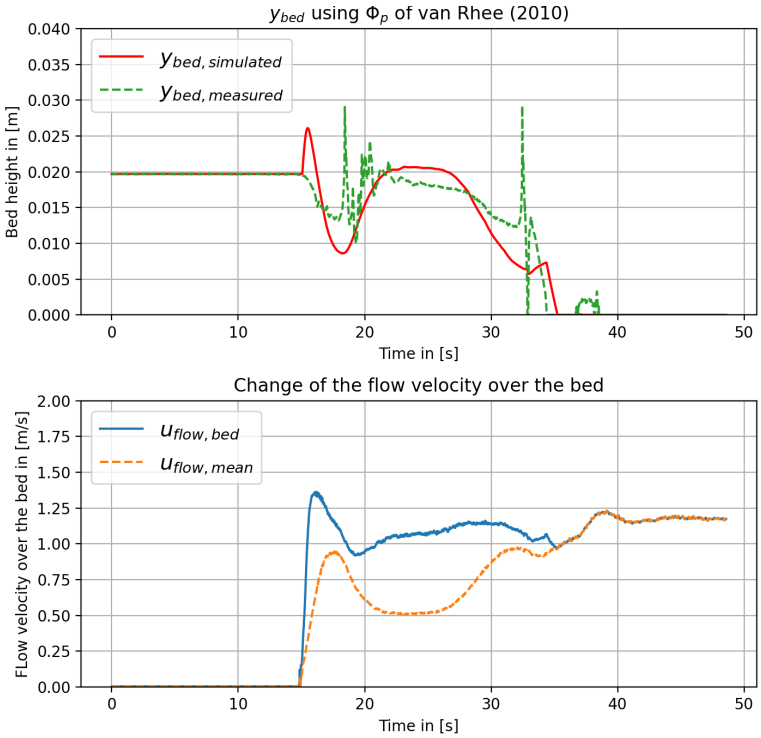

Figure F.47: Outcomes of simulation using the van Rhee (2010) pick-up function for Dorsilit nr.7 with a mixture concentration of 20%

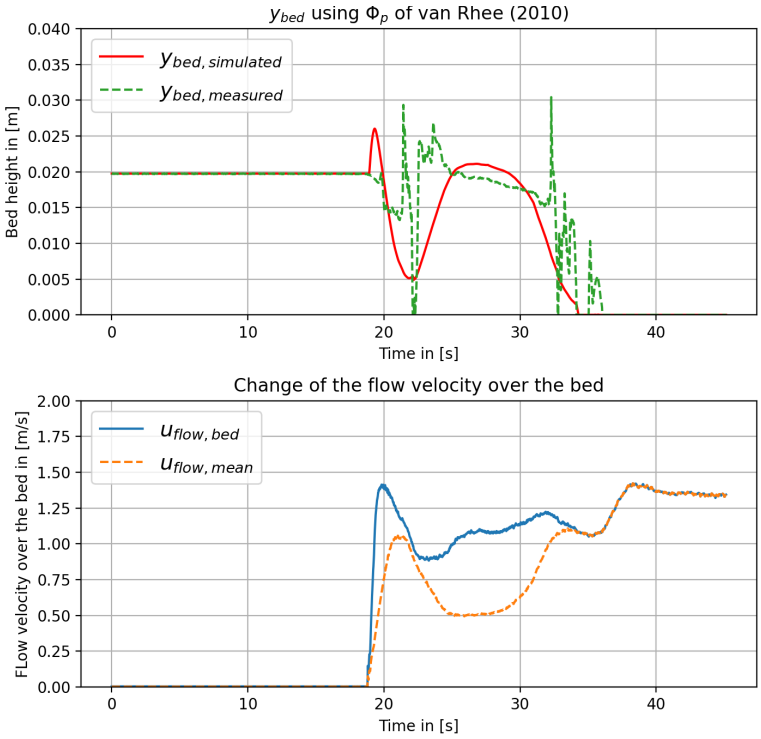

Figure F.48: Outcomes of simulation using the van Rhee (2010) pick-up function for Dorsilit nr.7 with a mixture concentration of 30%

F.3.3 *Dorsilit nr.8*

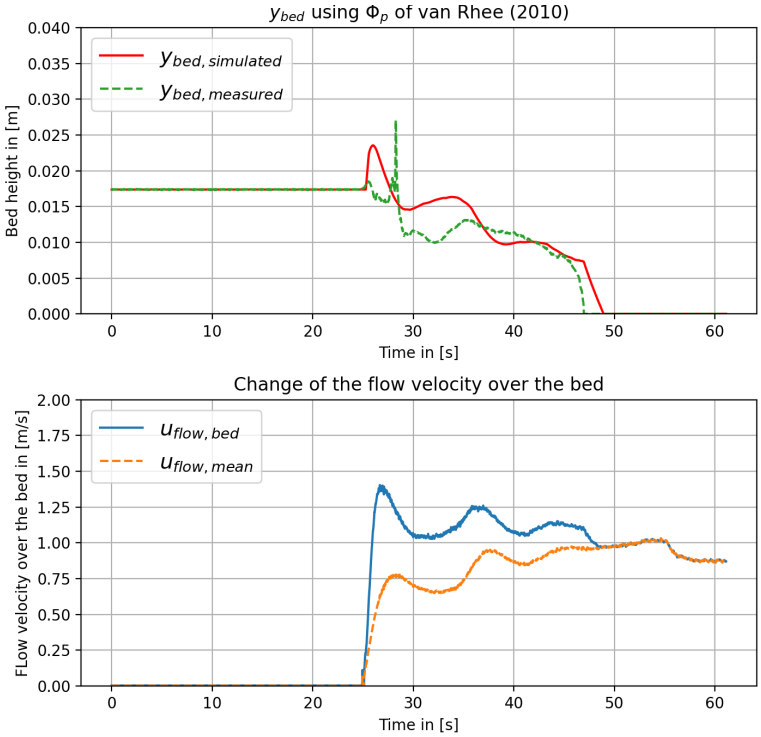

Figure F.49: Outcomes of simulation using the van Rhee (2010) pick-up function for Dorsilit nr.8 with a mixture concentration of 5%

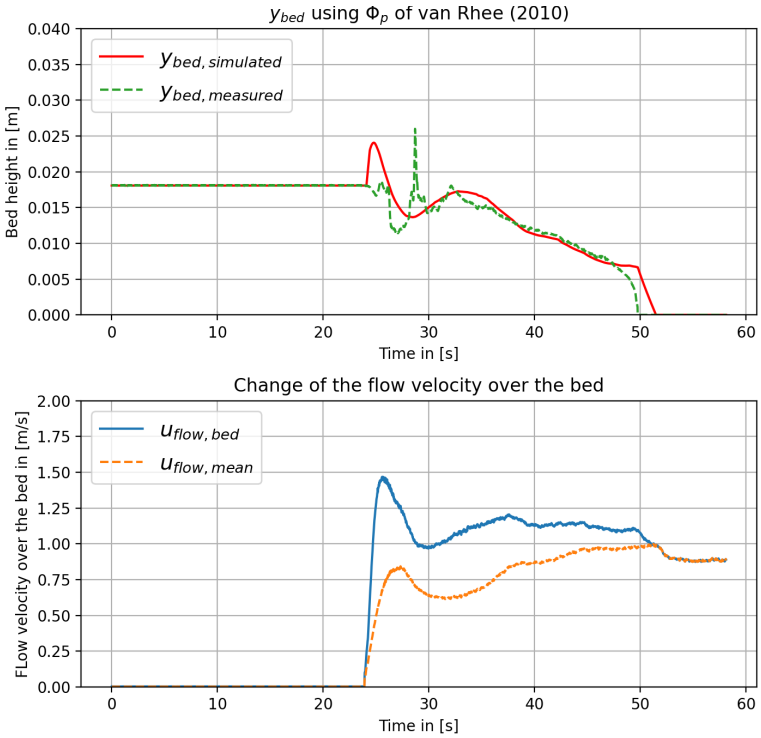

Figure F.50: Outcomes of simulation using the van Rhee (2010) pick-up function for Dorsilit nr.8 with a mixture concentration of 10%

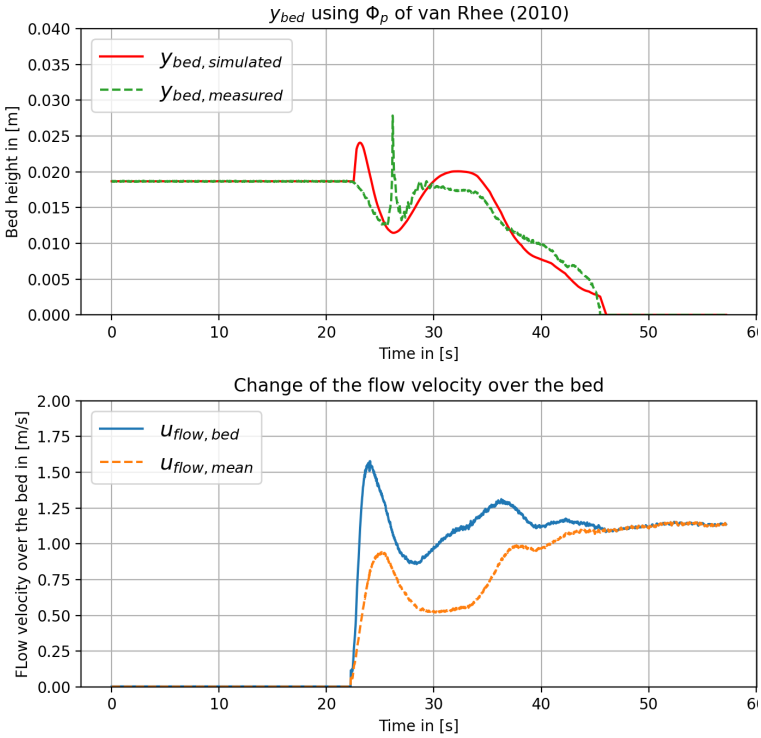

Figure F.51: Outcomes of simulation using the van Rhee (2010) pick-up function for Dorsilit nr.8 with a mixture concentration of 20%

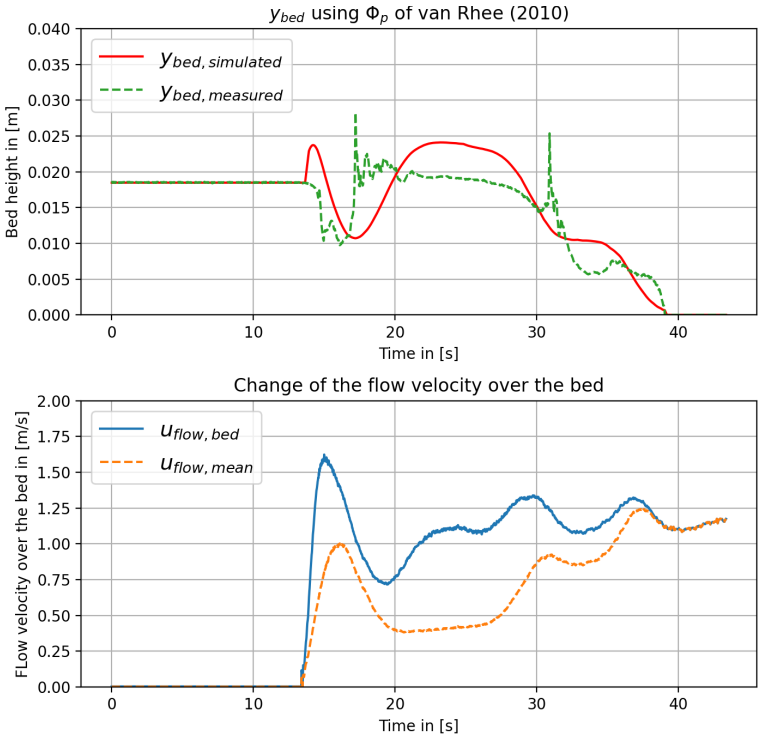

Figure F.52: Outcomes of simulation using the van Rhee (2010) pick-up function for Dorsilit nr.8 with a mixture concentration of 30%

F.3.4 *Zilverzand*

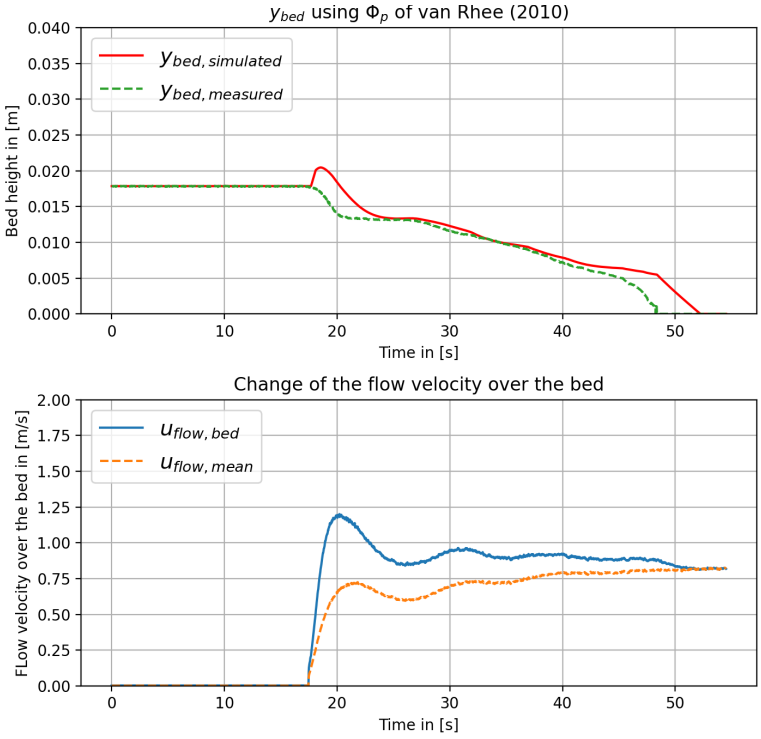

Figure F.53: Outcomes of simulation using the van Rhee (2010) pick-up function for Zilverzand with a mixture concentration of 5%

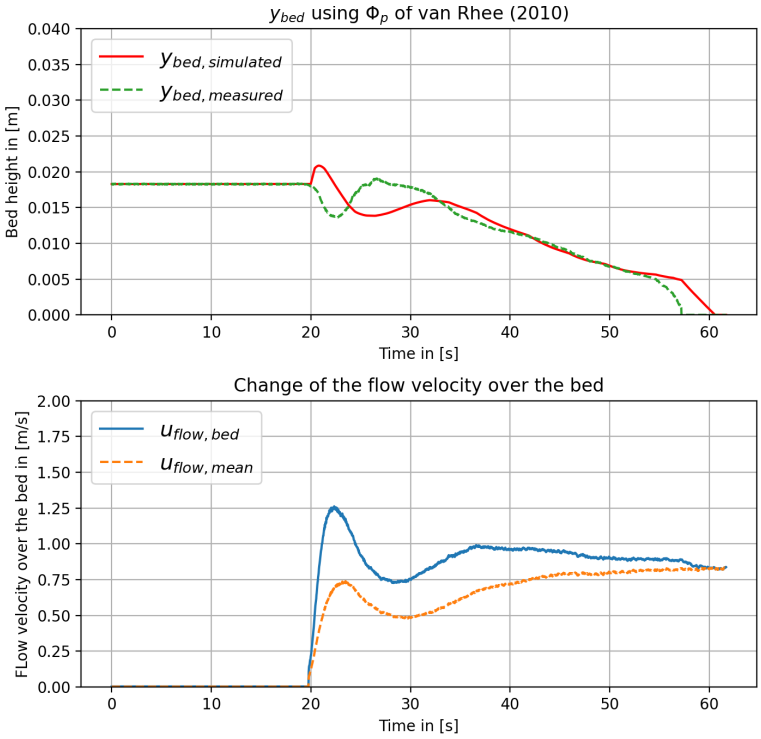

Figure F.54: Outcomes of simulation using the van Rhee (2010) pick-up function for Zilverzand with a mixture concentration of 10%

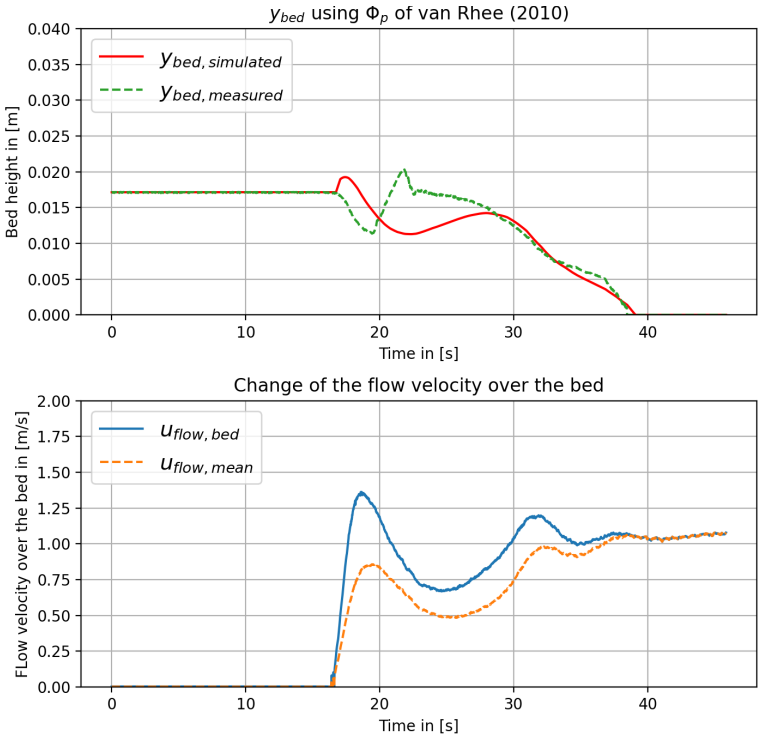

Figure F.55: Outcomes of simulation using the van Rhee (2010) pick-up function for Zilverzand with a mixture concentration of 20%

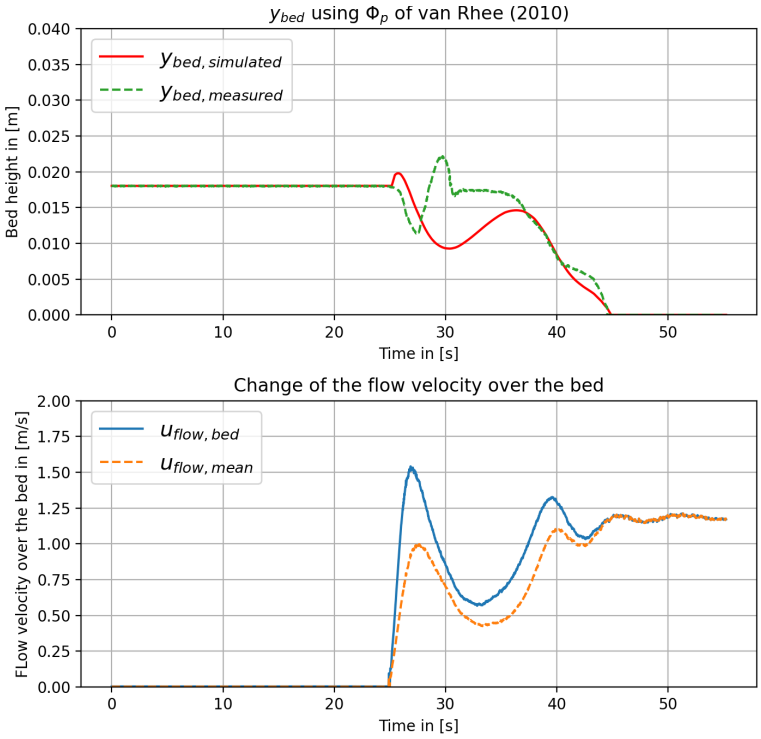

Figure F.56: Outcomes of simulation using the van Rhee (2010) pick-up function for Zilverzand with a mixture concentration of 30%

F.3.5 *GEBA*

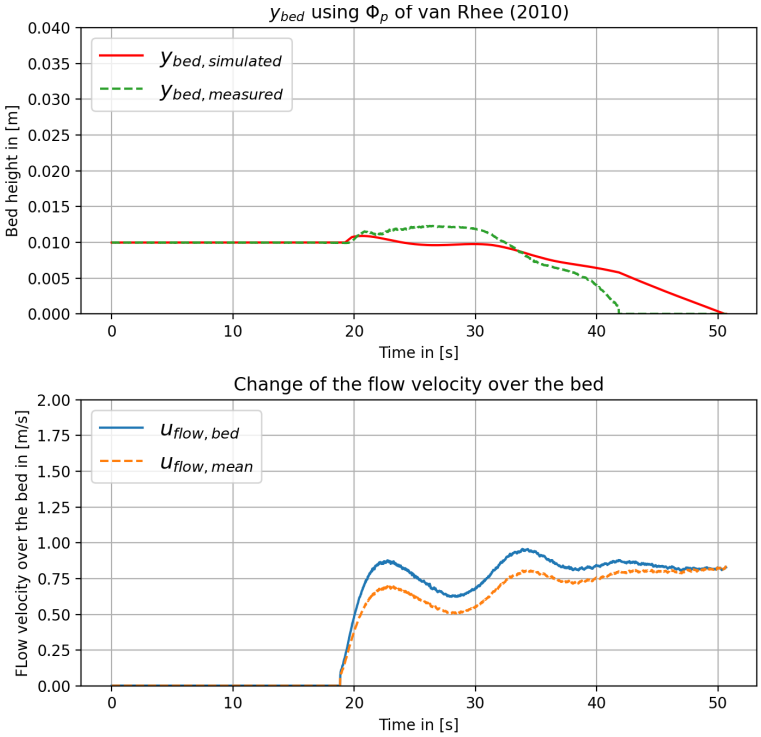

Figure F.57: Outcomes of simulation using the van Rhee (2010) pick-up function for GEBA with a mixture concentration of 5%

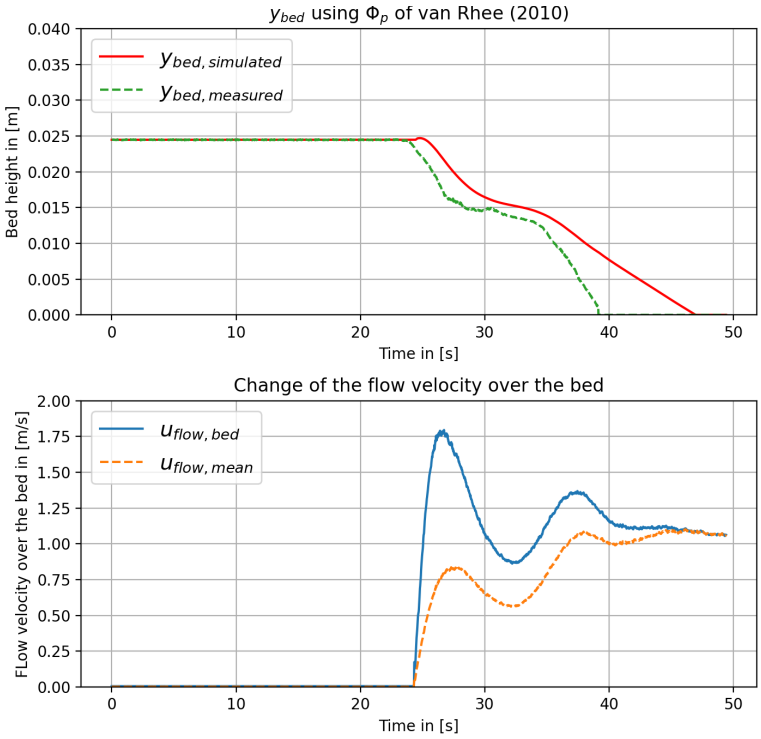

Figure F.58: Outcomes of simulation using the van Rhee (2010) pick-up function for GEBA with a mixture concentration of 10%

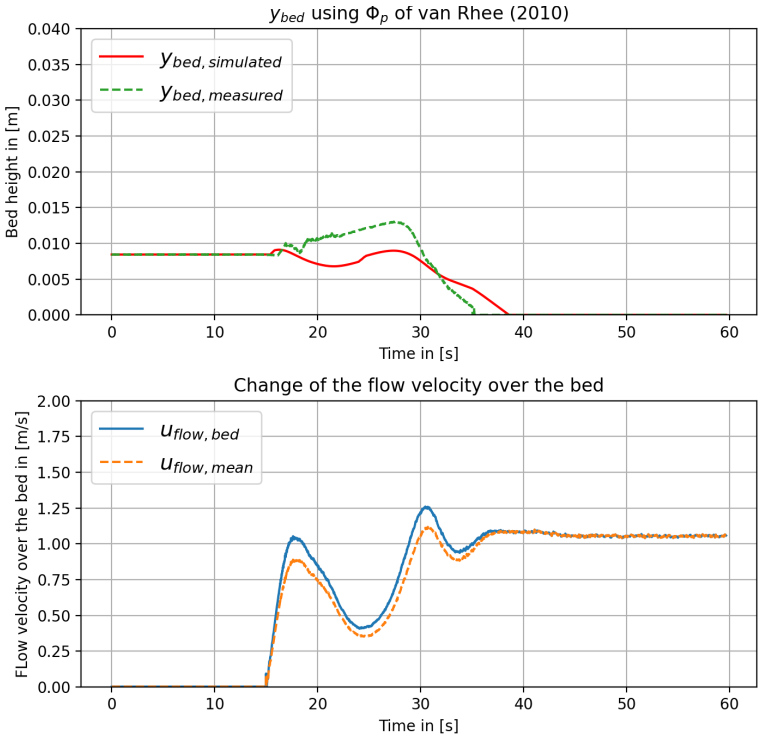

Figure F.59: Outcomes of simulation using the van Rhee (2010) pick-up function for GEBA with a mixture concentration of 20%

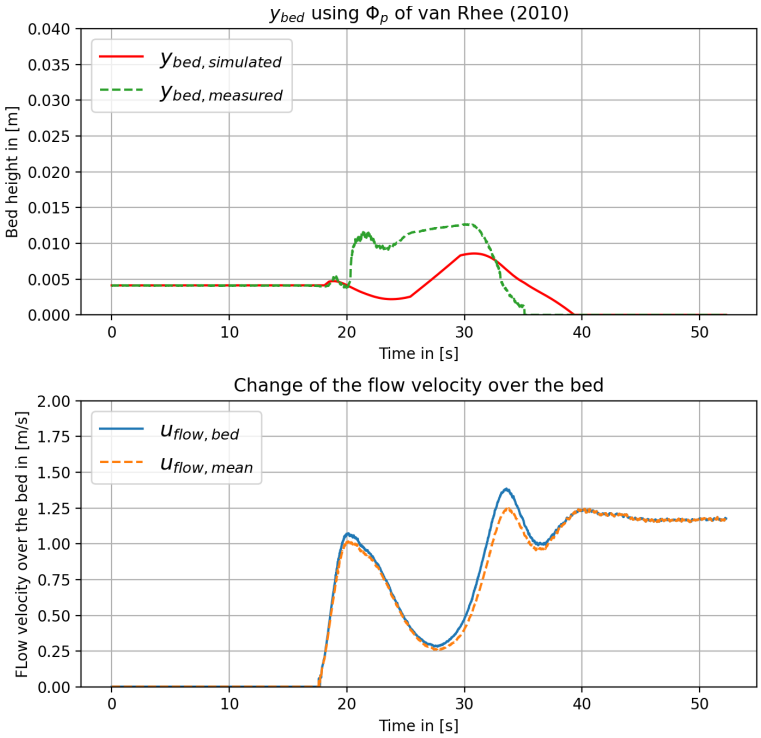

Figure F.60: Outcomes of simulation using the van Rhee (2010) pick-up function for GEBA with a mixture concentration of 30%

F.4 Pick-up Function of van Rhee and Talmon (2010)

F.4.1 *Dorsilit nr.5G*

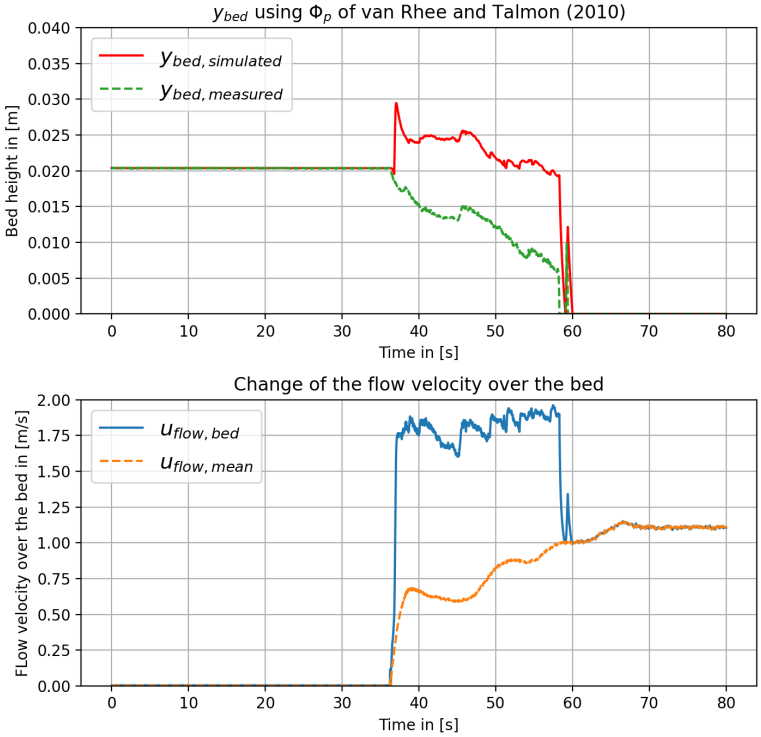

Figure F.61: Outcomes of simulation using the van Rhee and Talmon (2010) pick-up function for Dorsilit nr.5G with a mixture concentration of 5%

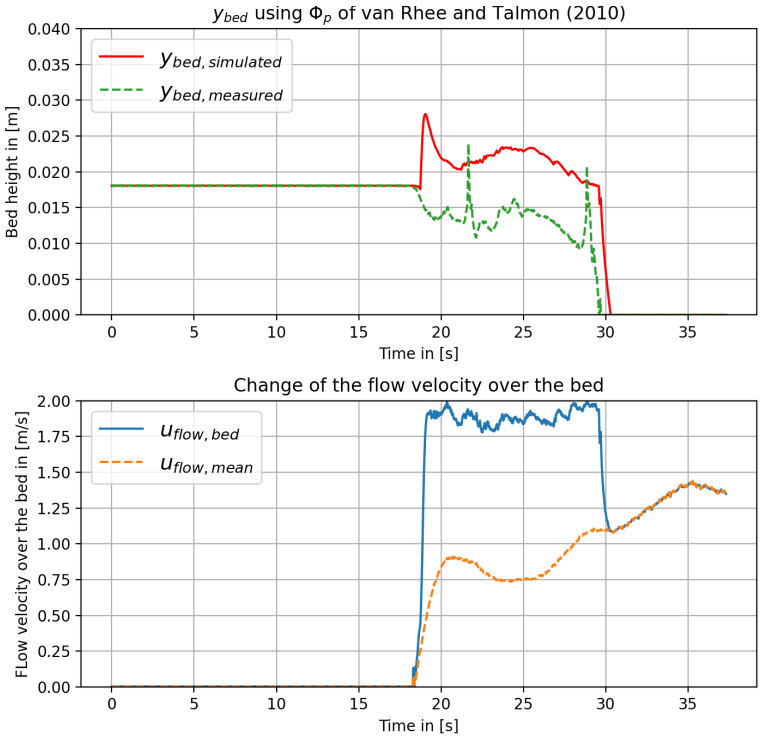

Figure F.62: Outcomes of simulation using the van Rhee and Talmon (2010) pick-up function for Dorsilit nr.5G with a mixture concentration of 10%

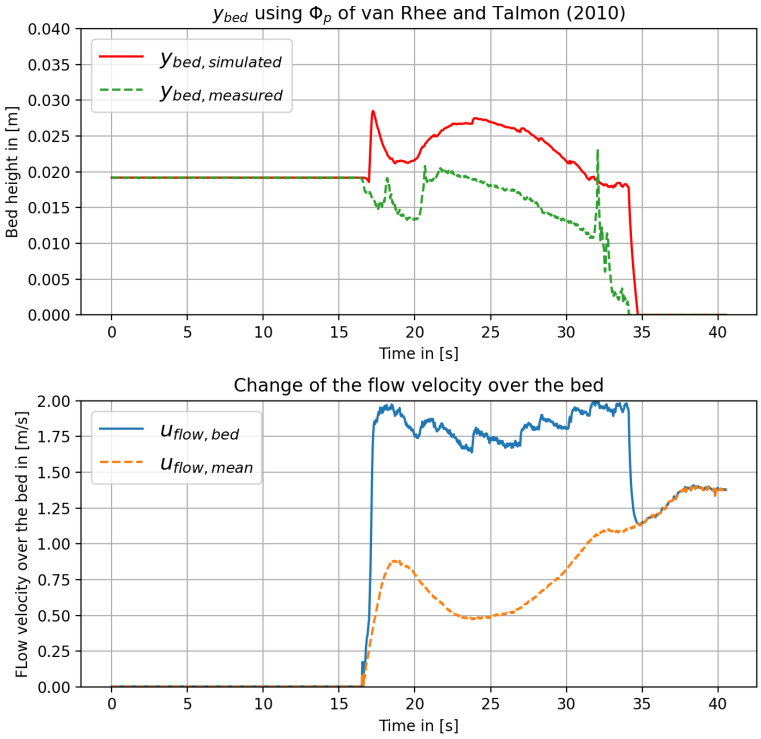

Figure F.63: Outcomes of simulation using the van Rhee and Talmon (2010) pick-up function for Dorsilit nr.5G with a mixture concentration of 20%

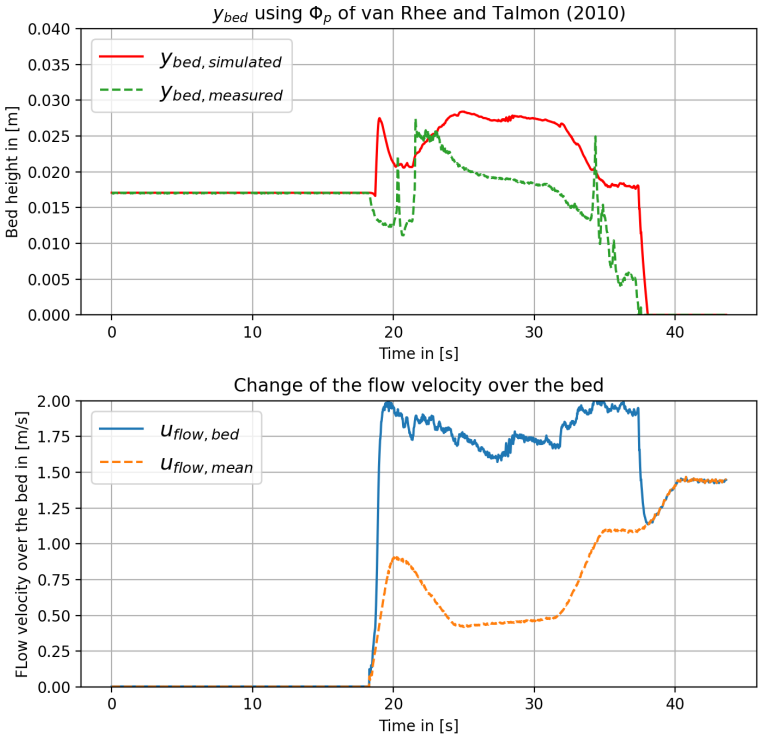

Figure F.64: Outcomes of simulation using the van Rhee and Talmon (2010) pick-up function for Dorsilit nr.5G with a mixture concentration of 30%

F.4.2 *Dorsilit nr.7*

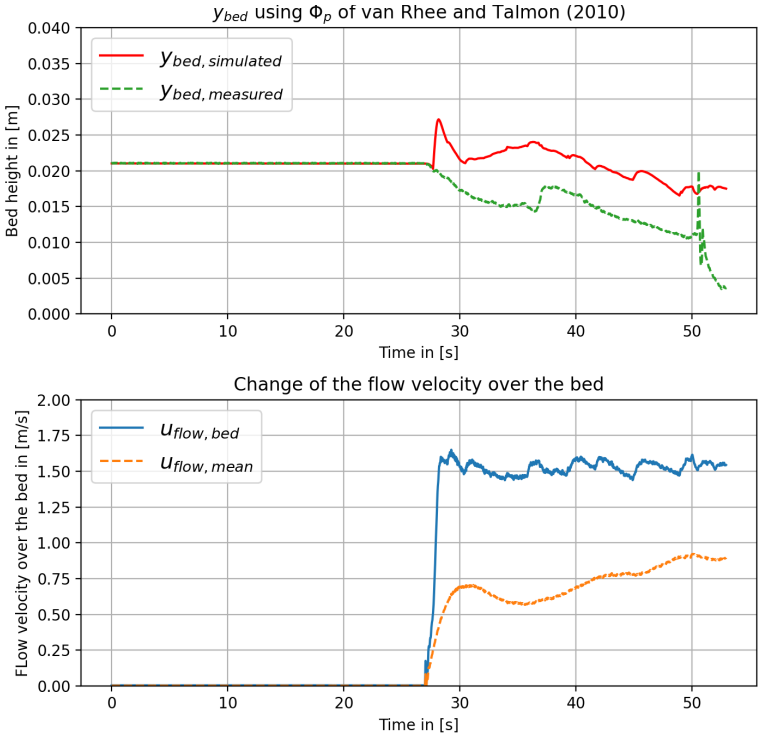

Figure F.65: Outcomes of simulation using the van Rhee and Talmon (2010) pick-up function for Dorsilit nr.7 with a mixture concentration of 5%

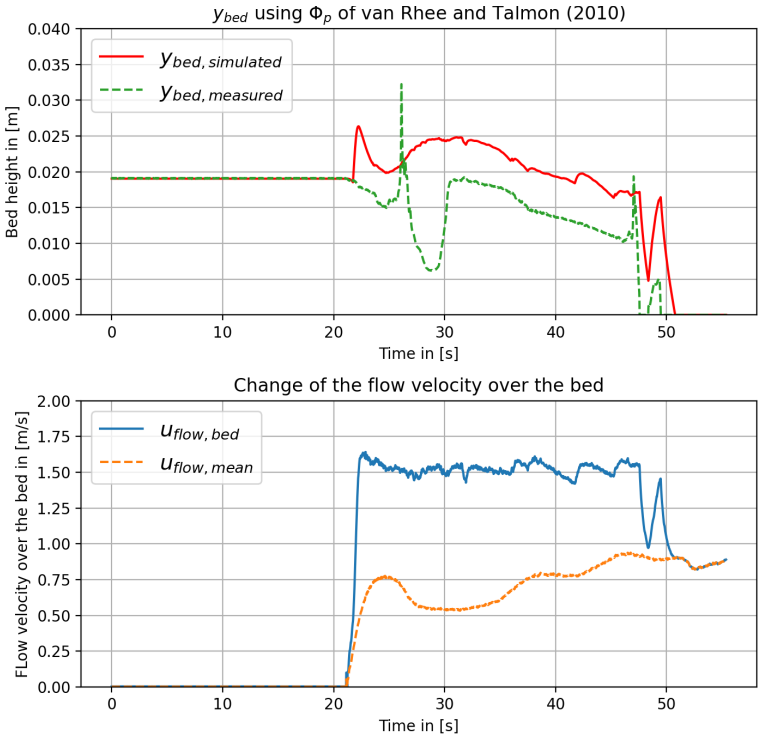

Figure F.66: Outcomes of simulation using the van Rhee and Talmon (2010) pick-up function for Dorsilit nr.7 with a mixture concentration of 10%

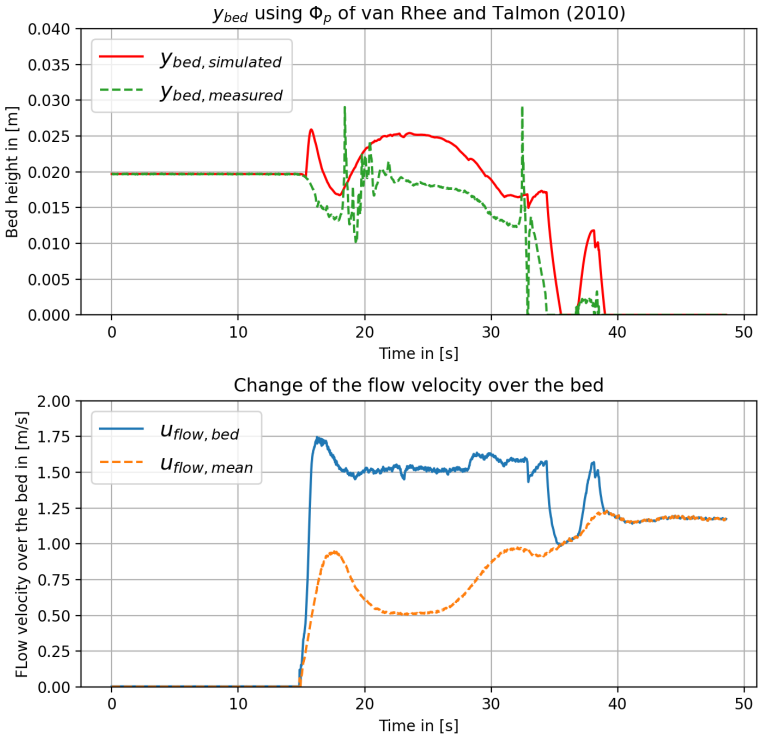

Figure F.67: Outcomes of simulation using the van Rhee and Talmon (2010) pick-up function for Dorsilit nr.7 with a mixture concentration of 20%

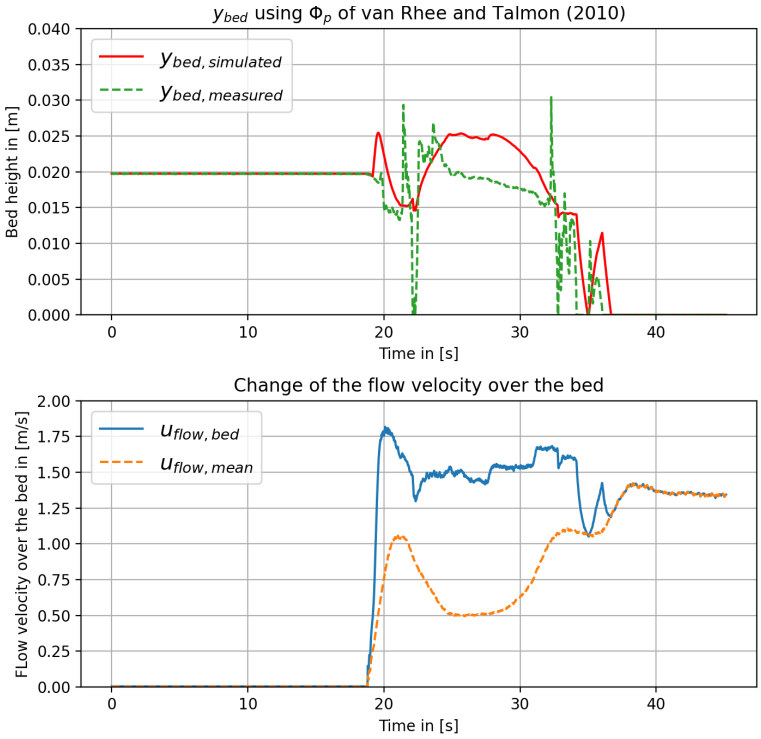

Figure F.68: Outcomes of simulation using the van Rhee and Talmon (2010) pick-up function for Dorsilit nr.7 with a mixture concentration of 30%

F.4.3 *Dorsilit nr.8*

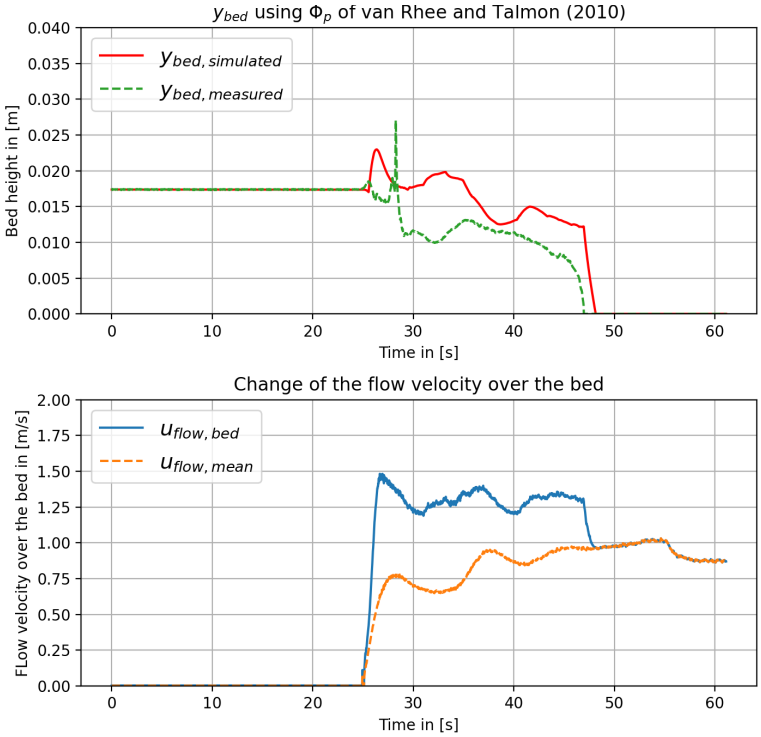

Figure F.69: Outcomes of simulation using the van Rhee and Talmon (2010) pick-up function for Dorsilit nr.8 with a mixture concentration of 5%

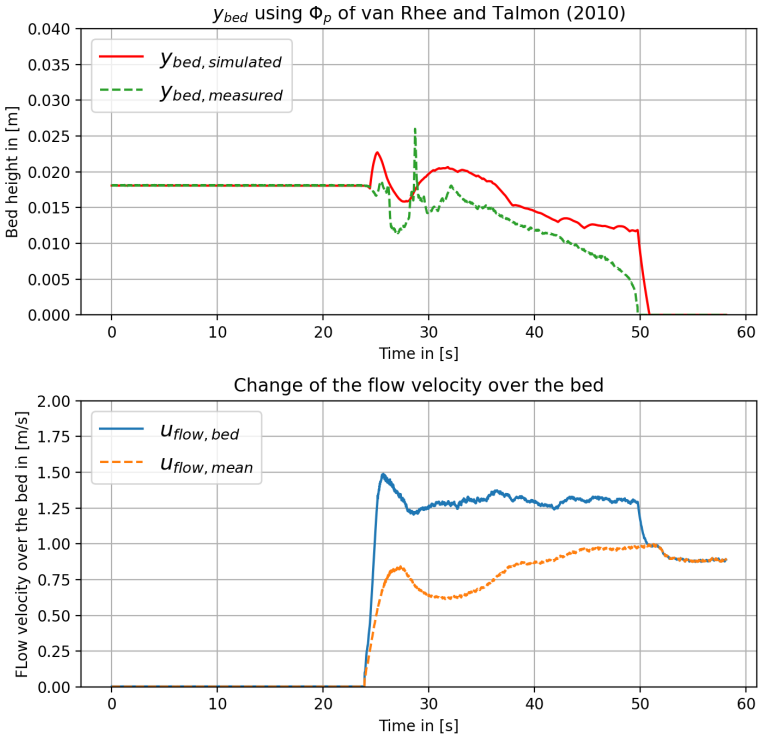

Figure F.70: Outcomes of simulation using the van Rhee and Talmon (2010) pick-up function for Dorsilit nr.8 with a mixture concentration of 10%

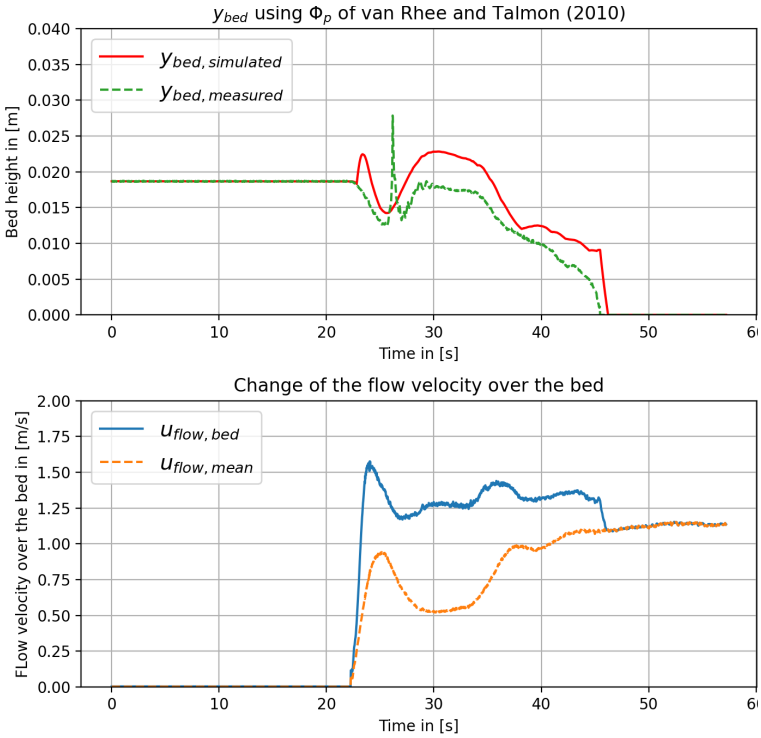

Figure F.71: Outcomes of simulation using the van Rhee and Talmon (2010) pick-up function for Dorsilit nr.8 with a mixture concentration of 20%

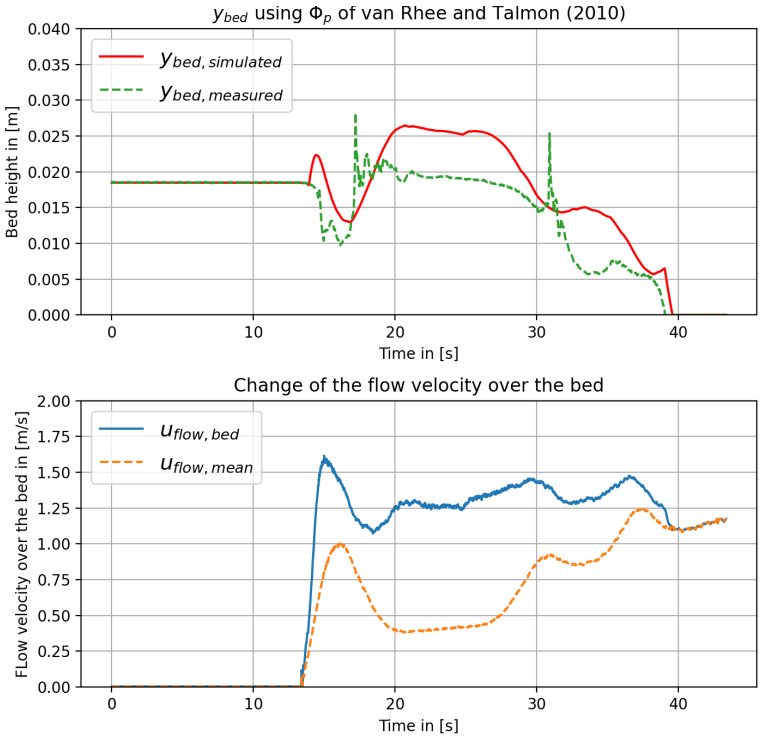

Figure F.72: Outcomes of simulation using the van Rhee and Talmon (2010) pick-up function for Dorsilit nr.8 with a mixture concentration of 30%

F.4.4 *Zilverzand*

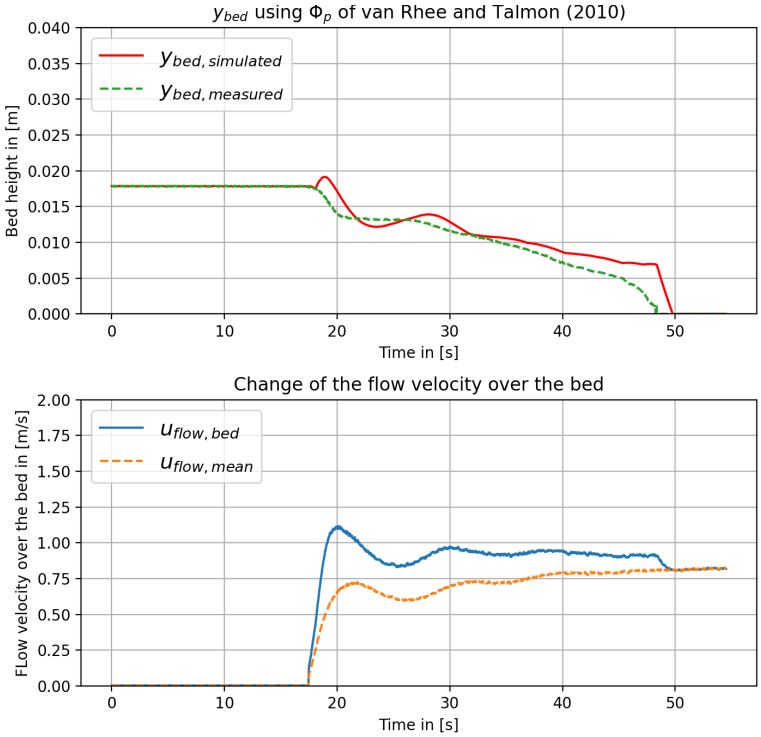

Figure F.73: Outcomes of simulation using the van Rhee and Talmon (2010) pick-up function for Zilverzand with a mixture concentration of 5%

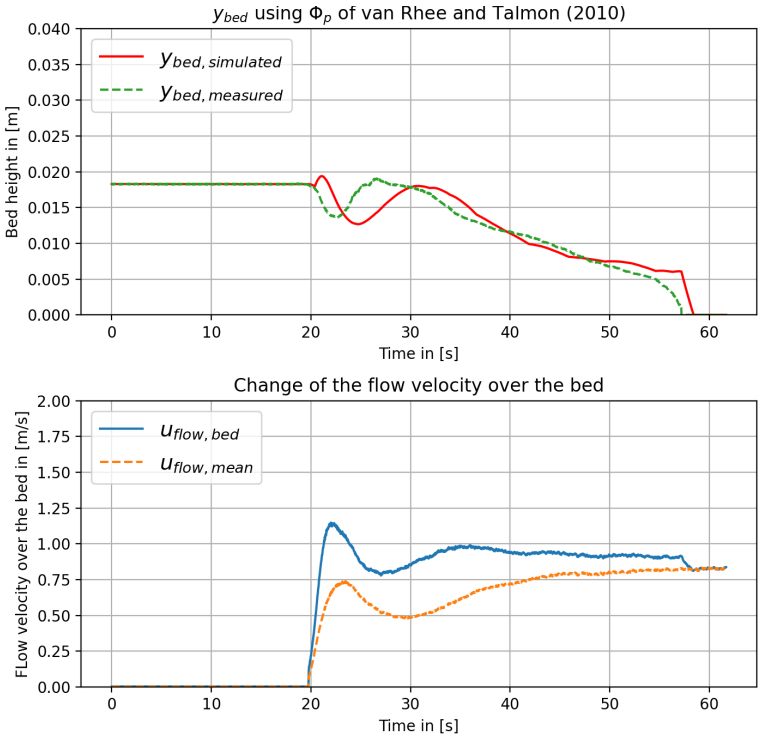

Figure F.74: Outcomes of simulation using the van Rhee and Talmon (2010) pick-up function for Zilverzand with a mixture concentration of 10%

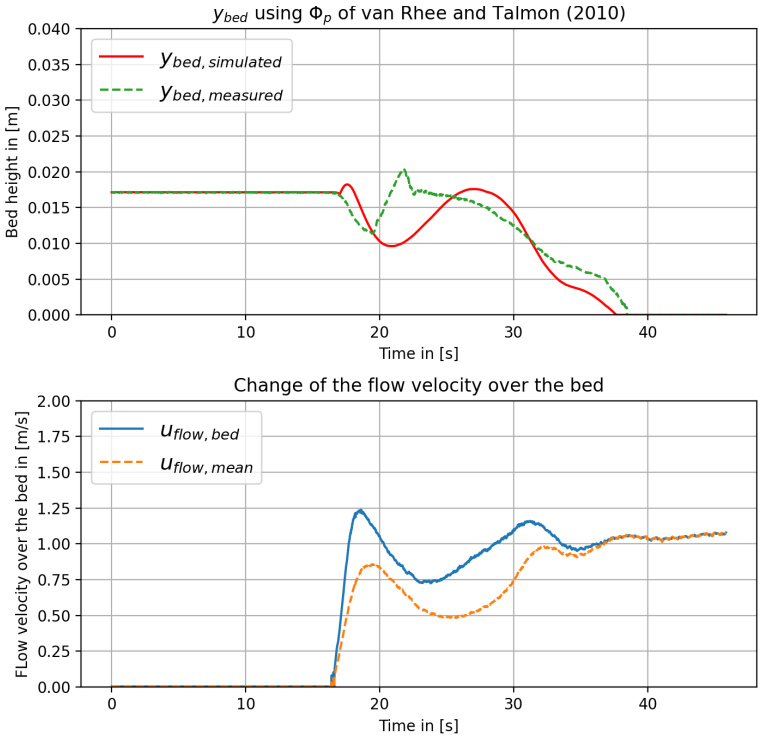

Figure F.75: Outcomes of simulation using the van Rhee and Talmon (2010) pick-up function for Zilverzand with a mixture concentration of 20%

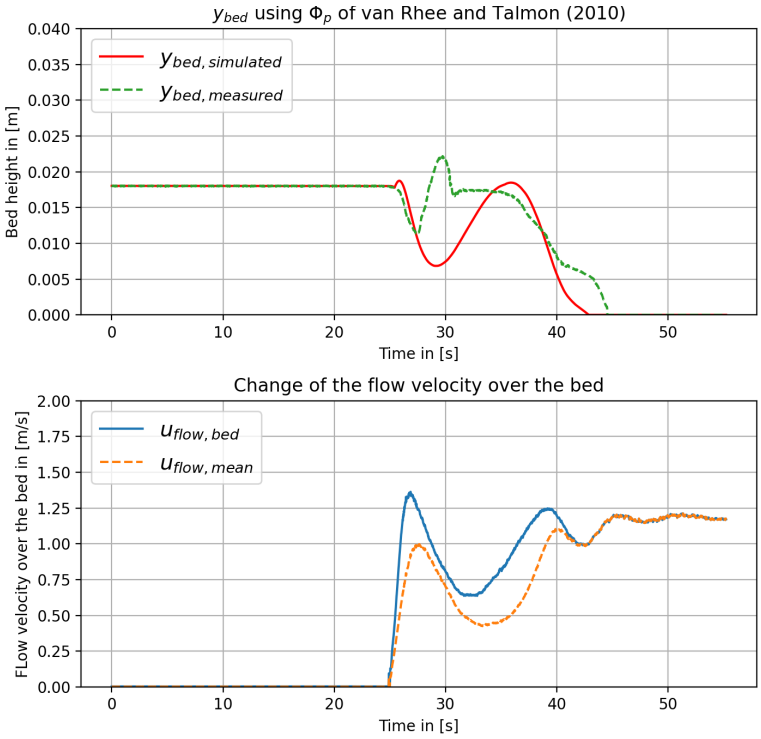

Figure F.76: Outcomes of simulation using the van Rhee and Talmon (2010) pick-up function for Zilverzand with a mixture concentration of 30%

F.4.5 *GEBA*

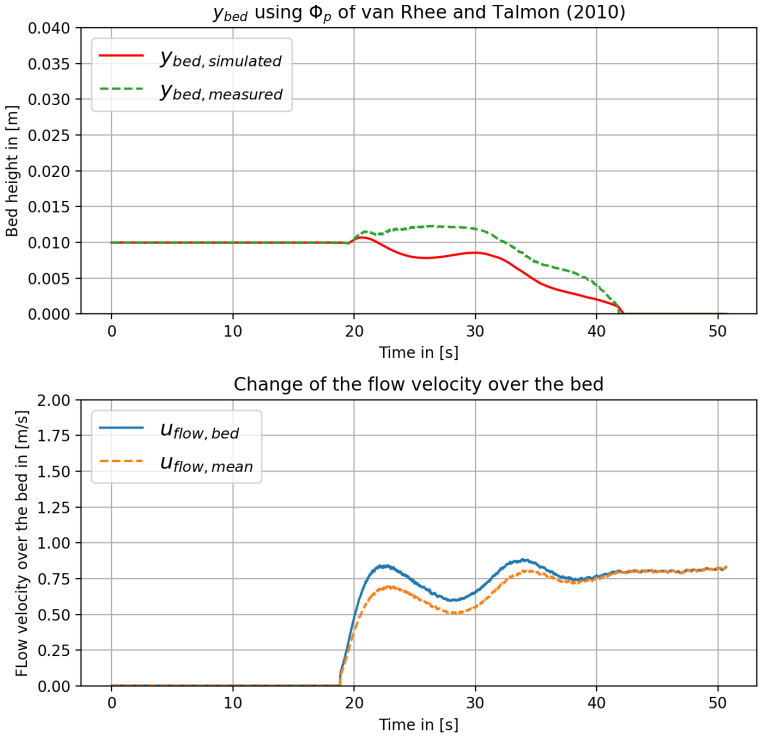

Figure F.77: Outcomes of simulation using the van Rhee and Talmon (2010) pick-up function for GEBA with a mixture concentration of 5%

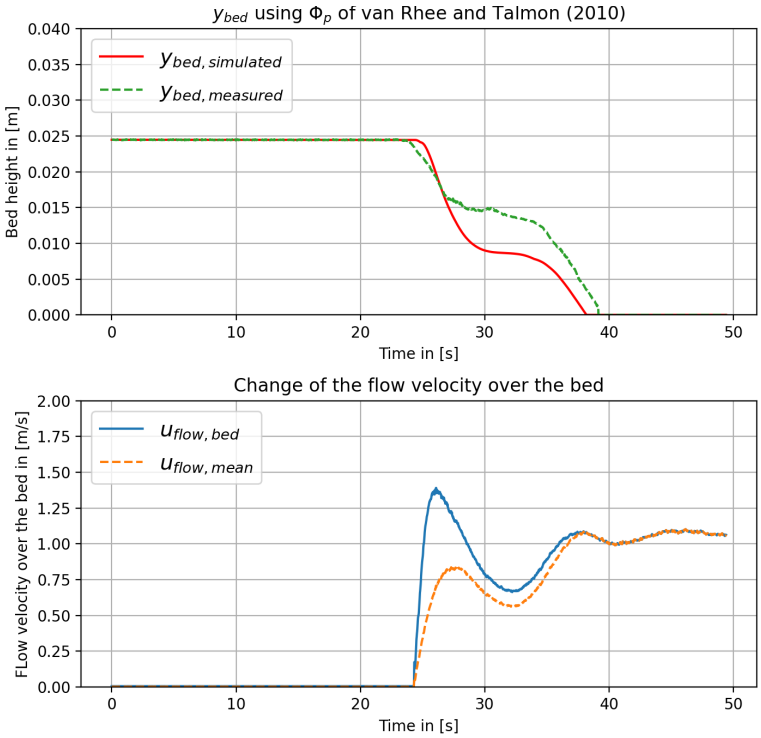

Figure F.78: Outcomes of simulation using the van Rhee and Talmon (2010) pick-up function for GEBA with a mixture concentration of 10%

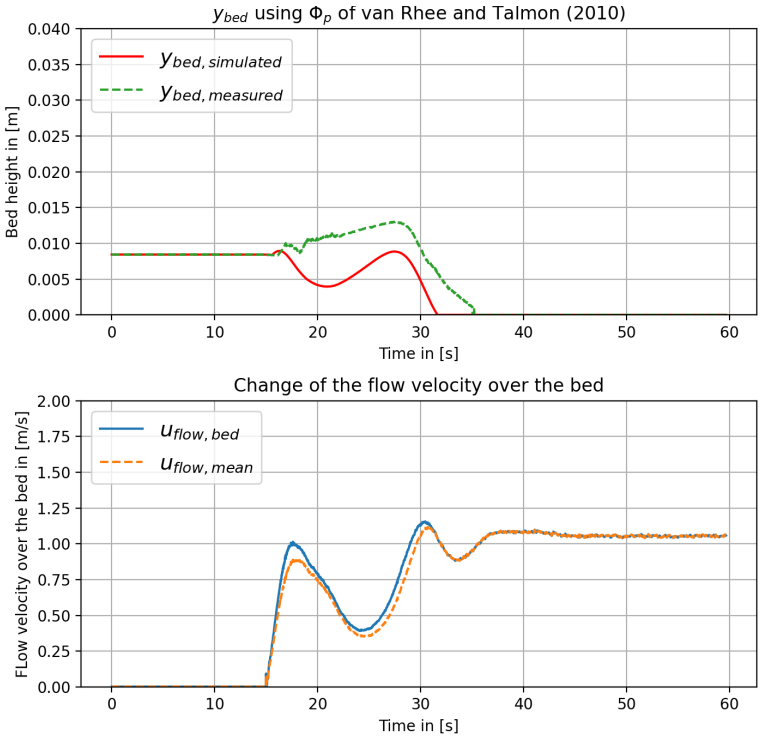

Figure F.79: Outcomes of simulation using the van Rhee and Talmon (2010) pick-up function for GEBA with a mixture concentration of 20%

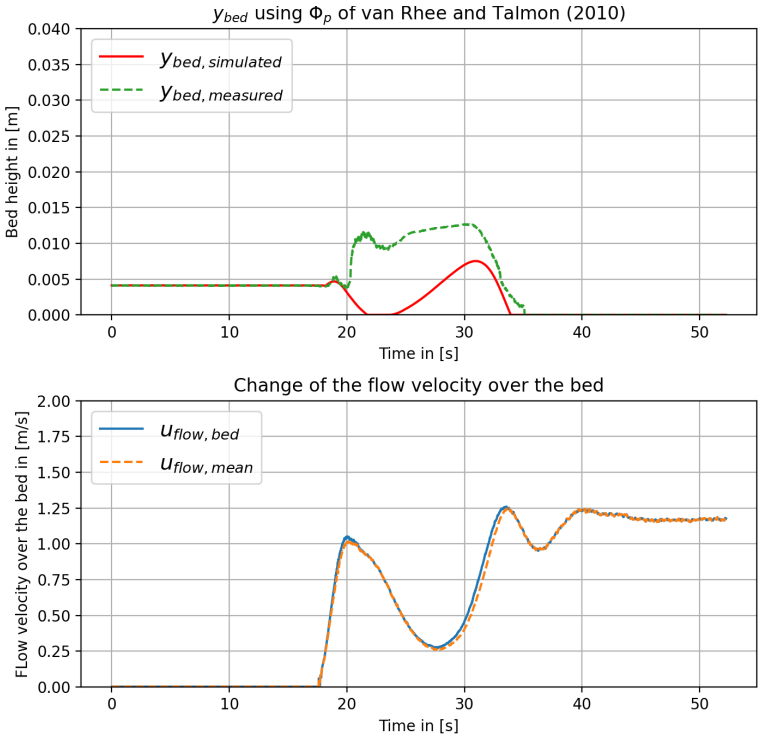

Figure F.80: Outcomes of simulation using the van Rhee and Talmon (2010) pick-up function for GEBA with a mixture concentration of 30%

F.5 Pick-up Function of Bisschop (2018)

F.5.1 *Dorsilit nr.5G*

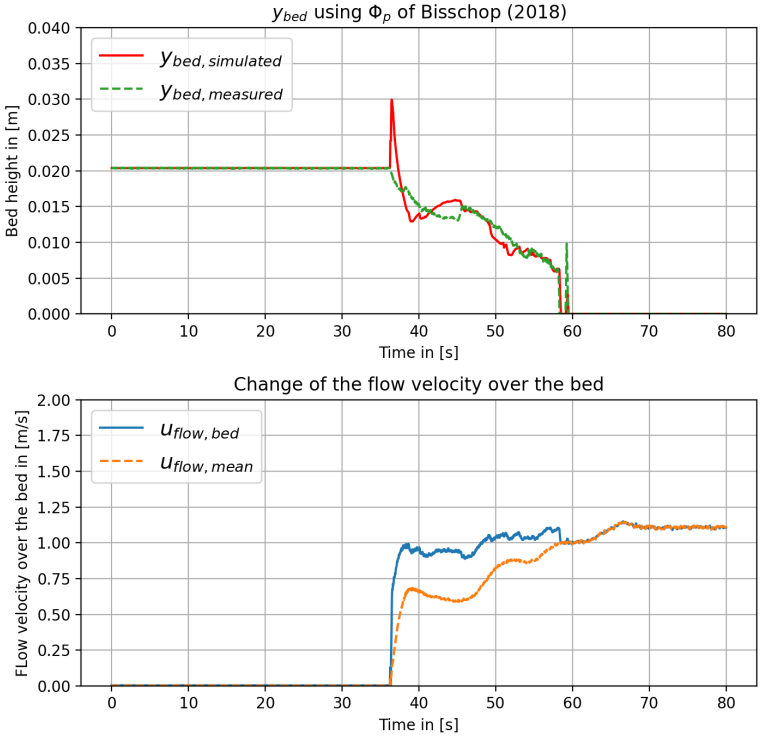

Figure F.81: Outcomes of simulation using the Bisschop (2018) pick-up function for Dorsilit nr.5G with a mixture concentration of 5%

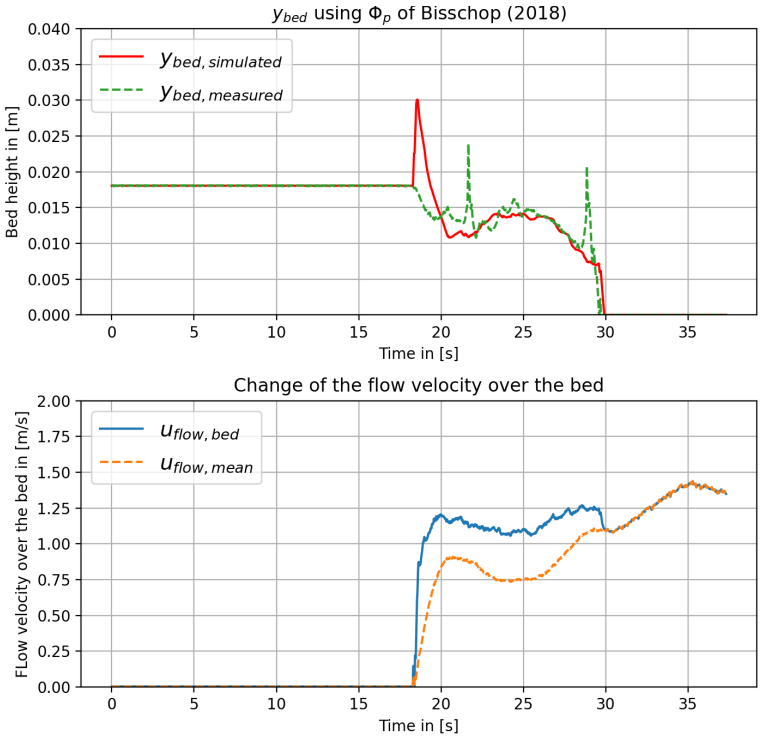

Figure F.82: Outcomes of simulation using the Bisschop (2018) pick-up function for Dorsilit nr.5G with a mixture concentration of 10%

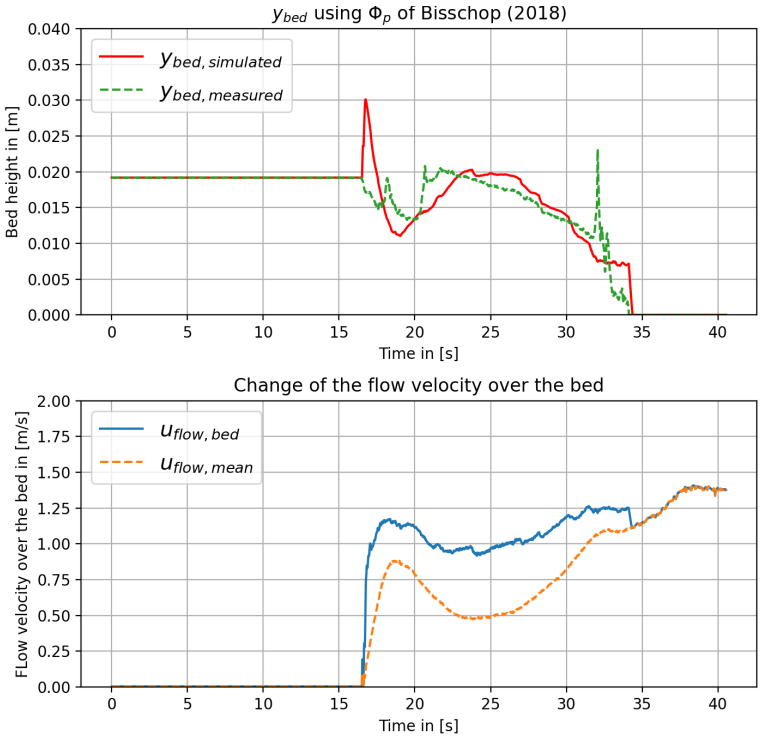

Figure F.83: Outcomes of simulation using the Bisschop (2018) pick-up function for Dorsilit nr.5G with a mixture concentration of 20%

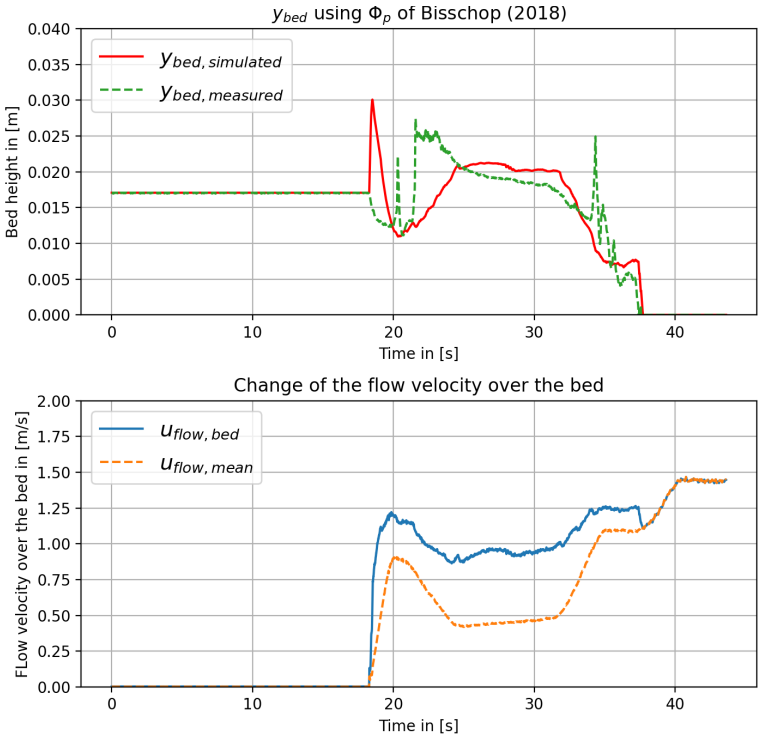

Figure F.84: Outcomes of simulation using the Bisschop (2018) pick-up function for Dorsilit nr.5G with a mixture concentration of 30%

F.5.2 *Dorsilit nr.7*

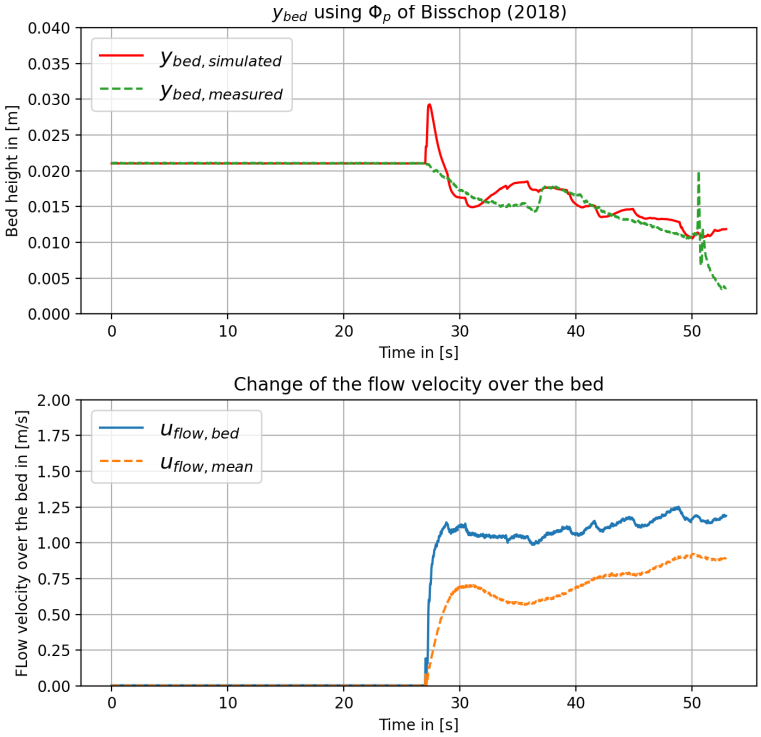

Figure F.85: Outcomes of simulation using the Bisschop (2018) pick-up function for Dorsilit nr.7 with a mixture concentration of 5%

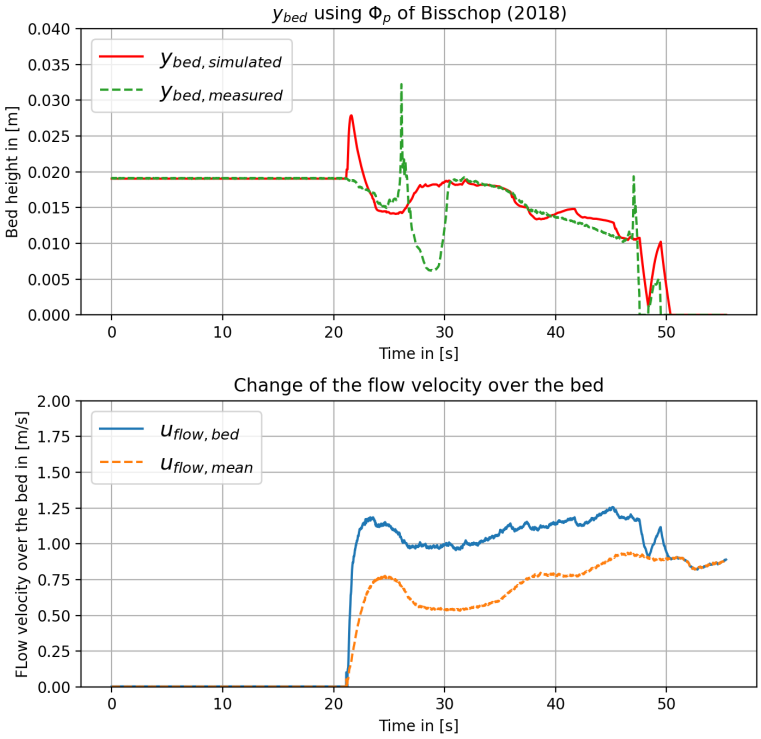

Figure F.86: Outcomes of simulation using the Bisschop (2018) pick-up function for Dorsilit nr.7 with a mixture concentration of 10%

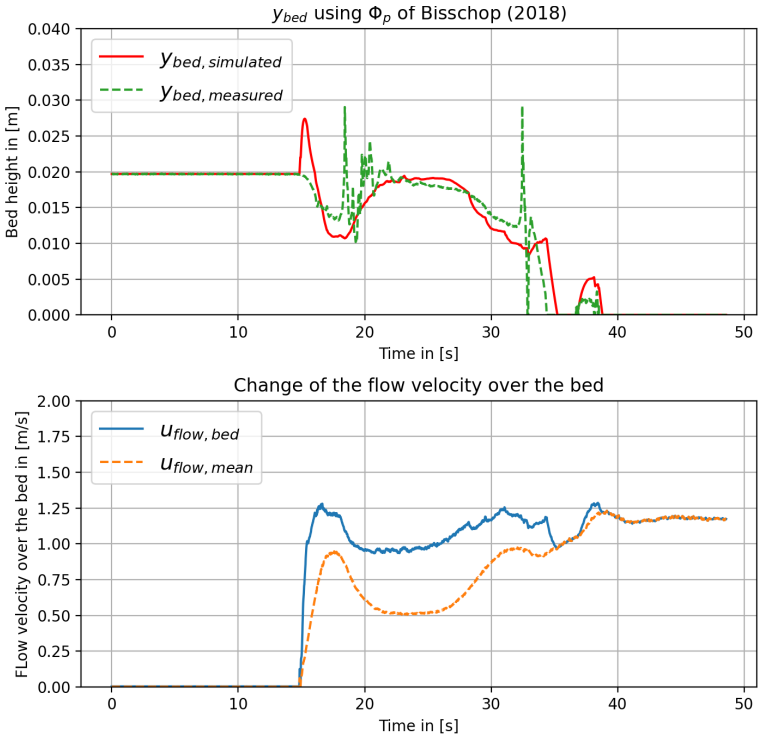

Figure F.87: Outcomes of simulation using the Bisschop (2018) pick-up function for Dorsilit nr.7 with a mixture concentration of 20%

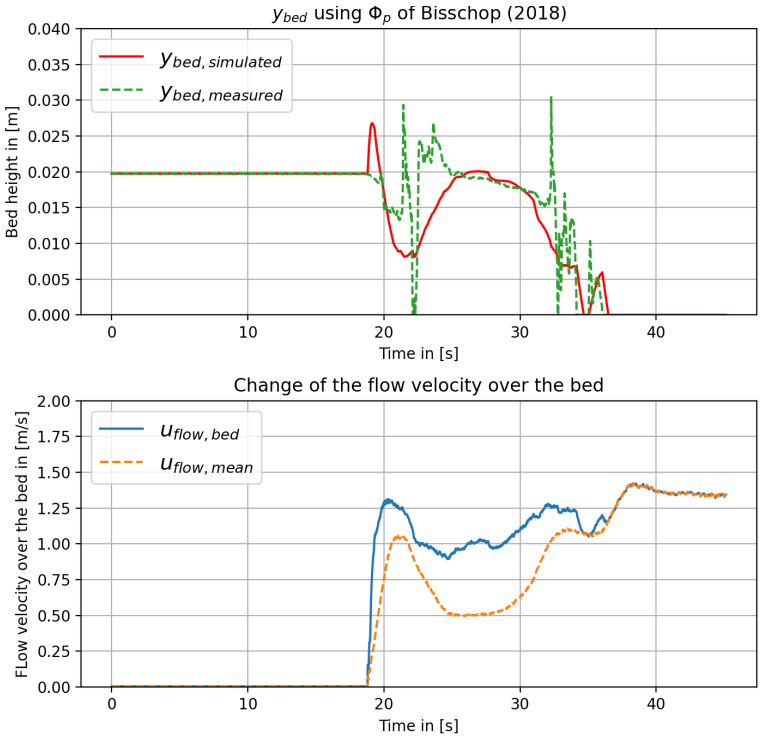

Figure F.88: Outcomes of simulation using the Bisschop (2018) pick-up function for Dorsilit nr.7 with a mixture concentration of 30%

F.5.3 *Dorsilit nr.8*

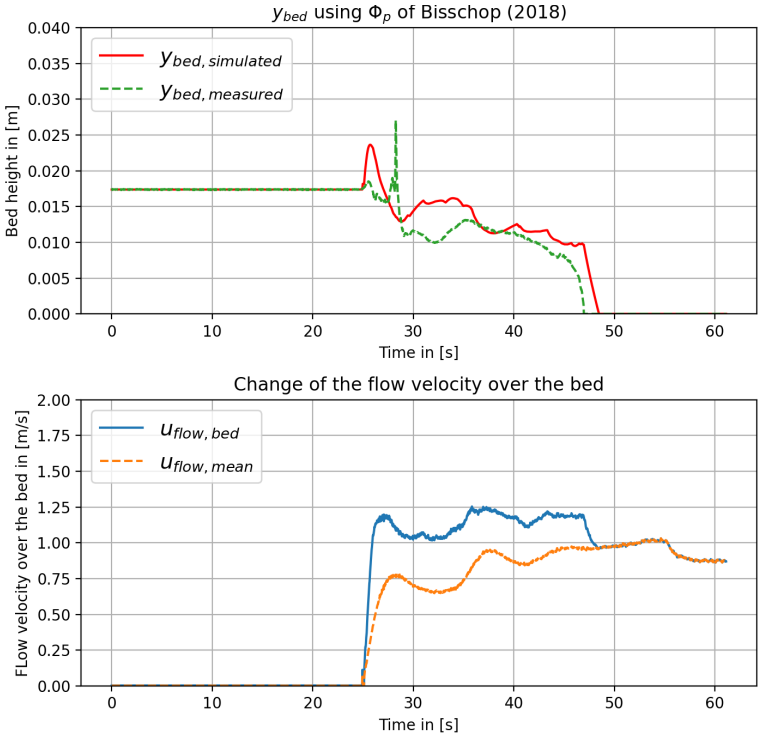

Figure F.89: Outcomes of simulation using the Bisschop (2018) pick-up function for Dorsilit nr.8 with a mixture concentration of 5%

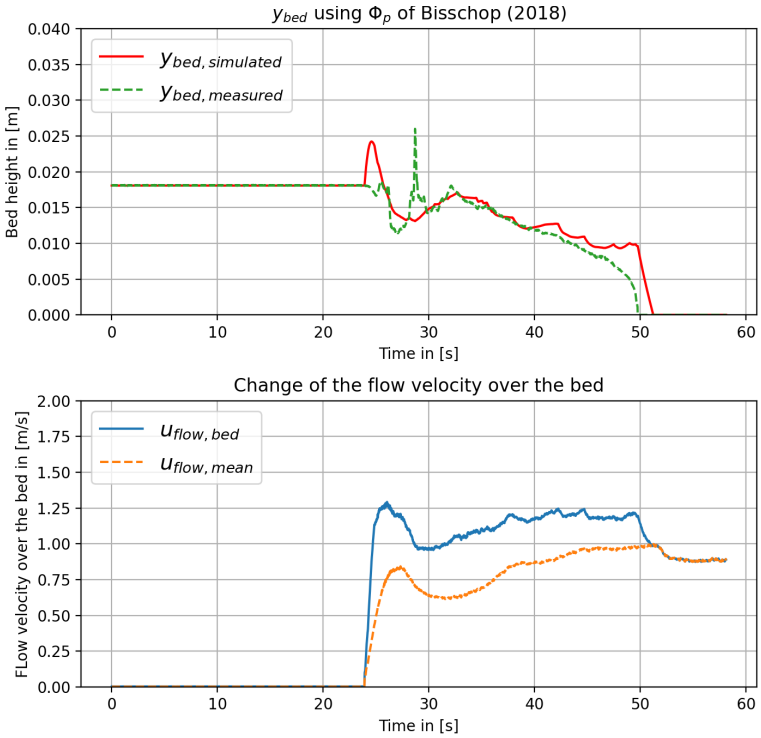

Figure F.90: Outcomes of simulation using the Bisschop (2018) pick-up function for Dorsilit nr.8 with a mixture concentration of 10%

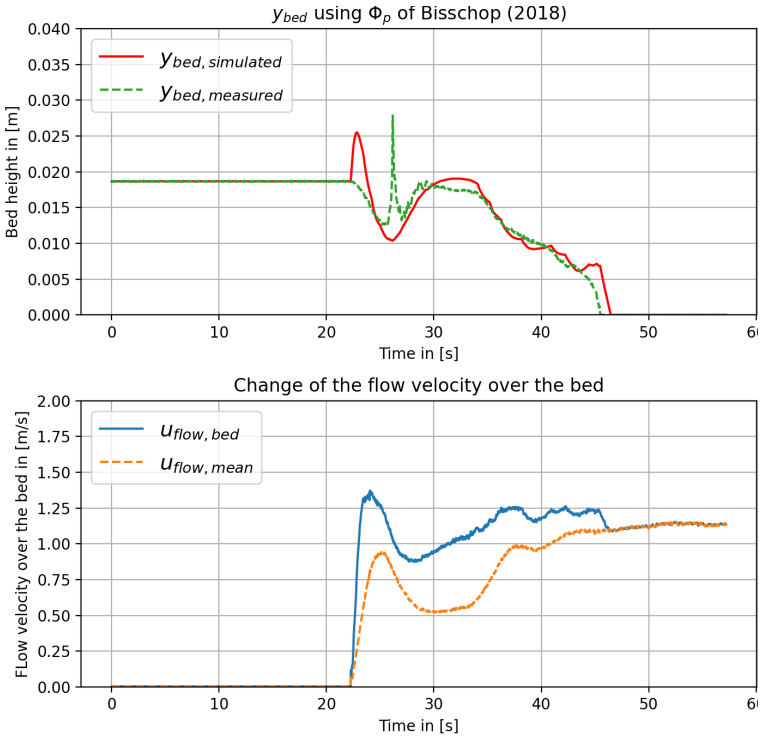

Figure F.91: Outcomes of simulation using the Bisschop (2018) pick-up function for Dorsilit nr.8 with a mixture concentration of 20%

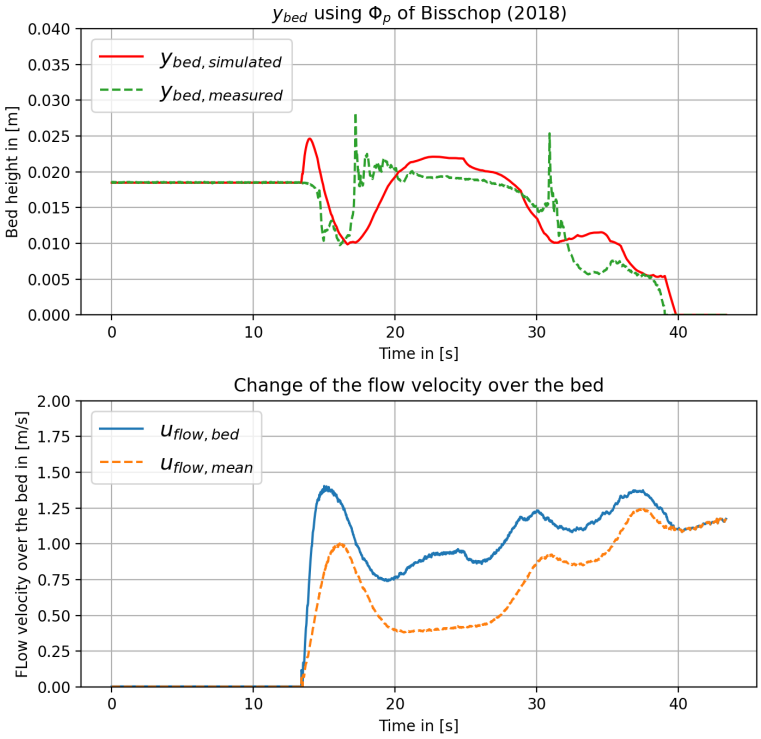

Figure F.92: Outcomes of simulation using the Bisschop (2018) pick-up function for Dorsilit nr.8 with a mixture concentration of 30%

F.5.4 *Zilverzand*

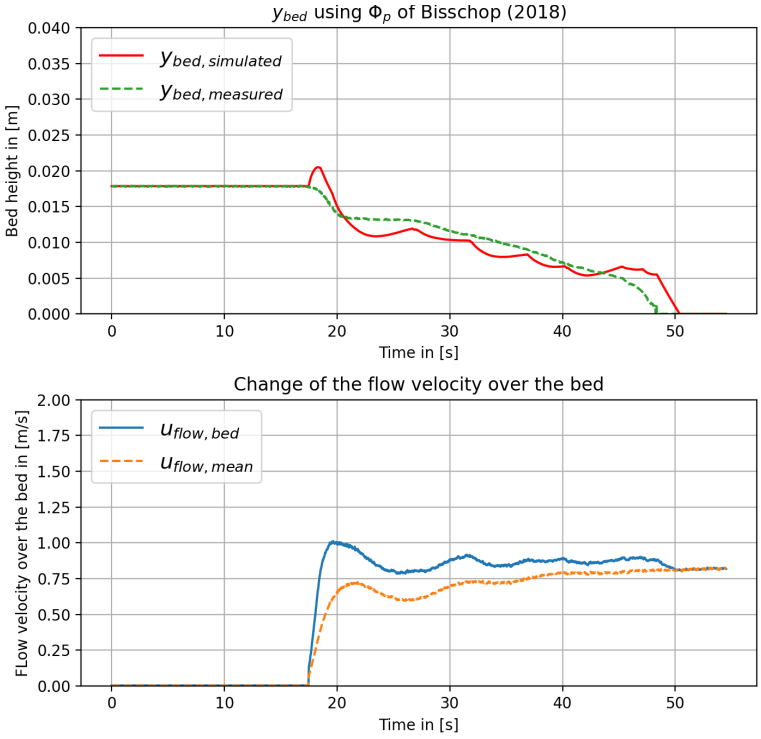

Figure F.93: Outcomes of simulation using the Bisschop (2018) pick-up function for Zilverzand with a mixture concentration of 5%

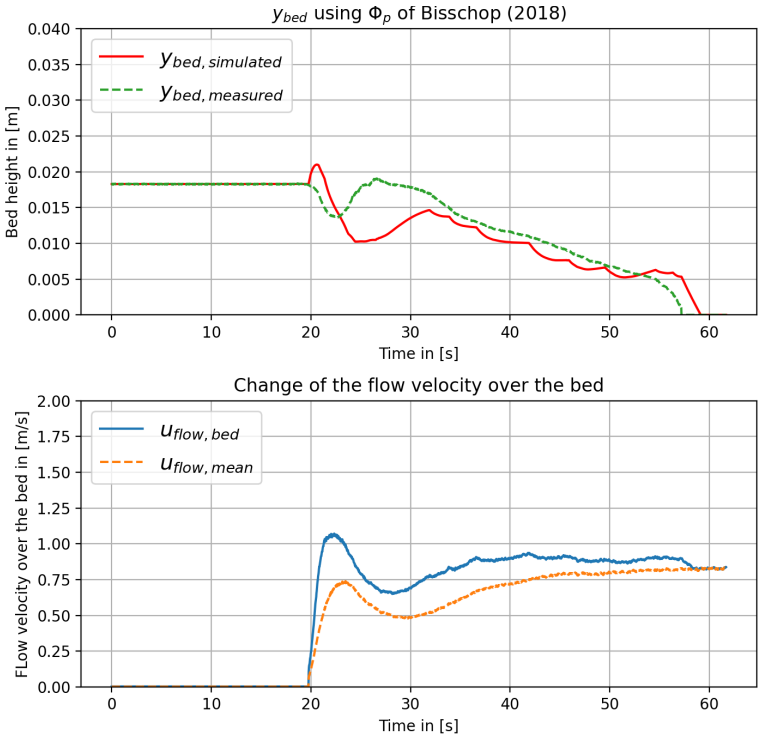

Figure F.94: Outcomes of simulation using the Bisschop (2018) pick-up function for Zilverzand with a mixture concentration of 10%

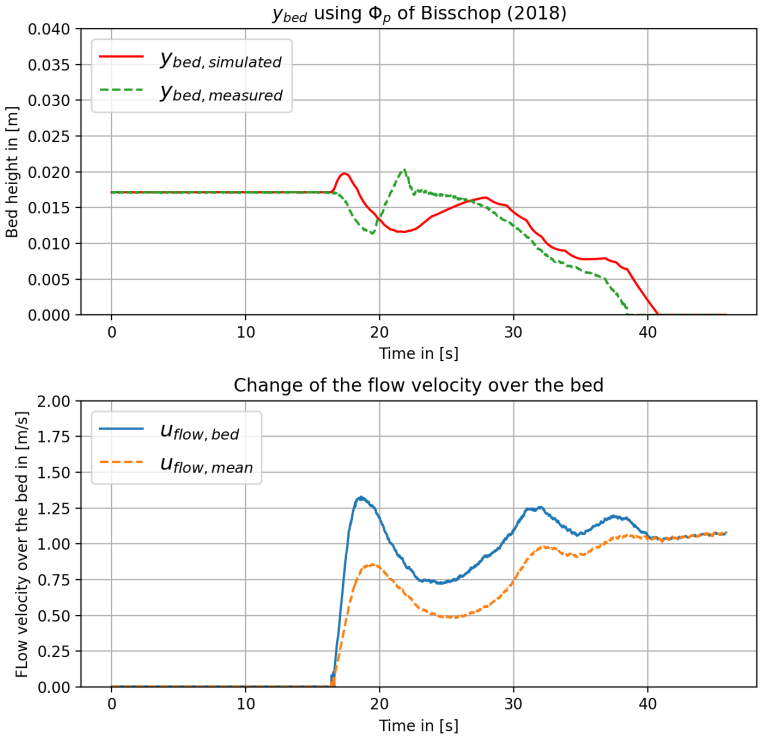

Figure F.95: Outcomes of simulation using the Bisschop (2018) pick-up function for Zilverzand with a mixture concentration of 20%

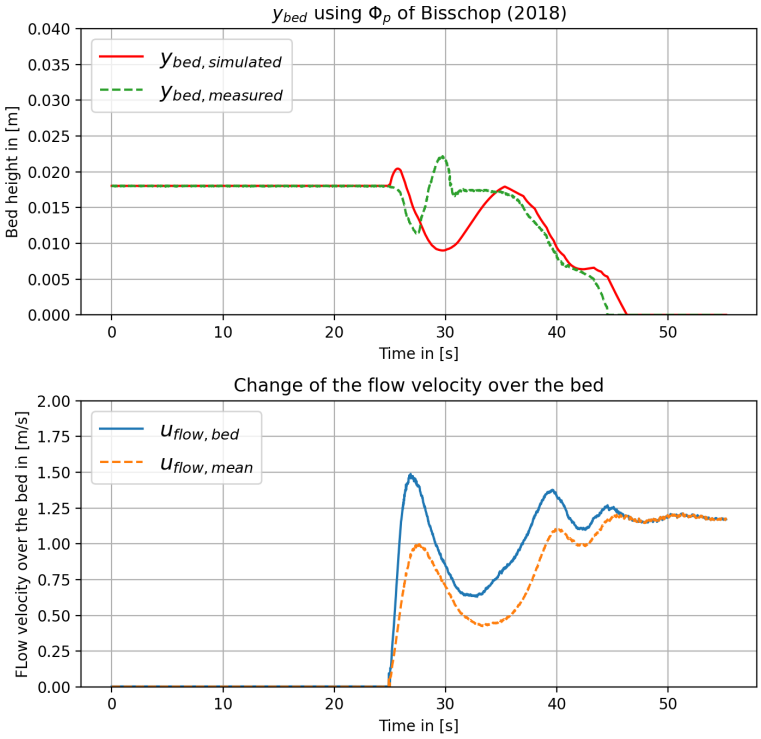

Figure F.96: Outcomes of simulation using the Bisschop (2018) pick-up function for Zilverzand with a mixture concentration of 30%

F.5.5 *GEBA*

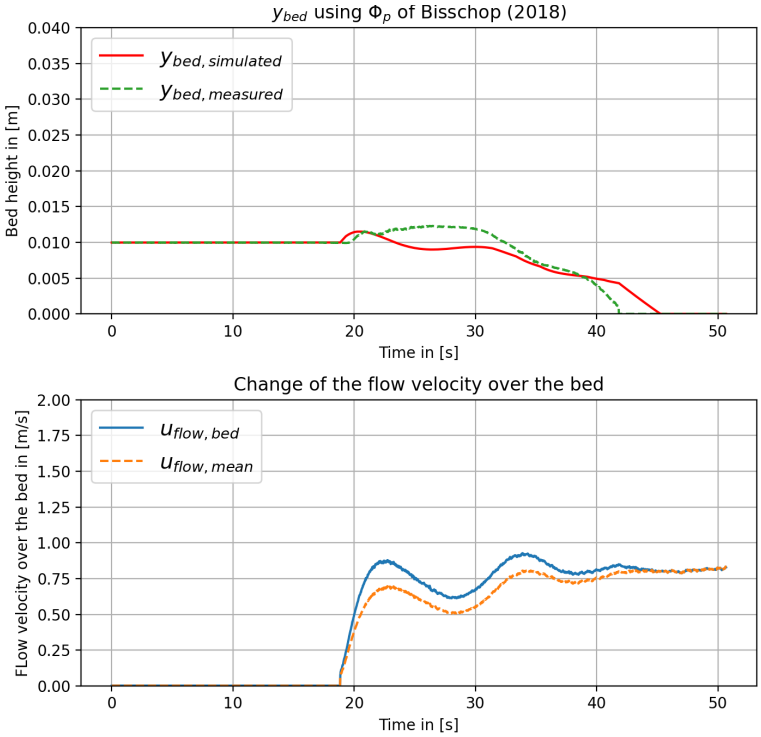

Figure F.97: Outcomes of simulation using the Bisschop (2018) pick-up function for GEBA with a mixture concentration of 5%

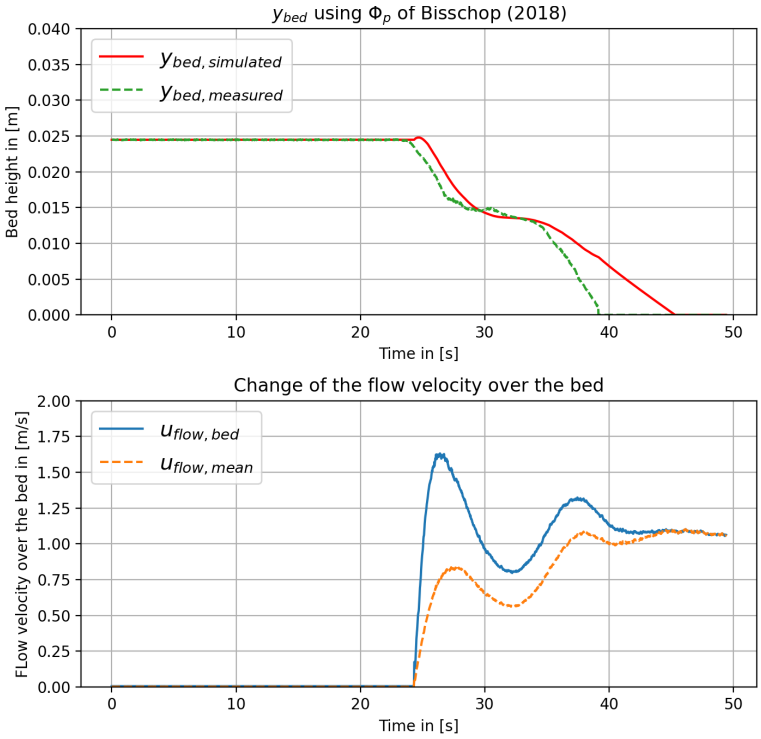

Figure F.98: Outcomes of simulation using the Bisschop (2018) pick-up function for GEBA with a mixture concentration of 10%

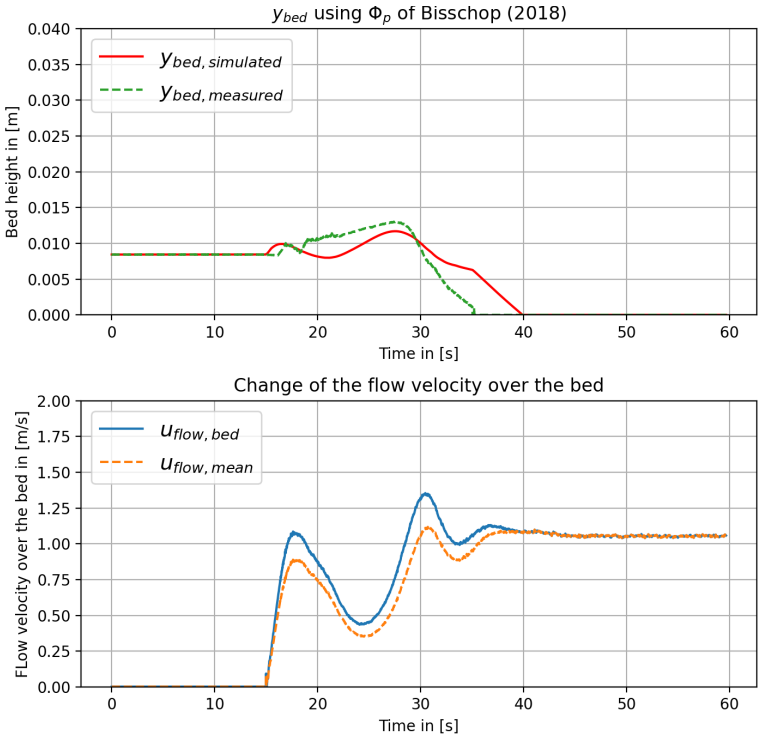

Figure F.99: Outcomes of simulation using the Bisschop (2018) pick-up function for GEBA with a mixture concentration of 20%

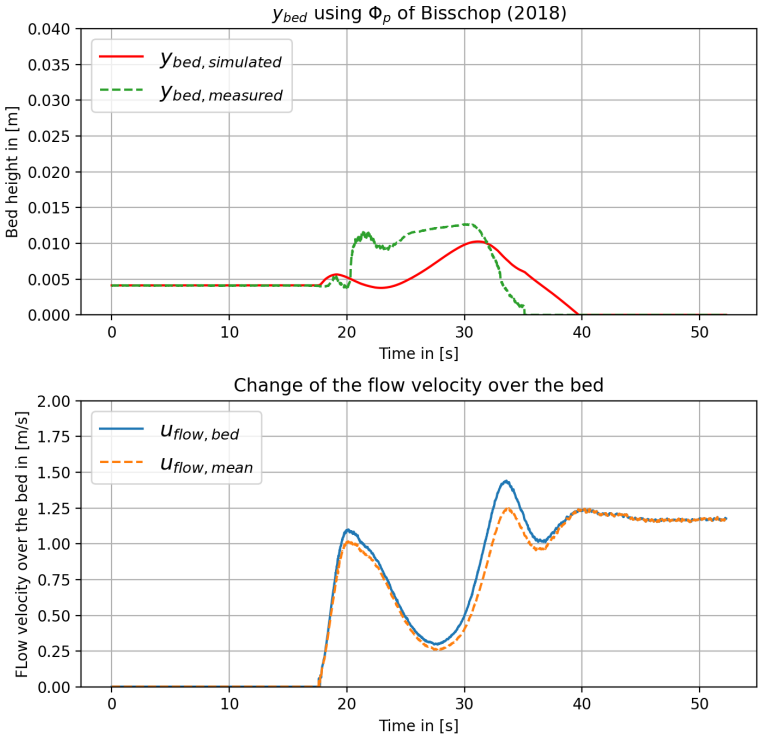

Figure F.100: Outcomes of simulation using the Bisschop (2018) pick-up function for GEBA with a mixture concentration of 30%

F.6 Pick-up Function of van Rijn (2019)

F.6.1 *Dorsilit nr.5G*

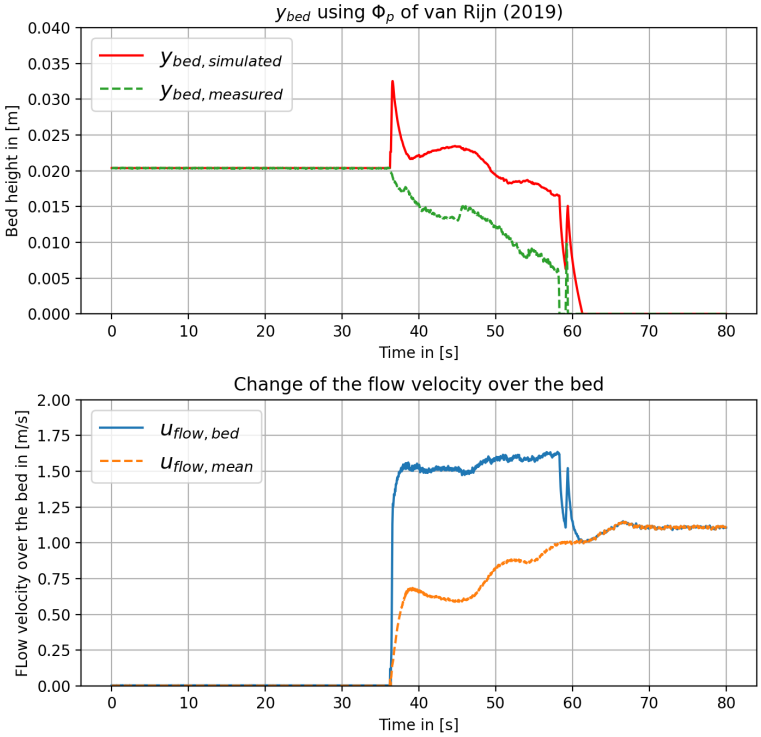

Figure F.101: Outcomes of simulation using the van Rijn et al. (2019) pick-up function for Dorsilit nr.5G with a mixture concentration of 5%

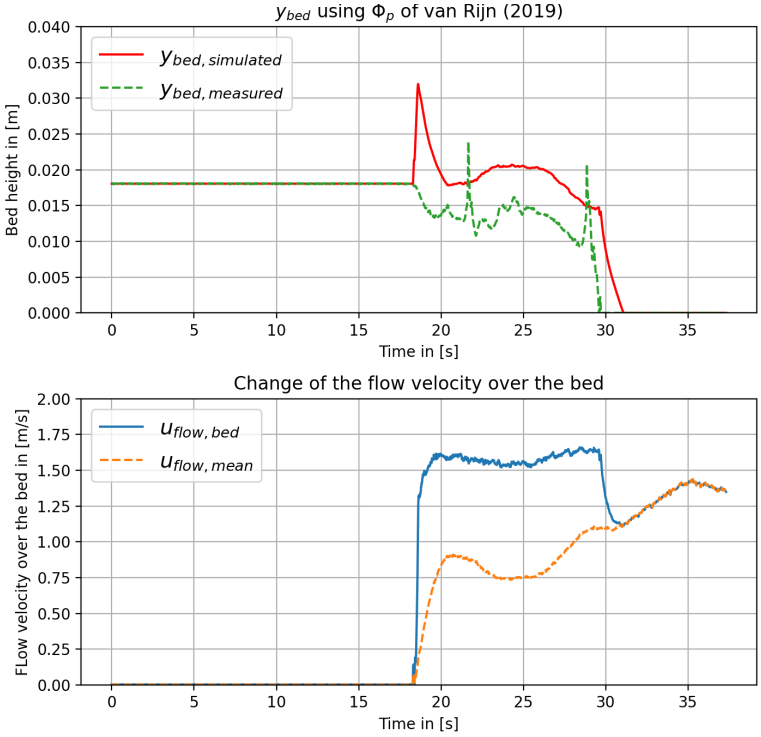

Figure F.102: Outcomes of simulation using the van Rijn et al. (2019) pick-up function for Dorsilit nr.5G with a mixture concentration of 10%

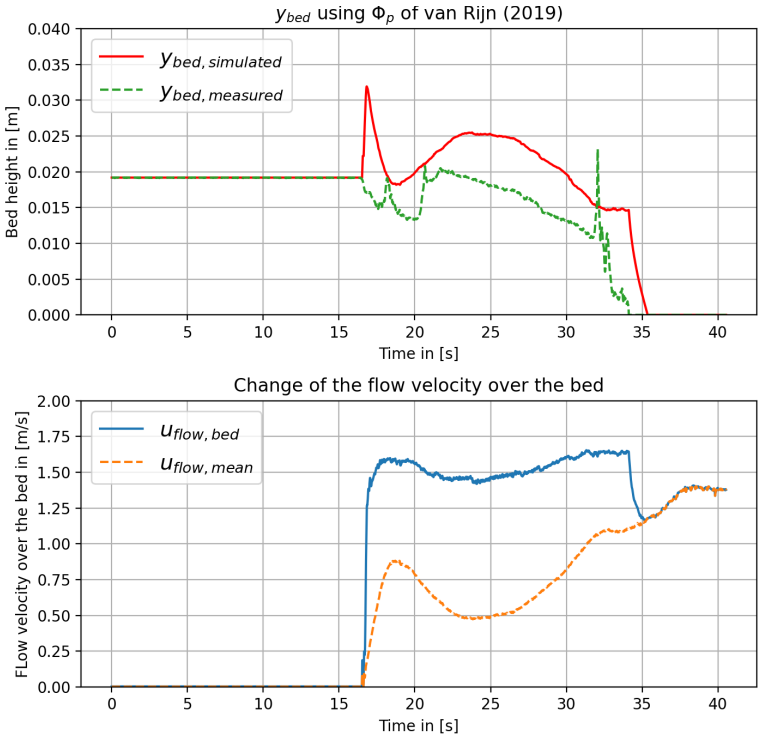

Figure F.103: Outcomes of simulation using the van Rijn et al. (2019) pick-up function for Dorsilit nr.5G with a mixture concentration of 20%

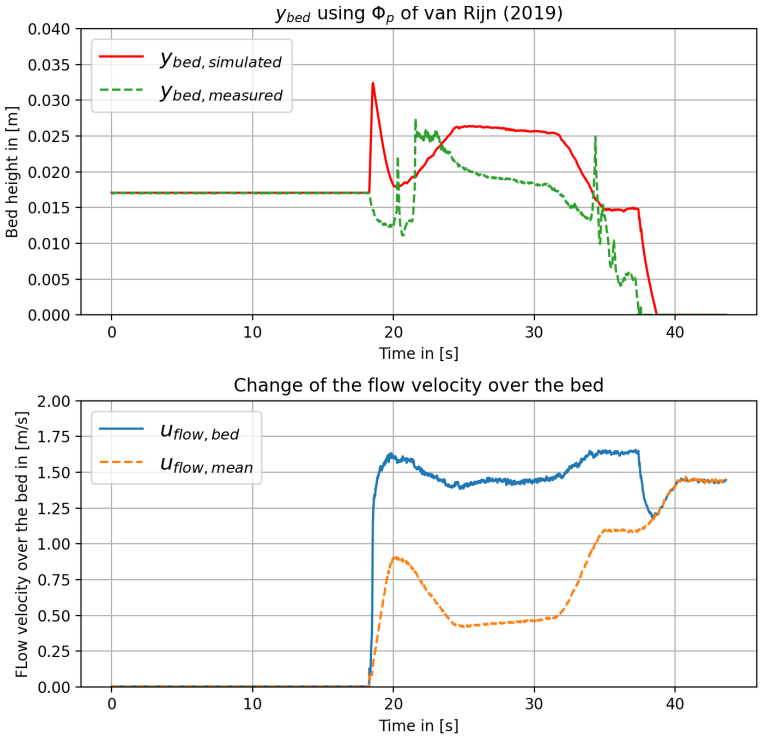

Figure F.104: Outcomes of simulation using the van Rijn et al. (2019) pick-up function for Dorsilit nr.5G with a mixture concentration of 30%

F.6.2 *Dorsilit nr.7*

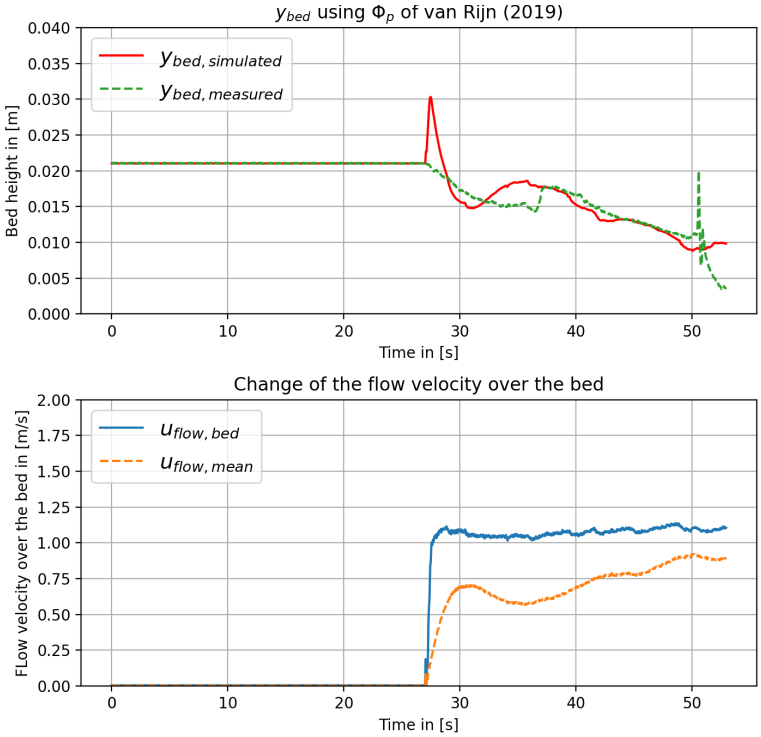

Figure F.105: Outcomes of simulation using the van Rijn et al. (2019) pick-up function for Dorsilit nr.7 with a mixture concentration of 5%

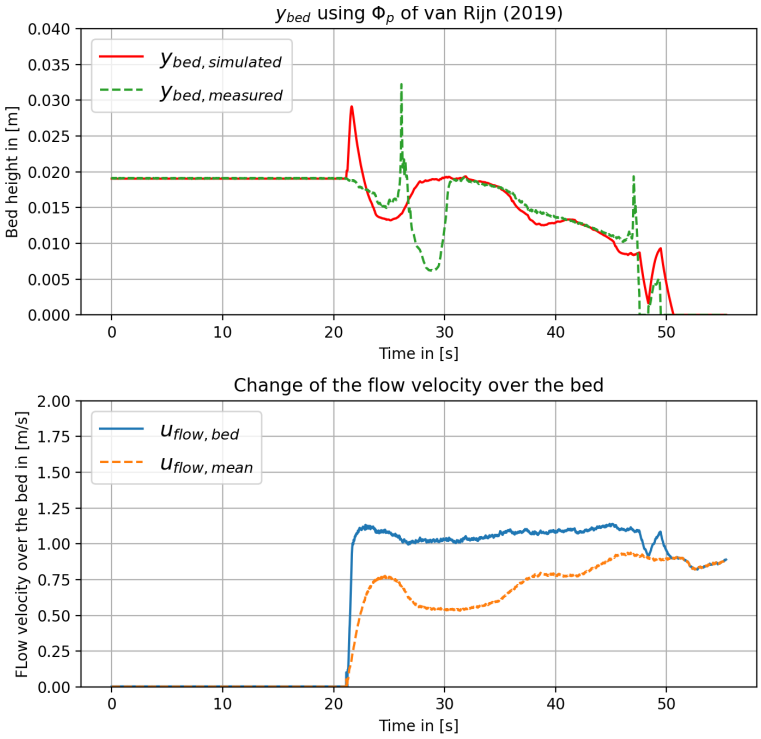

Figure F.106: Outcomes of simulation using the van Rijn et al. (2019) pick-up function for Dorsilit nr.7 with a mixture concentration of 10%

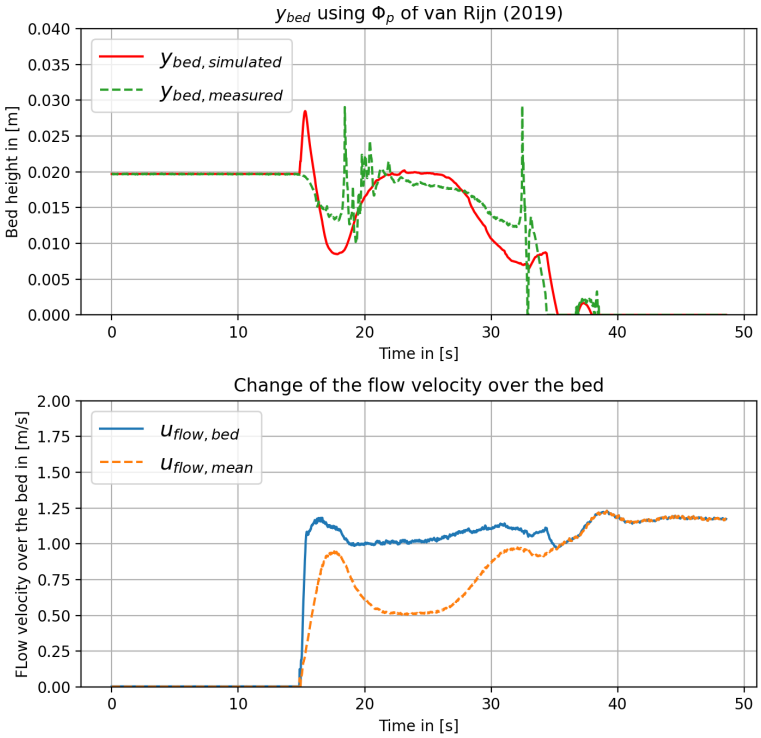

Figure F.107: Outcomes of simulation using the van Rijn et al. (2019) pick-up function for Dorsilit nr.7 with a mixture concentration of 20%

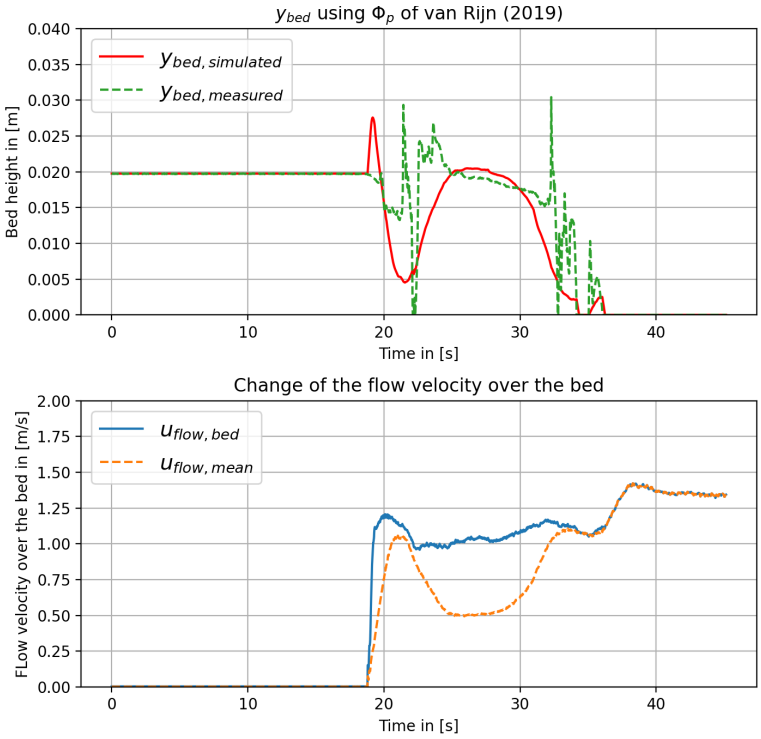

Figure F.108: Outcomes of simulation using the van Rijn et al. (2019) pick-up function for Dorsilit nr.7 with a mixture concentration of 30%

F.6.3 *Dorsilit nr.8*

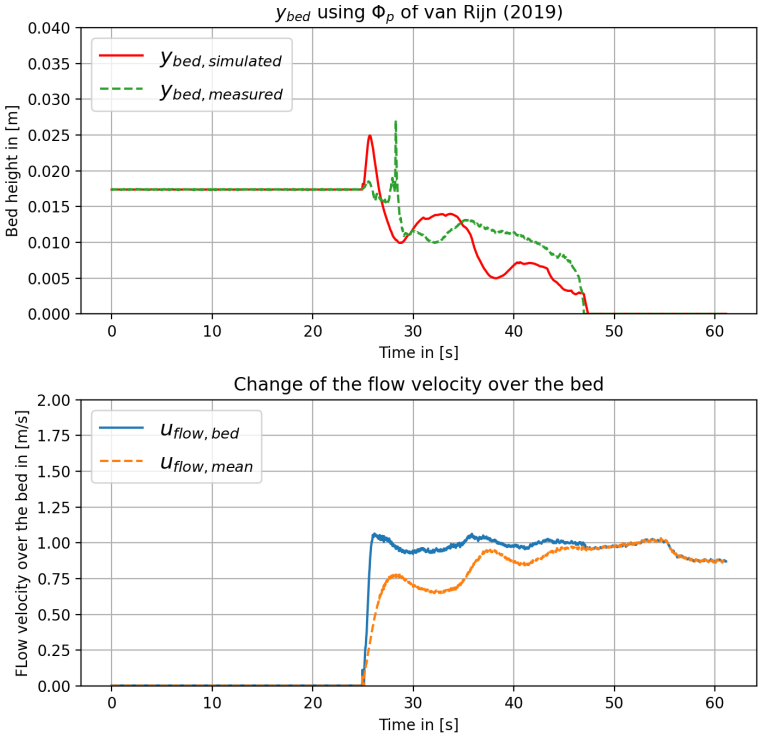

Figure F.109: Outcomes of simulation using the van Rijn et al. (2019) pick-up function for Dorsilit nr.8 with a mixture concentration of 5%

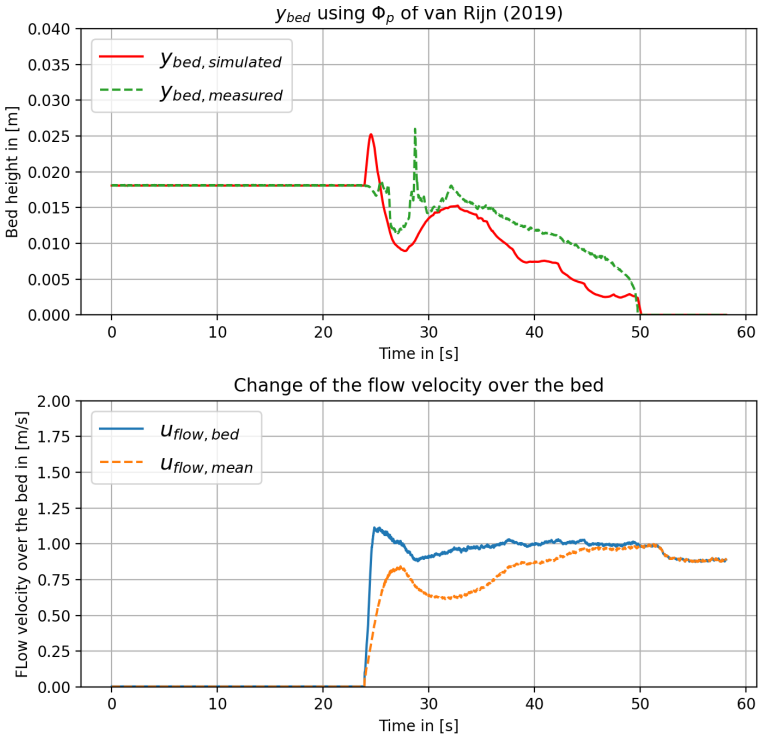

Figure F.110: Outcomes of simulation using the van Rijn et al. (2019) pick-up function for Dorsilit nr.8 with a mixture concentration of 10%

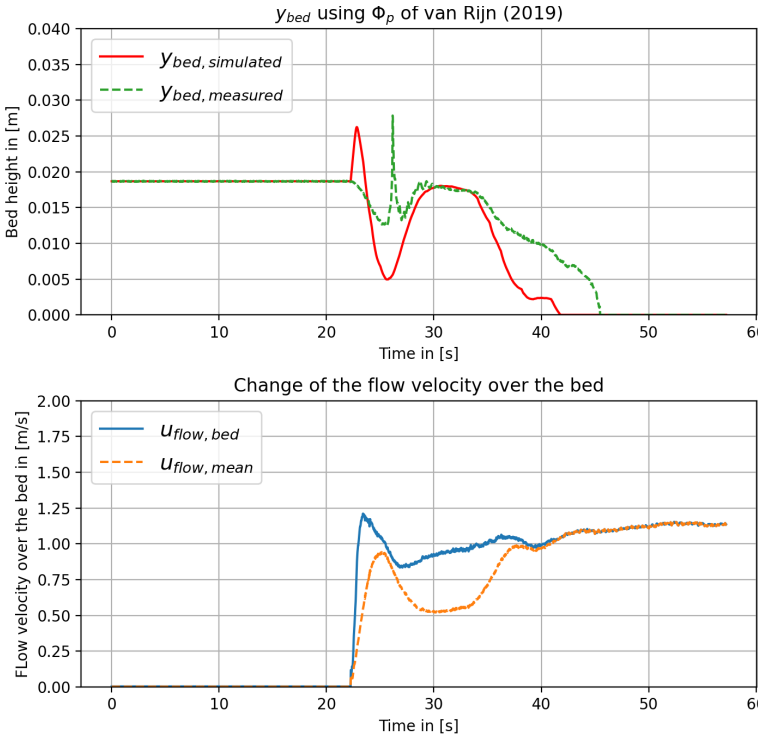

Figure F.111: Outcomes of simulation using the van Rijn et al. (2019) pick-up function for Dorsilit nr.8 with a mixture concentration of 20%

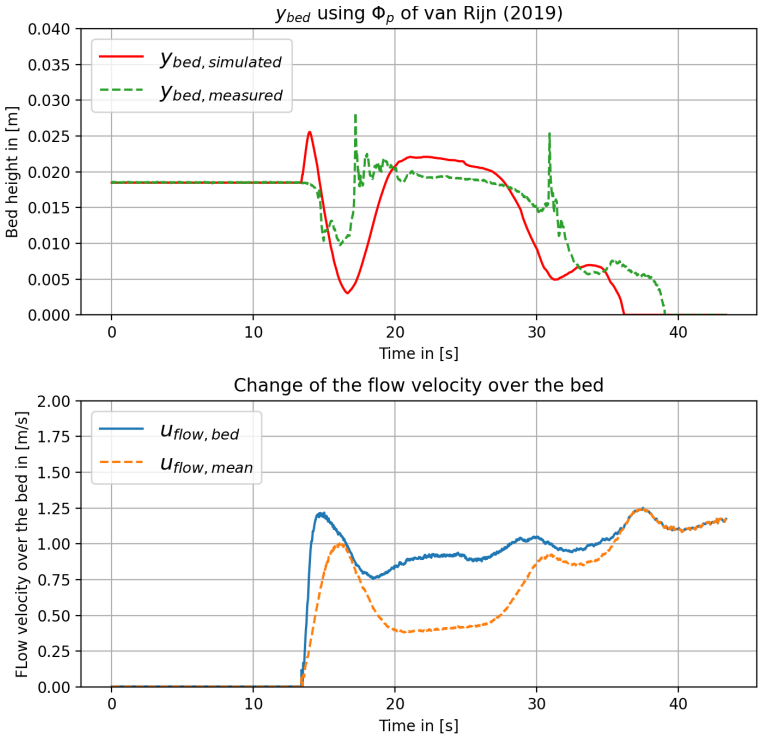

Figure F.112: Outcomes of simulation using the van Rijn et al. (2019) pick-up function for Dorsilit nr.8 with a mixture concentration of 30%

F.6.4 *Zilverzand*

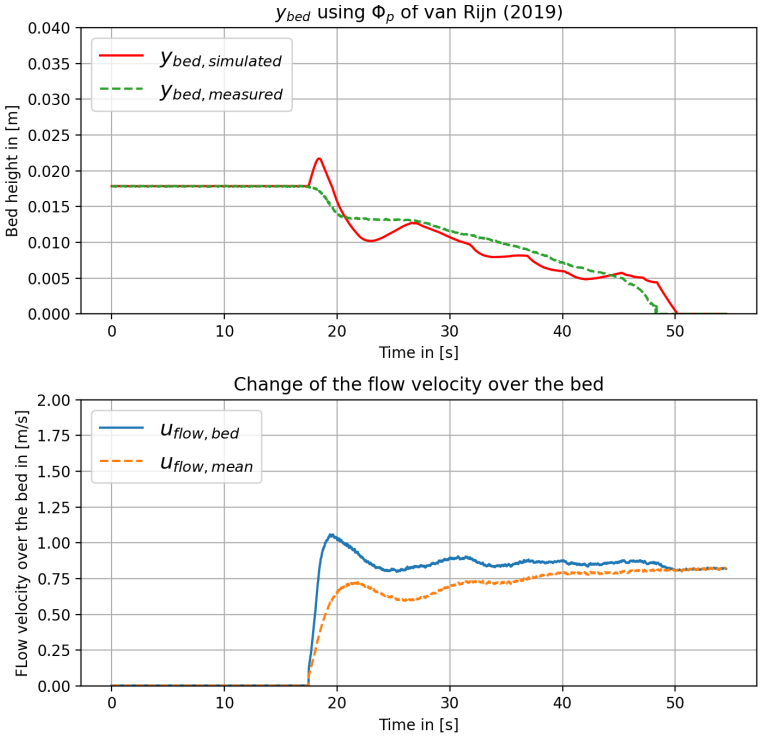

Figure F.113: Outcomes of simulation using the van Rijn et al. (2019) pick-up function for Zilverzand with a mixture concentration of 5%

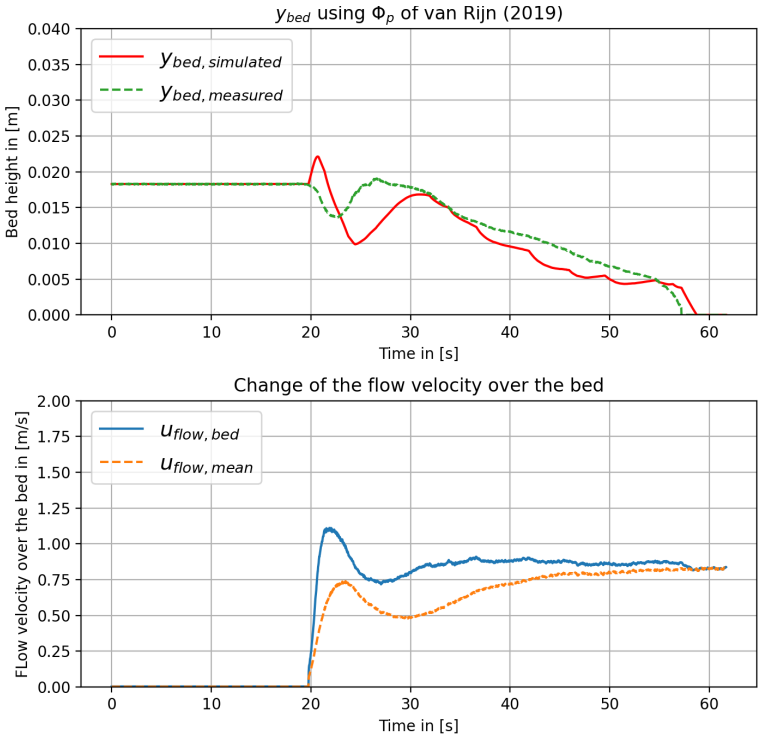

Figure F.114: Outcomes of simulation using the van Rijn et al. (2019) pick-up function for Zilverzand with a mixture concentration of 10%

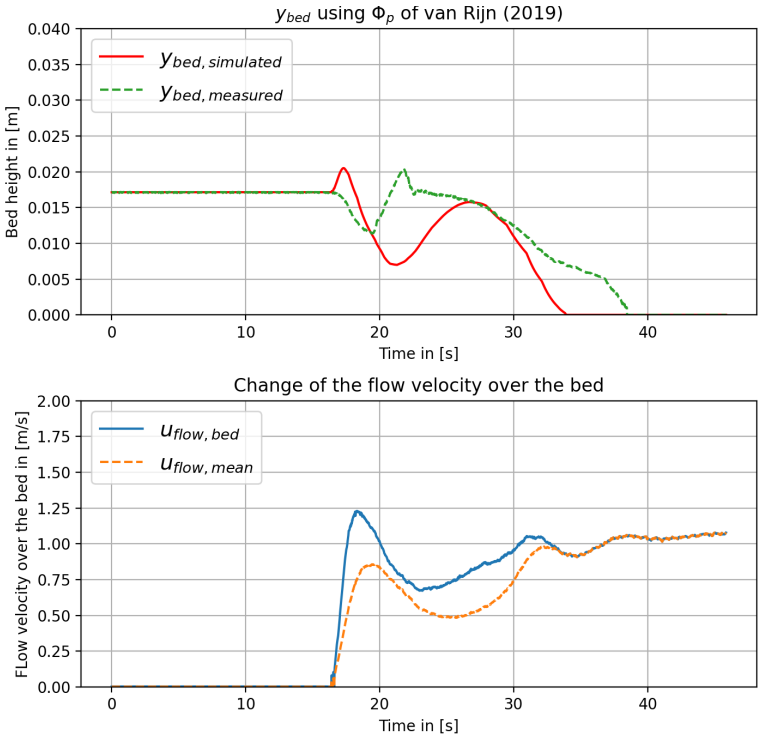

Figure F.115: Outcomes of simulation using the van Rijn et al. (2019) pick-up function for Zilverzand with a mixture concentration of 20%

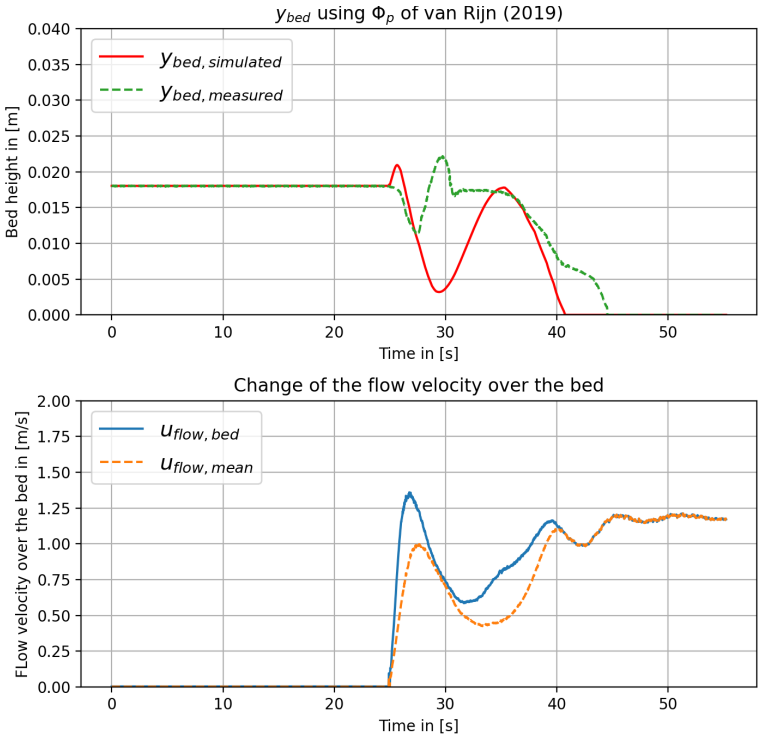

Figure F.116: Outcomes of simulation using the van Rijn et al. (2019) pick-up function for Zilverzand with a mixture concentration of 30%

F.6.5 *GEBA*

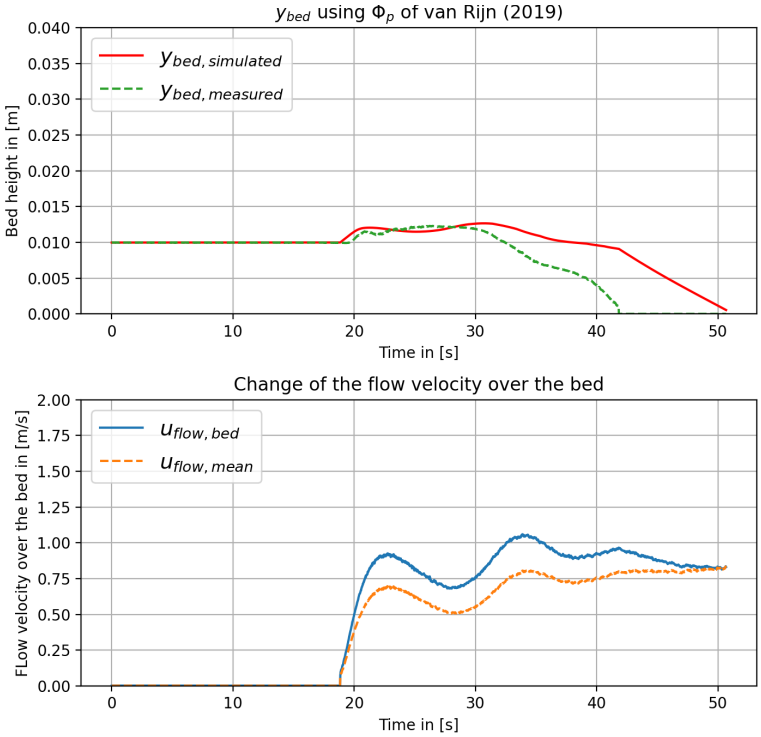

Figure F.117: Outcomes of simulation using the van Rijn et al. (2019) pick-up function for GEBA with a mixture concentration of 5%

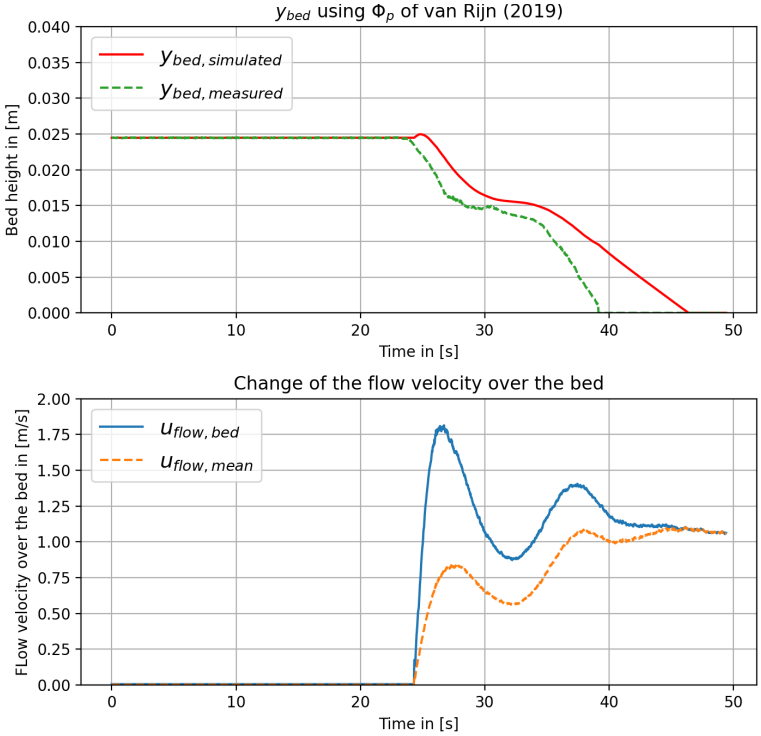

Figure F.118: Outcomes of simulation using the van Rijn et al. (2019) pick-up function for GEBA with a mixture concentration of 10%

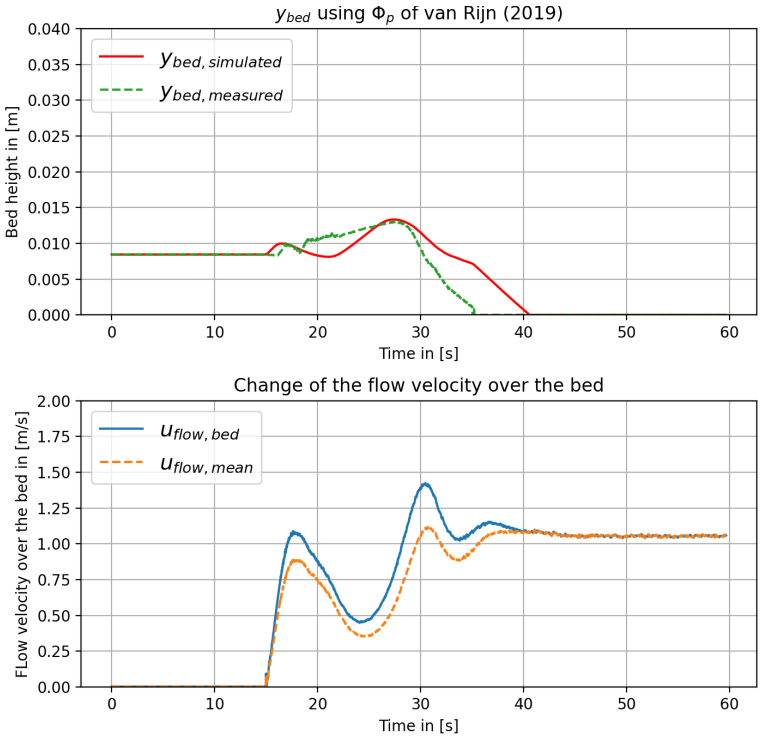

Figure F.119: Outcomes of simulation using the van Rijn et al. (2019) pick-up function for GEBA with a mixture concentration of 20%

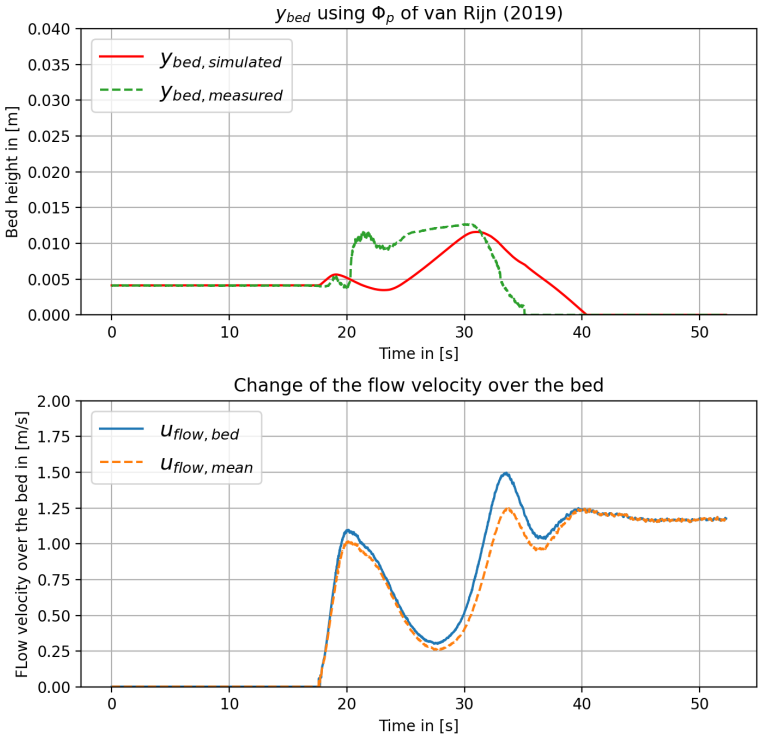

Figure F.120: Outcomes of simulation using the van Rijn et al. (2019) pick-up function for GEBA with a mixture concentration of 30%